Exact Results in Gauge Theories

by

João Silva

A thesis
presented to the University of Waterloo
in fulfillment of the
thesis requirement for the degree of
Doctor of Philosophy
in
Physics

Waterloo, Ontario, Canada, 2015

Author's Declaration

I hereby declare that I am the sole author of this thesis. This is a true copy of the thesis, including any required final revisions, as accepted by my examiners.

I understand that my thesis may be made electronically available to the public.

Abstract

This thesis is devoted to the study of observables in the four dimensional superconformal $\mathcal{N} = 4$ Yang-Mills theory. We will be focused on the problem of computing higher point correlation functions, scattering amplitudes and Wilson loops. Integrability is the main actor in this context and will allow us to obtain answers that would be inconceivable without it. In the case of correlation function, we will study them in the weak and strong coupling limits separately where integrability possesses different incarnations. For the case of scattering amplitudes and Wilson loops, we provide a non-perturbative solution.

Acknowledgements

I had the luck of having Pedro Vieira as my PhD advisor. For his enthusiasm, creativity, generosity and hard working it is hard to conceive what a better advisor could be. He has been my main source of inspiration and his approach to physics has certainly moulded my view of doing science. I am indebted to him for all the care he devoted to me. Thank you Pedro!

I am also obliged to my co-advisor Miguel Costa, with whom I had the first contact with theoretical physics. Without him, I would not have had all the great opportunities to do physics in Porto and in Canada. Thank you Miguel!

I am very thankful to my collaborators Benjamin Basso, Lucía Córdova, Jorge Escobedo, Thiago Fleury, Amit Sever, Jon Toledo from whom I learned so much and for inspiring me. I also want to thank Romuald Janik, Spiro Karigiannis, Rob Mann and Rob Myers for being part of my committee.

During the PhD, I have met some great people that influenced me. I want to thank them all, most notably, Jon Toledo, for his friendship, collaboration, and for being such an awesome company in all the trips we did together during the PhD; Jorge Escobedo, for his great help in the first (painful) months of the PhD and for my first scientific collaboration; Peter Lunts, for his great company and friendship throughout the PhD. I want also to thank all other people I have met in Perimeter during these years (and that is a lot), the Bistro staff for making the environment so unique and stimulating, Debbie and Diana for all the help and care. From CFP, I want to thank everyone especially to Vasco Goncalves, Miguel Zilhão, João Penedones (with some overlap in Canada) and Florbela Martins that made my stays in Porto always pleasant and stimulating. From King's College London, where I spent the last year of my PhD, I am indebted to the several people I have met, especially Nikolay Gromov, Fedor Levkovich-Maslyuk and Grigrory Sizov for a warm hospitality. I would like to thank all my friends outside the scientific environment, especially Luís and João.

I also want to thank FCT for funding me through the grant SFRH/BD/69084/2010 and the GATIS network.

Finally, my family has been the greatest source of support, confidence and comfort. I want to thank my parents, my brother and my goddaughters. This thesis is for them.

Aos meus pais, Adriano e Fernanda,
ao meu irmão Tiago,
à Carolina e à Matilde.

Table of Contents

II Scattering amplitudes from Integrability

4 Overview of Scattering Amplitudes

Chapter 1

Fields, strings and integrability

Fundamental particles in nature seem to be well described by gauge theories at least up to the energy scales we are currently able to measure. As of middle 2015, this scale is set at some impressive 13 TeV [1]. The standard model of elementary particles is certainly the most successful scientific theory we have developed as it seems to explain pretty much everything we have been observing. In this theory, the strong force is described by quantum chromodynamics (QCD) with a $SU(3)$ gauge group, with the quarks being in its fundamental representation. This is an example of a Yang-Mills gauge theory.

Despite its tremendous success, there are several features of QCD that are badly understood. One such example is how to describe it at low energies where it is strongly coupled and thus sits outside the reach of perturbation theory. In particular, in this regime quarks are confined and a solid explanation of this phenomena is one of the biggest open questions in physics. Even at high energies, the Feynman diagram expansion is clearly inefficient making it very hard to improve the precision of theoretical results by going to higher loops.

The poor comprehension of strongly coupled gauge theories incited over the past decades the study of simpler toy models with more symmetry or particular limits of known theories. One prominent example is to consider $SU(N)$ QCD in the limit where the number of colours N goes to infinity keeping the combination $g_{\mathrm{YM}}^2 N$ fixed, where g_{YM} is the Yang-Mills coupling. This idea was first put forward by Gerard 't Hooft [2] and paved the way towards a entire new field of research. Taking the large N limit reorganizes the Feynman diagram series in terms of the parameter $1/N$. Each term in this expansion corresponds to a different topology of the Feynman diagrams, pretty much like in string theory the perturbation theory is organized in terms of topologies of the string worldsheet

and characterized in terms of the number of handles and holes of the surface. In fact, this analogy is not accidental and reveals a deep connection between the gauge and string theory which later gave rise to holography. We will come back to this point.

Large N QCD revealed yet another remarkable feature: the emergence of integrability for the first time in the context of gauge theories. In [3], Lipatov suggested that the asymptotic behaviour of the hadron-hadron scattering amplitudes in the limit of large invariant energy s and fixed transferred momentum t could be described by means of some one-dimensional lattice model. It turned out that this model is in fact integrable, in the sense that the corresponding Hamiltonian can be exactly diagonalized by means of the Bethe ansatz [4]. Beyond simpler cases like this, large N QCD is still a tremendous problem and it is far from being solved.

It seems natural to consider supersymmetric Yang-Mills theories as they are typically simpler. The particular case of maximally supersymmetric Yang-Mills in four dimensions, $\mathcal{N} = 4$ SYM, is the most studied example. It is known to be conformal (the beta function is zero) and hence the coupling constant does not run being simply a free parameter.

The AdS/CFT correspondence [5] identifies this theory with type II B superstring theory in ten dimensional curved $AdS_5 \times S^5$ spacetime. This can be regarded as a realization of the 't Hooft idea of relating a gauge and a string theory in the large N limit. Among many interesting features of the duality is the fact that the strong coupling regime of the gauge theory is related to weakly coupled string theory, which is tractable. The physical picture that emerges in the strong coupling is rather interesting as in several cases the computation of physical observables boils down to pure geometrical problems. It is a standard fact in string theory that the string vibrational modes in $AdS_5 \times S^5$ correspond to particles or fields propagating in this same background. In particular, a closed string involves the massless fields of supergravity (of which the graviton is an example) and also an infinite set of massive modes. These massive modes decouple as the coupling constant goes to infinity and the computation of physical observables in the gauge theory turns into gravitational problems with some geometrical meaning in AdS. This is the case for several cases studied in literature, like some two and three point functions involving protected operators. However, for most of the problems the massive modes are relevant not only when we go away from the large 't Hooft coupling limit and the string dynamics plays an important role. This is what happens for correlation functions involving non-protected operators or scattering amplitudes. Fortunately, remarkably simple structures emerged in the perturbative expansion of several physical observables that finally allowed for exact results at any value of the coupling even when these massive modes enter into the game. The most notable case is the appearance of integrability in the computation of anomalous dimensions, correlation functions, scattering amplitudes and expectation values of Wilson

loops.

Integrability   Integrable field theories form a class of quantum field theories for which one can often obtain exact results for some observables, like S-matrices for scattering of asymptotic states, spectrum of energies, or in some cases even the full correlation functions. These theories live in two dimensions and their special properties result from the existence of an infinite set of higher spin conserved charges. The existence of these tower of charges restricts dramatically the dynamics of the theory. For instance, when we consider the scattering of excitations we observe that no particle production is allowed and the momenta of the particles are simply permuted during the scattering. More importantly, the scattering of any number of particles factorizes into products of two to two scatterings. Hence, all the information about the dynamics is contained in the two body S-matrix and this factorizability property is mathematically encoded on the so-called Yang- Baxter equation. This is the fingerprint of integrability in field theories.

A famous example of an integrable field theory is the sine-Gordon defined by the following action in 1+1 dimensions,

$$S = \int d^2x \left(\frac{1}{2} \partial_\mu \phi \partial^\mu \phi + \frac{m^2}{\beta^2} \cos(\beta \phi) \right) . \tag{1.1}$$

The standard approach would be to consider the limit of small coupling constant β, define a set of vertices for the field ϕ (which in this case would be an infinite set) and do the usual perturbation theory. Then one would eventually obtain the first few orders of the scattering matrix for the asymptotic states of the theory.

However, it was shown that this theory actually possesses an infinite number of conservation laws both at classical and quantum levels. With this knowledge, it was possible to obtain the exact and explicit formula for the quantum S-matrix for any pair of particles of the theory (which are a soliton, anti-soliton and their bound states)[1]. It is a clear example that shows how integrability can be used to obtain information that otherwise would be unthinkable to obtain.

Let us emphasize once more that the natural arena for integrability are the two dimensional models. An infinite set of conserved charges in higher dimensional field theories renders them trivial - only the free field theory is integrable in higher dimensions [7]. This is the reason why four dimensional $\mathcal{N} = 4$ SYM is not integrable in the sense above explained.

---

[1]More specifically, this S-matrix bootstrap was based on Yang-Baxter, unitarity, crossing symmetry and analyticity, see more in [6].

What happens is that for each observable in this theory that we aim at computing, we will need to find an auxiliary two dimensional problem where integrability is manifest and can then be used in its full glory. This is highly nontrivial though and in fact there is not a canonical procedure to uncover the good auxiliary two dimensional integrable problem.

Perhaps the most successful and well studied instance where integrability was revealed is the problem of computing the spectrum of conformal dimensions of the operators in $\mathcal{N} = 4$ SYM. Let us start by reviewing some basic facts of this theory and then illustrate how integrability comes about in this problem with some concrete example.

1.1 The field theory $\mathcal{N} = 4$ SYM

The action of $\mathcal{N} = 4$ SYM was given for the first time in [8], from the dimensional reduction of $\mathcal{N} = 1$ SYM in ten dimensions. The action of $\mathcal{N} = 1$ SYM in ten dimensions is

$$S = \int d^{10}x \, \mathrm{tr} \, \left(-\frac{1}{2} F_{MN} F^{MN} + i \bar{\lambda} \Gamma^M D_M \lambda \right) . \tag{1.2}$$

where Γ are the Dirac matrices in ten dimensions, F_{MN} is the field strength and λ represents a Majorana-Weyl spinor which has sixteen real independent components. The dimensional reduction to four dimensions consists in imposing that the fields do not depend on six of the ten spacetime coordinates, namely

$$\partial^{4+m} A^N = 0 , \quad \partial^{4+m} \Psi = \partial^{4+m} \Psi = 0 , \quad m = 1, \ldots, 6 . \tag{1.3}$$

Then we split the ten dimensional gauge field into a four dimensional gauge field A_μ and six scalars,

$$A_M = (A_\mu(x), \phi_i(x)) , \quad \text{with} \quad \mu = 0, \ldots, 3 \quad \text{and} \quad i = 1, \ldots, 6 . \tag{1.4}$$

where we assume these fields are independent of the remaining six coordinates. Finally, the Majorana-Weyl spinor can be expressed in terms of four Weyl plus four anti-Weyl spinors of the four dimensional theory

$$\lambda^t = [(0, \bar{\psi}^{\dot{\alpha}}_{a=1}), \ldots, (0, \bar{\psi}^{\dot{\alpha}}_{a=4}), (\psi^{a=1}_\alpha, 0), \ldots, (\psi^{a=4}_\alpha, 0)] . \tag{1.5}$$

One still needs to choose a convenient representation of the ten dimensional Γ matrices in terms of four and six dimensional γ matrices [9]. Furthermore, one can rewrite the six scalar fields arising from the internal components of the gauge field into components of

the tensor Φ^{ab} in the antisymmetric representation of $SU(4)$. Upon expanding the original action (1.2) we obtain the $\mathcal{N} = 4$ SYM lagrangian density

$$
\begin{aligned}
\mathcal{L} \;=\; & \mathrm{tr} \left(-\frac{1}{2} F_{\mu\nu} F^{\mu\nu} + 2\mathcal{D}_\mu \Phi_{ab} \, \mathcal{D}^\mu \Phi^{ab} + 2i\psi^{\alpha a} \sigma^\mu_{\alpha\dot\alpha} (\mathcal{D}_\mu \bar\psi_a)^{\dot\alpha} \right. \\
& \left. + 2g_{\mathrm{YM}}^2 [\Phi^{ab}, \Phi^{cd}][\Phi_{ab}, \Phi_{cd}] - 2\sqrt{2} g_{\mathrm{YM}} \left([\psi^{\alpha a}, \Phi_{ab}]\psi^b_\alpha - [\bar\psi_{\dot\alpha a}, \Phi^{ab}]\bar\psi^{\dot\alpha}_b \right) \right).
\end{aligned}
\tag{1.6}
$$

The field content of this theory consists then of a gauge field A_μ, four Weyl fermions ψ^a_α and six real scalars $\Phi^{ab} = -\Phi^{ba}$ and all these fields are in the adjoint representation of the gauge group $SU(N)$. Moreover it can be shown that the action is invariant under the $\mathcal{N} = 4$ on-shell supersymmetry transformations, as a result of the $\mathcal{N} = 1$ supersymmetry of the original action, and it is also exactly conformal.

1.2 Integrability in the spectrum problem

Weak coupling In a conformal field theory, it is always possible to find a basis of (renormalized) operators such that the two point function has the form

$$
\langle \mathcal{O}_A(x_1) \mathcal{O}_B(x_2) \rangle = \frac{\delta_{AB}}{|x_{12}|^{2\Delta_A}},
\tag{1.7}
$$

where Δ_A are the conformal dimensions. In general, if the operators carry some Lorentz indices the RHS of the above equation will involve some conformally invariant tensor structure. Let us suppose we want to determine the conformal dimensions at one loop where we expect it to have the following perturbative expansion

$$
\Delta_A = d_A + g^2 \gamma_A + \dots
\tag{1.8}
$$

Here d_A is the classical dimension of the operator $\mathcal{O}_A$, γ_A is its one-loop anomalous dimension and $g^2 = \frac{g_{\mathrm{YM}}^2 N}{16\pi^2}$ is the 't Hooft coupling.

We start with some bare operator $\mathcal{O}_A$ and we consider its two point function with some probe operator made out of arbitrary fields. It has the generic form

$$
\langle \mathcal{O}_A^{(0)}(x_1) \mathcal{O}^{(\mathrm{probe})}(x_2) \rangle = \frac{\mathcal{N}}{|x_{12}|^{2\,d_A}} \left(\hat{1} - g^2 \hat{H} \log |x_{12}\Lambda|^2 \right),
\tag{1.9}
$$

where $\mathcal{N}$ is some normalization constant that might depend on the coupling. The matrix $\hat{H}$ is the so-called mixing matrix. The renormalized operator is then obtained from the bare operators by

$$
\mathcal{O}_A = \left(\hat{1} + g^2 \hat{H} \log |\Lambda/\mu| \right)_{AB} \mathcal{O}_B^{(0)},
\tag{1.10}
$$

where μ is some renormalization scale. $\hat{H}$ is such that the correlation function of $\mathcal{O}_A$ with any other operator is finite. Once we find this matrix, its diagonalization renders the anomalous dimensions γ_A. The eigenvectors of this matrix which are made from a linear combination of the bare operators then renormalize multiplicatively by μ^{γ_A}.

Throughout this thesis we will be considering single trace gauge invariant operators made out of the adjoint fields of the theory. Let us restrict ourselves for now to a particular class of these single trace operators in which the fields involved are just a scalar $Z \equiv \phi^{34}$ and a component of a Weyl fermion $\Psi \equiv \psi^4_{\alpha=1}$. We will be analysing these operators in greater detail in the forthcoming chapter. An example is

$$\mathcal{O} = \operatorname{tr}\, (Z \ldots \Psi \ldots Z) \tag{1.11}$$

where the dots stand to any of the fields Z or Ψ and the number of fields of the operator is L (also called the *length* of the operator).

We want to find the one-loop spectrum of anomalous dimensions for operators made out of these fields following the logic above. The computation of all Feynman diagrams is given in figure A.2 of appendix A.

In the end, we sum over all the diagrams as illustrated in figure 1.1. The mixing matrix can be written as a sum of local operators acting on neighbouring fields inside the trace as follows

$$\hat{H} = 2 \sum_{j=1}^{L} (I_{j,j+1} - SP_{j,j+1}) \tag{1.12}$$

where the indices correspond to the position of the fields inside a trace. I is the identity operator and SP refers to the superpermutation operator that exchanges the position of two fields and picks up a minus sign when these two fields are fermionic.

The outcome of this computation can be regarded as an Hamiltonian acting on a closed spin chain state where each field inside the trace corresponds to a site of the spin chain. What is remarkable about (1.12) is that this Hamiltonian is known to be integrable (see [10] for a related discussion). In fact, this is nothing but a fermionic version of the Heisenberg Hamiltonian which is diagonalizable by means of the Bethe ansatz. Therefore integrability allows us to compute the anomalous dimensions for arbitrary operators made out of these two kinds of fields. The computation we presented here parallels an analogous computation by Minahan and Zarembo in 2002 [11] for operators made out of scalars, that triggered the field of integrability in $\mathcal{N} = 4$ SYM.

Let us emphasize that the 1+1 dimensional auxiliary problem where integrability turns up for the spectrum problem at weak coupling is the spin chain model. The factorizability

7
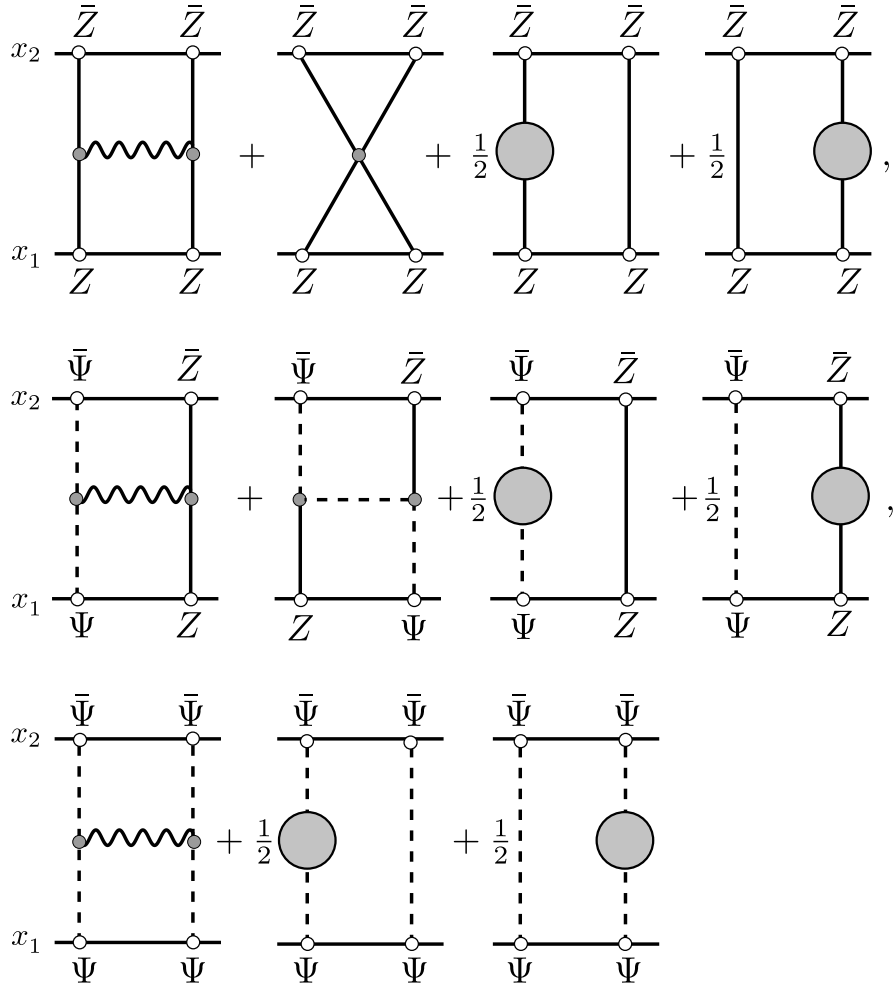
Figure 1.1: Using the results of figure A.2, the sum of the graphs appearing in this figure gives precisely the Hamiltonian of (1.12).

happens at the level of the S-matrix for the excitations in this spin chain model, and it is not connected (at least directly) with the properties of the spacetime S-matrix of $\mathcal{N} = 4$ SYM.

Strong coupling The AdS/CFT duality identifies the single trace gauge invariant operators with closed string states in $AdS_5 \times S^5$. Moreover, the conformal dimensions of the operators are in correspondence with the energy of the corresponding closed string states.

The world-sheet of the closed string in $AdS_5 \times S^5$ has a topology of a cylinder and can be parametrized by a pair of coordinates (σ, τ). Then the embedding coordinates in $AdS_5 \times S^5$ will be functions of the cylinder coordinates $X^\mu(\sigma, \tau)$. They are then promoted to quantum fields and their dynamics is described by an action that is determined by the geometry of the background. This action includes additionally some fermionic degrees of freedom. When restricted to the bosonic degrees of freedom the action is simply the Polyakov action with target space $AdS_5 \times S^5$. The point we want to emphasize is that string theory naturally provides a two dimensional quantum field theory and this model turns out to be integrable. The classical integrability of the model was shown in [12]. The appearance of integrable structures on both sides of the duality was a sign that integrability somehow persisted further at quantum level and in particular that the 2D worldsheet theory is fully quantum integrable.

Recent developments The weak coupling integrability was afterwards extended to other sectors and to higher loops [10, 13–15], eventually leading to the all loop conjecture of the Asymptotic Bethe Ansatz (ABA) for long operators [16, 17]. On the other side of the correspondence, the semiclassical quantization of the folded string (GKP string) [18] and agreement with the ABA [19] provided the first non-trivial interpolation between weak and strong coupling. The developments on the spectrum problem culminated in the 2009's solution given by the Thermodynamic Bethe Ansatz [20–22] originated from the Y-system [23]. This was refined in the subsequent years to the Quantum Spectral Curve [24], which is probably the ultimate simplification of the spectrum problem. An extensive review of the integrability in the spectrum problem (and much more!) is given in [25].

1.3   Outline of the thesis

We will now focus our attention on the exact computation of observables other than the conformal dimensions. Integrability will also be the main player for higher point correlation functions, scattering amplitudes and Wilson loops, even though the corresponding auxiliary two dimensional problems might be different.

I was co-author of the following papers: [26–30]. This thesis will not cover [26] and will be based on the other papers. It is split in two main parts, each one covering a different observable. The first part will be devoted to the correlation functions. The chapter 2 consists on the study of three point functions at weak coupling and its material strongly overlaps with the paper [28]. The chapter 3 is about the strong coupling limit of four

point functions and is built on the contents of [27]. The second part covers the scattering amplitudes/ Wilson loop problem. We will see that these two observables are actually equivalent. The chapter 4 is a brief review of the subject, and the chapter 5 is based on the papers [29, 30]. We end up with some final remarks in chapter 6. Additionally, we include several appendices that complement the main text with mostly technical aspects.

Part I

Correlation functions from Integrability

Chapter 2

Correlation functions at weak coupling

We now study the first class of observables of this thesis, namely the higher point correlation functions of local operators in planar $\mathcal{N} = 4$ Super Yang-Mills. The computation of correlators is a whopping task. In standard gauge theories, one typically relies on perturbation theory for a small value of the coupling constant but one can hardly go further in the perturbative order as the number of Feynman diagrams increases dramatically. Integrability turns out to be pivotal in making the task feasible at weak coupling and as recently reported in [31] to finally generate a non-perturbative solution for the three point case.

The problem of three point functions in a conformal field theory is known to be reduced to the computation of the so-called structure constants, as the spacetime dependence is completely fixed from symmetry considerations. Moreover, the structure constant together with the conformal dimensions of the operators contain all the dynamical information appearing in the OPE decomposition. Therefore we can reconstruct all higher point functions from them. The non-perturbative knowledge of these two observables constitutes what one would call a *solution* of $\mathcal{N} = 4$ SYM.

The first attempts to compute three point functions go back to the early days of the AdS/CFT correspondence [32] where it was found that for protected operators (chiral primary operators) the structure constant is in fact coupling independent. Therefore, it equals the tree level result and agrees with the string theory calculation. For non-protected operators, the comparison is difficult because of the weak/strong coupling nature of the duality. Nevertheless, there were several attempts to perform these computations at weak

coupling (in particular with the use of integrability) [33–42], and also at strong coupling mostly in the classical limit [43–52].

We aim at reviewing how integrability tools can help in this problem at weak coupling using the pedagogical example of the three point functions in the so-called $\mathfrak{su}(1|1)$ subsector of $\mathcal{N} = 4$ Super Yang-Mills.

2.1 Three-point functions at leading order

In this section, we perform the computation of the structure constants at leading order. The setup that will be used for the calculation involves composite operators made out of both fermionic and scalar fields. Each of these operators is thought of as a state of a closed spin chain with the fermionic fields being excitations over a ferromagnetic vacuum. The advantage of this approach is that the connection with the integrability tools of quantum spin chains becomes manifest (see for instance [25]) and facilitates the combinatorial problem.

The smallest (closed) sector of $\mathcal{N} = 4$ SYM containing both fermionic and bosonic fields is the $\mathfrak{su}(1|1)$. The field content of this sector consists of one complex scalar that we will denote as $Z = \Phi^{34}$ and a complex chiral fermion that shares with the scalar one R-charge index, for instance $\Psi = \psi^4_{\alpha=1}$. The setup for the calculation of the planar three-point functions that we will be considering involves an operator $\mathcal{O}_1$ given by a linear combination of single traces made out of products of these fields. More precisely,

$$\mathcal{O}_1 = \sum_{1 \leq n_1 < n_2 < \ldots < n_{N_1} \leq L_1} \psi^{(1)}(n_1, n_2, \ldots, n_{N_1}) \mathrm{tr} \left(Z \ldots \underset{n_1}{\Psi} \ldots \underset{n_2}{\Psi} \ldots Z \right), \qquad (2.1)$$

where L_1 is the length of the operator, N_1 is the number of its fermionic fields and n's are the positions of the excitations along the chain of Z's. We designate the coefficients $\psi^{(1)}$ in this linear combination by wave-function. It is natural to consider the second operator $\mathcal{O}_2$ made out of the complex conjugate fields, namely

$$\mathcal{O}_2 = \sum_{1 \leq n_1 < n_2 < \ldots < n_{N_2} \leq L_2} \psi^{(2)}(n_1, n_2, \ldots, n_{N_2}) \mathrm{tr} \left(\bar{Z} \ldots \underset{n_1}{\bar{\Psi}} \ldots \underset{n_2}{\bar{\Psi}} \ldots \bar{Z} \right). \qquad (2.2)$$

In our conventions, the complex conjugate fields are given by

$$\bar{Z} = (Z)^* = \Phi_{34} = \Phi^{12}, \qquad (2.3)$$
$$\bar{\Psi} = (\Psi)^\dagger = \bar{\psi}_{4, \dot{\alpha}=\dot{1}}.$$

15
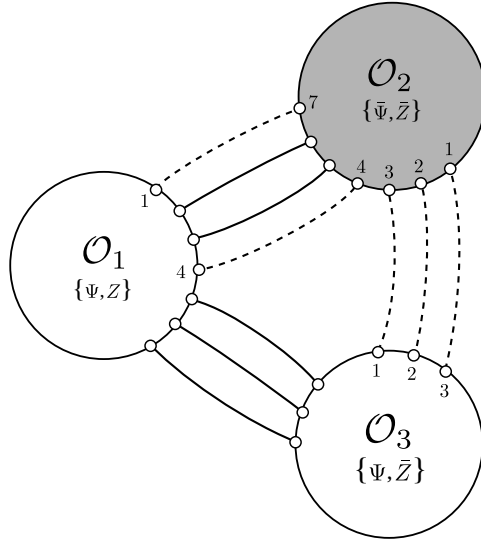
Figure 2.1: The leading order contribution to the three-point functions. The solid lines represent a bosonic propagator and the dashed lines represent a fermionic propagator. We also indicate our conventions for labelling the positions of the excitations. Notice that in our setup the first N_3 excitations of the operator $\mathcal{O}_2$ have always their position fixed.

From now on, we will omit the Lorentz spinorial indices at several places keeping in mind that they are always kept fixed.

As a consequence of the R-charge conservation, it is clear that we cannot take the third operator to be also in the same $\mathfrak{su}(1|1)$ sector to which $\mathcal{O}_1$ and $\mathcal{O}_2$ belong, if we want to have a non-vanishing result and avoid extremal correlation functions[1]. Instead, we consider a "rotated" operator constructed by applying $\mathfrak{su}(4)$ generators several times to a $\mathfrak{su}(1|1)$ operator of the type $\mathcal{O}_1$. The idea is to get a composite operator having a term with only Ψ and $\bar{Z}$ fields in order to allow non-vanishing Wick contractions between all pairs of operators (see figure 2.1 for an example of a non-extremal three-point function). More precisely, let us suppose that we start with a state made out of Ψ and Z fields. In order to convert a single Z into a $\bar{Z}$ we must apply a pair of $\mathfrak{su}(4)$ generators that rotate its two R-charge indices. In sum, we can generate a term with Ψ's and $\bar{Z}$'s by considering the

---

[1]The extremal case presents additional subtleties related to the mixing with double-trace operators, see [33]. We will not investigate such issues in this thesis and therefore only non-extremal three-point functions will be considered.

following operation

$$\mathcal{O}_3 = \frac{1}{(L_3 - N_3)!^2} (r^2{}_4 r^1{}_3)^{L_3 - N_3} \sum_{1 \le n_1 < \ldots < n_{N_3} \le L_3} \psi^{(3)}(n_1, \ldots, n_{N_3}) \mathrm{tr}\ (Z \ldots \Psi \ldots \Psi \ldots Z)\ ,$$

(2.4)

where $r^a{}_b$ are $\mathfrak{su}(4)$ generators and they act on the fields inside the trace. Now, the $\mathfrak{su}(4)$ generators may also act on the field Ψ which carries one R-charge index. Therefore, this operation will generate several terms coming from the different ways of acting with the generators,

$$\mathcal{O}_3 = \sum_{1 \le n_1 < \ldots < n_{N_3} \le L_3} \psi^{(3)}(n_1, \ldots, n_{N_3}) \Bigg[\quad \mathrm{tr}\ \left(\bar{Z} \ldots \Psi \ldots \Psi \ldots \bar{Z} \right) +$$

$$+ \quad \mathrm{tr}\ \left(\bar{Z} \ldots \psi^2 \ldots \Psi \ldots \Phi^{14} \right) + \ldots \Bigg],\ (2.5)$$

where in the first line we have the term where all the $\mathfrak{su}(4)$ generators act on the scalar fields Z. In the second line, we represent the terms where some of the generators also act on the fermionic fields Ψ. As an example of how the formula given above is evaluated consider,

$$(r^2{}_4 r^1{}_3) \cdot \mathrm{Tr}\ (\Psi Z) = (r^2{}_4 r^1{}_3) \cdot \mathrm{Tr}\ (\psi^4 \Phi^{34}) = \mathrm{Tr}\ (\psi^2 \Phi^{14}) + \mathrm{Tr}\ (\psi^4 \Phi^{12})\ .$$

At tree-level, the terms in the second line of (2.5) do not give any contribution due to the R-charge conservation. In other words, one always has a zero Wick-contraction. Therefore, at leading order, only the first line contributes and we get a tree-level diagram of the type represented in figure 2.1. At one-loop, the terms in the second line will also need to be taken into account. We emphasize that the operators $\mathcal{O}_1$ in (2.1) and $\mathcal{O}_3$ in (2.4) are spinorial operators with N_1 and N_3 indices $\alpha = 1$ respectively. This follows from the definition of the field Ψ given previously. The operator $\mathcal{O}_2$ in (2.2) has N_2 Lorentz indices $\dot{\alpha} = \dot{1}$ associated to each of the fermions $\bar{\Psi}$.

In a conformal field theory, the two-point functions are completely fixed by the symmetries up to a normalization constant. For two operators having spinorial indices as shown below, we have

$$\langle \mathcal{O}_{i\,;\,1_1 \ldots 1_{N_i}}(x_1)\, \bar{\mathcal{O}}_{i\,;\,\dot{1}_1 \ldots \dot{1}_{N_i}}(x_2) \rangle = \mathcal{N}_i \frac{(J_{12,1\dot{1}})^{N_i}}{|x_{12}|^{2\Delta_i}}\ ,$$

(2.6)

where $\mathcal{N}_i$ is a constant associated to the normalization of the operator, Δ_i is its conformal

dimension and the tensorial structure is[2]

$$J_{ij,1\dot{1}} = \frac{x_{ij}^\mu \left(\sigma_\mu^E\right)_{1\dot{1}}}{(2\pi)^2 |x_{ij}|}, \qquad \text{with} \qquad x_{ij}^\mu = x_i^\mu - x_j^\mu. \tag{2.7}$$

In the case of three-point functions of generic operators having spinorial indices, one has many inequivalent tensor structures consistent with the conformal symmetry, and the result of the correlation function is a linear combination of these structures. The constraints following from conformal symmetry on the higher point functions were studied for instance in [53–55]. However, for the setup considered in this work there is only one possible tensor and the three-point functions is of the form

$$\langle \mathcal{O}_{1;1_1\dots 1_{N_1}}(x_1)\, \mathcal{O}_{2;\dot{1}_1\dots \dot{1}_{N_2}}(x_2)\, \mathcal{O}_{3;1_1\dots 1_{N_3}}(x_3)\rangle = \tag{2.8}$$

$$\frac{(J_{12,1\dot{1}})^{N_1}(J_{23,1\dot{1}})^{N_3}\sqrt{\mathcal{N}_1\mathcal{N}_2\mathcal{N}_3}\, C_{123}(g^2)}{|x_{12}|^{\Delta_1+\Delta_2-\Delta_3}|x_{13}|^{\Delta_1+\Delta_3-\Delta_2}|x_{23}|^{\Delta_2+\Delta_3-\Delta_1}},$$

where we are considering $N_2 = N_1 + N_3$ and $g^2 = \frac{\lambda}{16\pi^2}$ with λ the 't Hooft parameter.

The structure constant $C_{123}(g^2)$ has a perturbative expansion when g^2 is small, and its leading order will be designated by $C_{123}^{(0)}$. Using the figure 2.1, we observe that the only non-trivial Wick contractions occur between operators $\mathcal{O}_1$ and $\mathcal{O}_2$. The structure constant $C_{123}^{(0)}$ is then given by the product of the three wave-functions with a sum over the positions of the excitations between these two operators,

$$\left|C_{123}^{(0)}\right| = \alpha \left| \psi_{1,\dots,N_3}^{(3)} \sum_{N_3 < n_1 < \dots < n_{N_1} \le L_2} \psi_{L_2+1-n_{N_1},\dots,L_2+1-n_1}^{(1)} \psi_{1,\dots,N_3,n_1,\dots,n_{N_1}}^{(2)} \right|. \tag{2.9}$$

α is a normalization factor that comes from the fact that we are normalizing the operators such that their two-point functions has the canonical form (2.6) with $\mathcal{N}_i = 1$. It is given by

$$\alpha = \sqrt{\frac{L_1 L_2 L_3}{\mathcal{N}^{(1)}\mathcal{N}^{(2)}\mathcal{N}^{(3)}}}, \quad \text{with} \quad \mathcal{N}^{(j)} = \sum_{1 \le n_1 < \dots < n_{N_j} \le L_j} (\psi_{n_1,\dots,n_{N_j}}^{(j)})^* (\psi_{n_1,\dots,n_{N_j}}^{(j)}). \tag{2.10}$$

The main goal of this section is to find a closed formula for $C_{123}^{(0)}$.

---

[2]See Appendix A.1 for our conventions.

2.1.1 The one-loop Bethe eigenstates and structure constants

To compute $C_{123}^{(0)}$ we must consider states with definite one-loop anomalous dimension [33]. The one-loop $\mathfrak{su}(1|1)$ integrable Hamiltonian and S-matrix can be found in [10, 14] or in the introduction of this thesis where it was computed directly. It can be written in terms of the Pauli matrices as

$$H_1 = 2g^2 \sum_{n=1}^{L} \left((1 - \sigma_n^3) - \frac{1}{2}(\sigma_n^1 \sigma_{n+1}^1 + \sigma_n^2 \sigma_{n+1}^2) \right) , \tag{2.11}$$

where L is the length of the spin chain. At leading order the two-excitation S-matrix is independent of their momenta and simply given by

$$S(p_1, p_2) = -1 . \tag{2.12}$$

In order to find the eigenstates of the Hamiltonian given above, we use the usual coordinate Bethe ansatz. A N-magnon state of a spin-chain of length L is of the form

$$|\psi_N\rangle = \sum_{1 \leq n_1 < n_2 < \ldots < n_N \leq L} \psi_N(n_1, n_2, \ldots, n_N)|n_1, \ldots, n_N\rangle , \tag{2.13}$$

where the n_i's in $|n_1, \ldots n_N\rangle$ indicate the position of the fermionic excitations Ψ on the chain (for details about the coordinate Bethe ansatz see [25, 33]). Notice that the ket $|n_1, \ldots n_N\rangle$ represents the trace in (2.1). The wave-function $\psi_N(n_1, \ldots, n_N)$ is a combination of plane waves with as many terms as the number of possible permutations of the momenta with the relative coefficients being the S-matrices. Since the leading order $\mathfrak{su}(1|1)$ S-matrix is just -1, the several terms in the wave-function will appear with alternating signs which we write as

$$\psi_N(n_1, n_2, \ldots, n_N) = \sum_{P} \text{sign } P \, \exp(ip_{\sigma_P(1)}n_1 + ip_{\sigma_P(2)}n_2 + \ldots + ip_{\sigma_P(N)}n_N) \tag{2.14}$$

where P indicates sum over all possible permutations σ_P of the elements $\{1, \ldots, N\}$, and sign P is the sign of the permutation. Moreover, we should impose the periodicity condition by requiring the momenta p_i to satisfy the Bethe equations

$$e^{ip_i L} = 1 . \tag{2.15}$$

The cyclic property of the trace is implemented by imposing the zero momentum condition of the state,

$$\sum_{i=1}^{N} p_i = 2\pi \times \text{integer} . \tag{2.16}$$

Having determined the eigenstates of the one-loop $\mathfrak{su}(1|1)$ Hamiltonian, we can proceed to compute the leading order structure constant $C_{123}^{(0)}$ given in (2.9) by following some simple steps. First, we notice that since the positions of the excitations of the third operator are fixed, we can use (2.14) to write $\psi^{(3)}$ explicitly. It is simple to see that we obtain a Vandermonde determinant which can be also presented as a simple product,

$$\left|C_{123}^{(0)}\right| = \alpha \left| \prod_{j<k}^{N_3} \left[e^{ip_j^{(3)}} - e^{ip_k^{(3)}} \right] \sum_{N_3<n_1<...<n_{N_1}\leq L_2} (\psi_{n_1,...,n_{N_1}}^{(1)})^* \, \psi_{1,...,N_3,n_1,...,n_{N_1}}^{(2)} \right|. \qquad (2.17)$$

Moreover we have replaced $\psi_{L_2+1-n_{N_1},...,L_2+1-n_1}^{(1)}$ by $(\psi_{n_1,...,n_{N_1}}^{(1)})^*$ since they differ by at most a sign.

Notice that the first N_3 excitations of the wave-function $\psi^{(2)}$ have their positions fixed or *frozen*. In order to make the computation of this sum simpler, we consider an auxiliary problem where we add N_3 extra excitations to the wave-function $\psi^{(1)}$ and liberate the fixed N_3 roots of $\psi^{(2)}$ with their positions being summed over too,

$$\mathcal{S}_{aux} \equiv \sum_{1\leq n_1<...<n_{N_3+N_1}\leq L_2} (\psi_{n_1,...,n_{N_3+N_1}}^{(1)})^* \, \psi_{n_1,...,n_{N_3+N_1}}^{(2)}. \qquad (2.18)$$

The advantage of considering this auxiliary problem is that the sum (2.18) can be easily computed due to the form of the wave-functions. Moreover, we can relate it with the original sum appearing in (2.17) as we now explain. Indeed, let us consider that N_3 momenta, say $\{p_1^{(1)}, \ldots, p_{N_3}^{(1)}\}$, are complex. We can then dynamically localize the wave-function around the original N_3 positions by taking the limit of these momenta going to minus infinity. More precisely, we send $\{e^{-ip_1^{(1)}}, \ldots, e^{-ip_{N_3}^{(1)}}\}$ to zero in such a way that

$$e^{-ip_1^{(1)}} \ll \cdots \ll e^{-ip_{N_3}^{(1)}}. \qquad (2.19)$$

Thus, given the explicit form of the wave-function (2.14), we observe that in this limit the sum over the positions of the extra roots in (2.18) is dominated by the term for which $n_1 = 1, \ldots, n_{N_3} = N_3$. This procedure of sending roots to a particular limit in order to freeze their positions is the coordinate Bethe ansatz counterpart of the *freezing trick* used in [34] at the level of the six-vertex model. Neglecting all the subleading terms, we get that in this limit, (2.18) is reduced to

$$\mathcal{S}_{aux} \to \left(\prod_{k=1}^{N_3} e^{-ip_k^{(1)} k} \right) \sum_{N_3<n_1<...<n_{N_1}\leq L_2} (\psi_{n_1,...,n_{N_1}}^{(1)})^* \, \psi_{1,...,N_3,n_1,...,n_{N_1}}^{(2)}, \qquad (2.20)$$

where we recognize precisely the original sum of (2.17).

Returning to our auxiliary problem, we use again that the wave-function is completely antisymmetric in its arguments to extend the limits of the sum (2.18). In compensation, we merely have to introduce a trivial overall combinatorial factor. Using the explicit form of the wave-function we write the sum (2.18) as

$$\mathcal{S}_{aux} = \frac{1}{N_2!} \sum_{\{n_i\}} \sum_{P,Q} \text{sign} \, P \, \text{sign} \, Q \, \prod_{a=1}^{N_1+N_3} e^{\left(ip_{P(a)}^{(2)} - ip_{Q(a)}^{(1)}\right)n_a} \, . \tag{2.21}$$

We emphasize again that we now sum without restrictions, $1 \leq n_i \leq L_2$, for all n_i. These sums over n_i can be explicitly computed as they are geometric series. Using the Bethe equations and the total momentum condition for the operator $\mathcal{O}_2$, we can then simplify (2.21) to

$$\mathcal{S}_{aux} = \left[\prod_{a=1}^{N_1+N_3} \left(1 - e^{-ip_a^{(1)}L_2}\right) \right] \frac{1}{N_2!} \sum_{P,Q} \text{sign} \, P \, \text{sign} \, Q \, \prod_{a=1}^{N_1+N_3} \frac{1}{e^{ip_{Q(a)}^{(1)}} - e^{ip_{P(a)}^{(2)}}} \, . \tag{2.22}$$

The remaining sum in the previous expression is manifestly the definition of a Cauchy determinant and, therefore, it can be written explicitly as a simple product as follows

$$\mathcal{S}_{aux} = \left[\prod_{a=1}^{N_1+N_3} \left(1 - e^{-ip_a^{(1)}L_2}\right) \right] \frac{\prod_{j<k} (e^{ip_j^{(1)}} - e^{ip_k^{(1)}})(e^{ip_k^{(2)}} - e^{ip_j^{(2)}})}{\prod_{j,k}(e^{ip_j^{(1)}} - e^{ip_k^{(2)}})} \, . \tag{2.23}$$

Notice that this expression contains as a limit the norm of an operator.[3] It is given by

$$\mathcal{N}^{(j)} = L_j^{N_j} \, . \tag{2.24}$$

Finally, we take the limit of (2.23) when $\{e^{-ip_1^{(1)}}, \ldots, e^{-ip_{N_3}^{(1)}}\}$ vanish as in (2.19). Plugging the resulting limit and taking into account the overall product multiplying the sum in (2.20), we obtain our final result

$$\left| C_{123}^{(0)} \right| = \left[\prod_{i=1}^{3} L_i^{\frac{1-N_i}{2}} \right] \left| \left[\prod_{j=1}^{N_1} \left(1 - e^{ip_j^{(1)}L_2}\right) \right] \frac{\prod_{a=1}^{3} \prod_{j<k}^{N_a} (e^{ip_j^{(a)}} - e^{ip_k^{(a)}})}{\prod_{j=1}^{N_1} \prod_{k=1}^{N_2} (e^{ip_j^{(1)}} - e^{ip_k^{(2)}})} \right| \, . \tag{2.25}$$

---

[3]If we set $N_3 = 0$ and consider $p_j^{(1)} \to p_j^{(2)}$ we get the expression for $\mathcal{N}^{(2)}$ after using the Bethe equations (2.15).

Let us remark that this expression is considerably simpler than the ones found for the $\mathfrak{su}(2)$ [34] and $\mathfrak{sl}(2)$ [39] sectors. This is perhaps not surprising given that at leading order we are dealing with a theory of free fermions so that the form of the $\mathfrak{su}(1|1)$ wave-function becomes quite simple. However, we will see that the one-loop result persists to be simpler than in the other sectors.

2.2 One-loop three-point functions

In this section, we compute the structure constants at first order in the 't Hooft coupling λ for our setup. There are two main ingredients in this computation. Firstly, one has to consider Bethe eigenstates that diagonalize the two-loop dilatation operator as these states are of order λ. Secondly, one has to compute the relevant Feynman diagrams at this order in perturbation theory. This second contribution can be compactly taken into account through the insertion of an operator at specific points of the spin chains as will be reviewed.

2.2.1 Two-loop coordinate Bethe eigenstates and Norms

The two-loop Bethe eigenstates are determined by diagonalizing the long-range Hamiltonian H [10]

$$H = H_1 + H_2 \,, \tag{2.26}$$

where H_1 is given in (2.11) and

$$H_2 = 4g^2 \sum_{n=1}^{L} \Big(2(\sigma_n^3 - 1) - \frac{1}{4}(\sigma_n^3 \sigma_{n+1}^3 - 1) + (\sigma_n^1 \sigma_{n+1}^1 + \sigma_n^2 \sigma_{n+1}^2)\Big(\frac{9}{8} - \frac{1}{16}\sigma_{n+2}^3\Big) \tag{2.27}$$
$$-\frac{1}{16}\sigma_n^3(\sigma_{n+1}^1 \sigma_{n+2}^1 + \sigma_{n+1}^2 \sigma_{n+2}^2) - \frac{1}{8}\sigma_n^1(1 + \sigma_{n+1}^3)\sigma_{n+2}^1 - \frac{1}{8}\sigma_n^2(1 + \sigma_{n+1}^3)\sigma_{n+2}^2 \Big),$$

where σ^i are the Pauli matrices. In order to diagonalize it, we start with the usual coordinate Bethe ansatz which works when the excitations are at a distance bigger than the range of the interaction, i.e. when $|n_i - n_j| > 2$. In this region all we need is the two-loop S-matrix which reads

$$S(p_1, p_2) = -1 - 8ig^2 \sin\Big(\frac{p_1}{2}\Big) \sin\Big(\frac{p_1 - p_2}{2}\Big) \sin\Big(\frac{p_2}{2}\Big) \,. \tag{2.28}$$

Given the long-range nature of the Hamiltonian (2.26), we expect the form of the wave-function to be modified with respect to the usual Bethe ansatz (2.14). In fact, when magnons are placed at neighbouring positions on the spin chain they interact in a non-trivial way. Therefore, the wave-function must be refined by the inclusion of the so-called *contact terms*. For instance, in the case of three magnons we write it as

$$\psi(n_1, n_2, n_3) = \phi_{123} + \phi_{213}S_{21} + \phi_{132}S_{32} + \phi_{312}S_{31}S_{32} + \phi_{231}S_{31}S_{21} + \phi_{321}S_{32}S_{31}S_{21}\,,$$

where we have used the notation $S_{ab} = S(p_a, p_b)$ and

$$\phi_{abc} = e^{ip_a n_1 + ip_b n_2 + ip_c n_3}\Big(\quad 1 \quad + g^2\,\mathbb{C}(p_a, p_b)\,\delta_{n_2,n_1+1}\delta_{n_3>n_2+1} + g^2\mathbb{C}(p_b, p_c)\,\delta_{n_2>n_1+1}\delta_{n_3,n_2+1}$$
$$+ \quad g^2\,\mathbb{C}(p_a, p_b, p_c)\,\delta_{n_2,n_1+1}\delta_{n_3,n_2+1}\Big)\,. \tag{2.29}$$

The functions $\mathbb{C}$ are the contact terms which are fixed by solving the energy eigenvalue problem. In the case of N-magnons, the wave-function has a similar structure. It consists of $N!$ terms coming from the permutations of $\{p_1, \ldots, p_N\}$ and $N - 1$ types of contact terms namely $\mathbb{C}(p_i, p_j), \ldots, \mathbb{C}(p_1, ..., p_N)$.

Unexpectedly, we have found that up to seven magnons the contact terms are simply given by

$$\mathbb{C}(p_1, \ldots, p_N) = \frac{N - 1}{2}\,. \tag{2.30}$$

Even though we have not proved the validity of this formula for an arbitrarily high number of magnons, the pattern emerging up to seven magnons is quite suggestive. Given the form of the contact terms in the $\mathfrak{su}(2)$ and $\mathfrak{sl}(2)$ sectors, the simplicity of the $\mathfrak{su}(1|1)$ result is quite surprising. In particular, notice that they are independent of the momenta of the colliding magnons. This might be pointing towards the existence of a new algebraic description of these states yet to be unveiled.

As already explained, in order to correctly compute the three-point functions we need to know the norm of the Bethe eigenstates as we are normalizing the result by the two-point functions. Remarkably, we have checked numerically up to six-magnons that the two-loop (coordinate) norm is given by

$$\mathcal{N} = \det_{j,k \leq N} \frac{\partial}{\partial p_j}\left[Lp_k + \frac{1}{i}\sum_{m \neq k}^{N} \log S(p_m, p_k)\right]\,. \tag{2.31}$$

Interestingly, this formula is precisely the well-known Gaudin norm for the one-loop $\mathfrak{su}(2)$ Bethe states. Still within the $\mathfrak{su}(2)$ sector, it was recently shown in [37] that this expression

23

remains valid at higher loops leading to an all-loop conjecture for the norm. Moreover, the two-loop norm for $\mathfrak{sl}(2)$ Bethe states was found to be precisely of the type (2.31) as described in [39]. In all these cases, the contact terms recombine exactly to preserve the determinant form. This is very suggestive of an underlying hidden structure that is worth investigating.

2.2.2 One-loop perturbative calculation

Loop computations will give rise to divergences which require the introduction of a regularization scheme. A very convenient one and the one that will be used in this work is the *point splitting* regularization. At one-loop, only neighbouring fields inside any of the single-trace operators interact and the divergences arise because the two fields are at the same spacetime point. The idea behind the point splitting regularization is to separate these two fields by a distance ϵ which will act as a regulator [4].

Consider a $\mathfrak{su}(1|1)$ bare operator which is an eigenstate of the one-loop dilatation operator. Its non-vanishing two-point function is of the form

$$\langle \mathcal{O}_{i\,;\,1_1\ldots 1_{N_i}}(x_1)\,\bar{\mathcal{O}}_{i\,;\,\mathrm{i}_1\ldots\mathrm{i}_{N_i}}(x_2)\rangle = \mathcal{N}_i\,\frac{(J_{12,1\mathrm{i}})^{N_i}}{|x_{12}|^{2\Delta_{0,i}}}\left(1 + 2g^2\,a_i - \gamma_i\log\left(\frac{x_{12}^2}{\epsilon^2}\right)\right)\,, \qquad (2.32)$$

where the tensor on the right-hand side was defined in (2.7). In the expression above, $\Delta_{0,i}$ and γ_i are the free scaling dimension and the one-loop anomalous dimension of the operator $\mathcal{O}_i$ respectively, $\mathcal{N}_i$ is a normalization constant and a_i is a scheme dependent constant. In addition, the three-point function of three $\mathfrak{su}(1|1)$ bare operators that diagonalize the one-loop dilatation operator is, in our setup, fixed by conformal symmetry and takes the form (see [35] for details)

$$\langle \mathcal{O}_{1\,;\,1_1\ldots 1_{N_1}}(x_1)\,\mathcal{O}_{2\,;\,\mathrm{i}_1\ldots\mathrm{i}_{N_2}}(x_2)\,\mathcal{O}_{3\,;\,1_1\ldots 1_{N_3}}(x_3)\rangle = \qquad (2.33)$$

$$\frac{(J_{12,1\mathrm{i}})^{N_1}(J_{23,1\mathrm{i}})^{N_3}\,\sqrt{\mathcal{N}_1\mathcal{N}_2\mathcal{N}_3}}{|x_{12}|^{\Delta_{0,1}+\Delta_{0,2}-\Delta_{0,3}}|x_{13}|^{\Delta_{0,1}+\Delta_{0,3}-\Delta_{0,2}}|x_{23}|^{\Delta_{0,2}+\Delta_{0,3}-\Delta_{0,1}}}\,C_{123}^{(0)}\,\times$$

$$\left(1 + g^2\left(C_{123}^{(1)} + a_1 + a_2 + a_3\right) - \frac{\gamma_1}{2}\log\left(\frac{x_{12}^2 x_{13}^2}{x_{23}^2\epsilon^2}\right) - \frac{\gamma_2}{2}\log\left(\frac{x_{12}^2 x_{23}^2}{x_{13}^2\epsilon^2}\right) - \frac{\gamma_3}{2}\log\left(\frac{x_{23}^2 x_{13}^2}{x_{12}^2\epsilon^2}\right)\right)$$

---

[4]In order to preserve the gauge invariance, one can introduce a Wilson line between the two shifted fields. This will in principle introduce extra diagrams at one-loop, coming from the gluon emission from the Wilson line. However, we will show in the Appendix A.4 that this additional contribution actually vanishes at this order in perturbation theory.
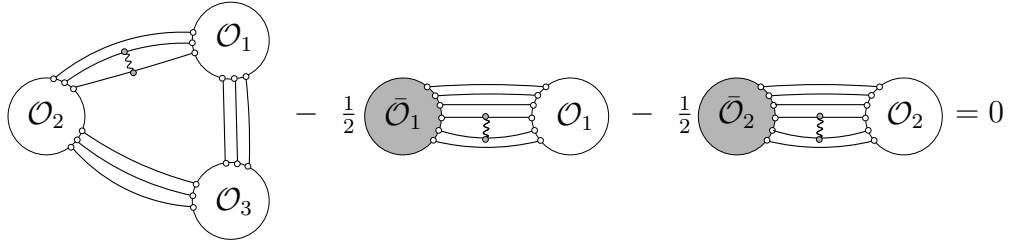
Figure 2.2: The wavy-line in the figure is just a representation of a one-loop diagram (for example, a gluon exchange). When the contribution of the square root of the two-point functions is subtracted (this is the reason for the factor $\frac{1}{2}$), all the diagrams involving just two operators are canceled.

where we have factored out the tree-level constant $C_{123}^{(0)}$.

To extract the regularization scheme independent structure constant $C_{123}^{(1)}$ from the expression above, we have to divide the three-point function by the square root of the two-point functions of all the operators to get rid of the constants a_i's. After performing this division, one can then read the meaningful structure constant.

From the Feynman diagrams computation point of view, it is actually simpler to calculate $C_{123}^{(1)}$ instead of the combination $(C_{123}^{(1)} + a_1 + a_2 + a_3)$. In fact, because we have to divide by the square root of the two-point functions, all one-loop diagrams in the three-point function involving only two operators are canceled. The figure 2.2 has an example of a such cancellation.

The conclusion is that one is left with the computation of only genuine three-point diagrams, i.e., the diagrams involving fields from the three operators[5]. The allowed positions of the spin chains where it is possible to have those genuine diagrams are commonly called the *splitting points*. We are then seeking the constants coming from the genuine three-point diagrams subtracted by the constants coming from the same diagrams but now seen as two-point processes. This is exemplified in the figure 2.3.

The details of the Feynman diagram computation are given in the Appendix A and here we just provide the results. In the figure 2.4, we list all diagrams giving a non-zero contribution to the three-point functions as well as the result of the respective scheme independent constants. A relevant aspect of this computation is that some terms in the second line of (2.5) are now important at one-loop level. Indeed, from figure 2.4 we realize that the second graph of the second row mixes up the R-charge indices of the scalar and the fermion. In particular, the scalar Φ^{14} and the fermion ψ^2 in the second line of (2.5)

---

[5]This fact was dubbed the *slicing argument* in [36]
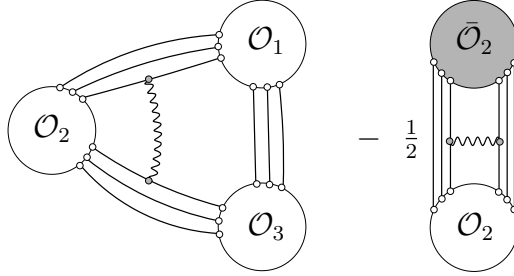
Figure 2.3: A genuine three-point diagram to which we subtract half of the same diagram but seen as a two-point process is shown. The constant coming from this combination of diagrams is regularization scheme and normalization independent.

can be converted into a Ψ and a $\bar{Z}$ through this diagram. The resulting state can then be contracted with the remaining external operators and give a non-vanishing contribution.

From the results of figure 2.4, we can directly read off an operator acting on the two fields at the splitting points of an external state and that gives those same constants after contraction with the remaining states. We denote this operator by $\mathcal{F}$ and define it by the following matrix elements

$$\langle\, \psi^a\, \psi^b\, |\, \mathcal{F}\, |\, \psi^c\, \psi^d\, \rangle = -\, \delta^{ac}\delta^{bd}\,, \qquad (2.34)$$

$$\langle\, \Phi^{ef}\, \Phi^{gh}\, |\, \mathcal{F}\, |\, \Phi^{ab}\, \Phi^{cd}\, \rangle = 2\, \bar{\delta}^{gh,ab}\, \bar{\delta}^{ef,cd} - 2\, \bar{\delta}^{ef,ab}\, \bar{\delta}^{gh,cd} -\, \epsilon^{abcd}\, \epsilon^{efgh}\,,$$

$$\langle\, \Phi^{de}\, \psi^f\, |\, \mathcal{F}\, |\, \Phi^{ab}\, \psi^c\, \rangle = -\, \delta^{fc}\bar{\delta}^{ab,de}\,, \qquad \langle\, \psi^f\, \Phi^{de}\, |\, \mathcal{F}\, |\, \psi^c\, \Phi^{ab}\, \rangle = -\, \delta^{fc}\bar{\delta}^{ab,de}\,,$$

$$\langle\, \Phi^{de}\, \psi^f\, |\, \mathcal{F}\, |\, \psi^c\, \Phi^{ab}\, \rangle = \delta^{ce}\bar{\delta}^{ab,df}\,, \qquad \langle\, \psi^f\, \Phi^{de}\, |\, \mathcal{F}\, |\, \Phi^{ab}\, \psi^c\, \rangle = \delta^{ce}\bar{\delta}^{ab,df}\,,$$

where $\bar{\delta}^{ab,cd} \equiv \delta^{ac}\delta^{bd} - \delta^{ad}\delta^{bc}$ and in the second line we recognize the $\mathfrak{so}(6)$ Hamiltonian [11, 35, 36]. It is simple to check that the operator $\frac{g^2}{2}\mathcal{F}$ reproduces the constants of figure 2.4.

For the specific setup that we are considering only the diagrams of figure 2.4 are relevant, since additional diagrams either cancel among them or vanish, see Appendix A for details. In the case of a more general setup, the operator $\mathcal{F}$ defined receives corrections from new diagrams.

In what follows, the operator $\mathcal{F}$ will appear with additional indices as $\mathcal{F}_{ij}$, which indicate
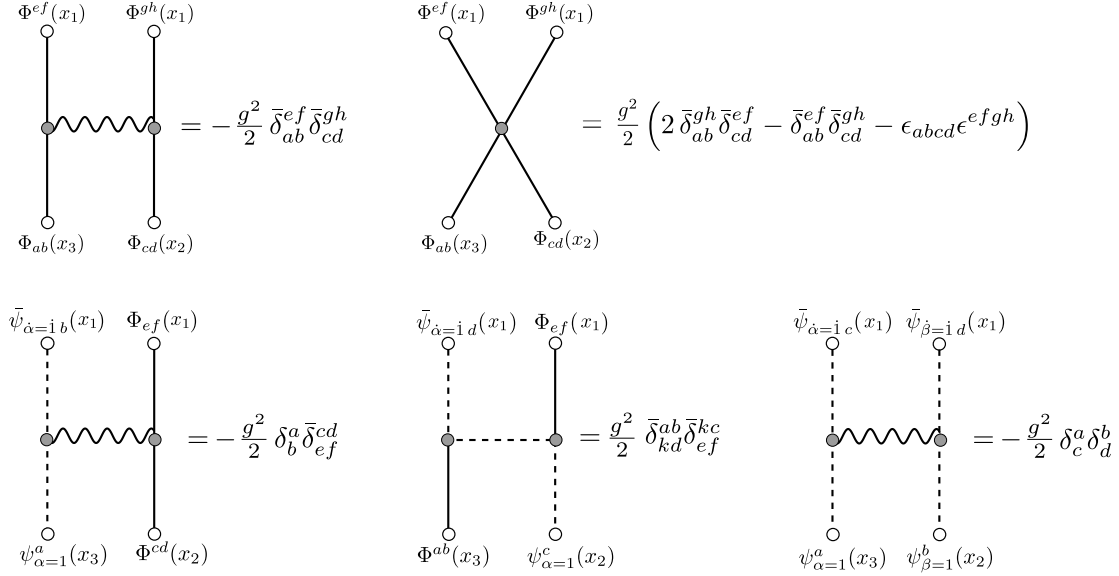
Figure 2.4: These are the relevant one-loop diagrams for the three-point functions. All other graphs give a zero contribution. The solid, wiggly and dashed lines represent the scalars, gluons and fermions, respectively. The constants are obtained by combining the three-point and two-point graphs as illustrated in figure 2.3. We have used the point splitting regularization and the Feynman gauge. For three-point diagrams we take the limit where a pair of dots (either top or bottom) are brought to the same spacetime points. For the two-point function, both pairs of dots (top and bottom) are brought to the same spacetime points. We are using the definition $\bar{\delta}^{ab}_{cd} \equiv \delta^a_c \delta^b_d - \delta^b_c \delta^a_d$.

the sites in the spin chain where the operator acts. As an example, we have that

$$\langle \dots \overset{i}{\Psi}\overset{j}{Z} \dots | \frac{g^2}{2}\mathcal{F}_{ij} | \dots \overset{i}{\Psi}\overset{j}{Z} \dots \rangle = -\frac{g^2}{2} \,,$$

which reproduces the result of the first diagram of the second row of figure 2.4. It is important to note that when the operator $\mathcal{F}_{ij}$ acts on non-neighbouring sites, it can pick up additional minus signs due to statistics, for example,

$$\langle \Psi \dots \underbrace{\Psi \dots \Psi}_{n \text{ fermions}} \dots Z | \frac{g^2}{2}\mathcal{F}_{1L} | Z \dots \underbrace{\Psi \dots \Psi}_{n \text{ fermions}} \dots \Psi \rangle = (-1)^n \frac{g^2}{2} \,,$$

where n denotes the number of fermionic excitations between the first and last sites and we have used the last rule of (2.34).

27

2.2.3 Final result

We now give the complete expression for the structure constants up to one-loop in the setup considered in this work. It reads

$$C_{123} = \alpha \times \Big(\quad \langle \mathbf{1}^f | 1 + \frac{g^2}{2} \mathcal{F}_{L_3-N_3, L_3-N_3+1} + \frac{g^2}{2} \mathcal{F}_{L_1,1} | \underbrace{\bar{Z} \dots \bar{Z}}_{L_3-N_3} i_1 \dots i_{L_2-N_3} \rangle \quad (2.35)$$

$$\langle \underbrace{\bar{\Psi} \dots \bar{\Psi}}_{N_3} i_1 \dots i_{L_2-N_3} | 1 + \frac{g^2}{2} \mathcal{F}_{N_3, N_3+1} + \frac{g^2}{2} \mathcal{F}_{L_2,1} | \mathbf{2} \rangle \Big) \times$$

$$\langle \underbrace{\Psi \dots \Psi}_{N_3} \underbrace{\bar{Z} \dots \bar{Z}}_{L_3-N_3} | 1 + \frac{g^2}{2} \mathcal{F}_{N_3, N_3+1} + \frac{g^2}{2} \mathcal{F}_{L_3,1} | \mathbf{3} \rangle \,,$$

where we have that

$$\alpha = \sqrt{\frac{L_1 L_2 L_3}{\mathcal{N}^{(1)} \mathcal{N}^{(2)} \mathcal{N}^{(3)}}} \,, \tag{2.36}$$

with $\mathcal{N}^{(i)}$ being the respective norms and we are using the conventions

$$\langle \sigma_{i_1} \sigma_{i_2} \cdots \sigma_{i_L} | \sigma_{j_1} \sigma_{j_2} \cdots \sigma_{j_L} \rangle = \delta_{i_1 j_1} \delta_{i_2 j_2} \cdots \delta_{i_L j_L} \,,$$

where σ is any field.

In the formula (2.35), i_a can be either $\bar{Z}$ or $\bar{\Psi}$ and a sum over all these intermediate states is implied. Moreover, we have included a superscript f in the bra associated to the operator $\mathcal{O}_1$ to emphasize that the state was *flipped*[6], see [33] for details. The external states are the two-loop corrected Bethe eigenstates as described in section 2.2.1, for instance

$$|\mathbf{1}\rangle = |1\rangle^{(0)} + g^2 |1\rangle^{(1)} + \mathcal{O}(g^4) \,. \tag{2.37}$$

We have checked that for the simple case of three half-BPS operators, the one-loop correction to the structure constant vanishes as expected from the non-renormalization theorem of [56], see Appendix A.3 for details.

The expression (2.35) can now be evaluated as an explicit function of the Bethe roots by using the known form of the two-loop Bethe states. As the number of excitations on the

---

[6]In short, the *flipping* operation $\mathcal{F}l$ introduced in [33] is defined as $\mathcal{F}l: \ \psi(n_1, \dots, n_N)|n_1, \dots, n_N\rangle \mapsto \psi(n_1, \dots, n_N)\langle L - n_N + 1, \dots, L - n_1 + 1| \hat{C}$, where $\hat{C}$ means charge conjugation which exchanges $Z \leftrightarrow \bar{Z}$ and $\Psi \leftrightarrow \bar{\Psi}$.

external states increases, such task becomes tedious and the result gets lengthy obscuring possible simplifications. Nevertheless, we can easily deal with states of arbitrary length but only a few magnons. It turns out that the manipulation of the resulting expressions for these simple cases reveals a strikingly compact structure that can be easily generalizable for arbitrary complicated states. We then resort to the numerical approach in order to confirm that such generalization actually holds. In the end, we find a formula given by a very simple and natural deformation of the tree-level result (2.25), as follows

$$
C_{123} = \mathcal{C} \, \frac{\prod_{k=1}^{3} \prod_{i<j}^{N_k} \mathfrak{f}(y_i^{(k)}, y_j^{(k)})}{\prod_{i=1}^{N_1} \prod_{j=1}^{N_2} \mathfrak{f}(y_i^{(1)}, y_j^{(2)})} \prod_{k=1}^{N_1} \left[1 - (y_k^{(1)})^{L_2} \prod_{i=1}^{N_2} \left(-S(y_i^{(2)}, y_k^{(1)}) \right) \right] , \tag{2.38}
$$

where we are using the notation $y_k^{(i)} = e^{i p_k^{(i)}}$ and the normalization factor $\mathcal{C}$ is given by

$$
\mathcal{C} = \sqrt{\frac{L_1 L_2 L_3}{\mathcal{N}^{(1)} \mathcal{N}^{(2)} \mathcal{N}^{(3)}}} \left[1 + g^2 \left(N_3^2 - 1 \right) - \frac{1}{4} \sum_{i=1}^{3} \gamma_i \right] , \tag{2.39}
$$

with γ_i being the anomalous dimension of the operator $\mathcal{O}_i$. As described in the section 2.2.1, the norms $\mathcal{N}^{(i)}$ are given by the formula

$$
\mathcal{N}^{(i)} = \det_{j,k \leq N_i} \frac{\partial}{\partial p_j^{(i)}} \left[L p_k^{(i)} + \frac{1}{i} \sum_{m \neq k}^{N_i} \log S(p_m^{(i)}, p_k^{(i)}) \right] . \tag{2.40}
$$

The most important and non-trivial part of the final result is the function $\mathfrak{f}$ which reads

$$
\mathfrak{f}(s,t) = (s-t) \left[1 - \frac{g^2}{2} \left(\frac{s}{t} + \frac{t}{s} - \frac{1}{s} - s - \frac{1}{t} - t + 2 \right) \right] . \tag{2.41}
$$

The momenta $p_k^{(j)}$ of the fermionic excitations must satisfy the Bethe equations which take the form

$$
e^{i p_k^{(j)} L_j} = \prod_{i \neq k}^{N} \left(-S(p_k^{(j)}, p_i^{(j)}) \right) , \tag{2.42}
$$

and the total momentum condition (2.16).

This ends this chapter. We have computed the full one-loop structure constant for operators in $\mathfrak{su}(1|1)$ sector and expressed it as a simple factorized formula depending solely on the Bethe roots characterizing each operator. We add that these weak coupling integrability methods inspired a new non-perturbative approach to the three-point function problem in [31]. In the next chapter, we turn to an example of a strong coupling computation where integrability appears in a completely different vestment.

29

Chapter 3

Correlation functions at strong coupling

At strong coupling, the problem of computing the correlation function is that of finding the area of the minimal surface in $AdS_5 \times S^5$ that goes to the AdS boundary at the operator insertion points x_a. In this section, we compute the AdS part of the correlation function for four arbitrary heavy scalar operators inserted along a line. The method used here is inspired by the integrability techniques originally developed for the Null Polygonal Wilson loop problem [57] and later applied to the computation of three-point functions [46–49]. As in these previous applications, integrability allows one to compute the minimal AdS action without knowing the explicit classical solution. For the four point correlation function the connection with Hitchin systems and the formalism developed in [58] is used intensely. As in [46,47,57] the starting point of the method is the map of the string equations of motion in AdS to a certain auxiliary linear problem by Pohlmeyer reduction. Ultimately the solution takes the form of a set of functional equations that we call a χ-*system*. These functional equations are similar in spirit to the Y-system appearing in [57] and which naturally arise in the solutions of integrable QFT's.

For some specific BPS operators dual to strings spinning on the same great circle of S^5 the sphere contribution is well know. In this case we can construct the full strong-coupling correlation function. We emphasize that these 4-point functions are generically neither extremal nor protected. Non-protected results for correlation functions of heavy operators at strong coupling are quite rare. For example, in [46], the AdS part of the three-point function was computed. Additionally, the only complete, non-protected result that we know of are [48] where the strong-coupling three-point functions of GKP strings is computed and [49] that complemented [46] by computing the sphere part of the correlation

function.[1] Furthermore, the new non-perturbative approach of [31] opened a window of opportunity of exploring the physics of correlation functions at strong coupling.

3.1   Four point function generalities

For large 't Hooft coupling λ, the semi-classical computation of correlation functions corresponds to the evaluation of the AdS_5 and S^5 actions for classical solutions with the topology of a four punctured sphere. The boundary conditions are that the solution close to each puncture P_a, which is associated with the gauge theory operator $\mathcal{O}_a(x_a)$, approaches the AdS boundary at the point x_a in the same way as a 2-point function involving $\mathcal{O}_a(x_a)$ and some other heavy, scalar operator. In this chapter, we study the simplest case where the operators are inserted on a line in $\mathbb{R}^4$. This implies that the string solution is contained in a Euclidean AdS_2 subspace of AdS_5. Moreover, there is only one independent cross-ratio. The conformal symmetry of $\mathcal{N} = 4$ constrains the four-point correlation function to take the form

$$\langle \mathcal{O}_1(x_1)\mathcal{O}_2(x_2)\mathcal{O}_3(x_3)\mathcal{O}_4(x_4) \rangle = f(u) \prod_{a>b}^{4} (x_{ab})^{\Delta_{ab}} \,, \tag{3.1}$$

where $x_{ab} = x_a - x_b$, Δ_a is the dimension of operator $\mathcal{O}_a$, $\Delta_{ab} = \left(\sum_c \Delta_c\right)/3 - \Delta_a - \Delta_b$ and u is the conformal cross-ratio

$$u = \frac{x_{14}x_{23}}{x_{12}x_{34}} \tag{3.2}$$

Both the AdS and sphere contributions contain divergences as the string approaches the position of the operators at the boundary of AdS, which requires a cut-off $z = \mathcal{E}$. To describe the world-sheet we use complex variables $w, \bar{w}$. On the 4-punctured sphere, the physical cut-off $\mathcal{E}$ corresponds to cutting out small disks of radius ϵ_a around each puncture P_a at w_a. Ultimately, we will need to establish a precise relation between the cut-off's ϵ_a and $\mathcal{E}$. As we will review later, this is possible given the data accessible from integrability [46].

In this chapter, we will consider operators with charges scaling as $\sqrt{\lambda}$, and without spin in AdS. Following the prescription developed in [45, 46], we account for the states in the sphere by introducing an extra contribution of wave-functions. Therefore, the semi-classical

---

[1]Using the results of this chapter it may be possible to extend the results of [48] to the complete N-point functions of GKP strings at strong coupling since the mathematical problem is similar to the one treated here.
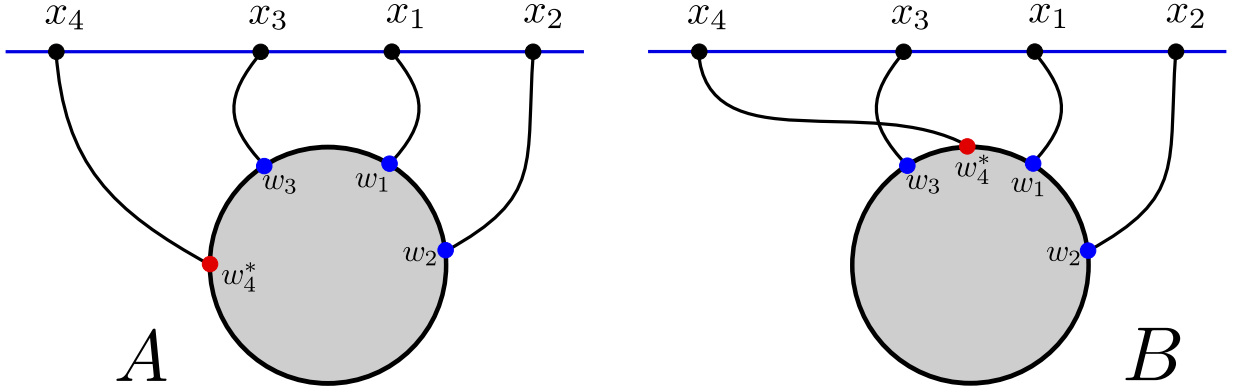
Figure 3.1: Insertions on the 4-punctured sphere. The gray ball represents the world-sheet (the complex plane plus the point at infinity, or simply 'the sphere') and the black boundary of the ball represents the equator of the sphere. The points w_a are the punctures on the sphere corresponding to the operators inserted at the positions x_a at the boundary of AdS_2, which is represented by the straight line. We fix the points w_1, w_2, w_3 and x_1, x_2, x_3 using the world-sheet and target-space conformal symmetry respectively. The position of the fourth insertion w_4 should be fixed by imposing the Virasoro constraint (i.e. the vanishing of the full stress energy tensor). Alternatively, it should correspond as well to the saddle point of the integrand of (3.3). By symmetry we expect this point to also be along the real axis, and thus we have a notion of an ordering of the 4 punctures. In particular, there is three distinct ranges for the location of w_4. Consider the ordering of the x_a shown in this figure. Depending on the parameters of the problem (that is, the charges and cross ratio), if the point is located between w_2 and w_3 (as in panel A) then the insertions will not cross and the string embedding will look schematically like the one shown in figure 3.2A. If it is located between w_3 and w_1 (as in panel B) or between w_1 and w_2 then the insertions cross each-other and we expect the string embedding to look like the one shown in figure 3.2B.

four-point function is given schematically by

$$\int d^2 w_4 \, e^{-\frac{\sqrt{\lambda}}{\pi} \int_{\Sigma \backslash \{\epsilon_a\}} \mathcal{L}_{AdS_2}} e^{-\frac{\sqrt{\lambda}}{\pi} \int_{\Sigma \backslash \{\epsilon_a\}} \mathcal{L}_{S^5}} \Psi_1 \Psi_2 \Psi_3 \Psi_4 \tag{3.3}$$

where the actions are evaluated on a classical (Euclidean) string solution approaching the boundary of AdS at the positions of the insertion points x_a.

In principle, there is an integral over all four insertion-points on the worldsheet. In (3.3) we only integrate over the insertion w_4 since the position of the other punctures can

be fixed by conformal transformations. Since we are considering the $\lambda \to \infty$ limit, one can evaluate the integral over w_4 by saddle point and the end result is the integrand of (3.3) evaluated at the dominant saddle point. Alternatively, we can use the Virasoro constraint (i.e. vanishing of the full stress energy tensor) which provides a condition on the insertion position w_4. For the case we will study, the Virasoro constraint can be straightforwardly solved as we will see.

The position of the fourth insertion turns out to have interesting consequences. There are two issues here: the positions of the operators on the boundary and the positions of the insertion points on the sphere. We can use the target-space conformal symmetry to place three of the operators at $x_1 = 1$, $x_2 = \infty$, $x_3 = -1$ and the world-sheet conformal symmetry to fix $w_1 = 1$, $w_2 = \infty$, $w_3 = -1$. The position x_4 is an input since we can put $\mathcal{O}_4$ anywhere along the line that contains $\mathcal{O}_{1,2,3}$. On the other hand, once we choose x_4 the position of the fourth puncture is fixed at $w_4 = w_4^*$ by the Virasoro constraint. By symmetry we expect it to be located on the real axis and in this case we have a notion of an ordering of the punctures. In particular, there are three possible in-equivalent orderings depending on the position of w_4. Figure 3.1 shows two of these possibilities. If the ordering of the x_a is the same as the w_a then the insertions do not cross each other, as in figure 3.1A. If the ordering of the x_a is different from that of the w_a, then the insertions will cross as in figure 3.1B. These two possibilities lead to two types of string embeddings with distinctly different properties as is shown in figure 3.2. We will see that two types of solutions arise naturally in our construction. We are able to characterize the qualitative features of the spacetime embeddings and compute the minimal AdS action of both types of solutions. We will return to this topic below.

3.2 AdS_2 Pohlmeyer reduction

In this section we briefly review the Pohlmeyer-reduction process. We begin with a discussion of the string equations of motion and the stress-energy tensor, which is the starting point of the reduction. We then introduce the function γ in terms of which the AdS Lagrangian can be written. It turns out that γ satisfies a non-linear but *scalar* equation of motion that is a modified version of the well-know sinh-Gordon equation. Next we show how the different types of string embeddings discussed in section 3.1 are encoded though the boundary conditions imposed on γ. Finally we use the function γ to write the AdS action in a form where integrability is more readily applied.
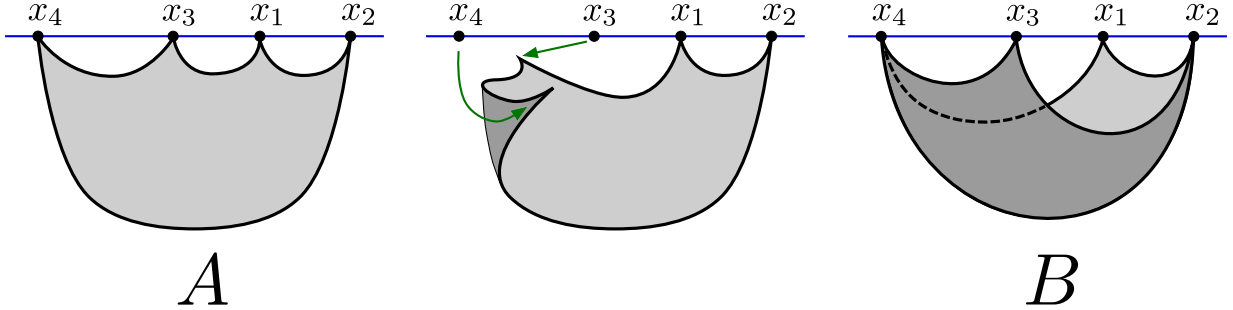
Figure 3.2: Two different possible string embeddings in AdS_2 which obey the required boundary conditions. These two solutions are shown in panels A and B. The center panel shows how to generate the configuration of panel B from that of panel A by interchanging the order in which the insertions on the sphere attach to the boundary; this interchange results in the characteristic folding shown in the embedding of panel B. These two types of solutions arise from the possibility that for a given choice of operator insertion points x_a the insertion point w_4^* (see figure 3.1) can be located in any of the three possible intervals (w_2, w_3), (w_3, w_1), (w_1, w_2).

3.2.1 Equations of motion and stress-energy tensor

Recall that we can consider (euclidean) AdS_2 as a surface in $R^{1,2}$ obeying the constraint

$$Y \cdot Y = (Y_1)^2 - (Y_2)^2 + (Y_3)^2 = -1. \tag{3.4}$$

We write the action for a string in AdS_2 as

$$S = \frac{1}{2} \int d^2\sigma \left[\partial_\alpha Y \cdot \partial^\alpha Y + \lambda \left(Y \cdot Y + 1 \right) \right] \tag{3.5}$$

and the resulting equations of motion as

$$\Box Y = \left(\partial Y \cdot \bar\partial Y \right) Y \tag{3.6}$$

The first term in the action is just the free string action in $R^{1,2}$; the second term is a Lagrange multiplier term that imposes (3.4).

The equations of motion (3.6) must be supplemented by the Virasoro constraints and boundary conditions. The Virasoro constraint requires $T_{AdS} + T_S = 0$. In particular, the AdS contribution to the stress-energy tensor does not vanish. Fortunately the boundary conditions allow us to completely fix the form of $T_{AdS} = -T_S$. Here we are interested

34
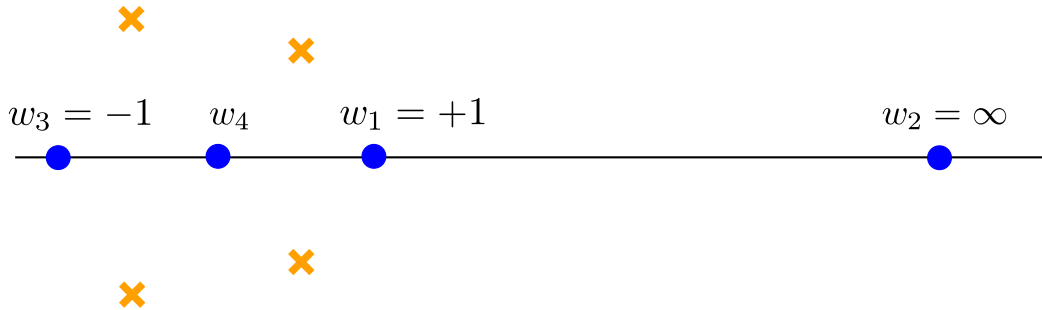
Figure 3.3: Schematic analytic structure of T. The blue dots represent the (double) poles of T at locations w_a and corresponding to the operator insertions $\mathcal{O}_a(x_a)$. The yellow crosses indicated zeros of T. We have fixed the positions of w_1, w_2 and w_3 using the world-sheet conformal symmetry. We have arbitrarily placed w_4 in the interval (w_3, w_1) although generically it can be located in any of the three intervals along the real axis.

in solutions with the topology of a four-punctured sphere where the punctures are at the position of the operator insertions and thus the boundary conditions give the behavior of the string solutions near the insertion points. The correct prescription is to demand that the string goes to the boundary at the insertion points. Furthermore, it should approach the boundary in a specific way as dictated by the vertex operators. The behavior of the solution near the boundary will be dominated by the operator inserted there, independent of the properties or number of other operators inserted at different points. This means that the behavior near the insertion points can be determined from the 2-point function, where the string solution is know explicitly. From the explicit solution for the 2-point function one finds that the desired property of the solution near insertion point w_a is [46]

$$(\partial Y)^2 \equiv T(w) \sim \frac{\Delta_a^2}{4(w - w_a)^2} \qquad (w \to w_a) \tag{3.7}$$

where $T(w)$ is the holomorphic component of T_{AdS}. The corresponding property also is required for the anti-holomorphic component $\bar{T}(\bar{w})$. Thus we know that T should be an analytic function on the (4-punctured) Riemann sphere with double-pole singularities at the punctures. This fixes T to be a specific rational function.

First consider the denominator of the rational function T. The polynomial in the denominator is determined by the positions of the insertions. Three of the insertions can be fixed by conformal symmetry, leaving one final insertion. Furthermore, one can apply the Virasoro constraint $T_{AdS} + T_S = 0$ that will fix the location of the fourth insertion point. Alternatively, we can regard the integrand of (3.3) as a function of this final insertion

35

point. In the limit $\sqrt{\lambda} \to \infty$ the integral localizes at the saddle point $w_4 = w_4^*$, thus fixing completely the denominator of T.

Now consider the numerator of T. Without loss of generality we can consider the case where there is no insertion at infinity since we can perform a transformation that maps any arbitrary point to infinity. Then the polynomial in the numerator can be at most of degree 4 (otherwise T would not be regular at infinity) and therefore it is characterized by 5 parameters. Four of these parameters are fixed by the condition (3.7). The final unfixed parameter, which we will call U, parameterizes the single cross-ratio of the four operators (recall that four points in a line have only one independent cross-ratio). The precise map between the parameter U and the cross-ratio u is quite involved but fortunately we will not need it since the cross-ratio will be encoded in the χ-system in a simple way. The analytic structure of T is shown schematically in figure 3.3. We will use this sort of figure to represent T throughout this chapter.

3.2.2 The function γ

Our objective is to evaluate the AdS part of the string action. In Poincaré coordinates the on-shell action becomes[2]

$$\partial Y \cdot \bar{\partial} Y = \frac{\partial x \bar{\partial} x + \partial z \bar{\partial} z}{z^2} = \sqrt{T\bar{T}} \cosh \gamma \qquad (3.9)$$

where the above formula defines the function $\gamma(w, \bar{w})$. It follows from the equations of motion that γ satisfies the modified sinh-Gordon equation

$$\partial \bar{\partial} \gamma = \sqrt{T\bar{T}} \sinh \gamma. \qquad (3.10)$$

It is well known that this equation is classically integrable, and in what follows we exploit this integrability to compute the AdS action.

Now let us determine what boundary conditions should be imposed on γ. For the 2-point function $\gamma = 0$. Recall that the string solution should approach that of the 2-point function as the string approaches the boundary at the operator insertion points x_a. Therefore we should require that $\gamma \to 0$ as $w \to w_a$ [46]. Furthermore, in order to have

---

[2]The AdS_2 Poincaré coordinates are given by

$$Y^1 = -\frac{1}{2z}\left(1 - x^2 - z^2\right), \quad Y^2 = \frac{1}{2z}\left(1 + x^2 + z^2\right), \quad Y^3 = \frac{x}{z}. \qquad (3.8)$$

a non-singular world-sheet metric the right-hand side of (3.9) should never vanish. Thus when T has a zero γ must have a logarithmic singularity to cancel it. In summary, the boundary conditions on γ are

$$\gamma \quad \rightarrow \quad \pm\frac{1}{2}\log T\bar{T} \quad (w \rightarrow z_a) \tag{3.11}$$

$$\gamma \quad \rightarrow \quad 0 \quad\quad\quad\quad (w \rightarrow w_a) \tag{3.12}$$

where z_a denotes a zero of T and w_a a pole of T. Notice that the regularity of the world-sheet metric does not fix the sign of the logarithmic 'spike' in (3.11) and, in principle, different choices are possible at each zero (recall that generically T will have 4 zeros for the 4-point function, as follows from the discussion of the previous section). These different choices correspond to different string solutions having differing properties, and generically different total action. We will refer to the spikes with the $+$ $(-)$ sign as u-spikes (d-spikes). We will now describe how the choice of these signs is related to the string embeddings shown in figure 3.2.

3.2.3 Spikes, fold-lines and string embeddings

As mentioned in the previous section there are 4 zeros of T and at each zero we have a $\mathbb{Z}_2$ ambiguity (see equation (3.11)) in the choice of spikes of γ. A priori there are 2^4 different choices for the spikes. However, it turns out that there are only 2 distinct choices that correspond to target-space solutions with the desired properties. These two possibilities are shown in figure 3.4. A discussion of why these are the only two possible choices is given in appendix C.[3] These two different possibilities correspond precisely to the two different possible string solutions shown in figure 3.2. The key ingredient in making this correspondence is the observation that contours on the world-sheet where $\gamma = 0$ correspond to fold-lines in the string embedding (see appendix C). The location of these contours is directly connected with the choice of spikes. For example, between a u-spike and a d-spike we know that there must be at least one such contour. In figure 3.4 the $\gamma = 0$ contours are indicated by the black curves. In appendix C we discuss in detail how the structure of these contours is inferred from the choice of spikes.

Let us describe in more detail how we relate the two spike configurations in figure 3.4 to the two string embeddings in figure 3.2. As mentioned above, the key ingredient is to study the fold lines in the two figures. First consider the target-space solution. In figure

---

[3]The main ideas are: first, configurations related by $\gamma \rightarrow -\gamma$ are not distinct since this is a symmetry of (3.10), and second, one should choose the spikes such that $\gamma \rightarrow -\gamma$ under reflection about the real axis. See appendix C.
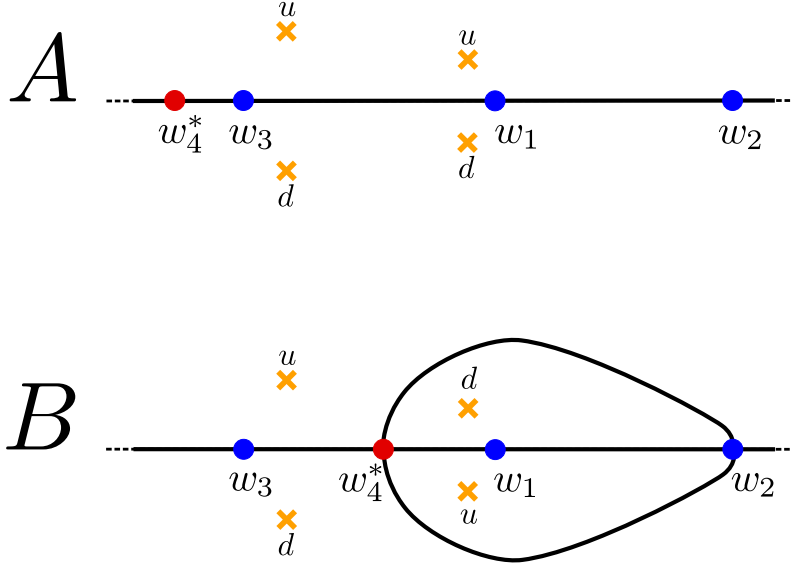
Figure 3.4: Contours where $\gamma = 0$ based on the choice of signs in equation (3.11). These contours are shown schematically by the black curves. The label u (d) at a zero indicates the choice of sign $+$ $(-)$ in equation (3.11). We give a detailed discussion of why these are the only possible structures for these contours in appendix C. The key in relating these figures to the embeddings in figure 3.2 is that contours on the world-sheet where $\gamma = 0$ map onto folds of the embedding.

3.2A it is clear that there is a single fold-line that runs through each of the punctures in sequence. That is, there is a fold-line directly connecting x_4 with x_3 then x_3 with x_1, etc. This is in agreement with the fold-structure implied by figure 3.4A since for this choice of spikes we can deduce that there is a single contour where $\gamma = 0$ running along the real axis connecting w_4 to w_3 then w_3 to w_1, etc. Thus the spike configuration of figure 3.4 describes a string embedding of the type shown in figure 3.2A.

Now consider the folds of the embedding shown in figure 3.2B. Insertions x_1 and x_3 are both connected by fold lines directly to the insertions x_2 and x_4. Furthermore, x_2 and x_4 are connected to each other by *two* fold-lines. This is because this configuration is double-folded along that line, as one can see from the construction shown in the center panel of figure 3.2. All of this is in perfect agreement with the fold-structure implied by figure 3.4B. In particular, for this choice of spikes both w_1 and w_3 are directly connected to w_2 and w_4^* by contours where $\gamma = 0$. Moreover, w_2 and w_4^* are connected by *two* contours where $\gamma = 0$, precisely corresponding to the double-fold line connecting x_2 and x_4 in figure

3.2B.

Let us comment on a subtle point regarding figure 3.4. Note that we have placed w_4^* in different intervals in the two figures. On one hand, we should do this in order to be in agreement with figures 3.1 and 3.2. However, as we will see, given a cross-ratio u and the insertion position w_4^*, the fold structure is fixed. So, to compare two different fold structures for a given cross ratio we are forced to consider w_4^* in different intervals. This is in perfect agreement with the intuitive perspective of figures 3.1 and 3.2. We will return to this point in section 3.5.2.

3.2.4 The action as a wedge product

We will now return to the computation of the minimal AdS action (see equation (3.3)). Explicitly, the quantity we want to evaluate is

$$-\frac{\sqrt{\lambda}}{\pi} \int_{\Sigma \backslash \{\epsilon_a\}} \frac{\partial x \bar{\partial} x + \partial z \bar{\partial} z}{z^2} \tag{3.13}$$

where $\Sigma \backslash \{\epsilon_a\}$ denotes the sphere with small disks of radius ϵ_a cut out at each puncture. These cut-offs are not independent and are all fixed in terms of the single target-space cut-off $z = \mathcal{E}$; this is important in recovering the spacetime dependence of the correlation function and we will return to this point below [46]. It is convenient to separate the action into a piece that is independent of the cut-offs, and a piece where the dependence can be explicitly evaluated. This can be done because the solution near the punctures is know. In particular, we may write [46, 57]

$$\mathcal{A} = -\frac{\sqrt{\lambda}}{\pi} \int_{\Sigma} \sqrt{T\bar{T}} \left(\cosh \gamma - 1\right) - \frac{\sqrt{\lambda}}{\pi} \int_{\Sigma \backslash \{\epsilon_a\}} \sqrt{T\bar{T}} \tag{3.14}$$

To extend the integration to the full sphere in the first term we have used the fact that the action (3.9) goes like $\sqrt{T\bar{T}}$ near the punctures as follows from (3.12). We will refer to the first and second term in (3.14) as A_{fin} and A_{div} respectively. Since T is known A_{div} can be evaluated explicitly in terms of the ϵ_a, but to eliminate the ϵ_a in terms of $\mathcal{E}$ requires detailed information about the string solution itself. Fortunately, the tools necessary for computing A_{fin} will also provide the necessary information to complete the calculation of A_{div}. Thus, let us focus for the time being on the computation of A_{fin} and return to A_{div} afterwards.

We would like to write A_{fin} in a form where the integrability of (3.10) is more readily

usable. Following [46, 57] we introduce the forms

$$\omega = \sqrt{T} dw \tag{3.15}$$

$$\eta = \frac{1}{2} \sqrt{\bar{T}} \left(\cosh \gamma - 1 \right) d\bar{w} + \frac{1}{4} \frac{1}{\sqrt{T}} \left(\partial \gamma \right)^2 dw \tag{3.16}$$

and then from a direct computation it follows that

$$A_{fin} = \frac{i}{2} \int_{\widetilde{\Sigma}} \omega \wedge \eta \tag{3.17}$$

where $\widetilde{\Sigma}$ denotes the double cover of the sphere defined by $y^2 = T(w)$. Extending the integration from Σ to $\widetilde{\Sigma}$ simply involves a factor of 2 since each form is odd under sheet-exchange. An important property of these forms is that they are both closed. The form ω is clearly closed since it is holomorphic, and the closure of η follows from the equations of motion for γ. Notice that (3.17) would be true for any choice of the dw component of η. The specific coefficient appearing in (3.16) is necessary for the closure of the form.

Now we would like to apply the Riemann bilinear identity (RBI) to reduce (3.17) to one-dimensional integrals over cycles on $\widetilde{\Sigma}$. There are two caveats in doing this – the singularities in ω and the singularities in η. These issues where resolved in [46], and we follow the approach used there (see [46] for a more detailed treatment and also [47] for a different approach). The basic idea of the RBI is to write one of the forms of the wedge product as an exact form, $\omega = dF$ where $F = \int_{P_0}^{P} \omega$, which is always possible on a Riemann surface minus some contour, L. In the present case ω has single poles and thus F will have logarithmic cuts which need to be accounted for. A way to side-step this complication is to spread the single poles in ω into a small square-root cuts such that F has only square-root cuts and no singularities. The cost of doing this is that the genus of $\widetilde{\Sigma}$ increases, but the upside is that the application of the RBI is simplified. This takes care of the singularities in ω. Now consider the form η which behaves as $\eta \sim (w - z_a)^{-5/2}$ near the zeros of T. The prescription of [46] is to remove the points z_a from the domain by taking L to be the sum of the standard contour for a Riemann surface of genus g and small contours C_a encircling the points z_a. The integrand of (3.17) can then be written as $d\left(F\eta\right)$ (since $d\eta = 0$ on the domain) and then Stokes theorem can be used to reduce the surface integral to a line integral over the usual boundary of the genus g Riemann surface and the contours C_a. The end result is that each boundary C_a contributes a correction of $\pi/12$ to A_{fin} in (3.17) while the integral over the boundary of $\widetilde{\Sigma}$ gives the usual sum over cycles on $\widetilde{\Sigma}$ and thus we have [46]

$$A_{fin} = (\text{number of zeros}) \frac{\pi}{12} - \frac{i}{2} \left(\oint_{\gamma_a} \omega \right) I_{ab}^{-1} \left(\oint_{\gamma_b} \eta \right) \tag{3.18}$$

40

where $\{\gamma_a\}$ is a complete basis of cycles on $\widetilde{\Sigma}$ and I_{ab} is their intersection matrix. For the four-point function there is generically 4 zeros and 4 poles. When we spread the four poles we introduce an additional 4 cuts and thus the surface is genus 5 and there will be 5 a-cycles and 5 b-cycles; that is $\{\gamma_a\} = \{\gamma_{a_1}, \gamma_{b_1}, \gamma_{a_2}, ..., \gamma_{a_5}, \gamma_{b_5}\}$. The main point is that we have reduced the computation of the surface integral (3.17) into a sum of 1-dimensional cycle integrals of a closed form. Such integrals are precisely what integrability is good at computing. In the following section we will see how to compute the cycles $\oint_{\gamma_a} \eta$ by exploiting the integrability of (3.10).

3.3   The linear problem

To compute the η-cycles appearing in (3.18) it is useful to consider the linear problem associated with equation (3.10). Consider a function ψ obeying

$$(\partial + J_w)\,\psi = 0, \qquad (\bar{\partial} + J_{\bar{w}})\,\psi = 0 \tag{3.19}$$

where the components of the connection $J = J_w dw + J_{\bar{w}} d\bar{w}$ are given by

$$J_w = A_w + \frac{1}{\xi}\Phi_w, \qquad J_{\bar{w}} = A_{\bar{w}} + \xi\Phi_{\bar{w}} \tag{3.20}$$

where A and Φ are independent of the spectral parameter ξ and given in terms of γ and $T, \bar{T}$. We give the explicit forms of A and Φ in appendix B. Note that we will frequently write the spectral parameter as $\xi = e^\theta$.

Compatibility of equations (3.19) for all ξ is equivalent to the flatness of J, which is satisfied if γ obeys the equation of motion (3.10) and T ($\bar{T}$) is purely holomorphic (anti-holomorphic). In the following section we will discuss the relation between the solutions of the (3.19) and the η-cycles appearing in (3.18).

3.3.1   Basic properties

There are a few aspects of the linear problem which will be essential for the following analysis. Let us comment on each of them in turn.

- *Solutions near punctures.* Using (3.7) and (3.12) one can show that near the punctures P_a there are two linear-independent solutions of the form (see Appendix B)

$$\hat{\psi}^{\pm}(w) \;\equiv\; \left(T/\bar{T}\right)^{1/8} e^{\pm \frac{1}{2}\int^w \xi^{-1}\omega + \xi\bar{\omega}}|\pm\rangle \tag{3.21}$$

$$\sim\; (w - w_a)^{\pm\frac{1}{4}\Delta_a\xi^{-1}-\frac{1}{4}}\left(\bar{w} - \bar{w}_a\right)^{\pm\frac{1}{4}\bar{\Delta}_a\xi+\frac{1}{4}}|\pm\rangle \tag{3.22}$$

41

where $|\pm\rangle$ are the eigenvectors of σ^3. Notice that there is a solution that is exponentially big and one that is exponentially small as one approaches the puncture P_a.[4]

- *'Small' solutions.* Demanding that a function is both a solution of the linear problem and also small at some puncture P uniquely defines that solution (up to overall normalization). Thus there is a family of 'small' solutions s_a each of which is small at puncture P_a. On the other hand, specifying that a solution has the big asymptotic near P does not uniquely determine the solution since one could create another solution obeying the same boundary conditions by adding an arbitrary multiple of s_P.

- $\mathbb{Z}_2$ *symmetry and 'big' solutions.* Even though one cannot uniquely specify a solution by demanding that it has the big asymptotic near P, there is nevertheless a special solution big near P that is uniquely defined. This follows from the $\mathbb{Z}_2$ symmetry of the connection (3.20) which is given by

$$U J(\xi) U^{-1} = J(e^{i\pi}\xi) \tag{3.23}$$

where $U = i\sigma^3$. This symmetry implies that if $s_P(\xi)$ (we are suppressing the w, $\bar{w}$ dependence) is the solution to (3.19) small at P then

$$\tilde{s}_P \equiv \sigma^3 s_P(e^{-i\pi}\xi) \tag{3.24}$$

is another solution of the linear problem. Moreover, from (3.21) it follows that $\tilde{s}_P$ is *big* at P. Thus we have a second uniquely defined family of solutions $\tilde{s}_a$, each of which is big at puncture P_a.

- *Products of solutions.* Given two solutions of the linear problem ψ_1 and ψ_2, there is a natural SL_2 invariant inner product

$$(\psi_1 \wedge \psi_2) \equiv \mathrm{Det}\left[\{\psi_1, \psi_2\}\right] \tag{3.25}$$

This inner product is equivalent to the Wronskian of the two solutions. Important properties of this Wronskian are that it is independent of w and $\bar{w}$, and thus only depends on the spectral parameter ξ. Further, the product will vanish if the two solutions are linearly *dependent*.

---

[4]In going from (3.21) and (3.22) we have been careless about the branches of ω. In particular, we may choose a particular branch at some P_a such that the near-puncture solutions take the form (3.22) but then if we smoothly continue $\sqrt{T}$ to some other puncture P_b it is possible that the small and big solutions correspond to the opposite components from the small and big solutions at P_a. This will be very important below, since it will usually be the case in the construction we will use.

Now that we have introduced these basic facts of the linear problem, we can state what is perhaps the key ingredient in the whole computation.[5] We claim that the $\xi \to 0$ expansion of the inner product of two small solutions is the following [46, 57]

$$(s_a \wedge s_b) \sim \exp\left[\frac{1}{2}\xi^{-1}\varpi_{ab} + \frac{1}{2}\xi\bar{\varpi}_{ab} + \xi \int_a^b \eta + \mathcal{O}\left(\xi^2\right)\right] \tag{3.26}$$

where η is precisely the same form (3.16) that appears in the action formula (3.18) and ϖ_{ab}, $\bar{\varpi}_{ab}$ are explicitly known in terms of integrals of ω and $\bar{\omega}$.[6] A derivation of (3.26) is given in appendix B.4. The point is that by computing the inner products $(s_a \wedge s_b)(\xi)$ we can extract the "puncture-puncture" integrals $\int_a^b \eta$ by extracting the $\mathcal{O}(\xi)$ coefficient of this inner product. All of the η-cycles appearing in (3.18) can be written in terms of linear combinations of these puncture-puncture integrals. Thus, we can compute area (3.18) by computing the inner products $(s_a \wedge s_b)$. The rest of this section is devoted to explaining how we compute such inner products using techniques from integrability.

3.3.2 Defining solutions globally

Let us now comment on how to globally define the small solutions. Suppose that we want to construct the small solution s_P away from puncture P, say at some generic point A. To do this we need to use the connection to transport the solution along some path from the neighbourhood of P to the point A. However, it is clear from (3.21) that the solutions of the linear problem have non-trivial monodromies around the punctures and therefore homotopically different paths on the 4-punctured sphere will result in different values of the small solution at A. In other words, solutions of the linear problem live on a (generically infinite-sheeted) Riemann surface with branch points at the punctures. For the purposes of calculating it is convenient to fix some conventions for dealing with the multivaluedness of the solutions. We first define the sheets by cutting the Riemann surface as shown in figure 3.5. The cuts all join at a common point and the monodromy about that point is the identity since a path passing through all the cuts is contractable on the sphere. We then define the value of the small solution associated with puncture P at some point A as follows. Draw any curve from the neighbourhood of P to A. In the neighbourhood of P one starts with s_P. For every time the path crosses a cut emanating from some puncture

---

[5]To our knowledge the following fact first appear in [57]. Later it was used in [46,47] for 3-point function computations. We give a derivation in appendix B.4; A different derivation appears in [47].

[6]To be more precise, this expansion will be true for certain s_a and s_b depending on certain conditions stemming from the form of T and also depending on the value of $\text{Arg}(\xi)$. Furthermore, the contour of integration will be precisely defined by these conditions. We will discuss these conditions in detail below.

$$(M_3 s_4)|_A = (M_2^{-1} M_1^{-1} M_4^{-1} s_4)|_A$$
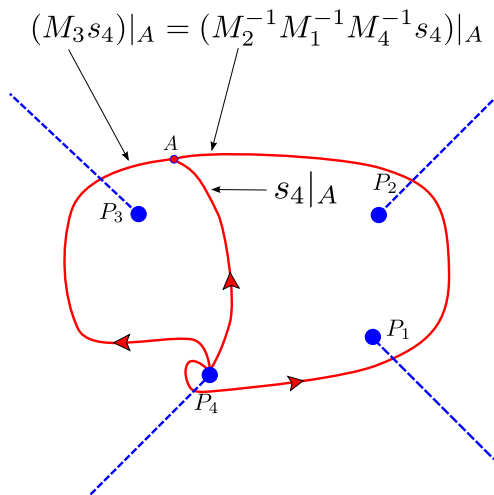
Figure 3.5: Our conventions for defining the solutions globally. The dashed blue lines emanating from the punctures indicate the conventions for 'cutting' the full Riemann surface, thus defining the sheets. The red lines indicate the parallel transport of a solution from P_4 to the point A along three paths. Two of the paths are homotopically equivalent due to the triviality of the total monodromy $M_4 M_3 M_2 M_1 = 1$ (which follows from the fact that any path encircling all the punctures with the same orientation is contractable on the sphere). The third path is homotopically distinct from the other two, and thus the value of the solution at A will differ by monodromy factors.

Q in the *clockwise* (*counterclockwise*) sense attach a factor M_Q (M_Q^{-1}).[7] In this way, if we transport along a path that is homotopically equivalent to a path that does not cross any cuts then the small solution at A will be $s_P|_A$. If the path crosses the cut emanating from puncture Q once in the clockwise sense, then the value of the small solution at A will be $(M_Q s_P)|_A$, and so on (see figure 3.5). In the case when s_P is transported around the puncture P one can see from the explicit form (3.21) of s_P near P that the result will be multiplication by a constant. That is

$$M_P s_P = \mu_P s_P \tag{3.27}$$
$$M_P \tilde{s}_P = \tilde{\mu}_P \tilde{s}_P \tag{3.28}$$

---

[7]Note that the result of a monodromy can be expressed as the linear map M since both s and Ms are solutions of the linear problem. Therefore they can both be expanded in terms of two linearly independent solutions of the linear problem, and thus they are related to each other simply by a linear map, or in other words simply by multiplication by some matrix, M.

so that s_P and $\tilde{s}_P$ are eigenvectors of M_P with eigenvalues μ_P and $\tilde{\mu}_P = 1/\mu_P$ respectively. One cannot repeat such an analysis to evaluate $M_Q s_P$ since generically one does not know the explicit form of s_P in the neighbourhood of Q.

3.3.3 WKB approximation and WKB Curves

As we will discuss shortly, it will be essential to have control over the $\xi \to 0, \infty$ asymptotics of the inner products $(s_P \wedge s_Q)(\xi)$. It is clear from $(3.19) - (3.20)$ that these are both singular limits, and the basic idea of extracting this singularity – which is called the *WKB approximation* – is as follows.[8] As discussed above, we have good control over the solutions in the neighbourhood of the punctures. Thus we would like to study, in the limits $\xi \to 0, \infty$, the transport of small s_P along a curve $w(t)$ which connects a neighbourhood of a puncture P with a neighbourhood of another puncture Q. Let us consider the transport away from P (see figure 3.6). We will discuss the $\xi \to 0$ limit since the $\xi \to \infty$ limit is similar.
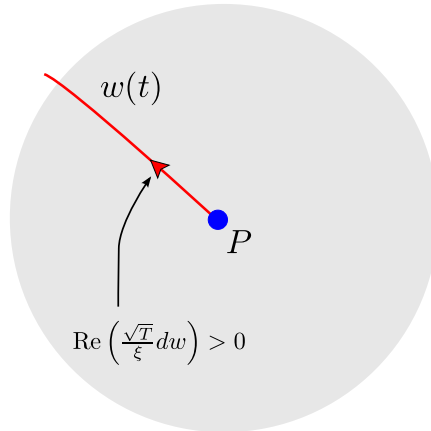
Figure 3.6: Transporting s_P away from P along $w(t)$. We have chosen the branch of Φ in (3.29) such that $s_P \propto |+\rangle$ near w_P. In other words, we have chosen the branch of Φ such that $\mathrm{Re}\left(\langle +| - \Phi_w/\xi dw|+\rangle\right) = \mathrm{Re}\left(dw\sqrt{T}/\xi\right) > 0$ for dw pointing along $w(t)$ *away* from P and thus $\exp\left(\int_{w'_P}^{w(t)} dw\sqrt{T}/\xi\right)$ is exponentially diverging as $\xi \to 0$.

At any point in Σ the matrix Φ has the two eigenvalues $\mp\omega/2 = \mp\sqrt{T}/2\,dw$ (which are

---

[8]See appendix B.4 or [58] for a more detailed treatment.

single valued on the double cover $\widetilde{\Sigma}$), and thus we can choose a gauge along $w(t)$ where Φ is diagonal and given by

$$\Phi = \frac{1}{2} \begin{pmatrix} -\omega & 0 \\ 0 & \omega \end{pmatrix} = \frac{1}{2} \begin{pmatrix} -\sqrt{T}dw & 0 \\ 0 & \sqrt{T}dw \end{pmatrix} \tag{3.29}$$

In the limit $\xi \to 0$ some component of Φ/ξ will dominate and thus the leading contribution to s_a at some point w along $w(t)$ will be given by

$$e^{-\int_{w'_a}^{w} \Phi/\xi} |\sigma\rangle \tag{3.30}$$

where the value of $\sigma = \pm$ depends on the branch of Φ we have chosen (recall that $|\pm\rangle$ are the eigenvectors of σ^3). This is the singular contribution in the limit $\xi \to 0$ for the same reason that it is the small solution – namely, because

$$\mathrm{Re}\left(\langle\sigma|\left(-\Phi/\xi\right)|\sigma\rangle\right) > 0 \tag{3.31}$$

along a path traveling *away* from P_a. The basic statement of the WKB approximation is that so long as we transport along paths such that (3.31) is true along the whole path then the leading contribution to s_P in the $\xi \to 0$ limit is indeed given by (3.30). In other words, as long as we transport along curves satisfying (3.31) everywhere, then we can reliably extract the singularity as $\xi \to 0$ as it is simply given by (3.30). The curves along which (3.31) is satisfied most strongly are those for which

$$\mathrm{Im}\left(\langle\sigma|\left(-\Phi/\xi\right)|\sigma\rangle\right) = 0 \tag{3.32}$$

Curves satisfying this condition are called *WKB curves*. If we transport along some curve satisfying (3.32) for $\mathrm{Arg}\,(\xi) = \phi$, then the condition (3.31) will be satisfied for $\mathrm{Arg}\,(\xi) \in (\phi - \pi/2, \phi + \pi/2)$. In fact, we will need to control the asymptotics of s_P in precisely such a wedge of the ξ-plane, and thus we should always transport along WKB lines. We will give the a very brief overview of the properties of these lines in the next subsection. For a detailed treatment see [58].

3.3.4 WKB triangulation

As we discussed in section 3.3.2 we define the solutions of (3.19) globally by transporting along specific paths. Transport of solutions along homotopically equivalent paths will lead to the same result, whereas transport along homotopically inequivalent paths generically will give different results. For this reason it is useful to set up a system of fiducial paths

| A: generic point | B: pole | C: zero |
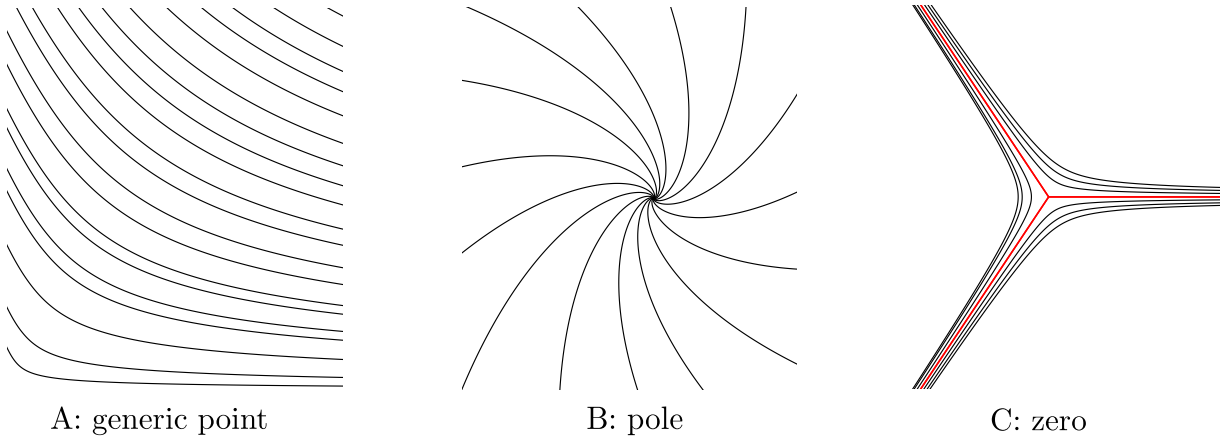
Figure 3.7: Local structure of WKB lines in the neighbourhood of, A: a generic point; B: a double pole of T; C: a simple zero of T. In the case of a generic point the WKB curves form continuous non-intersecting lines. In the case of a singular point they form logarithmic spirals for generic values of $\mathrm{Arg}(\xi)$. The exact nature of these spirals will not be important. What is important is that the singular points act as sources/sinks of WKB curves. In the case of a zero, there are three special WKB curves that asymptote to the zero which are the red curves in panel C. These special curves, called separating curves, determine the global structure of the WKB foliation.

between the punctures which we will use to globally define the solutions. Because we will need to control the large/small ξ asymptotics of the Wronskians, it is best to choose these paths to be WKB curves – i.e. curves satisfying (3.32).

We will first consider the local structure of WKB curves. In the neighbourhood of a generic point on the punctured sphere the WKB curves are smooth and non-intersecting (see figure 3.7A). In the neighbourhood of a (double) pole of T the WKB curves follow logarithmic spirals that asymptote to the singular point (see figure 3.7B). All that will be important here is that the poles act as sources/sinks of WKB curves but the exact nature of these spirals will not be important. Finally, working in the neighbourhood of a simple zero of T one can show that there are three special WKB curves that asymptote to the zero and which govern the WKB lines near the zero (see figure 3.7C).

Now consider the global structure of the WKB curves. All WKB curves fall into one of the following types [58]

- *Generic WKB curves* which are those that asymptote in both directions to a pole of

47
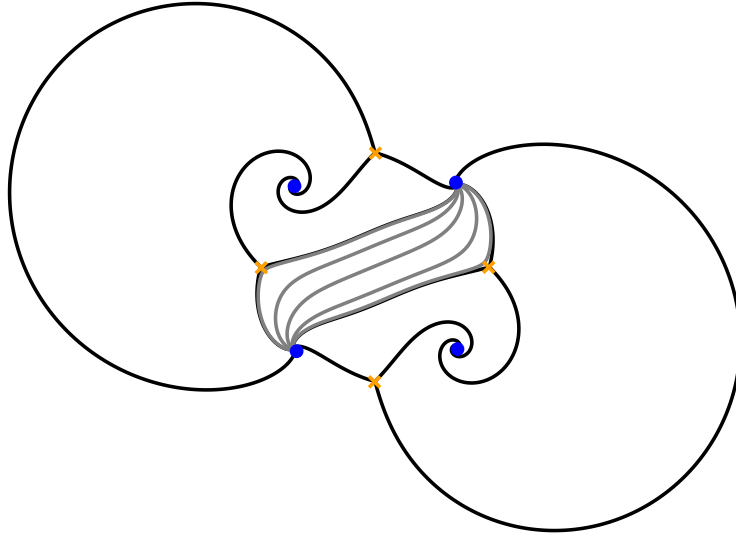
Figure 3.8: Global WKB structure for an example with 4 punctures. The separating curves are shown in black. In one cell we show several examples of homotopically equivalent curves (shown in gray) that sweep the cell. Each cell defined by the separating curves has a 1-parameter family of such curves. By choosing a representative curve from each family we obtain the triangulation shown in figure 3.9. Notice that near each puncture (the blue dots) we see the spiral structure shown in panel B of figure 3.7 and near each zero (yellow ×) we see the local structure shown in panel C of figure 3.7.

T (potentially the same one);

- *Separating WKB curves* which asymptote to a zero of T in one direction and to a pole of T in the other;

- *Finite WKB curves* which are closed or asymptote in both directions to a zero of T (potentially the same one).

We will now describe how we use the WKB curves to set up a system of fiducial paths, or more specifically, a *triangulation*. By triangulation we mean a triangulation of the punctured sphere with all vertices at the punctures and at least one edge incident on each vertex. Consider fixed T and $\text{Arg}(\xi)$ such that there are no finite WKB curves (this can always be done since such curves only appear at special, discrete values of $\text{Arg}(\xi)$). First draw all of the separating WKB curves – there will be $3N_Z$ of these, where N_Z is the number of zeros of T (since for the moment we are not allowing finite WKB curves). These
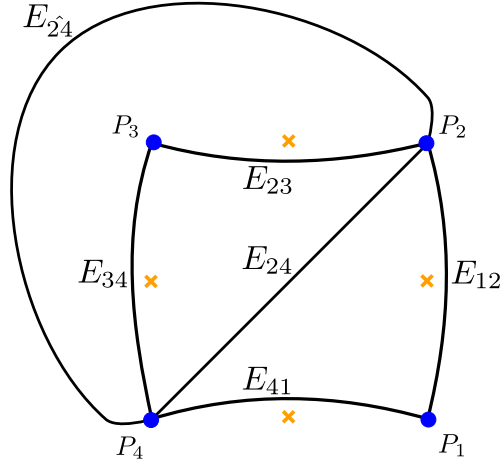
Figure 3.9: The WKB triangulation of the 4-punctured sphere following from the WKB foliation shown in figure 3.8. Each edge E_{ab} of the triangulation is a representative from one of the families of homotopotically equivalent lines in each cell of figure 3.8. This triangulation will be of central interest in the 4-point function computation.

curves will divide the punctured sphere up into cells with each cell defining a family of homotopically equivalent *generic* WKB curves as shown in figure 3.8 for an example of the 4-punctured sphere. To construct the triangulation, choose a representative curve from each cell, e.g. any one of the silver curves shown in figure 3.8. The claim is that the collection of these representative curves, which we will call *edges*, gives the desired triangulation [58].[9] As a concrete example, the triangulation associated with the cell-construction of figure 3.8 is shown in figure 3.9. This same triangulation will play an important role in the 4-point function computation below.

We have now finished the discussion of how to construct the WKB triangulation for a given T and $\mathrm{Arg}\,(\xi)$. Before moving on the the next section let us discuss one final point. In the following it will be useful to lift edges of the triangulation to the double cover $\widetilde{\Sigma}$ and to endow the lifted edges with an orientation. Recall that $\omega = \sqrt{T}dw$ is a single valued form on $\widetilde{\Sigma}$. Let ∂_t be a tangent vector of the lifted edge E at a point on $\widetilde{\Sigma}$. There are of course two possible orientations for ∂_t. Note that by virtue of (3.32) we have $e^{-i\phi}\omega \cdot \partial_t \in \mathbb{R}$. We define the orientation of the lifted edge E by the condition $e^{-i\phi}\omega \cdot \partial_t > 0$. Notice that

---

[9]To see this in general consider a single zero of T as shown in figure 3.7. The zero is on the boundary of three cells. Choosing edges from the family of curves in each cell we see that they form a triangle. Thus the edges form a triangulation of the punctured sphere with each triangle containing a zero of T.
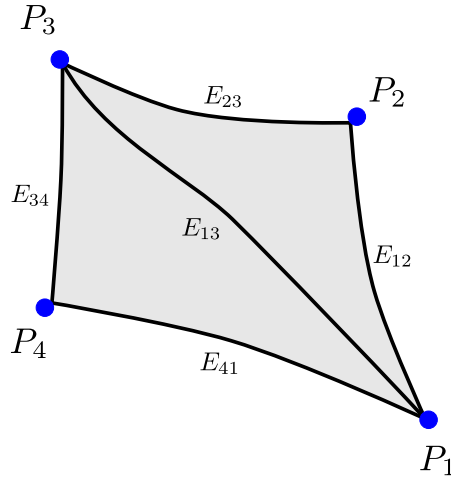
Figure 3.10: The two triangles sharing the edge E_{13}. These two triangles define the quadrilateral $Q_{E_{13}}$, which is shown in gray shading. Each blue dot represents a puncture, which are the vertices of the triangulation and each black line and is an edge.

each edge on the punctured sphere will lift to two edges – one on each sheet of $\widetilde{\Sigma}$ and that these two edges will have opposite relative orientation. Picking a particular orientation of some edge is equivalent to picking a particular sheet of $\widetilde{\Sigma}$.

3.3.5 Coordinates

From the WKB triangulation we will now construct the so-called Fock-Goncharov coordinates [58]. These are natural objects to work with because they are gauge invariant and independent of the normalization of the small solutions. From the coordinates we will be able to extract the η-cycles that we need to compute the action (3.18).

Consider some edge E of the triangulation. This edge is shared by precisely two triangles, and these triangles form the quadrilateral Q_E (see figure 3.10). Number the vertices of Q_E as shown in figure 3.10 with E going between P_1 and P_3. As we mentioned in section 3.3.1, associated with each puncture P_a there is a small solution s_a. The solutions cannot be made globally smooth and single valued on the punctured sphere due to the monodromy around each puncture. However, we can define them such that they are single valued and
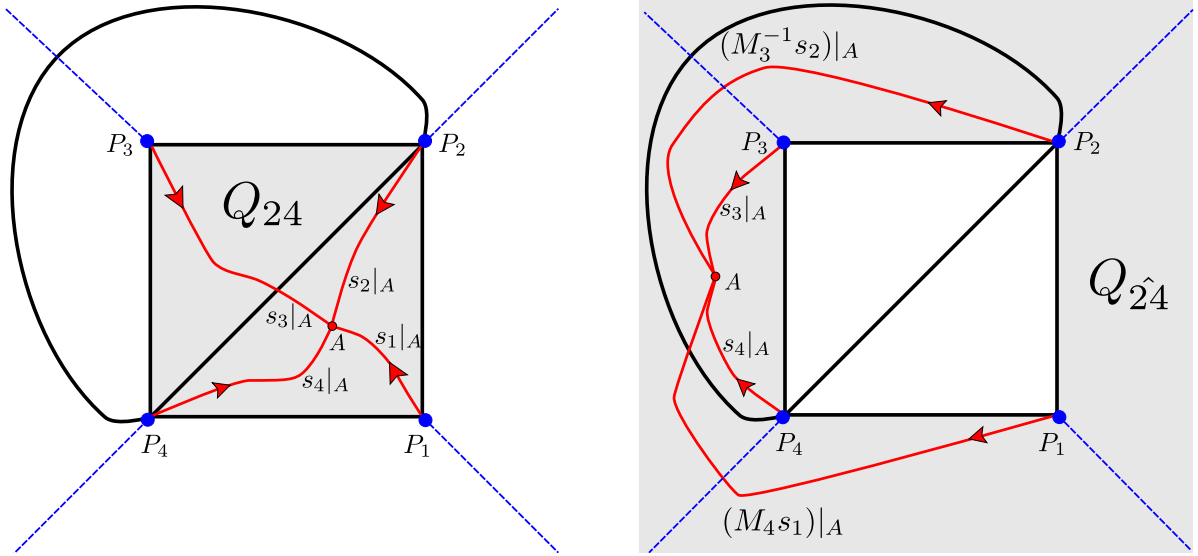
Figure 3.11: Here we show how to construct the coordinates χ_{24} (left panel) and $\chi_{\hat{2}4}$ (right panel) of the triangulation of figure 3.9. The gray shaded regions represent Q_{24} and $Q_{\hat{2}4}$ respectively. These figures should be pictured on the sphere. The dashed blue lines emanating from the punctures indicate our conventions for defining the sheets of the small solutions as explained in section 3.3.2. The red lines indicate how we globally define the solutions s_a by transporting away from P_a using the connection. We use paths that never leave the quadrilateral such that the solutions used to form the coordinates are guaranteed to be single-valued and smooth throughout the quadrilateral, as required.

smooth throughout Q_E.[10] We then define the Fock-Goncharov coordinate as [58]

$$\chi_E = (-1)\frac{(s_1 \wedge s_2)(s_3 \wedge s_4)}{(s_2 \wedge s_3)(s_4 \wedge s_1)} \tag{3.33}$$

where all the s_a are evaluated at a common point in Q_E.

As a concrete example consider the triangulation of the 4-punctured sphere shown in figure 3.9. In figure 3.11 we show how to apply the procedure just described to construct the coordinates corresponding to edges E_{24} and $E_{\hat{2}4}$. Consider first the left panel of 3.11. We define each solution s_a throughout Q_{24} by parallel transporting from each P_a where the explicit form of the solutions is known – see (3.21). The red lines indicate the parallel

---

[10]We will show this in some concrete examples momentarily.

51
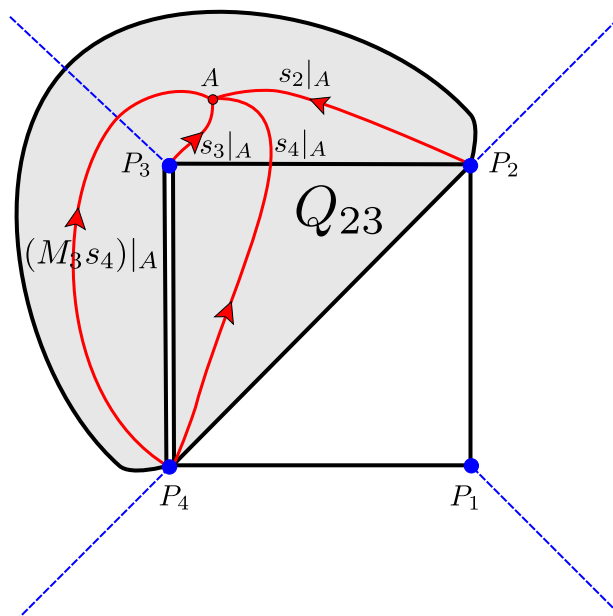
Figure 3.12: Here we describe the construction of the coordinate for the slightly degenerate case where the coordinate corresponds to an edge ending at a vertex that has only two incident edges (e.g. P_2 has only 2 incident edges: E_{12} and E_{23}). We construct the coordinate for edge E_{23} of the triangulation shown in figure 3.9. The quadrilateral prescription described above still applies, but one must take care to correctly define Q_E and the solutions inside Q_E. First of all, in order to have single-valued and smooth solutions throughout Q_{23} we must exclude a region between P_3 and P_4. Otherwise Q_{23} would contain P_3 and thus the solutions could not be single valued in Q_{23} (there would be a monodromy around P_3). Since the boundaries of the quadrilateral must be edges of the triangulation, the only choice is to remove a thin region running along edge E_{34} and then to treat the two 'sides' of E_{34} as different edges. In the figure we have represented this process by showing E_{34} as doubled and with the region between the new edges excluded from Q_{23}. We then define the solutions throughout Q_{23} in the same way as described in figure 3.11, by analytically continuing the solutions along paths from P_a to A that stay within Q_{23} which is represented as the shaded region. Once we have defined the solutions at a common point we form the coordinate χ_{23} given in equation (3.35).

transport of each s_a from P_a to a common point A; clearly we can define the small solutions at any point $A \in Q_{24}$ in this way. Further, if the paths never leave the quadrilateral (or at

52

least is always homotopically equivalent to a paths that never leave the quadrilateral) then the solution defined in this way is guaranteed to be single-valued and smooth throughout the quadrilateral, as required. With the solutions defined at a common point in the quadrilateral we can construct the coordinate χ_{24}, which is independent of the choice of $A \in Q_{24}$. Now consider the right panel of figure 3.11 where the grey shading indicates the quadrilateral associated to edge $Q_{\hat{2}4}$. These figures should be imagined on the sphere. Now to transport the small solutions to a common point one cannot avoid passing under a cut onto new sheets of some of the small solutions. For example s_2 must pass onto a new sheet in order to be smoothly continued to the point A. This is because if we were to compare the s_2 of the left panel and the s_2 of the right panel (by moving each respective A to a common point A' along the edge E_{34}, for example) the two paths of continuation would differ by a holonomy around P_3, and thus the values at the point A' would not coincide but would differ by the action of $M_3^{\pm 1}$. Of course which solution we call s_2 and $M_3^{\pm 1}s_2$ is purely a matter of convention. Similarly, which solutions acquire factors of M_a depends on the choice of the point A. We stress that the coordinates are independent of all such ambiguities, as one can easily check using identities such as $(M_c s_a \wedge s_b) = (s_a \wedge M_c^{-1} s_b)$, etc. Then from figure 3.11 we read off

$$\chi_{24} = (-1)\frac{(s_2 \wedge s_3)(s_4 \wedge s_1)}{(s_3 \wedge s_4)(s_1 \wedge s_2)}, \qquad \chi_{\hat{2}4} = (-1)\frac{(M_3^{-1}s_2 \wedge M_4 s_1)(s_4 \wedge s_3)}{(M_4 s_1 \wedge s_4)(s_3 \wedge M_3^{-1}s_2)}. \tag{3.34}$$

We will also need to construct coordinates in the slightly degenerate case where the coordinate corresponds to an edge ending at a vertex that has only two incident edges (including the edge under consideration) for example all edges in figure 3.9 except E_{24} and $E_{\hat{2}4}$. We show how to construct this coordinate in figure 3.12. Using the procedure described there we find

$$\chi_{23} = (-1)\frac{(s_2 \wedge M_3 s_4)(s_3 \wedge s_4)}{(M_3 s_4 \wedge s_3)(s_4 \wedge s_2)}, \qquad \chi_{12} = (-1)\frac{(s_1 \wedge M_1^{-1}s_4)(s_2 \wedge s_4)}{(M_1^{-1}s_4 \wedge s_2)(s_4 \wedge s_1)} \tag{3.35}$$

The other two coordinates χ_{34} and χ_{14} are computed in a similar way.

We have now completed our discussion of how to construct the coordinates. Before we continue, let us comment on a useful property of these objects. Consider multiplying all of the coordinates associated with edges meeting a given puncture P. For example, the edges ending at P_2 in the triangulation of figure 3.9 are E_{12}, $E_{\hat{2}4}$, E_{23} and E_{24}. Using (3.34)-(3.35) we have

$$\chi_{12}\chi_{\hat{2}4}\chi_{23}\chi_{24} = \mu_2^2. \tag{3.36}$$

This property is true in general since the inner-products in the coordinates telescopically cancel in the product and the only thing that remains is the effect of the monodromy

$$(s_2 \wedge s_3) \sim e^{\frac{1}{2} \int_3^2 \omega/\xi}$$

$$(s_3 \wedge s_4)^{-1} \sim e^{\frac{1}{2} \int_4^3 \omega/\xi}$$

$$\gamma_{24}$$

$$(s_1 \wedge s_2)^{-1} \sim e^{\frac{1}{2} \int_2^1 \omega/\xi}$$

$$(s_4 \wedge s_1) \sim e^{\frac{1}{2} \int_1^4 \omega/\xi}$$
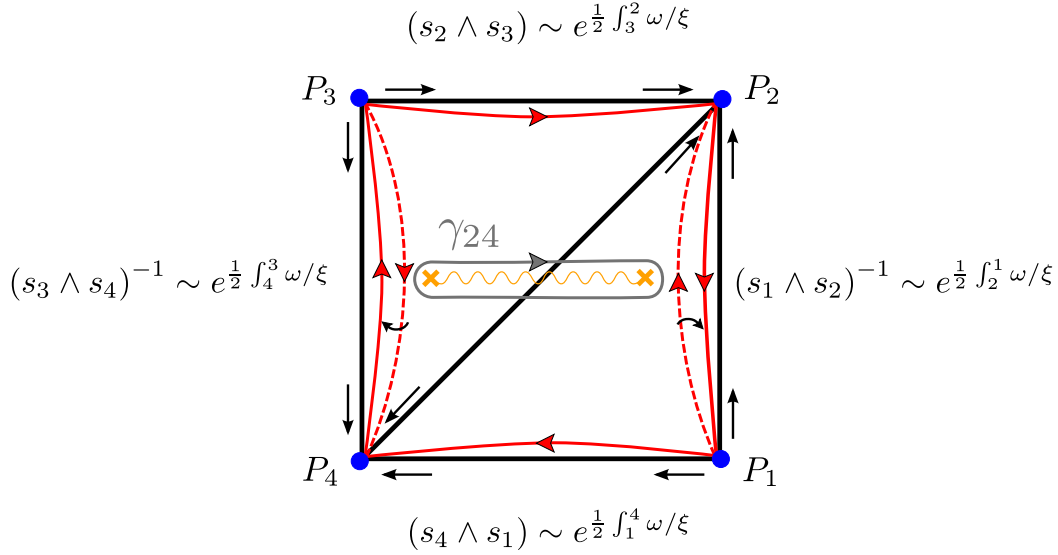
Figure 3.13: Computing the $\xi \to 0$ asymptotic of the coordinate χ_{24} for a typical WKB triangulation. The blue disks represent the punctures and the black lines represent edges of the triangulation. A yellow $\times$ represents a zero of ω and the wavy yellow line shows our convention for defining the sheets of $\widetilde{\Sigma}$. The black arrows running along the edges indicate the choice of the direction for the edges. Each red curve indicates the transport of a small solutions in the limit $\xi \to 0$. The dashed red lines correspond to the transport of a solution appearing in the *denominator* of the coordinate. The transports used to form the coordinate combine into the continuous integral of ω near the boundary of Q_{24}, which can then be deformed into the cycle integral γ_{24} shown in gray.

around the puncture which produces a μ_P^2 factor. Thus we have the general rule [58]

$$\prod_{E \text{ meeting } P} \chi_E = \mu_P^2. \tag{3.37}$$

3.3.6 WKB asymptotics of the coordinates

The advantage of using the WKB triangulation is that the $\xi \to 0, \infty$ asymptotics of the coordinates of the triangulation are easily extracted given the discussion of section 3.3.3. That is, because we have maximum control over the large/small ξ asymptotics of the small solutions when we transport along WKB curves. We give only the basic idea of the

54

derivation of these asymptotics here and refer the reader to appendix $B.4$ and [58] for details.

To obtain the asymptotic of some χ_E one simply needs to use expression (3.30) for each inner-product of the coordinate, taking care to account for the direction of the WKB lines. Consider the coordinate associated with edge E_{24} in figure 3.13. The expression for this coordinate in terms of the small solutions is given in (3.34). We will now use formula (3.30) to compute the asymptotic of this coordinate in the $\xi \to 0$ limit. Let us take the directions of the WKB lines to be as given in figure 3.13. To evaluate the inner product $(s_2 \wedge s_3)$ we must transport the solutions to a common point. Since there is a WKB line flowing from P_3 to P_2 we can safely use (to leading order) expression (3.30) to transport s_3 to the neighbourhood of P_2, giving a contribution of the form $(s_2 \wedge s_3) \sim e^{\frac{1}{2} \int_3^2 \omega / \xi}$. To evaluate $(s_3 \wedge s_4)$ we must transport s_3 to P_4 since that is the direction of the WKB line and thus we get the contribution $(s_3 \wedge s_4) \sim e^{\frac{1}{2} \int_3^4 \omega / \xi}$. We may then reverse the order of integration in $(s_3 \wedge s_4)$ and also move it to the numerator of the coordinate. Then the integrations from $(s_2 \wedge s_3)$ and $(s_3 \wedge s_4)$ combine nicely into a continuous integral running just inside the boundary of Q_{24} from the neighbourhood of P_2 to P_3 to P_4. Repeating this analysis for the remaining two brackets one obtains a closed cycle integral passing along the boundary of Q_{24}. Recall from the discussion of section 3.3.4 that each triangle in the WKB triangulation encloses one zero of ω. The integral of ω thus encloses two zeros and so it can be deformed to the cycle integral shown in figure 3.13. Thus the non-vanishing contribution in the limit $\xi \to 0$ is given by

$$\chi_E \sim (-1) \exp\left(\frac{1}{2} \xi^{-1} \int_{\gamma_E} \omega + C_E^{(0)} \right) \tag{3.38}$$

The contour γ_E is the cycle encircling the two zeros contained in Q_E and its direction is the same as that of the WKB lines corresponding to the brackets in the numerator of the coordinate. The term $C_E^{(0)}$ is the $\mathcal{O}(\xi^0)$ contribution to the WKB expansion, which we will discuss momentarily. The overall (-1) prefactor in (3.38) is the same (-1) appearing in the definition of the coordinate (3.33).

To derive the subleading WKB corrections (in the $\xi \to 0$ limit, for example) is essentially a matter of perturbation theory once the singular contribution has been extracted. We give a detailed discussion of this in appendix $B.4$. Here we will simply focus on the result and its implications. We find the first subleading contribution is given by

$$C_E^{(0)} = \log(-1)^{u_E} \pm i\pi \tag{3.39}$$

where u_E is the number of u-spikes enclosed by γ_E.

Finally the $\xi \to \infty$ asymptotic follows in the same way as the $\xi \to 0$ and leads to a

cycle integral around Q_E of $\xi\bar{w}$.

To summarize, the $\xi \to 0, \infty$ asymptotics for χ_E are given by

$$\chi_E \sim (-1)^{u_E} \exp\left[\frac{1}{2}\int_{\gamma_E}\left(\xi^{-1}\omega + \xi\bar{\omega}\right)\right] \tag{3.40}$$

where γ_E is the cycle encircling the two zeros contained in Q_E and its direction is the same as that of the WKB lines corresponding to the brackets in the numerator of the coordinate. Now it is clear how the choice of spikes (i.e. the choice of signs in (3.11)) is encoded into the coordinates – via the constant term in the WKB expansion which contributes the $(-1)^{u_E}$ factor in (3.40). Recall that u_E is the number of u-spikes encircled by γ_E.

3.3.7 Shift relation.

In section 3.3.1 we explained that there are two special solutions s_P, $\tilde{s}_P$ associated with each puncture P and that they are related to each other by a shift in the spectral parameter: $\tilde{s}_P(\xi) = \sigma^3 s_P(e^{-i\pi}\xi)$. Here we give an alternative relation between the small and big solutions that does not involve shifting the spectral parameter. The solutions s_P and $\tilde{s}_P$ are linearly independent and thus we can expand any solution s_Q in terms of them. In particular we have

$$s_Q = \left(\frac{\tilde{s}_P \wedge s_Q}{\tilde{s}_P \wedge s_P}\right) s_P + \left(\frac{s_P \wedge s_Q}{s_P \wedge \tilde{s}_P}\right) \tilde{s}_P \tag{3.41}$$

$$M_P s_Q = \left(\frac{\tilde{s}_P \wedge s_Q}{\tilde{s}_P \wedge s_P}\right) \mu_P s_P + \left(\frac{s_P \wedge s_Q}{s_P \wedge \tilde{s}_P}\right) \mu_P^{-1}\tilde{s}_P \tag{3.42}$$

For the second equality we have used (3.27)-(3.28). Combining these two equations it follows that

$$\left(\frac{M_P s_Q \wedge s_Q}{M_P s_Q \wedge s_P}\right) = (1 - \mu_P^2)\left(\frac{\tilde{s}_P \wedge s_Q}{\tilde{s}_P \wedge s_P}\right) \tag{3.43}$$

The utility of this equation is that it allows us to replace certain wronskians involving big solutions (as on the RHS of (3.43)) in terms of small solutions with monodromies. This will play a key role in the derivation of the functional equations that we present in the following section.

3.3.8 χ-system.

We will now derive a set of functional equations for the coordinates which, together with certain analytic properties, allows us to determine the coordinates completely. Our inspi-

56

ration comes from the solution of the bosonic Wilson-loop problem at strong coupling [57] where the solution involves a set of functional equations of the schematic form[11]

$$Y_a^+ Y_a^- = F_a(Y) \tag{3.44}$$

where $f^{n\times\pm} \equiv f(\theta \pm ni\pi/2)$. On the RHS of (3.44) the function F_a can depend on all of the Y_a, but with their arguments un-shifted. The only shifts in the spectral parameter occur on the LHS of (3.44). For the Wilson-loop problem the F_a are such that (3.44) takes the form of a so-called Y-system which commonly appear in the context of $1 + 1$ dimensional integrable QFT's. Here, using the general formalism of [58], we will arrive at a set of functional equations with the same schematic form as (3.44) but with the F_a of a different form than that occurring in the Wilson-loop problem. We will call this type of functional equation a χ-system.

To derive a relation of the form (3.44) we begin with the LHS. Using (3.24) we have

$$\chi_E \widetilde{\chi}_E = \chi_E \chi_E^{++} \tag{3.45}$$

where $\widetilde{\chi}_E$ is defined by taking χ_E and replacing each small solutions $s_a \to \tilde{s}_a$. To obtain the schematic form (3.44) we need to rewrite (3.45) in terms of only un-shifted small solutions. That is, we need to get rid of all the tildes without introducing any shifts in the spectral parameter. For this we can use (3.43) after applying the Schouten identity[12] to (3.45) to obtain

$$\chi_E \chi_E^{++} = \chi_E \widetilde{\chi}_E = \frac{(1 + A_{ab})(1 + A_{cd})}{(1 + A_{bc})(1 + A_{da})} \tag{3.46}$$

where we have defined the useful auxiliary quantity

$$A_{PQ} = (-1)\frac{(s_Q \wedge \tilde{s}_P)(s_P \wedge \tilde{s}_Q)}{(s_P \wedge \tilde{s}_P)(s_Q \wedge \tilde{s}_Q)} \tag{3.47}$$

$$= (-1)\left(1 + \mu_P^2\right)^{-1}\left(1 + \mu_Q^2\right)^{-1}\left(\frac{M_P s_Q \wedge s_Q}{M_P s_Q \wedge s_P}\right)\left(\frac{M_Q s_P \wedge s_P}{M_Q s_P \wedge s_Q}\right) \tag{3.48}$$

Here, the edge E is the edge ac in Q_E where the vertices are labeled $abcd$ in counter-clockwise order. To go from (3.47) to (3.48) we used the shift relation (3.43). The last step is to rewrite the wronskians appearing in (3.48) in terms of the coordinates. Once this is

---

[11]The linear problem associated with that problem is very similar to the one considered here and the Y_a are (up to shifts in the spectral parameter) the coordinates associated with that problem. We are referring here to the special case where the Wilson loop lives in an $\mathbb{R}_{1,1}$ subspace.

[12] $(s_a \wedge s_b)(s_c \wedge s_d) + (s_a \wedge s_c)(s_d \wedge s_b) + (s_a \wedge s_d)(s_b \wedge s_c) = 0.$
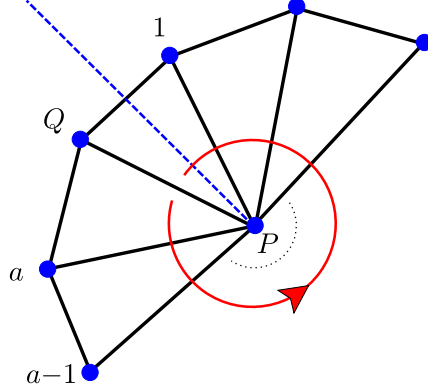
Figure 3.14: Graphical rules for constructing $\Sigma\left(P;Q\to Q\right)$. Start at edge E_{PQ} and continue in a *counterclockwise* fashion about P forming the nested product (3.49) by multiplying the coordinates for each edge encountered along the way (i.e. the coordinates associated with each edge intersected by the red line in the order indicated by the arrow). The dashed blue line indicates our convention for cutting the solutions to account for the monodromy around P. The small solutions used to form the coordinates are defined in the vicinity of P by analytically continuing them throughout the triangles along the direction indicated by the red arrow and thus if we use s_Q in $\chi_{P,a}$ then we must include a monodromy matrix when the solution is continued around P to form $\chi_{P,1}$.

done, combining $(3.45)-(3.48)$, we can assemble a functional equation of the form (3.44). To do this (following [58]) we introduce the quantity

$$\Sigma\left(P;Q\to Q\right)=1+\chi_{P,a}\left(1+\chi_{P,a-1}\left(1+...\chi_{P,2}\left(1+\chi_{P,1}\right)\right)\right) \tag{3.49}$$

The coordinates appearing in this object are shown in figure 3.14. By repeatedly applying the Schouten identity (see footnote 12) starting with $(1+\chi_{P,1})$ one can see that the Wronskians in (3.49) telescopically cancel so that[13]

$$\Sigma\left(P;Q\to Q\right)=\frac{(s_0\wedge s_{a+1})(s_P\wedge s_a)}{(s_{a+1}\wedge s_a)(s_0\wedge s_P)}=\frac{(s_P\wedge s_a)(M_Ps_Q\wedge s_Q)}{(s_Q\wedge s_a)(M_Ps_Q\wedge s_P)} \tag{3.50}$$

In going from the first equality to the second in (3.50) we have accounted for the monodromy acquired by the small solutions when they are analytically continued around P (see figure

---

[13]An easy way to see this in general is to use induction [58]. The case $a=1$ is simple to prove using Schouten identity. Then one can show (again using Schouten) that $\Sigma\left(P;Q_{a+2}\to Q_0\right)=1+\chi_{P,a+1}\Sigma\left(P;Q_{a+1}\to Q_0\right)$.

3.14). Then, from (3.50) and (3.48) we have

$$(1 + \mu_P)^2 (1 + \mu_Q)^2 A_{PQ} = \chi_{PQ} \Sigma (P; Q \to Q) \Sigma (Q; P \to P) \tag{3.51}$$

Finally, using (3.51) in (3.46) and noting (3.49) we obtain a closed functional equation for χ_E of the form (3.44). Repeating this procedure for the coordinate associated to each edge in a given triangulation gives the desired set of functional equations. Note that this procedure can be applied to derive the χ-system for an arbitrary number of punctures. In section 3.4 we will apply this procedure to the triangulation (3.9), which is one of the triangulations of interest for the four-point function computation.

3.3.9 Inverting χ-systems

In the previous section we showed how to derive the χ-system associated with a given triangulation of the N-punctured sphere. In this section we will discuss how to use the χ-system along with certain analytic properties of the coordinates to obtain integral equations that determine the χ_E uniquely.

The basic idea behind the inversion of a χ-system is to Fourier transform (the log of) each equation since in Fourier space these nonlocal relations become local as the shifts in the parameter θ can be undone in the usual way. For such a procedure to be successful one must have a certain amount of control of the analytic properties of the coordinates. Let us discuss this carefully. The equations that we want to Fourier transform have the form

$$\log \chi_E^- (\theta + i\phi) + \log \chi_E^+ (\theta + i\phi) = \log F_E \left(\chi^\pm (\theta + i\phi) \right) \tag{3.52}$$

where $F_E (\chi)$ is an explicit function of the coordinates which follows from the discussion of section 3.3.8. We have introduced the arbitrary shift ϕ for reasons that will be explained momentarily. Note that $\chi_E \chi_E^{++} = \chi_E \chi_E^{--}$ since the small solutions are $2\pi i$-periodic, which is why we can have either shift $F_E (\chi^\pm)$ on the RHS. The choice of this shift is arbitrary since the objects we will eventually compute (the η-cycles) are functionals of the coordinates only through A_{PQ} which is $i\pi$-periodic and thus does not care about the choice of shift. As a convention we choose the shift $-i\pi/2$.

To Fourier transform the relationship (3.52) one must be sure that the transform converges. Moreover, to undo the shifts on the LHS, one must account for the singularities (if any) of $\log \chi_E$ in the strip of width π centered along the line where the transform has been performed. We will now discuss each of these issues in turn.

The information from the WKB analysis will allow us to ensure the convergence of the Fourier transform, provided certain conditions are satisfied. First consider the LHS

of (3.52). We need to ensure that the transform of each *individual* term converges. We can ensure this if we know the asymptotics of the coordinates in the full strip $\text{Im}(\theta) \in (\phi - \pi/2, \phi + \pi/2)$. The coordinates should be derived from the triangulation that one has at $\text{Im}(\theta) = \phi$. Then the WKB analysis guarantees that the asymptotics are given by (3.40) in a strip that includes the region $\text{Im} \in (\phi - \pi/2, \phi + \pi/2)$. Each term on the LHS can be made safe to transform by making (on the LHS only) the replacement $\chi_E \to \chi_E / \chi_E^{(0)}$ where $\chi_E^{(0)}$ is the asymptotic (3.40). This replacement does not modify the equation since $\left(\chi_E^{(0)} \right) \left(\chi_E^{(0)} \right)^{++} = 1$.

Now consider the RHS of (3.52), which has the form (see equation (3.46))

$$\log F_E \left(\chi^{\pm} (\theta + i\phi) \right) = \log \left[\frac{(1 + A_{ab})(1 + A_{cd})}{(1 + A_{bc})(1 + A_{da})} (\theta \pm i\pi/2 + i\phi) \right] \tag{3.53}$$

Each A_{PQ} is computed by (3.51) and (3.49). For the RHS of (3.53) to be decaying it is sufficient for all of the A_{PQ} in (3.53) to be decaying. If all the χ-functions are decaying then from (3.51) and (3.49) it is clear that all of the A_{PQ} will decay; the μ-factors will decay by virtue of the rule (3.37). On the other hand, if all the χ-functions are growing the μ-factors in (3.51) will dominate the RHS of (3.51) so that A_{PQ} is still decaying; to see this one should re-express the μ-factors in terms of the coordinates using (3.37). Thus the RHS of (3.53) will decay if all of the χ-functions are growing, or alternatively if they are all decaying. For generic ϕ it will generally not be true that the RHS of (3.53) is well behaved, and one must try to find a range of ϕ-values for which the χ_E are all decaying or are all growing. If a suitable ϕ can be found, then (3.52) can be directly solved by Fourier-transform. In all of the examples we have considered (in particular, those relevant for the 4-point function) it has been possible to find such a ϕ.

Concerning the issue of singularities within the strip of inversion, it follows from (3.19) that the Wronskians $(s_a \wedge s_b)(\theta)$ are (in an appropriate normalization) analytic away from $\theta = \pm \infty$. It is, however, possible for these objects to have *zeros* and in the following it is an assumption that there are no zeros in the strip where we do the inversion.[14] In section 3.4.1 we perform numerical tests that support this assumption.

Finally, we use the Fourier analysis to obtain

$$\log X_E (\theta) = \log X_E^{(0)} (\theta) - \int_{\mathbb{R}} \frac{d\theta'}{2\pi i} \frac{\log F_E (X (\theta'))}{\sinh (\theta' - \theta + i0)} \tag{3.54}$$

---

[14] In the limit where the WKB approximation holds, i.e. when $\theta \to \pm \infty$ or in the limit of large zero modes $|Z_E| \to \infty$ [58], it is clear that (in an appropriate normalization) the Wronskians will not have any zeros since (suppose we compute the Wronskian near P_b) then s_a will be the *big* solution near P_b and is thus linearly independent of s_b which is small at P_b. For finite values of θ (or alternately of $|Z_E|$) we have no concrete way of arguing that these zeros are not present.

where $X_E(\theta) = \chi_E(\theta + i\phi - i\pi/2)$ and $X_E^{(0)}$ is the (shifted) asymptotic (3.40) and $F_E(X)$ is an explicit function of the coordinates which follows from the discussion of the previous section.

The equations (3.54) can easily be solved for the X_E by iterating them in a computer. In the next subsection we will show how to extract the η-cycles of formula (3.18) from the X_E which are computed using (3.54). We will then perform some numerical tests in section 3.4.1.

3.3.10 Extracting η-cycles

Once the coordinates are computed according to the prescription of the preceding section we extract the η-cycles as follows. What we need to compute are the individual Wronskians $(s_a \wedge s_b)$. For this, note that from (3.47) and footnote 12 we have

$$(1 + A_{ab}) = \frac{(s_a \wedge s_b)(\tilde{s}_a \wedge \tilde{s}_b)}{(s_a \wedge \tilde{s}_a)(s_b \wedge \tilde{s}_b)} \tag{3.55}$$

We can choose a gauge where $(s_P \wedge \tilde{s}_P) = 1$. The final result will be gauge independent. With this gauge choice we have

$$\log(s_a \wedge s_b)^- + \log(s_a \wedge s_b)^+ = \log\left(1 + A_{ab}^-\right) \tag{3.56}$$

Here we will use the notation $\theta \to \theta + i\phi$ where θ and ϕ are real. We then insert the zero-modes on the LHS in the same way as for the χ-system (see section 3.3.9). We are only interested in P_a and P_b that are connected by a WKB line when $\mathrm{Arg}\,(\xi) = \phi$, and thus we have good control over the asymptotics in the required strip. Performing the Fourier transforms we obtain

$$\log(s_a \wedge s_b)(\theta + i\phi) = \left(\frac{1}{2}e^{-\theta - i\phi}\varpi_{ab} + \frac{1}{2}e^{\theta + i\phi}\bar{\varpi}_{ab}\right) + \int_{\mathbb{R}} \frac{d\theta'}{2\pi} \frac{\log\left(1 + A_{ab}^-(\theta' + i\phi)\right)}{\cosh(\theta - \theta')} \tag{3.57}$$

where we have defined

$$\varpi_{ab} \equiv \lim_{w_a' \to w_a} \lim_{w_b' \to w_b} \left[\int_{E_{ab}} \sqrt{T}dw + \frac{\Delta_a}{2}\log(w_a - w_a') + \frac{\Delta_b}{2}\log(w_b - w_b')\right] \tag{3.58}$$

The integration in (3.58) is performed along edge E_{ab}. The direction of integration is the same as the direction of the edge E_{ab} (see appendix B.4). Note that the logarithmic terms precisely cancel the divergence from the endpoints of integration in (3.58) so that the ϖ_{ab}

are finite. In going from (3.56) to (3.57) we have used the asymptotics for $(s_a \wedge s_b)$ derived in appendix B.4.

Expanding (3.57) around $\theta \to -\infty$, and comparing with (3.26) with $\xi = e^{\theta + i\phi}$ we read off

$$\int_{E_{ab}} \eta = \int_{\mathbb{R}} \frac{d\theta}{\pi} e^{-\theta - i\phi} \log\left(1 + A_{ab}^-(\theta + i\phi)\right) \tag{3.59}$$

The contour of integration in $\int_{E_{ab}} \eta$ is along the WKB line connecting P_a and P_b and the direction of integration is the same as the direction of the edge E_{ab}. This formula allows us to compute the η-cycles from the χ-functions since the A_{PQ} are explicit functions of the coordinates.

3.4   The AdS action

3.4.1   Regularized AdS action

Now that we have introduced the needed tools we are ready to calculate the action (3.18). We will demonstrate for the case of the 4-point function, but the method is general and could be performed for any number of operators inserted along a line. The computation will be as follows. First we will introduce the relevant WKB triangulation which will be topologically equivalent to the triangulation shown in figure 3.9. Second, using the procedure of section 3.3.8 we will derive the χ-system satisfied by the coordinates of this triangulation. Supplementing these functional relations by the WKB asymptotics we will invert these functional relations using the technique of section 3.3.9 to obtain a set of integral equations that uniquely determine the coordinates. Finally, from coordinates we extract the η-cycles using the method of section 3.3.10. Once we have the η-cycles, we compute the action using (3.18).

Stress-energy tensor and WKB triangulation

For the purpose of the following computation, a useful parameterization of the stress energy tensor is

$$T(w) = \frac{1}{(w - w_4)^2}\left(c_\infty + \frac{c_0 + c_1 w + c_2 w^2 + U w^3}{(1 + w)^2(1 - w)^2}\right) \tag{3.60}$$

Here we have fixed three of the insertion points at $w_1 = +1$, $w_2 = \infty$, $w_3 = -1$ using the world-sheet conformal symmetry. The fourth insertion point is left at the position w_4
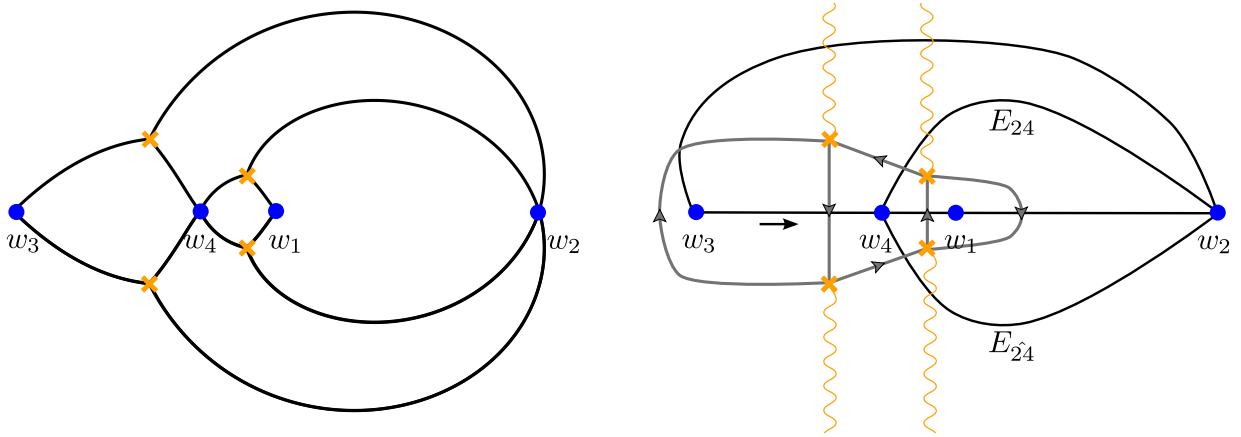
Figure 3.15: Constructing the triangulation for the 4-point function. In the left panel we show the WKB cells for $\text{Arg}\,(\xi) = 0$. The cell walls are formed by the separating WKB curves as described in section 3.3.4; as described there, inside each cell there is a 1-parameter family of generic WKB curves and by taking a representative curve from each family we obtain the triangulation shown in the right panel. In the right panel the black lines are the edges of the WKB triangulation and the wavy yellow lines show our convention for defining the branches of ω. Notice that this triangulation is topologically equivalent to the one shown in figure 3.9. This means that we can borrow the results derived for that example. In particular, the coordinates can be carried over from that example by making the proper identifications. The cycles corresponding to each coordinate are represented by the gray curves – we show only the portion of each cycle on the sheet of ω where the edge E_{34} has orientation *towards* P_4 as indicated by the black arrow along edge E_{34}.

which should be fixed by the Virasoro constraint. For the purpose of demonstration we will take w_4 to be between $w_3 = -1$ and $w_1 = +1$. When the fourth insertion point is located in one of the other intervals one can proceed by a similar procedure. The constants $c_a = c_a\,(w_4, \Delta)$ are functions of w_4 and dimensions of the operators and are fixed by the condition (3.7). Their explicit expressions are given in appendix D. The parameter U is unfixed by the condition (3.7) and implicitly parameterizes the cross ratio of the four operators (recall that they are inserted along a line in the boundary theory so that there is only one cross ratio). The analytic structure of T, the resulting WKB-structure and the WKB triangulation are shown in figure 3.15.

χ-system for the 4-point function

From equation (3.46) and figure 3.15 we have

$$\chi_{24}\chi_{24}^{++} = \left(\chi_{\hat{2}4}\chi_{\hat{2}4}^{++}\right)^{-1} = \frac{(1+A_{23})\,(1+A_{14})}{(1+A_{34})\,(1+A_{12})} \tag{3.61}$$

$$\chi_{12}\chi_{12}^{++} = \left(\chi_{14}\chi_{14}^{++}\right)^{-1} = \chi_{34}\chi_{34}^{++} = \left(\chi_{23}\chi_{23}^{++}\right)^{-1} = \frac{(1+A_{24})}{(1+A_{\hat{2}4})} \tag{3.62}$$

To compute each A_{PQ} we use formulas (3.51) and (3.49) along with the rules given in figure 3.14. In that way we find

$$A_{24} = \frac{\chi_{24}\,(1+\chi_{12}\,(1+\chi_{\hat{2}4}\,(1+\chi_{23})))\,(1+\chi_{43}\,(1+\chi_{\hat{4}2}\,(1+\chi_{41})))}{(1-\mu_2^2)\,(1-\mu_4^2)} \tag{3.63}$$

$$A_{23} = \frac{\chi_{23}\,(1+\chi_{34})\,(1+\chi_{24}\,(1+\chi_{12}\,(1+\chi_{\hat{2}4})))}{(1-\mu_2^2)\,(1-\mu_3^2)} \tag{3.64}$$

with the rest of the A_{PQ} being related by relabelling (see appendix D for the explicit formulas). These expressions and equations $(3.61) - (3.62)$ provide a closed system of functional equations for the 6 coordinates associated with the triangulation shown in figure 3.15.

These functional equations can be converted into integral equations of the form (3.54) using the technique described in section 3.3.9. To apply the procedure of section 3.3.9 one must find a ϕ such that the RHS of (3.52) is decaying, and for this one should appeal to the WKB analysis. The WKB cycles which determine the asymptotics of the coordinates are shown in figure 3.15. When $\Delta_1 \sim \Delta_3$ and $U \sim 0, w_4 \sim 0$ the cycles shown in figure 3.15 all have $\mathrm{Arg}(\oint_{\gamma_E} \omega) \sim \pi/2$.[15] In this case $\phi = 0$ is a suitable choice since then all χ_E^- will be growing and (3.53) will decay rapidly.[16] In summary, the integral equations in the region of present interest are given by equations (3.54) with F_E given by $(3.61) - (3.64)$. These equations will remain valid for all values of the parameters Δ_a, U, and w_4 such that the triangulation is unchanged. If one deforms these parameters too much the triangulation

---

[15]Interestingly, when $\Delta_1 = \Delta_3$ and $U = w_4 = 0$ there is a symmetry which causes the RHS of the χ-system to trivialize (i.e. to reduce to 1 for all χ_E) and the χ-functions can be computed explicitly (they are just equal to their zero-mode part). This is reminiscent of the case for the three-point function and, in fact, there is also a change of coordinates that maps the specific case $\Delta_1 = \Delta_3$ and $U = w_4 = 0$ to two copies of a three-point function.

[16]This will continue to be the case as long as the $\mathrm{Arg}(\oint_{\gamma_E} \omega)$ remain in the upper-half plane. In other-words, the inversion procedure will be valid for all U and w_4 such that the triangulation is unchanged since the triangulation will jump precisely when one of the $\oint_{\gamma_E} \omega$ crosses the real-axis [58].

will jump. One can then easily write the χ-system for the new triangulation and apply the same procedure to obtain the integral equations for that region of parameters.[17]

By numerically iterating these equations (using $\chi_E^{(0)}$ as the initial iterate for each χ_E) we obtain the χ-functions. The η-cycles are then extracted from the χ-functions using the procedure of section (3.3.10). In the following section we will write the regularized AdS action in terms of these η-cycles.

Finite part of AdS action

Now that we are able to compute the η-cycles (see previous subsection) we can use the formula

$$A_{fin} = \int_\Sigma \sqrt{T\bar{T}} \left(\cosh\gamma - 1\right) = \frac{\pi}{3} - \frac{i}{2} \left(\oint_{\gamma_a} \omega\right) I_{ab}^{-1} \left(\oint_{\gamma_b} \eta\right). \tag{3.65}$$

(see section 3.2.2 and equation (3.18)) to compute the regularized part of the AdS action. To use (3.65) there are few steps. These steps are simple but tedious and we will only list them here (see appendix D for a detailed implementation). As described in section 3.2.2 one should first modify T by spreading the double poles slightly such that $\omega = \sqrt{T} dw$ has an additional square-root cut at each of these points. Then one should choose a complete basis of a- and b-cycles (five of each is needed for the 4-point function). One can then apply formula (3.18) and then take the limit in which the small cuts close to form simple poles in ω. Once this is done the area will generically be expressed in terms of three different types of η-cycles: cycles connecting two punctures, cycles connecting a puncture with a zero and cycles connecting two zeros. The latter two can be expressed as linear combinations of the puncture-puncture cycles as described in appendix D. Once this is done, the final result takes the elegant form

$$A_{fin} = \frac{\pi}{3} - i \sum_{E \in \mathcal{T}} \omega_E \, \eta_E \tag{3.66}$$

where the sum runs over the edges in the triangulation (see figure 3.15), $\eta_{E_{ab}}$ is defined in (3.59) while $\omega_{E_{ab}}$ is the ω-cycles that intersects edge E_{ab} (i.e. the integral of ω that is associated with the coordinate χ_{ab}; these integrals are shown as the gray contours in figure 3.15).[18]

Formula (3.66) and the procedure of section 3.3 for computing the η-cycles solve the problem of computing the regularized AdS contribution to the 4-point function. In the

---

[17]Another (more elegant) approach would be to find a systematic way of analytically continuing the integral equations from one region of parameters to another as was done for the TBA equations of [57].

[18]Note that in formula (3.66) both integrals ω_E and η_E are the *segment* integrals between the appropriate limits. For example, the $\omega_E = \frac{1}{2} \oint_{\gamma_E} \omega$. In this sense we are abusive with the term 'cycle'.

U	Δ_3	Δ_4	Δ_1	Δ_2	Numerics	χ-system
1/5	1	2	1	2	0.84807	0.84812
1/2	1	2	1	2	0.82421	0.82423

Table 3.1: Comparison of the A_{fin} obtained by numerically integrating (3.10) and the area computed from the χ-system. The results are for the spike configuration of figure 3.4B.

next section we present some numerical tests of the procedure. Let us note that the procedure of section 3.3 is general and can be implemented for any number of punctures. Further, while we have only proved equation (3.66) for the case of the 4-point function, given its simplicity one might suspect that the formula holds in general (with $\pi/3 \rightarrow \pi/12 \times$ (#number of zeros of T), of course).[19] Even if the general result does not take the simple form (3.66), for a given T (i.e. for any number of punctures) the procedure described in section 3.2.2 is still valid and one can still write A_{fin} in terms of the η_E for the corresponding triangulation). In principle this solves the problem of computing the regularized AdS contribution to the N-point function. We have performed numerical tests only for the case of the 4-point function. We present these numerical results in the following section.

Numerical tests

We now present numerical tests of the method described above. We solved numerically the modified sinh-Gordon equation (3.10) for the function γ and then using this numerical solution to directly compute A_{fin} via

$$\int_\Sigma \sqrt{T\bar{T}}\,(\cosh\gamma - 1) \tag{3.67}$$

The general set-up of the numerical problem essentially follows that of [46] with some modifications. However, the numerical method that we use to solve the PDE (3.10) is quite different from that of [46].[20] We place the punctures at $w_3 = -1$, $w_4 = 0$, $w_1 = 1$, and $w_2 = \infty$. We then map the sphere to a square domain with the point at infinity mapping to the boundary of the square and the real axis mapping onto itself. Since γ must

---

[19]It would be a simple matter to check this, but we have not pursued this issue. We did check that the formula holds for the 3-point function (see appendix E).

[20]We are very grateful to Romuald Janik for providing us with a copy of the code used in [46] which was very useful in helping us to develop and test our own numerics.
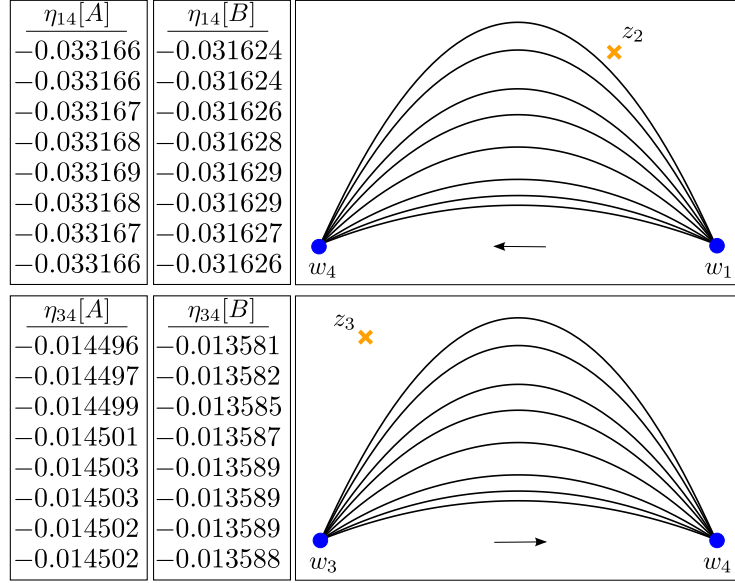
$\eta_{14}[A]$	$\eta_{14}[B]$
-0.033166	-0.031624
-0.033166	-0.031624
-0.033167	-0.031626
-0.033168	-0.031628
-0.033169	-0.031629
-0.033168	-0.031629
-0.033167	-0.031627
-0.033166	-0.031626

$\eta_{34}[A]$	$\eta_{34}[B]$
-0.014496	-0.013581
-0.014497	-0.013582
-0.014499	-0.013585
-0.014501	-0.013587
-0.014503	-0.013589
-0.014503	-0.013589
-0.014502	-0.013589
-0.014502	-0.013588

Figure 3.16: Here we show the values of η_{14} and η_{34} evaluated along several different contours. For example, the column labeled $\eta_{14}[A]([B])$ shows the values of η_{14} for the spike configuration of figure 3.4$A(B)$ for each of the contours shown to the right of the column. We use the parameter values $\Delta_3 = \Delta_1 = 1$, $\Delta_2 = \Delta_4 = 2$ and $U = 1/5$ for both spike configurations. There are five digits that we trust since they are unchanged for the different contours and they should be compared with our result from the functional equations that is $\eta_{14}^{\chi-\text{system}}[A] \approx -0.033169$, $\eta_{34}^{\chi-\text{system}}[A] \approx -0.014503$ and $\eta_{14}^{\chi-\text{system}}[B] \approx -0.031628$, $\eta_{34}^{\chi-\text{system}}[B] \approx -0.013588$. In the digits where the forms are closed there is perfect agreement with the analytic results.

vanish at the punctures, we should impose $\gamma = 0$ along the boundary of the square domain since w_2 maps to the boundary of the square in the new coordinates. Further, since for either configuration of spikes (see section 3.2.3 and figure 3.4) there is a fold-line along the real axis, we know $\gamma(x,0) = 0$ where we are using the coordinates $w = x + iy$ and writing $\gamma = \gamma(x,y)$. Thus we can solve the problem in half of the square with the Dirichlet boundary conditions $\gamma = 0$ on the boundaries. Lastly, we must remove the logarithmic singularities (3.11) in order to have a nice smooth function to solve for. A suitable function is

$$2\gamma_{reg} = \gamma + \frac{1}{2} \sum_a \sigma_a \log \left[\frac{(w - z_a)(\bar{w} - z_a)}{(1 + w\bar{w})} \right] \tag{3.68}$$

where we $\sigma_a = \pm 1$ is determined by $\gamma \sim -\sigma_a \frac{1}{2} \log T\bar{T}$ at z_a. The numerator of (3.68) removes the log divergences (3.11) in γ while the denominator is included to kill off these additional log terms at infinity. In the numerical implementation we fix the spike configuration we want to describe by choosing the set of $\{\sigma_a\}$. Finally, to numerically integrate the equation (3.10) (re-written in terms of γ_{reg}, of course) we use a standard relaxation method with an uniform grid.

In table 3.1 we compare the numerical results with the analytic results. The numerical results are obtained by the area computed using (3.67) with the numerical solution for γ. The analytic result is obtained from (3.66) with the η-cycles computed using the χ-system procedure. These results show a good agreement of our formula with the numerics.

A sharper measure of the agreement between the analytics and numerics is to compare directly the η-cycles. In figure 3.16 we show the numerical results for η_{14} and η_{34} computed along several different contours. This allows us to test the closure of the numerical η which we obtain from the numerical γ via (3.16). Note that closure of η implies that γ must obey (3.10) and thus this is a good measure of the numerical error. Indeed, one can see in figure 3.16 that the numerical cycles agree with the analytical predictions in all digits in which they are closed. That is, the numerics is in agreement with the analytics in all of the digits for which the numerics can be trusted.

Finally, it would be interesting to perform numerical tests for a larger portion of the parameter space (i.e. more values of the Δ_a, U and w_4). To perform a systematic study will probably require an improvement of our numerical method as our current method, while extremely simple, has very slow convergence.

3.4.2 Divergent part

In section 3.4.1 we completed the task of computing the first term in formula (3.14). In this section we will discuss the second term

$$ -\int_{\Sigma \backslash \{\epsilon_a\}} d^2w \sqrt{T\bar{T}} = -\frac{\pi}{2} \sum_a \Delta_a^2 \log \epsilon_a - A_{reg} \tag{3.69} $$

where A_{reg} is finite at $\epsilon_a \to 0$. The contribution A_{reg} can be computed by simple but tedious application of the Riemann bilinear identity and there are many ways to write the result. For example

$$ A_{reg} = i \sum_{E \in \mathcal{T}} \varpi_E \omega_E - i\frac{1}{2}(\varpi_{24} - \varpi_{\hat{24}})(\omega_{24} - \omega_{\hat{24}}) \tag{3.70} $$

where the sum is over the triangulation shown in figure 3.15 and $\varpi_{E_{ab}} \equiv \varpi_{ab}$ is defined in

(3.58). The ω_E are defined in the same way as in (3.66). One can check this formula by comparing with the direct 2D numerical integration of $\sqrt{T\bar{T}}$ with small circular disks cut out around the puncture (in Mathematica one can use NIntegrate along with the Boole command, for example).

We recall that (3.69) came from the regularization of the string action where we have added and subtracted $\sqrt{T\bar{T}}$ from the integrand of the AdS action. This integral depends explicitly on the cut-off ϵ_a around the punctures. It will be important to understand the connection with the physical cut-off $\mathcal{E}$ at the boundary of AdS. Fortunately we can extract the needed information from the linear problem since we have good analytic control over the solutions near the insertion points. To proceed by this route (which parallels the discussion of [46] for the 3-point function) we must first describe how the string embedding coordinates are recovered from the linear problem formalism, which is via the aptly-named *reconstruction formulas*. We will discuss this in the next subsection. After that, we will use the reconstruction formulas to eliminate the ϵ_a in favor of $\mathcal{E}$. From this procedure we will recover the standard spacetime dependence in (3.1) along with a contribution to the function $f(u,v)$. This will complete the computation of the semiclassical AdS contribution to (3.1).

Reconstruction formulas

The reconstruction formulas allow us to express the string embedding coordinates in terms of solutions of the linear problem. This point is crucial in our construction for the following reasons. First, we have introduced some regulators in the world-sheet, ϵ_a, that must be related to the physical cut-off in the boundary of AdS, $z = \mathcal{E}$. Second, by using them we will be able make the spatial dependence explicit in the final result, namely the insertion points x_a of the operators in the gauge theory.

Consider two solutions of the linear problem, ψ_A and ψ_B normalized as $(\psi_A \wedge \psi_B) = 1$, and construct a matrix Ψ as

$$\Psi = (\psi_A \ \psi_B). \tag{3.71}$$

The matrix Ψ obeys the same equations of motion as $\psi_{A,B}$ (3.19), namely

$$(\partial + J_w)\Psi = 0, \quad (\bar{\partial} + J_{\bar{w}})\Psi = 0. \tag{3.72}$$

where J_w and $J_{\bar{w}}$ are defined in (3.19)-(3.20). One can verify using (3.9) that the quantity

$$y^I \equiv -\frac{1}{2} \mathrm{tr} \ (\tilde{\sigma}^I \sigma^2 \Psi^T \sigma^1 \Psi)\big|_{\theta=0} \tag{3.73}$$

69

with $\tilde{\sigma}^1 = \sigma^1$, $\tilde{\sigma}^2 = -i\sigma^2$, $\tilde{\sigma}^3 = \sigma^3$, satisfies the same equations of motion as Y^I and also the constraint $y \cdot y = -1$ (with the *AdS* metric). In this way we establish a correspondence between target space coordinates and solutions of the linear problem,

$$\frac{1}{z} = Y^2 - Y^1 = 2i\,\Psi_{11}\Psi_{21}, \qquad \frac{x}{z} = Y^3 = i\,(\Psi_{11}\Psi_{22} + \Psi_{12}\Psi_{21}) \tag{3.74}$$

In order to relate the operator insertion points x_a and physical cut-off $\mathcal{E}$ with the linear problem data, it is convenient to express ψ_A and ψ_B in terms of the elementary solutions s_a and $\tilde{s}_a$ whose behavior close to the punctures is given by (3.21),

$$\psi_A = (\psi_A \wedge \tilde{s}_a)\,s_a + (s_a \wedge \psi_A)\,\tilde{s}_a, \qquad \psi_B = (\psi_B \wedge \tilde{s}_a)\,s_a + (s_a \wedge \psi_B)\,\tilde{s}_a \tag{3.75}$$

Close to the punctures the solution $\tilde{s}_a$ becomes dominant. Then, using (3.74) and the explicit form of $\tilde{s}_a$ close to the puncture P_a we get that

$$z = \frac{1}{i\,(s_a \wedge \psi_A)_0^2}|w - w_a|^{\Delta_a} \tag{3.76}$$

where the subscript 0 indicates that the solutions are evaluated at $\theta = 0$ (recall that this is the value where the physical problem is recovered – see equation (3.73)). Equation (3.76) is the relation needed to make the connection between the world-sheet and physical cut-off's

$$\Delta_a \log \epsilon_a = \log \mathcal{E} + \log |\,(s_a \wedge \psi_A)\,|_0^2 \tag{3.77}$$

Finally, using once again (3.74) we express the insertion points x_a of the operators in the gauge theory as

$$x_a = \frac{(s_a \wedge \psi_B)_0}{(s_a \wedge \psi_A)_0} \tag{3.78}$$

Physical regulator and spacetime dependence

We can now use (3.77) to eliminate the ϵ_a in (3.69) in favor of the physical cut-off at the boundary of AdS $z = \mathcal{E}$. We have

$$\sum_a \Delta_a^2 \log \epsilon_a = \left(\sum_a \Delta_a \log \mathcal{E} + \sum_a \Delta_a \log |\,(s_a \wedge \psi_A)\,|_0^2\right) \tag{3.79}$$

where a and A refer respectively to the small solution s_a and one generic solution ψ_A appearing in the reconstruction formulas. Now we will eliminate the factors $|\,(s_a \wedge \psi_A)\,|_0$

in terms of objects that we can compute.

The terms $|(s_a \wedge \psi_A)|_0^2$ can be related to the insertion points x_a in target space and overlaps of the elementary solutions evaluated at $\theta = 0$ through expression (3.78). Using Schouten's identity one can verify that

$$|(s_a \wedge \psi_A)|_0^2 = \frac{x_{bc}}{x_{ba} x_{ca}} \frac{|(s_b \wedge s_a)|_0| (s_c \wedge s_a)|_0}{|(s_c \wedge s_b)|_0} \tag{3.80}$$

for a, b, c distinct. This solution is unique up to different ways of rewriting the spatial dependence using the cross-ratio

$$u = \frac{x_{14} x_{23}}{x_{12} x_{34}} = \frac{(s_1 \wedge s_4)_0 \, (s_2 \wedge s_3)_0}{(s_1 \wedge s_2)_0 \, (s_3 \wedge s_4)_0} \tag{3.81}$$

where we have used (3.78). Note that we can compute the brackets appearing in (3.77)-(3.78) using (3.57). In particular we have

$$\log (s_a \wedge s_b)_0 = \left(\frac{1}{2} \varpi_{ab} + \frac{1}{2} \bar{\varpi}_{ab} \right) + \int_{\mathbb{R}} \frac{d\theta}{2\pi} \frac{\log \left(1 + A_{ab}^- \right)}{\cosh \theta} \tag{3.82}$$

This formula is valid when there is a WKB line connecting P_a and P_b. If a bracket appears for which we do not have a WKB line, we can simply use the cross ratio (3.81) to eliminate it in terms of brackets that can be computed using (3.82).

Finally, using (3.80) in (3.79) and massaging the resulting spacetime dependence by extracting multiples of u and $(1 + u)$ we find

$$e^{2 \times \frac{\sqrt{\lambda}}{2} \Delta_a^2 \log \epsilon_a} = \prod_{a > b}^4 \left(|s_a \wedge s_b|_0 \right)^{-\sqrt{\lambda} \Delta_{ab}} \left(\frac{x_{ab}}{\mathcal{E}} \right)^{\sqrt{\lambda} \Delta_{ab}} \tag{3.83}$$

where $\Delta_{ab} = \left(\sum_c \Delta_c \right)/3 - \Delta_a - \Delta_b$. The extra factor of 2 in the exponent on the left hand side of (3.83) anticipates the sphere regularization which turns out to be similar to the AdS part and will be treated in section 3.5.1.

We recognize in (3.83) the canonical spacetime dependence in the 4-point function of a conformal field theory (compare with equation (3.1)). The appearance of the cut-off in (3.83) is related to the renormalization of the operators. In fact, if we define $\tilde{\mathcal{O}}_{\Delta_a} \equiv \mathcal{E}^{\Delta_a} \mathcal{O}_{\Delta_a}$ this will cancel the $\mathcal{E}$ factors in (3.83). To be more precise, we should define a 4-point function that is independent of the operator renormalization. The standard procedure is to divide by the appropriate product of 2-point functions such that normalization factors cancel. The same factors of $\mathcal{E}$ will appear in these 2-point functions and will cancel with those in (3.83). We will thus drop the factors of $\mathcal{E}$ in the formulas below.

3.4.3 Summary of the AdS and divergent contributions

We have now computed all the parts of (3.14). In this section we summarize the full result. The semiclassical limit of the 4-point function (3.1) is given by

$$\left(f_{fin}^{AdS} f_{div}^{AdS\times S} f_{fin}^{S}\right)^{*} \prod_{a<b}^{4} (x_{ab})^{\Delta_{ab}} \,, \tag{3.84}$$

where the $*$ denotes evaluation at $w_4 = w_4^*$ and we define

$$f_{fin}^{AdS}(w_4) = e^{-\frac{\sqrt{\lambda}}{\pi} A_{fin}} \tag{3.85}$$

$$f_{div}^{AdS\times S}(w_4) = e^{-2\frac{\sqrt{\lambda}}{\pi} A_{reg}} \prod_{a>b}^{4} (|s_a \wedge s_b|_0)^{-\sqrt{\lambda}\Delta_{ab}} \tag{3.86}$$

and f_{fin}^{S} will be defined momentarily. The contribution A_{fin} is given by (3.66), A_{reg} is given in (3.70), the brackets in $f_{div}^{AdS\times S}$ are given by (3.82).

The sphere part of the correlation function contains divergences of the same type as AdS. We therefore regularize it also by subtracting $\sqrt{T\bar{T}}$. Such finite contribution is what we denote by f_{fin}^{S}

$$f_{fin}^{S} \equiv e^{-\frac{\sqrt{\lambda}}{\pi} \int_{\Sigma} \left(S^5 \text{ contribution} - \sqrt{T\bar{T}}\right)} \,. \tag{3.87}$$

where S^5 contribution stands for the S^5 Lagrangian and wavefunctions [46]. To compensate this subtraction, we include the factor of 2 in front of A_{reg} in expression (3.86). In general we cannot complete the construction of the 4-point function because we are unable to compute the contribution f_{fin}^{S}. Fortunately, for correlators involving only BPS operators of the same type (e.g. only Z and $\bar{Z}$) the sphere part is known and we can assemble the full result. This is the subject of the next section.

3.5 Full correlation function for BMN operators

In this section we compute the full correlation function for operators of the type tr Z^{Δ} when Δ scales as $\sqrt{\lambda}$. For these type of operators, the sphere part f_{fin}^{S} was already known [59] and therefore we can complete our computation. We stress that, unlike the three point function, this four point correlator is not protected. In section 3.5.2, we comment on how to fix the location of the puncture w_4 by the Virasoro constraint and discuss some issues on the multiple string embedding configurations. In section 3.5.3 we perform an analytical check of our procedure by studying the extremal limit where $\Delta_2 = \Delta_1 + \Delta_3 + \Delta_4$, which is known to be protected from quantum corrections.

3.5.1 Sphere part

The sphere part of the correlation function involves the classical wave-functions associated to the external states. We consider specifically the correlation function of four BMN operators[21]

$$\langle \text{tr } Z^{\hat{\Delta}_1}(x_1) \text{ tr } Z^{\hat{\Delta}_2}(x_2) \text{ tr } \bar{Z}^{\hat{\Delta}_3}(x_3) \text{ tr } \bar{Z}^{\hat{\Delta}_4}(x_4) \,\rangle, \tag{3.88}$$

for which the wave-functions are known [60, 61]. The string dual of these operators corresponds geometrically to a string that is point-like in the sphere and rotates around an equator [62]. The surface developed by the worldsheet is not extended in the sphere.

Let X_i $(i = 1, ..., 6)$ be the coordinates in S^5. This particular string state can be expressed as

$$X_1 + iX_2 = e^{i\varphi} \qquad\qquad X_i = 0, \quad i = 3, \ldots, 6 \tag{3.89}$$

where φ is an azimuthal angle of the sphere. The wave-functions for $\text{tr } Z^{\hat{\Delta}_a}$ and $\text{tr } \bar{Z}^{\hat{\Delta}_a}$ are given respectively by

$$\Psi_{\hat{\Delta}_a} = e^{i\hat{\Delta}_a \varphi(w_a, \bar{w}_a)}, \qquad \bar{\Psi}_{\hat{\Delta}_a} = e^{-i\hat{\Delta}_a \varphi(w_a, \bar{w}_a)} \tag{3.90}$$

where the field φ is evaluated at the puncture corresponding to the respective operator insertion.

As the wave-functions scale exponentially with $\sqrt{\lambda}$, they will act as sources for the equations of motion for φ. The total sphere contribution is then given by

$$\exp\left[-\frac{\sqrt{\lambda}}{\pi}\left(\int d^2w\, \partial\varphi\bar{\partial}\varphi + i\pi\left(\Delta_3\varphi_{w=-1} + \Delta_4\varphi_{w=w_4} - \Delta_1\varphi_{w=1} - \Delta_2\varphi_{w=\infty}\right)\right)\right]. \tag{3.91}$$

Considering both the contributions from the S^5 action and wave-functions as an effective action, we obtain the equations of motion for φ which are solved by

$$\varphi(w, \bar{w}) = i\left(\Delta_3 \log|w+1| + \Delta_4 \log|w-w_4| - \Delta_1 \log|w-1|\right). \tag{3.92}$$

This solution has an additional singularity at infinity with charge $-\Delta_3 - \Delta_4 + \Delta_1 (\equiv -\Delta_2)$, corresponding to the wave-function inserted at infinity. This is consistent with R-charge conservation. We may now plug (3.92) into (3.91), introducing cut-off's around the punctures to regulate this contribution. This amounts to evaluate the solution at a

---

[21]We are using the following notation for the dimensions of the operators $\hat{\Delta}_a = \sqrt{\lambda}\Delta_a$.

distance ϵ away from the punctures. As in the case of the AdS action, the logarithmic divergences

$$\exp\left[\frac{\sqrt{\lambda}}{2}\sum_i \Delta_i^2 \log \epsilon_i\right] \tag{3.93}$$

need to be regularized. We do this by subtracting $\sqrt{T\bar{T}}$ from the integrand. To compensate, we add a similar contribution to the divergent part, that was already treated in the previous section (indeed, this regularization procedure is responsible for the factor of 2 appearing in front of A_{reg} in expression for $f_{div}^{AdS\times S}$, see (3.86)). The dependence on the cut-off's then disappears yielding the following expression for the regularized sphere action and wave-functions

$$f_{fin}^S = \exp\left[\sqrt{\lambda}\left(A_{reg} - \log 2^{\Delta_3\Delta_1} - \log \frac{|w_4-1|^{\Delta_1\Delta_4}}{|w_4+1|^{\Delta_3\Delta_4}}\right)\right], \tag{3.94}$$

where f_{fin}^S was defined in (3.87)

3.5.2 Fixing the fourth insertion point

We have shown how to compute the quantities (3.85)-(3.86) as a general function of w_4. However, to compute (3.84) we must still consider the Virasoro constraint in order to fix this fourth insertion. Notice, that we have not made explicit use yet of this condition. The Virasoro constraint requires that the full stress energy tensor $T_{AdS} + T_S$ must vanish. This translates into the condition

$$T_{AdS} = -T_S = -(\partial_w\varphi)^2. \tag{3.95}$$

that can be used to fix the parameter w_4. The other parameter U translates the additional degree of freedom of the cross ratio and that is one of the inputs of the problem (the other inputs are the conformal dimensions of the operators). They are both related by

$$\chi_{24}(\theta=0;U) = \frac{x_{14}\,x_{23}}{x_{12}\,x_{34}} \equiv u \tag{3.96}$$

by formulas (3.81) and (3.34).

Using the specific solution (3.92) and the conservation of R-charge, $\Delta_2 = \Delta_3 + \Delta_4 - \Delta_1$, we obtain that w_4 is fixed to be

$$w_4 = \frac{\Delta_1(-(U-2)) + \Delta_3(U+2) + \Delta_4 U}{2\,(\Delta_1 - \Delta_3)}. \tag{3.97}$$

Depending on the external parameters of the problem (conformal dimensions and cross ratio), the fourth insertion point w_4 might be located in any of the three intervals on the real axis. This will automatically fix the spike configuration described in section 3.2.3 and consequently the string embedding. In order to see this, consider the example of the WKB triangulation we have been studying. There exist *a priori* two choices for the orientations of the spikes, as discussed in section 3.2.3 and appendix C. Therefore, once we fix a cross ratio u the overall sign of χ_{24} will be fixed as a consequence of the formula 3.40[22] and so does the spike configuration. The conclusion is that the external data determines the orientation of the spikes and thus the configuration of the string embedding. This is in perfect agreement with the mapping between figure 3.1 and 3.2 and it is non-trivial that the integral equations encode this mapping.

3.5.3 Extremal Limit

In this section, we study the correlation function

$$\langle \text{tr } \bar{Z}^{\hat{\Delta}}(x_1) \text{ tr } Z^{\hat{\Delta}_2}(x_2) \text{ tr } \bar{Z}^{\hat{\Delta}}(x_3) \text{ tr } \bar{Z}^{\hat{\Delta}_4}(x_4) \rangle \tag{3.98}$$

in the extremal limit when

$$\Delta_2 = 2\Delta + \Delta_4. \tag{3.99}$$

Such correlator is protected from quantum corrections as conjectured in [63] and later proved in [64]. Thus, we expect to obtain the tree level gauge theory result which in the planar limit is simply given by Wick contractions

$$\frac{1}{x_{12}^{2\hat{\Delta}} \, x_{23}^{2\hat{\Delta}} \, x_{24}^{2\hat{\Delta}_4}}. \tag{3.100}$$

The *AdS* part of our formula is universal in the sense that it only depends on the dimensions of the operators. On the other hand, the sphere part of the correlation function involves the precise details of the operators inserted. Compared to the previous sphere calculation (3.88), computing (3.98) just amounts to take the complex conjugate of the wave function located at x_1, due to the replacement of $Z \to \bar{Z}$.

Let us start by studying the case when the cross ratio is $u = 1$ which also fixes the

---

[22]Of course the corrections to χ_{24} from iterating the integral equations will differ for the two different spike configurations but they should not change the overall sign of $\chi_{24}^{(0)}$. We are taking this as a physically motivated assumption in this discussion. We have checked this assumption in a few examples and found that it holds.
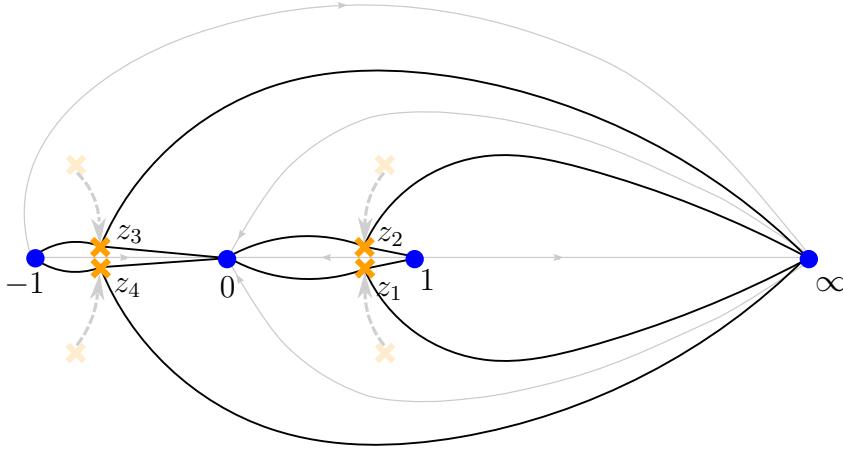
Figure 3.17: In the extremal limit, the main feature is that the zeros collide on the real axis. The black lines represent the WKB cells whereas the gray lines represent the WKB triangulation. At the exact extremal configuration, there are no WKB lines connecting 1 to 0 nor -1 to 0. We interpret this as a manifestation of the field theory fact that at tree level all operators are Wick contracted only to the fourth operator.

position of the fourth insertion at $w_4^* = 0$.[23] From this we will be able to see the general mechanism that gives the expected simplification of our result. The first important observation is that in this limit the zeros of $T(w)$ collide on the real axis as depicted in figure 3.17. Let us start by analyzing what this implies at the level of the χ-system. As the integrals ω_{14} and ω_{34} vanish, the χ's associated to these cycles, namely χ_{34} and χ_{14}, tend to -1. This observation has the remarkable consequence that the right hand side of all equations in the χ-system becomes trivially equal to 1 as one can easily verify [24]. As a re-

---

[23]One can argue for this as follows. Using conformal symmetry, we can fix three of the points in the target space at $x_3 = -1, x_1 = 1$ and $x_2 = \infty$ and also in the world-sheet at $w_3 = -1$, $w_1 = 1$ and $w_2 = \infty$. The fourth point x_4 will then be related to the cross ratio. For the particular choice of the cross ratio (3.81) equal to 1, the fourth point will be located at zero. Moreover if we choose the points at $x_3 = -1$ and $x_1 = +1$ to have the same conformal dimension and the same type of fields (say Z's) then this is a very symmetrical configuration. Going back to the worldsheet coordinates, by symmetry we expect to find $w_4^* = 0$. Of course, one can check this explicitly, by solving the χ-system.

[24]This trivialization of the χ-system is general and follows *just* from the fact that the two cycles ω_{14} and ω_{34} vanish which implies that the χ-functions χ_{34} and χ_{14} become -1. In the specific case of $U = w_4 = 0$ and $\Delta_1 = \Delta_3$, which turns out to correspond to cross ratio 1, the χ-system is already trivial because of the symmetry of the stress energy tensor in this particular point of the parameter space, see footnote 15). Nevertheless, we emphasize that the trivialization of the χ-system in general does not rely on this specific symmetry of the stress energy tensor.

sult, all χ-functions are *exactly* given by leading term of the WKB expansion (3.40)[25]. For convenience, let us introduce an infinitesimal δ defined by the condition $\delta = 2\Delta + \Delta_4 - \Delta_2$. At the end of the day, we will take $\delta \to 0$. In this limit, the solutions of the χ-system are then given by

$$\chi_{23} = \chi_{12} = -e^{-\frac{\pi(4\Delta-\delta)}{2}\cosh\theta}, \quad \chi_{34} = \chi_{14} = -e^{-\frac{\pi\delta}{2}\cosh\theta}, \quad \chi_{24} = \chi_{\hat{2}4} = e^{-\frac{\pi(2\Delta_z-\delta)}{2}\cosh\theta} \tag{3.101}$$

We may now plug this solution in the expression (3.51) and extract the cycles using as described in section $3.3.10$. We find that all A's vanish in the limit $\delta \to 0$ except for A_{14} and A_{34}, which tend to -1 as δ goes to zero. This implies that all $\eta_{E_{ab}}$ vanish except for η_{14} and η_{34}, which diverge since the integrand of these cycles becomes singular in this limit. However, one must go back to the area formula (3.66) and realize that such cycles are multiplied by a vanishing quantity. Indeed, (3.66) simplifies to

$$\frac{1}{4}\pi\delta\eta_{14} + \frac{\pi}{3} \, . \tag{3.102}$$

In the limit $\delta \to 0$, the first term of this expression is explicitly given by

$$\delta \int_0^\infty d\theta \, \cosh\theta \log\left(1 - e^{-\frac{1}{2}\pi\delta\cosh\theta}\right) + \mathcal{O}(\delta) = -\frac{\pi}{3} + \mathcal{O}(\delta). \tag{3.103}$$

Hence, it turns out that the finite AdS contribution vanishes in the extremal limit. We believe this is the general mechanism for any value of the cross ratio.

The computation of the sphere contribution follows the same steps as before, with a slight change on one vertex operator (recall that to get the extremal case, we replaced the operator located at x_1 in (3.88) by tr $\bar{Z}^{\hat{\Delta}}$). The new solution for the equations of motion is

$$\varphi(w, \bar{w}) = i\left(\Delta \log|w+1| + \Delta_4 \log|w| + \Delta \log|w-1|\right) . \tag{3.104}$$

Now when we compute the contribution of the sphere action and wavefunctions on this solution, we find that it *exactly* cancels the term $\sqrt{T\bar{T}}$ for Δ's satisfying (3.99). Consequently, the sphere part of the correlation function also vanishes in the extremal limit.

The divergent piece in the extremal becomes simply

$$e^{-\frac{\sqrt{\lambda}}{\pi}A_{reg}} \prod_{a>b}^4 (|s_a \wedge s_b|_0)^{-\sqrt{\lambda}\Delta_{ab}} \to \delta \int_{-\infty}^\infty \frac{d\theta}{2\pi\cosh\theta} \log(1-e^{-\frac{1}{2}\pi\delta\cosh\theta}) + \mathcal{O}(\delta) = \frac{\delta}{\pi}\log\frac{\pi\delta}{2} + \mathcal{O}(\delta) \tag{3.105}$$

---

[25]Indeed, when the right hand side of the χ-system is 1, the kernel term in equation (3.54) vanishes and we are left with leading WKB contribution.

which goes to zero as $\delta \to 0$. We are left with the spatial dependent part which, using that the cross-ratio is 1, can be written as

$$\frac{1}{\left(\frac{x_{12}}{\varepsilon}\right)^{2\hat{\Delta}} \left(\frac{x_{23}}{\varepsilon}\right)^{2\hat{\Delta}} \left(\frac{x_{24}}{\varepsilon}\right)^{2\hat{\Delta}_4}}. \tag{3.106}$$

This is nothing but the tree level result (3.100) of the gauge theory.

This section ends here. We have computed the AdS part of the four point function for heavy scalar operators in $\mathcal{N} = 4$ SYM in the classical limit. For the particular case of BPS operators on a line with a single scalar field, the sphere part is known and thus we can construct the full strong coupling four point function. We see no big obstacle in extending this computation for any number of operators using the method outlined here. With this we also conclude the first part of this thesis.

Part II

Scattering amplitudes from Integrability

Chapter 4

Overview of Scattering Amplitudes

We now devote our attention to another class of observables in $\mathcal{N} = 4$ SYM for which integrability serves as a precious tool in order to get non-perturbative results: the scattering amplitudes. Concretely, we will be interested in computing the color-ordered amplitudes and let us start by briefly review what they are (for a great review on scattering amplitudes see [67]). As a standard fact in a $SU(N)$ gauge theory with generators T^a with $a = 1, \ldots, N^2 - 1$, we are always able to decompose an $l-$loop amplitude into the so-called color ordered form

$$\mathcal{A}_n^{(l)} = N^l \sum_{\rho \in S_n/\mathbb{Z}_n} \mathrm{Tr}\left[T^{a_{\rho(1)}} \ldots T^{a_{\rho(n)}}\right] A_n^{(l)}\left(k_{a_{\rho(1)}} \ldots k_{a_{\rho(n)}}, \frac{1}{N}\right) + \text{multi-traces}. \quad (4.1)$$

The objects $A_n^{(l)}$ are often called the color-ordered amplitudes. We will consider the large N limit where we can neglect the multi-trace contributions as well as the subleading terms in N inside the color-ordered amplitude. These are the objects we are after and from now on we ignore any contribution from the color factors. The color-ordered amplitudes are functions of the momenta and the helicity configuration of the external particles.

Helicity structure   In order to handle the massless particles momenta, we now grasp over the spinor helicity formalism (see for instance [68]). The momentum p^μ of a given particle can be conveniently written in double index notation as

$$p^\mu = \sigma_{\alpha\dot\alpha}^\mu \, p^{\alpha\dot\alpha}. \quad (4.2)$$

The null momentum condition $p^2 = 0$ then translates into

$$\det(p^{\alpha\dot\alpha}) = 0, \quad (4.3)$$

which implies that it can be written as

$$p^{\alpha\dot\alpha} = \lambda^\alpha \tilde\lambda^{\dot\alpha} \,. \tag{4.4}$$

We then define the $SL(2)$ invariant contractions as

$$\langle \lambda\mu \rangle = \lambda^\alpha \mu^\beta \epsilon_{\alpha\beta} \,, \qquad [\lambda\mu] = \lambda_{\dot\alpha} \mu_{\dot\beta} \epsilon^{\dot\alpha\dot\beta} \tag{4.5}$$

and the ampitudes will then be expressed in terms of these brackets.

In $\mathcal{N}=4$ SYM the states are arranged into a CPT self-dual supermultiplet[1]. This is conveniently organized into a so-called superfield

$$\Phi(\eta) = g^+ + \tilde\eta^A \psi_A + \frac{1}{2}\tilde\eta^A \tilde\eta^B \phi_{AB} + \frac{1}{3!}\epsilon_{ABCD}\tilde\eta^A \tilde\eta^B \tilde\eta^C \bar\psi^D + \frac{1}{4!}\tilde\eta^4 g^- \,, \tag{4.6}$$

where the four $\tilde\eta$'s are Grassmann variables labeled by the $SU(4)$ index $A = 1,2,3,4$. Here $g^\pm$ is a gluon of positive/negative helicity, $\psi_A, \bar\psi^A$ are the four fermion pairs and $\phi_{AB} = -\phi_{BA}$ are the six real scalars.

These superfields can be considered as the superwavefunctions for the external lines of a superamplitude $\mathcal{A}_n(\Phi_1,\ldots,\Phi_n)$. The super amplitude is a polynomial in the η-variables which serve as bookkeeping variables of the particles being scattered. It is translational and supersymmetric invariant which allows us to write it as follows[2]

$$p_{\alpha\dot\alpha}\mathcal{A}_n = q_\alpha^A \mathcal{A}_n = 0 \Rightarrow \mathcal{A}_n(\Phi_1,\ldots,\Phi_n) = \delta^{(4)}(p_{\alpha\dot\alpha})\delta^{(8)}(q_\alpha^A)\mathcal{P}_n(\Phi_1,\ldots,\Phi_n)\,, \tag{4.7}$$

where $\delta^{(8)}(q_\alpha^A) = \prod_{A=1}^4 \prod_{\alpha=1,2} q_\alpha^A$ is a Grassmann delta function and $\mathcal{P}_n$ is a polynomial in the η variables. Given the fact that each variable $\tilde\eta_i^A$ carries one $SU(4)$ index and $\mathcal{P}$ should be a $SU(4)$ singlet, we conclude that this polynomial must contain only powers of 4 in the $\tilde\eta$ variables. More precisely, we write the scattering amplitude as sum of $SU(4)$ singlet homogeneous polynomials of degree multiple of 4

$$\mathcal{A}_n = \delta^{(4)}(p_{\alpha\dot\alpha})\,\delta^{(8)}(q_\alpha^A)\left(\mathcal{P}^{(0)} + \mathcal{P}^{(4)} + \mathcal{P}^{(8)} + \cdots + \mathcal{P}^{(4n-16)}\right)\,. \tag{4.8}$$

This function $\mathcal{A}_n$ can be regarded as a generating function for scattering amplitudes. Upon expanding in the η variables one can extract a particular amplitude corresponding to a specific configuration of external states. As an example, suppose we want to compute a

---

[1]This is due to the extended supersymmetry; in theories with less supersymmetry one would need a supermultiplet and its CPT conjugate separately.

[2]The supersymmetry generators are given by $q_\alpha^A = \lambda_\alpha \tilde\eta^A$ and $\bar q_{A,\dot\alpha} = \tilde\lambda_{\dot\alpha}\frac{\partial}{\partial\tilde\eta^A}$.

scattering amplitude with the i-th particle being a scalar. Then, using (4.6) one just needs to pick the term of the expansion with $\tilde{\eta}_i^A \tilde{\eta}_i^B$ for some A, B and similarly for other external states.

We note that the term $\delta^{(8)}(q_\alpha^A)$ is already of degree 8 in $\tilde{\eta}$. This means that the pure gluon amplitude must contain at least two negative helicity gluons. This is the maximally helicity violating (MHV) amplitude and corresponds to the first term $\mathcal{P}^{(0)}$ which is a polynomial of degree zero in $\tilde{\eta}$. The other terms correspond to NMHV, N²MHV, ... and the last term is the $\overline{\text{MHV}}$ which can be obtained from the MHV by CPT conjugation. For instance, the MHV amplitude is given at tree level by the famous Parke-Taylor formula [69],

$$\mathcal{P}_n^{(0)} = \frac{1}{\langle 12 \rangle \langle 23 \rangle \ldots \langle n-1\,n \rangle \langle n1 \rangle} \,. \tag{4.9}$$

IR divergences At loop level, the scattering amplitudes develop infrared divergences, with their origin either on the limit where a virtual gluon becomes soft (i.e. small energy limit) or in the limit where a virtual gluon becomes collinear with an external particle.

Let us consider the MHV amplitudes for an arbitrary number n of gluons and define the ratio

$$M_n = \mathcal{A}_n^{\text{MHV}} / \mathcal{A}_n^{\text{MHV,tree}} \,. \tag{4.10}$$

Because we are considering planar amplitudes, the exchange of the soft or collinear gluons processes ought to occur between neighbouring external particles and therefore the IR divergences will factorize into pieces that only depend on a single Mandelstam variable, namely $s_{i,i+1} = (p_i - p_{i+1})^2$. These infrared divergences were extensively studied in four dimensional gauge theories (see [65] and references therein). In particular, they are known to exponentiate. We are using here dimensional regularization and therefore the divergent piece will be a function of some cut-off ϵ and a scale μ_{IR}. Taking the log of the loop corrections M_n, we have [65],

$$\log M_n = \sum_{l=1}^{\infty} g^l \left[\frac{\Gamma_{\text{cusp}}^{(l)}}{(l\epsilon)^2} + \frac{\Gamma_{\text{col}}^{(l)}}{l\epsilon} \right] \sum_i \left(\frac{\mu_{IR}^2}{-s_{i,i+1}} \right)^{l\epsilon} + F_n^{\text{MHV}}(p_1, \ldots, p_n; g) + \mathcal{O}(\epsilon). \tag{4.11}$$

where the leading divergent term is governed by the cusp anomalous dimension Γ_{cusp}. Importantly, the divergent term is universal for the full superamplitude $\mathcal{A}_n$ (not only the MHV) and it completely factorizes. This factorized piece contains all the IR divergences of the amplitude.

This concludes our first look at the scattering amplitudes. We are now going to review a duality relating scattering amplitudes with Wilson loops, which will be central in the next chapter.

4.1 The Wilson Loop duality

Strong coupling   In the groundbreaking article [70], Alday and Maldacena suggested for the first time the existence of a duality between gluon scattering amplitudes and Wilson loops in the planar limit of $\mathcal{N} = 4$ SYM using the AdS/CFT correspondence.

They proposed a string theory prescription for computing scattering amplitudes at strong coupling, which we now review. In order to set up the argument, we start by considering the AdS$_5$ metric written in Poincaré coordinates,

$$ds^2 = R^2 \frac{dx_{3+1}^2 + dz^2}{z^2} \, . \tag{4.12}$$

The field theory asymptotic states are represented in the dual picture by open strings ending on a D-brane placed at some z_{IR}, which will serve as an infrared regulator, and in the end the limit $z_{IR} \to \infty$ will be taken. In sum, the problem consists of summing over worldsheets with topology of a disk with insertions at its boundary, embedded in AdS$_5$.

The field theory asymptotic gluon states carry 4-momentum k along the x direction, but on the D-brane, placed at z_{IR}, the proper momentum is instead $k_{pr} = k\frac{z_{IR}}{R}$. As z_{IR} is taken to infinity, with $z_{IR} \gg R$ and keeping the gluon momentum k fixed, the proper momentum becomes very large. We are left with a classical problem of finding the saddle point of the world sheet path integral, as was considered by Gross and Mende [71].

The boundary conditions for the saddle point are typically hard to formulate given the lack of explicit expressions for the vertex operators in AdS. Fortunately, in [70], it was proposed an efficient way of describing these boundary conditions. Let us define the T-dual variables as

$$\partial_\alpha y^\mu = \frac{iR^2}{z^2} \epsilon_{\alpha\beta} \partial_\beta x^\mu \, . \tag{4.13}$$

As argued in [70, 72], the boundary conditions in these variables become

$$\Delta y^\mu \equiv y^\mu(\sigma_{i+1}) - y^\mu(\sigma_i) = 2\pi k_i^\mu \tag{4.14}$$

where the k_i^μ is the momentum of the i-th gluon and σ_i the worldsheet position of the insertion. Importantly, once we define $r = \frac{R^2}{z}$, we recover again the AdS metric in the T-dual space,

$$ds^2 = R^2 \frac{dy_{3+1}^2 + dr^2}{r^2} \, . \tag{4.15}$$

This means that the regulator brane is now placed close to $r = 0$, which is the boundary of the AdS dual space. Moreover, the above boundary condition means that each vertex

operator insertion gets replaced by a segment line connecting two points whose separation is given by the 4-vector momentum carried by that vertex operator. Given that the gluons are massless and the conservation of total momentum is satisfied, the boundary condition for the worldsheet is a null polygon living on the boundary of the dual AdS space. This null polygon is constructed by concatenating the momenta of the scattered gluons one after another. Finally, the scattering amplitude at leading order at strong coupling is the area of the minimal surface[3] ending on this contour

$$A_n \propto \exp\left(-\frac{R^2}{2\pi} A_{min}\right) = \exp\left(-\frac{\sqrt{\lambda}}{2\pi} A_{min}\right) . \qquad (4.16)$$

It was further observed in [70], that this computation is formally identical to the computation of the expectation value of a Wilson loop on a light-like contour at strong coupling. This was the first hint towards the duality between Wilson loops and scattering amplitudes.

Weak coupling Inspired by this proposal, a similar relation between these two observables was found at weak coupling [73] shortly after [70]. Let us consider the MHV amplitudes for an arbitrary number n of gluons. The quantity M_n, defined in (4.10), splits into a divergent part Z_n^{MHV} which includes the IR divergences of the amplitude and a finite part F_n^{MHV} which we write down as

$$\ln M_n = Z_n^{\mathrm{MHV}} + F_n^{\mathrm{MHV}} . \qquad (4.17)$$

The piece F_n is a function of the momentum invariants $(p_i + \cdots + p_{i+j-1})^2$, and it is scheme independent (up to an additive constant). As we saw, the coefficient of the most divergent term of Z_n^{MHV} is given by the cusp anomalous dimension Γ_{cusp} and the subleading terms divergent terms are scheme dependent.

On the other side of the duality, we have the Wilson loop defined on a null polygonal contour C_n with light-like segments formed by the external on-shell gluon momenta,

$$k_i^\mu = x_{i+1}^\mu - x_i^\mu . \qquad (4.18)$$

The (bosonic) Wilson loop is defined as[4]

$$W[C_n] = \frac{1}{N} \mathrm{Tr}\, \mathcal{P} \exp\left[ig \int_{C_n} dt \frac{dx^\mu}{dt} A_\mu(x(t))\right] . \qquad (4.19)$$

---

[3]More precisely it has only to be the extremal surface, according to the discussion in [72].

[4]The Maldacena-Wilson loop introduced in [74] comprises an additional term involving scalars. However, for a light-like contour it coincides with the standard Wilson loop.

It also factorizes in a divergent factor Z_n^{WL} coming from the cusps and a finite piece F_n^{WL},

$$\ln W[C_n] = Z_n^{\mathrm{WL}} + F_n^{\mathrm{WL}}\,. \tag{4.20}$$

The statement of the duality is that the finite pieces coincide up to an unimportant additive constant c,

$$F_n^{\mathrm{MHV}} = F_n^{\mathrm{WL}} + c\,. \tag{4.21}$$

Moreover, the divergent pieces also coincide upon an identification of the parameters in the two renormalization schemes. In particular, both leading divergences (IR divergence on the amplitude side and UV divergence on the Wilson loop side) are governed by the cusp anomalous dimension. This equality was observed perturbatively up to two loops and for six particles [73].

Super Wilson loop The duality between MHV amplitudes and bosonic Wilson loops instigated research for its extension to super amplitudes and some sort of supersymmetric Wilson loop. Around the same time, two proposals for such a super Wilson loop were put forward in [75, 76]. The first proposal has its origin in the momentum twistor space and replaces the integral of the standard connection by an integral of a superfield over the supertwistor space.

The second proposal was designed exclusively for null polygonal contours and it is perhaps given in a more familiar language. It endows the Minkowski spacetime with Grassmann variables

$$\eta_i^A\,, \qquad i = \{1,\ldots,n\} \quad A = \{1,\ldots,4\}\,, \tag{4.22}$$

which[5] are assigned to each edge of the polygon (index i) and transform in the fundamental of the $SU(4)$ R-symmetry (index A). The proposed generalization of (4.19) is

$$W[C_n] = \frac{1}{N}\mathrm{Tr}\left(\mathcal{V}_{n1}\mathcal{W}_n\mathcal{V}_{n-1,n}\ldots\mathcal{W}_2\mathcal{V}_{12}\mathcal{W}_1\right)\,. \tag{4.23}$$

where $\mathcal{V}_{i,i+1}$ are some operator insertions at the cusps of the polygon with the property that $\mathcal{V}_{i,i+1} = 1 + \mathcal{O}(\eta)$. Additionally,

$$\mathcal{W}_j = \mathcal{P}\exp\left(ig\int dt\mathcal{E}_j(t)\right) \tag{4.24}$$

---

[5]These η-variables are related to the $\tilde\eta$-variables introduced before by the relation $\tilde\eta_i = (\langle i-1i\rangle\eta_{i+1} + \langle ii+1\rangle\eta_{i-1} + \langle i+1i-1\rangle\eta_i)/\langle i-1i\rangle\langle ii+1\rangle$

is a generalized parallel transport along the edge p_j with $\mathcal{E}_j = \frac{dx_j^\mu}{dt} A_\mu + \mathcal{O}(\eta)$. It is clear that the leading term in the η expansion is the the standard bosonic Wilson loop as in (4.19). The explicit expressions of $\mathcal{E}_j$ and $\mathcal{V}_{i.i+1}$ are such that $W[C_n]$ is supersymmetric in the sense $\mathcal{Q}_A W = 0$[6] and they can be found in [76]. It is this supersymmetric Wilson loop that is conjectured to be dual to super amplitudes. In particular, it has the following expansion

$$W_{\text{super}} = W_{\text{MHV}} + \eta_i^1 \eta_j^2 \eta_k^3 \eta_l^4 \ W_{\text{NMHV}}^{(ijkl)} + \eta_i^1 \eta_j^2 \eta_k^3 \eta_l^4 \eta_m^1 \eta_n^2 \eta_o^3 \eta_p^4 \ W_{\text{N}^2\text{MHV}}^{(ijkl)(mnop)} + \ldots \tag{4.25}$$

where $W_{\text{N}^k\text{MHV}}$ is the N^{k}MHV amplitude divided by the Parke-Taylor MHV factor.

Dual superconformal symmetry   Besides the standard conformal symmetry, the planar scattering amplitudes turned out to reveal an additional *dual conformal symmetry*. This new symmetry is the ordinary conformal symmetry from the Wilson loop point of view. Therefore, the existence of this extra symmetry in the amplitudes can be regarded as a natural consequence of the duality. Furthermore, it was later extended to a full dual superconformal symmetry. This is better exhibited by introducing the dual variables related to the standard ones $(\lambda_i, \tilde{\lambda}_i, \tilde{\eta}_i)$ by

$$\lambda_i^\alpha \tilde{\lambda}_i^{\dot\alpha} = x_i^{\dot\alpha\alpha} - x_{i+1}^{\dot\alpha\alpha}, \qquad \lambda_i^\alpha \tilde{\eta}_i^A = \theta_i^{\alpha A} - \theta_{i+1}^{\alpha A}, \tag{4.26}$$

where the periodicity conditions $x_{n+1} = x_1$ and $\theta_{n+1} = \theta_1$ are assumed. The first change of variables is nothing but the one appearing in (4.18). The dual superconformal generators are first order differential operators in the dual and standard $(\lambda_i, \tilde{\lambda}_i, \tilde{\eta}_i)$ variables and their expressions can be found in [118]. The dual superconformal symmetry can then be stated as follows. First, it was noticed that the full planar superamplitude $\mathcal{A}_n$ and its MHV component share the same IR divergences and they carry the helicity and the dual conformal weights of the scattered particles (so that they transform covariantly under the dual conformal symmetry). Hence it is convenient to factor out the MHV component and rewrite the superamplitude as

$$\mathcal{A}_n = \mathcal{A}_n^{\text{MHV}} \left(1 + R^{\text{NMHV}} + R^{\text{N}^2\text{MHV}} + \cdots + R^{\overline{\text{MHV}}} \right), \tag{4.27}$$

where $R^{\text{N}^k\text{MHV}}$ are called the ratio functions and are finite at all loops (i.e. free of IR divergences). These functions are *invariant* under the standard and dual superconformal

---

[6]These generators are the half of the dual supersymmetry generators, $\mathcal{Q} = (Q, \bar{S})$. The other half of the susy generators $\bar{\mathcal{Q}}$ do not annihilate the superloop due to anomalies originated by quantum corrections and give rise the so-called $\bar{\mathcal{Q}}$-equation.

transformations at tree level. At loop level, some of the dual superconformal symmetries are broken by quantum corrections and give rise to anomalous Ward identities (see [90] for a detailed treatment of dual superconformal symmetry).

4.2 The Operator Product Expansion program

The above duality mapped a scattering amplitude into another four dimensional observable, the Wilson loop. Despite the obvious richness and insight of this duality, it does not yet provide the natural playground for integrability, which only exhibits its power in two dimensions. Built upon the developments reviewed in the previous sections, the 2010's article [79] revealed the two dimensional arena for integrability and set a new path towards the exact solution for scattering amplitudes. It goes by the name of OPE for Wilson loops, and that is the core of the second part of this thesis. Later a refinement of these ideas gave rise to the pentagon OPE approach (POPE). Rehashing over the incarnation of integrability in the scattering problem is the topic of this and forthcoming sections.

4.2.1 The OPE for Wilson Loops

Let us start by reviewing how the standard OPE in conformal field theory works. Consider k operators inserted at the positions x_k. Pick two of them say $\mathcal{O}_1$ and $\mathcal{O}_2$ and surround them by a sphere according to the figure 4.1. This generates some state $|\Psi\rangle$ on the surface of the sphere, defined as

$$|\Psi\rangle = \mathcal{O}_1(x)\mathcal{O}_2(0)|0\rangle \tag{4.28}$$

This state can then be expanded in terms of eigenstates of the dilatation operator, which we refer to as energy eigenstates. Each of this energy eigenstates is in correspondence to a primary operator or its descendants inserted at the origin by the operator-state correspondence. So we can write

$$\mathcal{O}_1(x)\mathcal{O}_2(0)|0\rangle = \sum_{\text{primaries } \mathcal{O}_n} C_n(x, \partial_z)\mathcal{O}_n(z)|_{z=0}|0\rangle \,, \tag{4.29}$$

where $C_n(x, \partial_z)$ can be expanded in powers of the ∂_z. Let us consider for instance the contribution of a scalar primary $\mathcal{O}_n$. Then we have

$$C_n(x, \partial_z)\mathcal{O}_n(z)|_{z=0} = \frac{\text{constant}}{|x|^{E_n}} \left(\mathcal{O}_n(0) + \dots\right) \,, \tag{4.30}$$
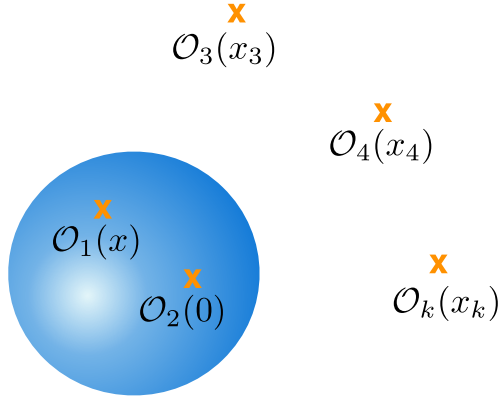
89

Figure 4.1: In the standard OPE for correlation functions of local operators, we surround two of the operators by a sphere which defines a state on its surface. We then decompose it over the eigenstates of the dilatation operator. These correspond to the primaries and their descendants.

for some constant E_n to be determined and the dots represent the descendants. This is the standard OPE expansion for a CFT. A further constraint on the form of this expansion comes from applying the dilatation operator to $\mathcal{O}_1$ and $\mathcal{O}_2$. That fixes the constant E_n to be $E_n = \Delta_1 + \Delta_2 - \Delta_n$, where Δ_n is the conformal dimension of the operator $\mathcal{O}_n$.

Now, let us suppose we want to compute the k-point function,

$$\langle \mathcal{O}_1(0)\mathcal{O}_2(x)\ldots\mathcal{O}_k(x_k)\rangle. \tag{4.31}$$

Using the OPE of the operators 1 and 2, we obtain that

$$\langle \mathcal{O}_1(0)\mathcal{O}_2(x)\ldots\mathcal{O}_k(x_k)\rangle = \sum_n e^{-E_n t}\, C_{12n}C_{n3\ldots k}\,. \tag{4.32}$$

Identifying the time t with $\log|x|$, we interpret this result as a sum over states that are propagating out of the sphere with energy E_n. The coefficients $C_{ij\ldots}$ are in principle complicated functions of all insertion points and contain dynamic information of the theory. The fundamental object is the three point vertex C_{12n}, from which all higher point correlators should be reconstructed.

This expansion is by no means unique as we could as well surround other set of operators by spheres and play the same game. The consistency of the expansion in different channels is required and it puts strong constraints on the correlation function, eventually determining it completely. This is known as the *conformal bootstrap* and it is currently a very active field of research (see for instance [77]).

The OPE for Wilson loops has its origin on a similar idea. Consider a null polygonal Wilson loop and pick two of its non intersecting edges. Then we divide the Wilson loop into a bottom and a top part by cutting it along some imaginary line intersecting these two edges as
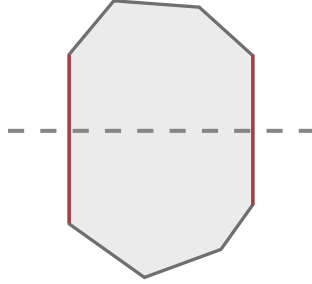
$$(4.33)$$

and we sum over the states that propagate through the cut. These states are in correspondence to the excitations of the flux tube that ends on these two selected null lines. They are well studied in literature and in the case of $\mathcal{N} = 4$ SYM they have different incarnations. They can be regarded as excitations around the infinite spin limit of high spin operators like $\text{Tr}[\Phi D_+^S \Phi]$ which have a spin chain description. Alternatively, using the gauge/gravity duality, they correspond to excitations around the GKP string. The dimensions of these operators can be computed at any value of the coupling constant following the work [80]. This sets the two dimensional integrable auxiliary problem we were after.

Finally, the geometry of the Wilson loop emerges when we act with some symmetries associated to these two selected null lines on the bottom part of the loop, in the same way as we acted with the dilatations on a subset of operators in the standard OPE for correlation functions. These symmetries are the ones that govern this OPE expansion and we now briefly review them.

Symmetries of a square Wilson loop   Let us first consider two null Wilson lines in $R^{1,3}$ which by conformal transformations can be mapped to the subspace $R^{1,1}$. In $R^{1,1}$, let us place one of the lines along x^- and the other at null infinity. The two lines break some symmetries of the full conformal group but preserve the following

- dilatations, D,

- boosts in $x^\pm$, M^{+-},

- rotations in the transverse directions, M^{12},

- translations in the x^- direction, P_-,

- special conformal transformations K^-.

If we consider the set of symmetries $\{D + M^{+-}, P_-, K_-\}$ then they form a subgroup $SL(2, R)$ that commutes with the remaining symmetries $\{D - M^{+-}, M^{12}\}$. This last set of symmetries keeps the points on the two null lines invariant, whilst the first set actually move points along those lines. In sum, this system of two null lines preserve $SL(2, R) \times R \times SO(2)$, where $SL(2, R)$ acts on x^-, R essentially corresponds to dilatations on x^+ and $SO(2)$ are the rotations in the transverse directions.

We now consider a null square which will play a major role in the precise construction of the OPE for Wilson loops. The square can be defined from the two infinite null lines system as we now describe. Take a point on one of the null lines to be a vertex of the square. Once that point is chosen, there will be another point in the other null line that is null separated from the first. That defines one edge of the null square. We complete the square by choosing another point on the null line according to the following figure
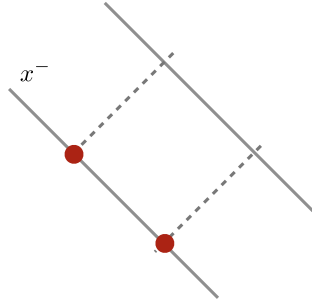
$$(4.34)$$

and in this way we define a null square. As far as the symmetries are concerned, it is clear that translations P_- and special conformal transformations K^- are broken since they do not preserve the two new edges of the square. Hence, the subgroup $SL(2, R)$ is broken down to R corresponding to the generator $D + M^{+-}$. Therefore, the three (commuting) symmetries of the null square are $R \times R \times SO(2)$. As a convention the generator $H \equiv D + M^{+-}$ is called the 'Hamiltonian' and the corresponding direction in which it moves points is parameterized by τ (so that the Hamiltonian acts as ∂_τ). Similarly, the generator $P \equiv D - M^{+-}$ is designated by 'momentum' and the conjugate coordinate is σ (so that momentum acts as ∂_σ) and finally the last generator $J \equiv M^{12}$ is dubbed as 'angular momentum' conjugated to the angle ϕ (and also acts as ∂_ϕ). We illustrate this parametrization of the square in figure 4.2.

The states propagating in this OPE expansion are characterized by the energy, momentum and spin in the transverse direction, precisely the eigenvalues of the symmetry generators of the square. To isolate the contribution of the various quantum numbers,
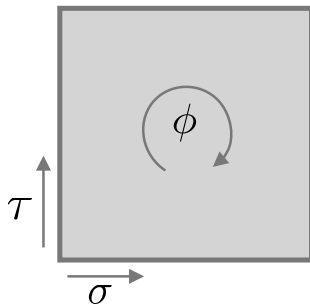
Figure 4.2: The three symmetries of the square are parametrized by the coordinates τ in the vertical direction, σ in horizontal direction and ϕ on the transverse direction to the plane where the square sits.

it turns out to be useful to introduce a three parameter family of polygons as we now describe.

Parametrizing a null polygon   To introduce a parametric family of polygons, we first break the null polygon in the way outlined above. Select two non consecutive null sides of the polygon and extend them to two null infinite lines. Then pick two points of one of the two null lines, see figure 4.3, and this defines a *reference* null square as described before. Moreover, we can cut the null Wilson loop into a bottom and a top part also illustrated in figure 4.3.

As we have seen the square preserves some symmetries, generated by

$$M = e^{\tau \partial_\tau + \sigma \partial_\sigma + \phi \partial_\phi} = e^{-\tau H + i\sigma P + i\phi J} \ . \tag{4.35}$$

We now act with these symmetries in the bottom part and leave the top part invariant, resembling the procedure we used in the OPE for correlation functions. This modifies the geometry of the polygon and such change is parametrized by τ, σ, ϕ, which are the conjugate coordinates to the three symmetries of the reference square.

The essential point now is to perform an expansion in terms of the eigenstates of the three operators generating the symmetries of the square. Those eigenstates correspond to the excitations of the color electric flux tube in between the two null lines that we selected to cut the Wilson loop. By introducing the parametric family of polygons we can now separate the different contributions of the different excitations of the flux tube according to their quantum numbers. Once again, this parallels the standard OPE for local operators where the expansion is organized in terms of their conformal dimension and spin.
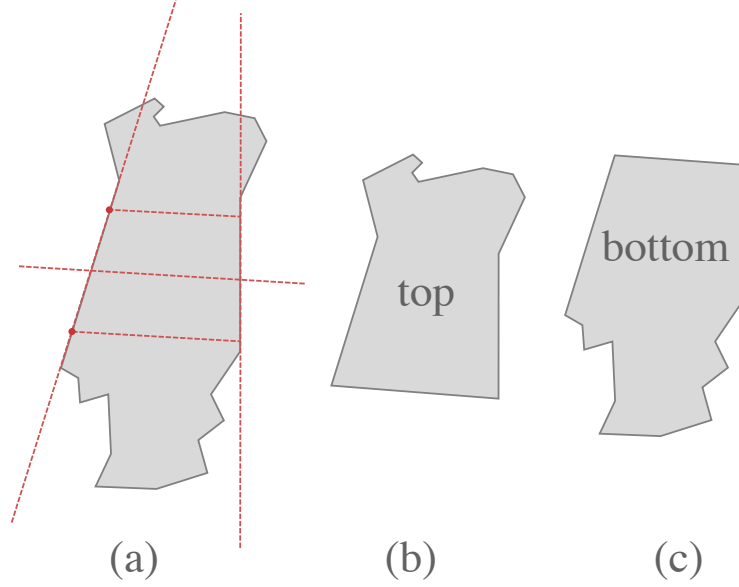
Figure 4.3: (a) In a general null polygon we define a square by first selecting two non consecutive edges and prolong them into two null lines. We then choose two points on these null lines. Once we choose them there will be two other points on the other null line that are null separated from the first. This defines a reference square. (b) We apply the symmetries of this reference square to the bottom cusps of the polygon. This parametrizes the polygon by the three coordinates of the reference square. In the limit of large τ, the bottom of the polygon is flattened and we get what we call the top part. This limit is usually known as the collinear limit. (c) Alternatively we could have applied the symmetries to the top half of the polygon. Then in the large τ limit we would flatten the top and we would get what we call the bottom part.

More precisely, we expect to have an expansion of the form

$$\langle W \rangle = \int dp \, e^{ip\sigma} \sum_m e^{im\phi} \sum_{E(m,p)} C(m,p) e^{-E(m,p)\tau} + \text{two particles} + \dots \tag{4.36}$$

where the function $C(m,p)$ factorizes into a contribution from the bottom and top

$$C = C_{\text{bottom}} C_{\text{top}} . \tag{4.37}$$

C_{bottom} (C_{top}) correspond to the overlap of the intermediate states with the bottom (top) part of the polygon. In order to make (4.36) precise one needs to take care of the UV

94

divergences of the Wilson loop that break these symmetries. However, these divergences are well understood and can be handled in several simple ways. We will come back to this point, but for now let us treat these symmetries as exact.

At large τ, it is clear that the lowest lying states (in particular the single particle states) dominate the expansion. The limit of large τ is called the collinear limit, and it corresponds to the flattening of the bottom part of the polygon. In other words, as $\tau \to \infty$ the polygon degenerates into the top part represented in figure 4.3 (b).

In the next section, we present a more concrete and refined version of these ideas that goes by the name of pentagon OPE, and it is the main subject of the second chapter of this part of the thesis.

4.3 The Pentagon OPE (POPE) in perspective

The POPE approach's main novelty with respect to what we have just seen is a different decomposition of the Wilson loop not only in a bottom and top parts, but rather into smaller building blocks: *squares* and *pentagons*.

There is a canonical way of breaking the null polygon in terms of squares as explained in figure 4.4. The middle squares, which result from the overlap of two pentagons, assume particular importance. In a n-sided polygon, there are $n-5$ such middle squares. Each of these squares has 3 symmetries, parametrized by the coordinates σ_i, τ_i, ϕ_i as we have just seen in the previous section, resulting in a total of $3(n-5)$ parameters. This number coincides precisely with the independent number of conformal cross ratios. We now act with each of this symmetries to the bottom cusps of the respective middle square. Therefore, we coordinatize all conformally independent n-sided polygons.

Concerning the dynamics, we start with a flux tube vacuum state on the bottom square. It undergoes a transition to the following square, governed by the so-called pentagon transition $P(0|\psi_1)$, where the zero in the first argument of P represents the vacuum. In this square (the first middle square), we sum over all possible flux tube states ψ_1, which correspond to the eigenstates of the operators that generate the symmetries of that square. These states propagate freely on the square and then undergo again into a transition to the following square governed by some pentagon transition $P(\psi_1|\psi_2)$. We repeat this procedure for all middle squares, summing over all flux tube states, and in the final square we have again the vacuum. In sum, we have the following sequence:

$$\text{vacuum} \to \psi_1 \to \psi_2 \to \cdots \to \psi_{n-5} \to \text{vacuum} \,. \tag{4.38}$$
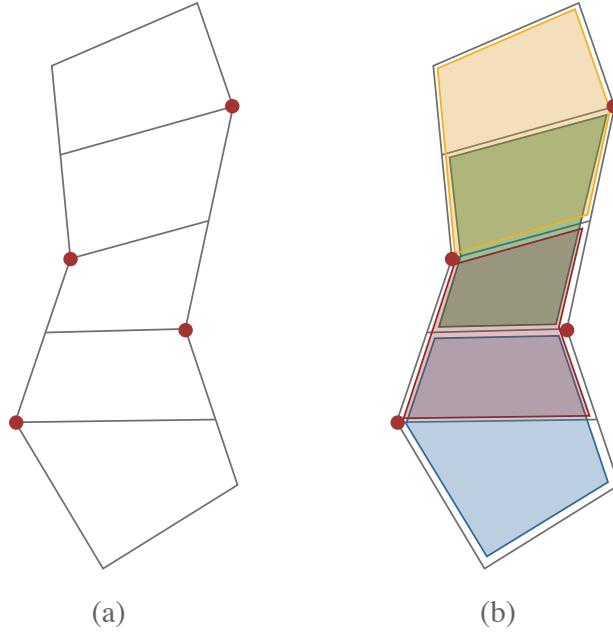
Figure 4.4: (a) We exemplify a canonical way of breaking a null polygon into a squares. Pick one of the lower cusps of the polygon (the lowest red point on the figure) and draw a null line emanating from it that intersects the polygon at another point. This defines the first square, in the very bottom of the polygon. Pick the next cusp (the next to lowest red point in the figure) and from it draw another null line that intersects the polygon at some other point. That defines another square. We proceed in this way until we reach the top of the polygon. (b) Each pair of squares define a pentagon. For instance, the two lowest squares together form the pentagon in blue.

Taking into account the pentagon transition between two eigenstates of the color flux tube, we get a representation of the Wilson loop $\mathcal{W}_n$ in the form of an infinite sum over all states,

$$\mathcal{W}_n = \sum_{\psi_i} P(0|\psi_1)P(\psi_1|\psi_2)\ldots P(\psi_{n-6}|\psi_{n-5})P(\psi_{n-5}|0)\, e^{\sum_j(-E_j\tau_j + ip_j\sigma_j + im_j\phi_j)}\,, \qquad (4.39)$$

with $\{\tau_i, \sigma_i, \phi_i\}$ a base of conformal cross ratios, which receive individually meaning of time, space and angle in the i'th OPE channel [79, 81].

We shall refer to the summand arising in this representation, as the *POPE integrand*. This integrand depends, amongst other things, on the $n-5$ flux tube states which propagate in each of the $n - 5$ middle squares. Such states are generically N-particle states which
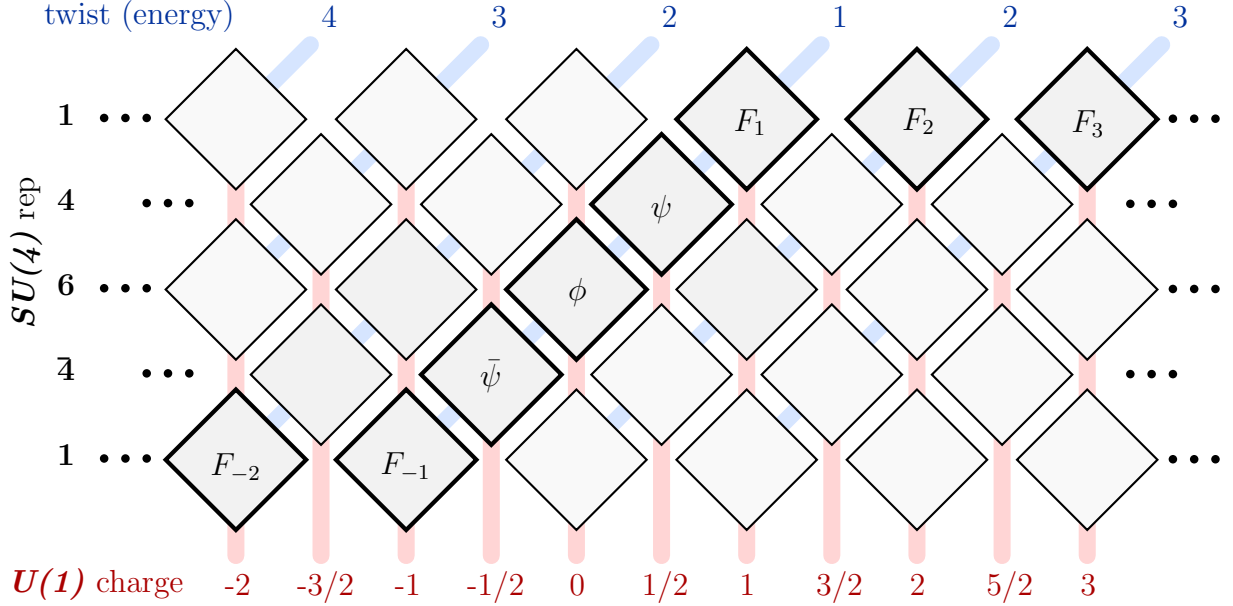
Figure 4.5: Fundamental excitations of the flux tube. In the main diagonal we have the gluons, scalars and fermions and in the top and bottom horizontal rows we have the gluon bound states. Here $F_1 \equiv F_{z-}$ and $F_{-1} \equiv F_{\bar{z}-}$, where the subscript $\mu = -$ in $F_{\mu\nu}$ denotes the light-like direction identified with the σ direction of the flux tube while $\nu = z = 1 + i2$ and $\nu = \bar{z} = 1 - i2$ stand for right- and left-handed polarizations with respect to the $1 - 2$ plane transverse to the flux tube. $F_{\pm a}$ is then a bound-state composed a excitations $F_{\pm 1}$.

correspond to N excitations on top of the GKP vacuum and N can be $0, 1, 2, \ldots$. Being an integrable system the charges of the state (energy, momentum and spin) are the sum of the individual charges of the excitations. The energy and momentum of each excitation can be parametrized by a Bethe rapidity u_i. Hence, a state is parametrized by a set of rapidities $\{u_1, \ldots, u_N\}$. The set of excitations is composed by scalars, fermions, gluons and bound-states of gluons [80] (see figure 4.5). For instance, we could have, in the i-th square, a state with two gluons of positive helicity, a bound state of two gluons of negative helicity, one scalar and a pair of fermions:[7]

$$\mathbf{\Psi}^{(i)} = \left\{ F_1(u_1), F_1(u_2), F_{-2}(u_3), \phi^{AB}(u_4), \psi^C(u_5), \psi^D(u_6) \right\} . \tag{4.40}$$

What makes this decomposition extremely powerful in planar $\mathcal{N} = 4$ SYM theory is

---

[7]Here A, B, C and D are $SU(4)$ R-charge indices and the indices on F indicate the helicity of the gluonic excitation.

that all of its building blocks can be computed at any value of the coupling thanks to the integrability of the underlying theory. Namely, the flux tube spectrum is, as we mentioned before, under total control [80] and the pentagon transitions can be bootstrapped [81–84] following (a slightly modified version of) the standard form factor program for integrable theories.

Through the celebrated duality between null polygonal Wilson loops and scattering amplitudes [73, 85], the decomposition (4.39) provides a fully non-perturbative representation of the so-called Maximal Helicity Violating (MHV) gluon scattering amplitudes in planar $\mathcal{N} = 4$ SYM theory.

In the next chapter, we will extend the OPE to the full super Wilson loop beyond the MHV paradigm. On the way, we will make this OPE expansion more precise and define the renormalized Wilson loop where the UV divergences are treated.

Chapter 5

The POPE for all Helicity Amplitudes

In this chapter we will argue that a suitable generalization of the pentagon transitions into super or *charged* pentagon transitions allows one to describe all amplitudes, for any number of external particles with arbitrary helicities and at any value of the 't Hooft coupling. We will then formulate precisely the POPE integrand and provide all its coupling dependent building blocks.

While the key ingredient in having an OPE expansion such as (4.39) is conformal symmetry, a central ingredient in the charged pentagon approach will be supersymmetry. The idea of charging the pentagons first appeared in [82] where certain charged transitions were introduced and successfully compared against N^kMHV amplitudes. More recently, further charged transitions were bootstrapped and matched with amplitudes in [84, 86, 87]. We are going to complete this picture by proposing a simple map between all possible helicity amplitudes and all the ways charged pentagons can be patched together into an OPE series like (4.39). An interesting outcome of this charged pentagons analysis is a simple proposal for how parity acts at the level of the super Wilson loop.

5.1   The Charged Pentagon Program

In the dual Wilson loop picture, N^kMHV amplitudes are computed as we have seen by a super Wilson loop decorated by adjoint fields inserted on the edges and cusps [76, 88]. It is this super loop that we want to describe within the pentagon approach.

At first, let us ask ourselves what would be a natural extension of (4.39) that allows for some regions of the loop to be *charged* due to the insertion of these extra fields. The minimal modification one could envisage is to generalize the pentagon transitions to super pentagon transitions or *charged* transitions, in which $P(\psi|\psi')$ stands as the bottom component. As for the $\mathcal{N} = 4$ on-shell super field, a pentagon would naturally come in multiple of five components

$$\mathbb{P} = P + \chi^A P_A + \chi^A \chi^B P_{AB} + \chi^A \chi^B \chi^C P_{ABC} + \chi^A \chi^B \chi^C \chi^D P_{ABCD} \,, \qquad (5.1)$$

where χ is a Grassmann parameter, $A = 1, 2, 3, 4$ an R-charge index, and where, for sake of clarity, we have suppressed the states ψ and ψ'. With these charged transitions at hand, we could now imagine building up charged polygons such as

$$\mathcal{P}_A \circ \mathcal{P}^A \equiv \sum_{\psi_1} P_A(0|\psi_1) P^A(\psi_1|0) e^{-E_1 \tau_1 + \cdots} \,,$$

$$\mathcal{P}_{AB} \circ \mathcal{P} \circ \mathcal{P}^{AB} \equiv \sum_{\psi_1, \psi_2} P_{AB}(0|\psi_1) P(\psi_1|\psi_2) P^{AB}(\psi_2|0) e^{-E_1 \tau_1 + \cdots} \,, \qquad (5.2)$$

$$\mathcal{P}_{AB} \circ \mathcal{P}_{CD} \circ \mathcal{P}^{AB} \circ \mathcal{P}^{CD} \equiv \sum_{\psi_1, \psi_2, \psi_3} P_{AB}(0|\psi_1) P_{CD}(\psi_1|\psi_2) P^{AB}(\psi_2|\psi_3) P^{CD}(\psi_3|0) e^{-E_1 \tau_1 + \cdots}$$

and so on. Here, an upper index represents a contraction with an epsilon tensor. Namely, we use $P^A = \epsilon^{ABCD} P_{BCD}$, $P^{AB} = \epsilon^{ABCD} P_{CD}$ and $P^{ABC} = \epsilon^{ABCD} P_D$ to compress the expressions above.

The most obvious change with respect to the MHV case is that R-charge conservation now forbids some of the processes which were previously allowed and vice-versa. For instance, in the creation amplitude $P_{AB}(0|...)$ we can produce a scalar ϕ_{AB} out of the vacuum, since this excitation has quantum numbers that match those of the charged pentagon. At the same time, neutral states such as the vacuum or purely gluonic states – which appeared in the non-charged transitions – can no longer be produced by this charged pentagon.

What stays the same is that all these charged transitions can be bootstrapped using integrability – as much as their bosonic counterparts. The *scalar* charged transition P_{AB} and the *gluon* charged transition P_{ABCD}, for instance, already received analysis of this sort in [82, 84].[1] The fermionic charged transitions, P_A and P_{ABC}, were more recently constructed in [86, 87].

The super pentagon hypothesis (5.1) and its OPE corollary (5.2) are the two main inputs in the charged pentagon program for helicity amplitudes. In the rest of this section

---

[1] Both were denoted by P_* in these works.

we present a simple counting argument supporting the equivalence between super OPE series and super amplitudes.

The important point is that not all the N^kMHV amplitudes are independent. Because of supersymmetry, many of them get linked together by means of so-called SUSY Ward identities. At given number n of particles, there is a basis of $\mathcal{N}(k,n)$ amplitudes in terms of which one can linearly express all the remaining ones.

The problem of eliminating this redundancy, such as to count the $\mathcal{N}(k,n)$ independent amplitudes, was beautifully analyzed in [89]. As explained below, the very same counting applies to inequivalent super OPE series like (5.2).

Counting the number of super OPE series is relatively easy:

At first, one notices that the R-charge of a polygon is always a multiple of four, as a consequence of $SU(4)$ symmetry. The first two cases in (5.2), for instance, involve charged pentagons with a total of 4 units, as for NMHV amplitudes, while the last example in (5.2) has a total of 8 units of charge, and should thus be related to N^2MHV amplitudes.

In the NMHV case, the amount of charge in each of the $n-4$ pentagons uniquely specifies the super OPE series and there is clearly $(n-1)(n-2)(n-3)(n-4)/4!$ ways of distributing four units of charge between the $n-4$ pentagons in our tessellation. Precisely this number is reported for $\mathcal{N}(1,n)$ in [89], see discussion below (3.12) therein.

This kind of partitions no longer enumerate all cases starting with N^2MHV amplitudes. For instance, there are three independent ways of charging all the four pentagons of an octagon with two units of charge,

$$ \mathcal{P}_{AB} \circ \mathcal{P}_{CD} \circ \mathcal{P}^{AB} \circ \mathcal{P}^{CD} \,, \quad \mathcal{P}_{AB} \circ \mathcal{P}^{AB} \circ \mathcal{P}_{CD} \circ \mathcal{P}^{CD} \,, \quad \mathcal{P}_{AB} \circ \mathcal{P}_{CD} \circ \mathcal{P}^{CD} \circ \mathcal{P}^{AB} \,, \quad (5.3) $$

with the last line in (5.2) being one of them. (We can understand this as coming from the three possible irreducible representations in $\mathbf{6}\otimes\mathbf{6}$ or, equivalently, as the three inequivalent ways of forming singlets in $\mathbf{6}\otimes\mathbf{6}\otimes\mathbf{6}\otimes\mathbf{6}$.) Therefore, to count the number of N^2MHV charged polygons we have to consider not only the number of ways of distributing eight units of charge within four pentagons but also to weight that counting by the number of inequivalent contractions of all the R-charge indices. Remarkably, this counting is identical to the one found in [89] based on analysis of the SUSY Ward identities. This is particularly obvious when looking at Table 1 in [89] where the number of independent N^2MHV components for 8 and 9 particles is considered. [2] In sum, our construction in (5.2) generates precisely

---

[2]The weight $3 = \mathcal{S}_{\lambda=[2,2,2,2]}$ in their table is precisely the one explained in our above discussion.
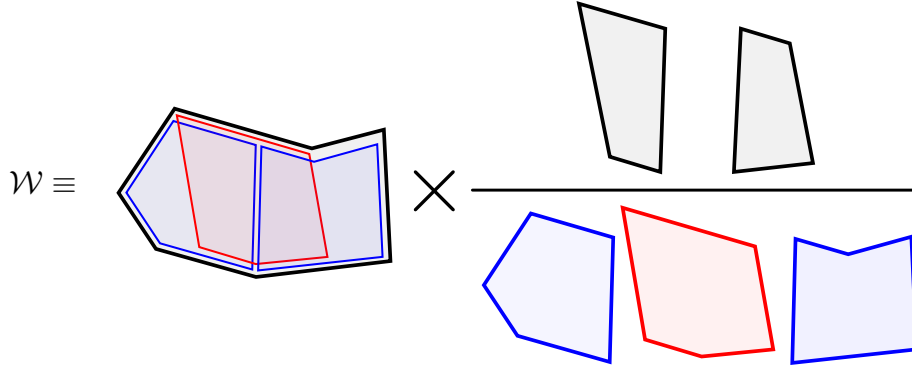
Figure 5.1: We study the conformally invariant and finite ratio $\mathcal{W}$ introduced in [81]. It is obtained by dividing the expectation value of the super Wilson loop by all the pentagons in the decomposition and by multiplying it by all the middle squares.

$\mathcal{N}(2,8) = 105$, $\mathcal{N}(2,9) = 490, \ldots$ different N^{2}MHV objects, in perfect agreement with the number of independent components arising from the study of the SUSY Ward identities.

It is quite amusing that the notation in [89] with a partition vector $\lambda = [\lambda_1, \ldots, \lambda_{n-4}]$ seems perfectly tailored to describe the charged pentagon approach where we have $n - 4$ pentagons with charges $\lambda_i \in \{0, 1, 2, 3, 4\}$. It also guarantees that the most general N^{k}MHV counting works the same for both amplitudes and OPE series, and concludes this analysis. The next step is to endow the charged pentagon construction with a precise dictionary between charged polygons and helicity configurations of scattering amplitudes.

5.2 The Map

As we have seen, a compact way of packing together all helicity amplitudes is through a generating function also known as the super Wilson loop with the expansion given in (4.25) and we reproduce here to fix some notation

$$W_{\text{super}} = W_{\text{MHV}} + \eta_i^1 \eta_j^2 \eta_k^3 \eta_l^4 \ W_{\text{NMHV}}^{(ijkl)} + \eta_i^1 \eta_j^2 \eta_k^3 \eta_l^4 \eta_m^1 \eta_n^2 \eta_o^3 \eta_p^4 \ W_{\text{N}^2\text{MHV}}^{(ijkl)(mnop)} + \ldots \tag{5.4}$$

The lower indices of the Grassmann η variables are associated to the edges of the polygon, $i = -1, 0, 1, \ldots, n - 2$.

Throughout this chapter we shall be using a rather unorthodox labelling of the edges of the polygon, which is represented in figure F.1. Namely, we number the edges from bottom

to top, with even numbers on one side and odd numbers on the other, like door numbers within a street. Given that we think of the Wilson loop as a sequence of flux-tube states propagating down this *street*, this is the most natural labelling from the OPE viewpoint. It makes it particularly simple to locate the j-th pentagon in the tessellation: it is the pentagon whose middle edge ends on edge j. The map between this labelling and the conventional cyclic ordering is explained in the caption of figure F.1.

Let us make a comment about the divergences of the (super) Wilson loop and how to deal with them. The super loop (5.4) has UV suppression factors associated to its cusps.[3] One can find in the literature several different ways of renormalizing the loop, such as to remove these factors. The one most commonly used is the *ratio function* $\mathcal{R} \equiv W_{\text{super}}/W_{\text{MHV}}$, first introduced in [90]. For our discussion, however, the OPE renormalization is better suited: it is obtained by dividing the super loop (5.4) by all the pentagons in its decomposition and by multiplying it by all the middle squares [82]

$$\mathcal{W} \equiv W_{\text{super}}/\mathrm{w} \qquad \text{with} \qquad \mathrm{w} \equiv \left(\prod_{i=1}^{n-4}\langle W_{i\text{'th pentagon}}\rangle\right)\Big/\left(\prod_{i=1}^{n-5}\langle W_{i\text{'th middle square}}\rangle\right), \quad (5.5)$$

as shown in figure 5.1. The ratio function $\mathcal{R}$ and the loop $\mathcal{W}$ are then easily found to be related to each other by $\mathcal{R} = \mathcal{W}/\mathcal{W}_{\text{MHV}}$. They are essentially equivalent, being both finite and conformally invariant functions of the η's and shape of the loop, but only $\mathcal{R}$ is cyclic invariant.

5.2.1 The Direct Map

Our goal in this section is to find the map between the different ways of gluing the charged transitions together, as in (5.2), and the components of the super loop (5.5). Put differently, we would like to find a map between the η's and the χ's such that $\mathcal{W}$ in (5.5) also admits the expansion

$$\mathcal{W} = \mathcal{P} \circ \mathcal{P} \circ \cdots \circ \mathcal{P} + \chi_1^1\chi_1^2\chi_1^3\chi_1^4 \mathcal{P}_{1234} \circ \mathcal{P} \circ \cdots \circ \mathcal{P} + \chi_1^1\chi_1^2\chi_1^3\chi_2^4 \mathcal{P}_{123} \circ \mathcal{P}_4 \circ \cdots \circ \mathcal{P} + \dots \quad (5.6)$$

in terms of the χ's.

There are two important properties of the super loop that will be relevant to our discussion. First, recall that an η is associated to an edge of the polygon while a χ is associated to a pentagon. As such, there are many more terms in the η-expansion (5.4) or

---

[3]These UV divergences are T-dual to the IR divergences of the on-shell amplitudes.
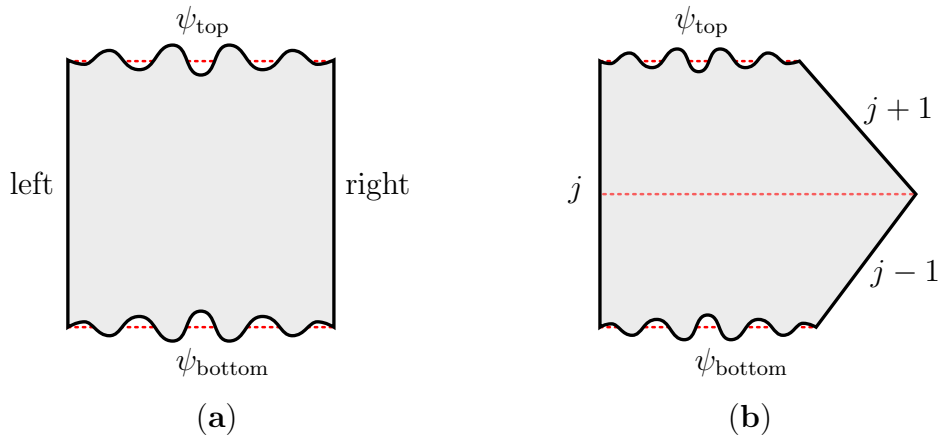
Figure 5.2: **a)** Any square in the OPE decomposition stands for a transition from the state at its bottom (ψ_{bottom}) to the state at its top (ψ_{top}). This transition is generated by a conformal symmetry of the right and left edges of that square (conjugate to the flux time τ). **b)** Similarly, the super pentagon $\mathbb{P}$ represents a transition from the state at its bottom to the state at its top. In the fermionic χ-directions, this transition is generated by a super-conformal symmetry of the $(j-1)$-th, j-th and $(j+1)$-th edges in this figure.

(5.5) of the super loop than there are in the χ-expansion (5.6). This is no contradiction, however. The reason is that the η-components are not all linearly independent, since, as mentioned before, they are subject to SUSY Ward identities. On the contrary, the χ-components *all* have different OPE interpretation and, in line with our previous discussion, should be viewed as defining a basis of independent components for the amplitudes. In other words, the map between χ- and η-components is not bijective if not modded out by the SUSY Ward identities. We can then think of the χ-decomposition as a natural way of getting rid of SUSY redundancy.

Second, the η-components of $\mathcal{W}$ are not 'pure numbers', since they carry weights under the little group; e.g., upon rescaling of the twistor[4] $Z_1 \to \alpha Z_1$ the component $\mathcal{W}^{1123}_{\text{NMHV}}$ transforms as $\mathcal{W}^{1123}_{\text{NMHV}} \to \mathcal{W}^{1123}_{\text{NMHV}}/\alpha^2$. These helicity weights cancel against those of the η's, so that $\mathcal{W}$ is weight free in the end. In contrast, the components in (5.6), as well as the corresponding χ's, are taken to be weightless. With this choice, the χ-components coincide with the ones predicted from integrability with no additional weight factors.

We now turn to the construction of the map. The question we should ask ourselves is: *What does it mean to charge a pentagon transition?* Said differently, how do we move from one pentagon-component to another in the χ decomposition of $\mathbb{P}$ in (5.1)? To find out, it

---

[4]See appendix F for a brief review of twistors.

helps thinking of the χ's as fermionic coordinates of sort and recall how usual (meaning bosonic) variables are dealt within the OPE set up.

The bosonic cross ratios are naturally associated with the symmetries of the middle squares. Namely, we can think of any middle square as describing a transition between two flux-tube states, one at its bottom and the other one at its top, as depicted in 5.2.**a**. Attached to this square are three conformal symmetries that preserve its two sides (left and right). To move in the space of corresponding cross ratios (τ, σ, ϕ) we act on the bottom state with these symmetries

$$\psi_{\text{bottom}} \quad \longrightarrow \quad e^{-H\tau + iP\sigma + iJ\phi}\,\psi_{\text{bottom}}\,. \tag{5.7}$$

Equivalently, we could act with the inverse transformations on the state at the top (ψ_{top}), since these are symmetries of the left and right sides sourcing the flux. In other words, the OPE family of Wilson loops is obtained by acting on all the twistors below each middle square with the conformal symmetries of that square.

Similarly, to move in the space of 'fermionic coordinates' we should act with a supercharge. In contrast to the previous case, these are now associated to the pentagons in the OPE decomposition. A pentagon transition represents the transition between two flux-tube states, one on the bottom square and the other on the top square – the transition being induced from the shape of the pentagon. So what we should do is to find the supercharge that preserves the three sides of the pentagon sourcing the two fluxes, i.e., the sides $j-1$, j and $j+1$ in figure 5.2.**b**, and act with it on the state at its bottom (ψ_{bottom}) or, equivalently, with the inverse symmetry on the state at its top (ψ_{top}). There is precisely one chiral supercharge that does the job, as we now describe.

Recall that we have 16 chiral supercharges at our disposal, that is, $\mathcal{Q}_A^a$ where A is an R-charge index and a is an $SL(4)$ twistor index. By construction they annihilate the super loop $\mathcal{W}$ on which they act as [91]

$$\mathcal{Q}_A^a = \sum_{i=-1}^{n-2} Z_i^a \frac{\partial}{\partial \eta_i^A} \qquad \text{with} \qquad \mathcal{Q}_A^a\,\mathcal{W} = 0\,. \tag{5.8}$$

By definition, for a given supercharge not to act on, say, the i-th side of the super loop, we need the coefficient of $\partial/\partial\eta_i^A$ to vanish. This can be achieved by contracting the $SL(4)$ index a with a co-twistor Y such that $Y \cdot Z_i = 0$. In our case, since we want $\mathcal{Q}$ to be a symmetry of the three sides of a pentagon, the co-twistor should be orthogonal to Z_{j-1}, Z_j and Z_{j+1}. There is exactly one such co-twistor:

$$Y_j \equiv Z_{j-1} \wedge Z_j \wedge Z_{j+1}\,. \tag{5.9}$$

106

It is then straightforward to define the operator $\partial/\partial\chi_j^A$ that charges the j-th pentagon. It acts as $Y_j \cdot \mathcal{Q}^A$ on the state ψ_{bottom} entering the j-th pentagon from the bottom or, equivalently, on what has created this state. In other words, $\partial/\partial\chi_j^A$ is defined as $Y_j \cdot \mathcal{Q}^A$ in (5.8) but with the summation restricted to edges lying below the j-th pentagon:

$$\frac{\partial}{\partial\chi_j^A} \equiv \frac{1}{(\mathbf{j}-\mathbf{1})_j\,(\mathbf{j})_j\,(\mathbf{j}+\mathbf{1})_j}\sum_{i=-1}^{j-2}Y_j\cdot Z_i\,\frac{\partial}{\partial\eta_i^A}\,. \tag{5.10}$$

Alternatively we could act on the state ψ_{top} at the top of the pentagon by restricting the summation to edges lying above the j-th pentagon and flipping the overall sign. These two prescriptions yield the same result since the two actions differ by $Y_j \cdot \mathcal{Q}^A$ where $\mathcal{Q}^A$ is the full supercharge annihilating the super loop.

The normalization factor multiplying the sum in (5.10) needs some explanation. It is introduced to make $\partial/\partial\chi_j^A$ weight free. In other words, it is defined such as to remove the weight of the co-twistor Y_j used to define our supercharge. In our notation, $(\mathbf{i})_j$ extracts the weight of the twistor Z_i in the j-th pentagon. This operation is unambiguous once we require it to be *local* with respect to the j-th pentagon, meaning that it should only make use of the five twistors of this pentagon. Indeed, given a pentagon p with five twistors $Z_a, \ldots, Z_e$, the unique conformally invariant combination carrying weight with respect to a is given by

$$(\mathbf{a})_p{}^4 = \frac{\langle abcd\rangle\langle cdea\rangle\langle deab\rangle\langle eabc\rangle}{\langle bcde\rangle^3}\,. \tag{5.11}$$

Uniqueness is very simple to understand. If another such expression existed, its ratio with (5.11) would be a conformal cross-ratio, which of course does not exist for a pentagon. A nice equivalent way of thinking of the weight (5.11) is as the NMHV tree level amplitude for the corresponding pentagon, that is

$$(\mathbf{i})_j^{-4} = W_{j\text{-th }\pentagon}^{(iiii)\ \text{tree}}\,. \tag{5.12}$$

(Stated like this, the idea of dividing out by such weights is not new, see discussion around (132) in [82].) Multiplying three such weights to make the normalization factor in (5.10), we would get

$$((\mathbf{j}-\mathbf{1})_j\,(\mathbf{j})_j\,(\mathbf{j}+\mathbf{1})_j)^4 = \frac{\left\langle Z_{j-1}, Z_{j+1}, Z_{t|j}, Z_j\right\rangle^3\left\langle Z_j, Z_{b|j}, Z_{j-1}, Z_{j+1}\right\rangle^3}{\left\langle Z_{j+1}, Z_{t|j}, Z_j, Z_{b|j}\right\rangle\left\langle Z_{b|j}, Z_{j-1}, Z_{j+1}, Z_{t|j}\right\rangle\left\langle Z_{t|j}, Z_j, Z_{b|j}, Z_{j-1}\right\rangle}\,, \tag{5.13}$$

where $Z_{t|j}/Z_{b|j}$ refer to the top/bottom twistors of the j-th pentagon respectively. Equivalently, $Z_{t|j}/Z_{b|j}$ are the middle twistors of the $(j+1)$-th/$(j-1)$-th pentagons, see figure F.1. For further discussion of these weights and their rewriting see appendix F.3.

Finally, there are two minor ambiguities in the above construction on which we should comment. One is the overall normalization of (5.11) or (5.12) which is not fixed by the symmetry argument above. The convention chosen here is equivalent to setting

$$\langle \mathcal{P}_{1234} \rangle = \left[\frac{\langle Z_0, Z_1, Z_2, Z_{-1} \rangle}{(\mathbf{0})_1 (\mathbf{1})_1 (\mathbf{2})_1} \right]^4 \mathcal{W}_{\text{pentagon NMHV}}^{(-1,-1,-1,-1)} = 1 \,. \tag{5.14}$$

A second minor ambiguity comes from the fourth power in (5.11) or (5.12). Due to its presence, to extract any weight we need to compute a fourth root, giving rise to a $\mathbb{Z}_4$ ambiguity. In practice we start from a point where the right hand side of (5.13) is real and positive for any j and pick the positive fourth root when extracting the weight on the left. Then everything is real and can be nicely matched against the integrability predictions. This seems reminiscent of the sort of positivity regions of [92]. It would be interesting to study the $\mathbb{Z}_4$ ambiguity further, and possibly establish a connection to the positivity constraints of [92].

5.2.2 Interlude : Sanity Check

As a check of our map (5.10) we consider an eight-leg scattering amplitude, i.e., an octagon or, equivalently, a sequence of four pentagons. For concreteness, we focus on the example of $\mathcal{P}_1 \circ \mathcal{P}_2 \circ \mathcal{P}_3 \circ \mathcal{P}_4 = \frac{\partial}{\partial \chi_1^1} \frac{\partial}{\partial \chi_2^2} \frac{\partial}{\partial \chi_3^3} \frac{\partial}{\partial \chi_4^4} \mathcal{W}$ at tree level and evaluate it in terms of the nine OPE variables $\{\tau_i, \sigma_i, \phi_i\}$. At this order, the OPE ratio $\mathcal{W}$ coincides with the ratio function $\mathcal{R}$ and we can easily extract components of the latter from the package [93]. For large OPE times we find that

$$\mathcal{P}_1 \circ \mathcal{P}_2 \circ \mathcal{P}_3 \circ \mathcal{P}_4 = e^{-\tau_1 - i\phi_1/2} \times e^{-\tau_2} \times e^{-\tau_3 + i\phi_3/2} \times f(\sigma_i) + \ldots \tag{5.15}$$

which is actually already a non-trivial check of our construction. Indeed, we have four charged pentagons each of which injects one unit of R-charge and one unit of fermion number. As such, the lightest states that will flow in the three middle squares are a fermion $\bar{\psi}_1$ (with helicity $-1/2$) in the first square, a scalar ϕ_{12} (with no helicity) in the second square and the conjugate fermion $\psi_{123} = \psi^4$ (with helicity $+1/2$) in the last middle square. In short, the leading process contributing to this amplitude should correspond to the sequence of transitions

$$\text{vacuum} \xrightarrow{\mathcal{P}_1} \bar{\psi}_1 \xrightarrow{\mathcal{P}_2} \phi_{12} \xrightarrow{\mathcal{P}_3} \psi_{123} \xrightarrow{\mathcal{P}_4} \text{vacuum} \,, \tag{5.16}$$
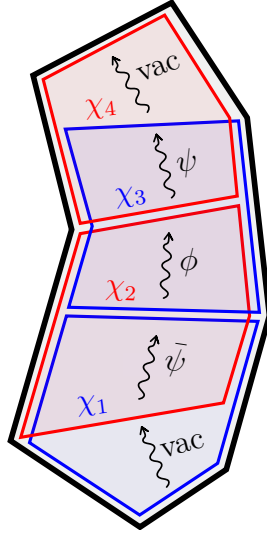
Figure 5.3: Leading OPE contribution to the NMHV octagon component $\mathcal{P}_1 \circ \mathcal{P}_2 \circ \mathcal{P}_3 \circ \mathcal{P}_4 = \frac{\partial}{\partial \chi_1^1} \frac{\partial}{\partial \chi_2^2} \frac{\partial}{\partial \chi_3^3} \frac{\partial}{\partial \chi_4^4} \mathcal{W}$. For this component, each of the four pentagons in the octagon decomposition carries one unit of R-charge and fermion number. From the flux tube point of view, this corresponds to the sequence of transitions in equation (5.16).

as represented in figure 5.3. The three exponential factors in (5.15) are in perfect agreement with this expectation.

Most importantly, the function $f(\sigma_i)$ should be given by the multiple Fourier transform of the sequence of pentagon transitions. It beautifully is. This type of checks will be given in section 5.5.

5.2.3 The Inverse Map

It is rather straightforward to invert the map (5.10) such as to obtain the $\partial/\partial\eta$'s in terms of the $\partial/\partial\chi$'s. For that aim, it is convenient to put back the weights in (5.10) and define

$$\mathcal{D}_A^{(j)} \equiv (\mathbf{j}-\mathbf{1})_j \, (\mathbf{j})_j \, (\mathbf{j}+\mathbf{1})_j \, \frac{\partial}{\partial \chi_j^A} = Y_j \cdot \sum_{i=-1}^{j-2} Z_i \, \frac{\partial}{\partial \eta_i^A} \, . \tag{5.17}$$

Given the triangular nature of this map, charging the first few edges at the bottom is as easy as writting the first few $\mathcal{D}$'s explicitly. For the bottom edge, for instance, we

immediately find that

$$\mathcal{D}_A^{(1)} = Y_1 \cdot Z_{-1} \frac{\partial}{\partial \eta_{-1}^A} \qquad \Rightarrow \qquad \frac{\partial}{\partial \eta_{-1}^A} = \frac{\mathcal{D}_A^{(1)}}{Y_1 \cdot Z_{-1}} \,, \tag{5.18}$$

while taking this into account and moving to the following edge yields

$$\frac{\partial}{\partial \eta_0^A} = \frac{(Y_1 \cdot Z_{-1})\mathcal{D}_A^{(2)} - (Y_2 \cdot Z_{-1})\mathcal{D}_A^{(1)}}{(Y_1 \cdot Z_{-1})(Y_2 \cdot Z_0)} \,, \tag{5.19}$$

and so on.

By following this recursive procedure we will eventually find that $\partial/\partial \eta_j$ is given as a linear combination of $\mathcal{D}^{(j+2)}$, $\mathcal{D}^{(j+1)}$, ..., $\mathcal{D}^{(1)}$. In plain words, it means that charging the edge j entails charging the entire sequence of pentagons lying all the way from that specific edge to the bottom of the polygon. The drawback is that it has be so even for an edge standing arbitrarily far away from the bottom of the polygon. This, however, is at odds with the locality of the OPE construction, in which a random pentagon in the decomposition only talks to its neighbours (through the flux-tube state that they share) and has little knowledge of how far it stands from the bottom. Besides, it introduces an artificial discrimination between bottom and top, despite the fact that our analysis could, at no cost, be run from the top. The way out is easy to find: the bottom tail of the inverse map is pure mathematical illusion, or, put differently, the inverse map beautifully truncates such as to become manifestly top/bottom symmetric.

In sum, instead of a sum over $j+2$ $\mathcal{D}$'s, what we find is that (for $3 \leq j \leq n-2$) $\partial/\partial \eta_j$ is given by the linear combination of the five neighboring pentagons only (see figure 5.4)

$$\boxed{\frac{\partial}{\partial \eta_j^A} = \frac{\langle Y_{j-2}, Y_{j-1}, Y_j, Y_{j+1} \rangle \mathcal{D}_A^{(j+2)} + \quad \dots \quad + \langle Y_{j-1}, Y_j, Y_{j+1}, Y_{j+2} \rangle \mathcal{D}_A^{(j-2)}}{(Y_{j-1} \cdot Z_{j+1})(Y_{j+1} \cdot Z_{j-1})(Y_{j-2} \cdot Z_j)(Y_{j+2} \cdot Z_j)}} \,. \tag{5.20}$$

Mathematically, this relation originates from the five-term identity

$$\langle Y_{j-2}, Y_{j-1}, Y_j, Y_{j+1} \rangle Y_{j+2} + \quad \dots \quad + \langle Y_{j-1}, Y_j, Y_{j+1}, Y_{j+2} \rangle Y_{j-2} = 0 \,, \tag{5.21}$$

which holds for any choice of five (co-)twistors and which simply follows from them having four components. Once we plug the definition (5.17) into the right hand side of (5.20), most terms cancel out because of this identity. Those that survive are boundary terms and
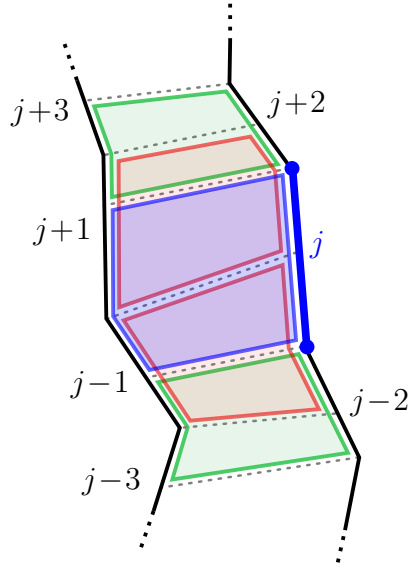
110

Figure 5.4: A remarkable feature of our construction is that the inverse map turns out to be local. Namely, charging edge j is done by charging the five pentagons touching this edge and these five pentagons alone. We notice in particular that the two outermost pentagons in this neighbourhood, which are shown in green above, are touching the endpoints of edge j only.

it is straightforward to work them out in detail. They precisely lead to the single term in the left hand side of (5.20).[5]

Actually, it is possible to interpret the inverse map (5.20) such that it also applies to the very first edges of the polygon, like in (5.18) and (5.19), provided that we properly understand what we mean by Y_0, Y_{-1}, Y_{-2} and Y_{-3}. (These co-twistors will show up when using (5.20) for $\partial/\partial\eta_2$, $\partial/\partial\eta_1$, $\partial/\partial\eta_0$ and $\partial/\partial\eta_{-1}$.) For this we can pretend that there are extra edges at the bottom of the polygon and the previous derivation would still go through.[6] Of course, for these bottom (or top) cases, it is easier to proceed recursively as

---

[5]To see that only the term proportional to $\partial/\partial\eta_j$ survives it is useful to note that the orthogonality relations $Y_{j-2}\cdot Z_{j-1} = Y_{j-1}\cdot Z_{j-1} = Y_j\cdot Z_{j-1} = 0$ allow us to freely extend slightly the summation range of some of the five terms in (5.20). In turn, these relations follow trivially from the definition (5.9) of the co-twistors. Finally, to check the overall normalization of both sides in (5.20), it is convenient to use the identity $\langle Y_{j-2}, Y_{j-1}, Y_j, Y_{j+1}\rangle = (Y_{j-1}\cdot Z_{j+1})(Y_{j+1}\cdot Z_{j-1})(Y_{j-2}\cdot Z_j)$.

[6]We can simply define $(Y_0, Y_{-1}, Y_{-2}, Y_{-3}) \equiv (Y_{\{0,-1,1\}}, Y_{\{*,0,-1\}}, Y_{\{-1,*,*\}}, Y_{\{*,*,*\}})$, with $Y_{\{i,j,k\}} \equiv Z_i\wedge Z_j\wedge Z_k$ and Z_* being arbitrary twistors, which drop out of the final result. At the same time, we also set $(\mathcal{D}_0\mathcal{W}, \mathcal{D}_{-1}\mathcal{W}, \mathcal{D}_{-2}\mathcal{W}, \mathcal{D}_{-3}\mathcal{W}) = (0,0,0,0)$.

in (5.18) and (5.19).

This concludes our general discussion of the map. The proposals (5.20) and (5.10) are the most important results.

5.2.4 Easy Components and the Hexagon

A polygon with n edges has a top pentagon and a bottom pentagon, plus $n-6$ pentagons which are neither top nor bottom and referred to as middle ones. Charging the bottom or the top pentagons is considerably simpler than charging any middle one. Let us focus on the bottom since the top is treated analogously. According to our general map (5.10), we see that the differential operator that charges the bottom pentagon, $\partial/\partial\chi_1$, is simply proportional to $\partial/\partial\eta_{-1}$,

$$\frac{\partial}{\partial\chi_1} = \frac{Y_1 \cdot Z_{-1}}{(\mathbf{0})_1(\mathbf{1})_1(\mathbf{2})_1} \times \frac{\partial}{\partial\eta_{-1}} \tag{5.22}$$

which we can further simplify to (see e.g. (F.19) in the appendix for a thorough explanation)

$$\frac{\partial}{\partial\chi_1} = (-\mathbf{1})_1 \times \frac{\partial}{\partial\eta_{-1}} . \tag{5.23}$$

In other words, up to a trivial factor which absorbs the weight in $\partial/\partial\eta_{-1}$, charging a bottom pentagon is the same as extracting components with η's at the very bottom of our polygon. Similarly, charging the top-most pentagon is equivalent to putting η's on the topmost edge. It could hardly be simpler. Explicitly, for any polygon, there are five NMHV components which are easy to construct:

$$\begin{aligned}
\mathcal{P}_{1234} \circ \mathcal{P} \circ \cdots \circ \mathcal{P} \circ \mathcal{P} &= w[4] \, \mathcal{W}^{(-1,-1,-1,-1)} , \\
\mathcal{P}_{123} \circ \mathcal{P} \circ \cdots \circ \mathcal{P} \circ \mathcal{P}_4 &= w[3] \, \mathcal{W}^{(-1,-1,-1,n-2)} , \\
\mathcal{P}_{12} \circ \mathcal{P} \circ \cdots \circ \mathcal{P} \circ \mathcal{P}_{34} &= w[2] \, \mathcal{W}^{(-1,-1,n-2,n-2)} , \\
\mathcal{P}_1 \circ \mathcal{P} \circ \cdots \circ \mathcal{P} \circ \mathcal{P}_{234} &= w[1] \, \mathcal{W}^{(-1,n-2,n-2,n-2)} , \\
\mathcal{P} \circ \mathcal{P} \circ \cdots \circ \mathcal{P} \circ \mathcal{P}_{1234} &= w[0] \, \mathcal{W}^{(n-2,n-2,n-2,n-2)} .
\end{aligned} \tag{5.24}$$

where $w[m] \equiv ((-\mathbf{1})_1)^m \, ((\mathbf{n}-\mathbf{2})_{n-4})^{4-m}$.

These are what we call the *easy components*. Morally speaking, from the first to the last line, we can think of the easy components as inserting an F, ψ, ϕ, $\bar{\psi}$, $\bar{F}$ excitation and their conjugate at the very bottom and top of our polygon.
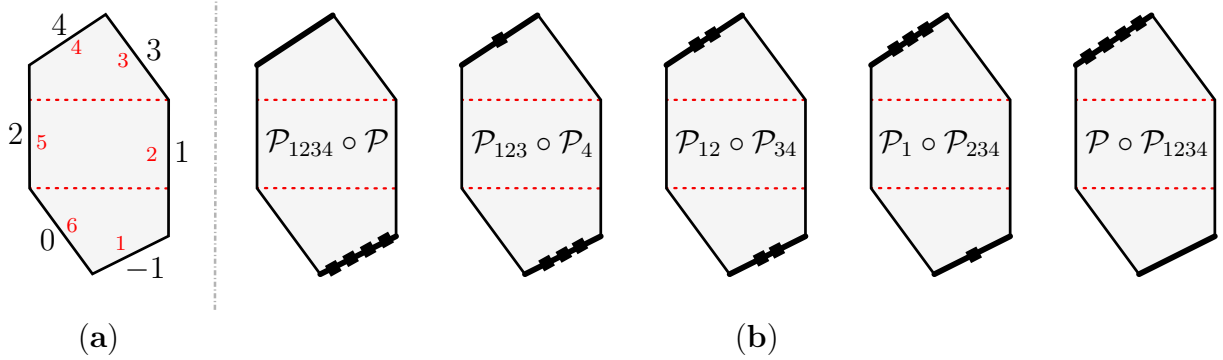
Figure 5.5: **(a)** OPE friendly edge labelling used in this chapter (big black outer numbers) versus the more conventional cyclic labelling (small red inner numbers) for the hexagon. **(b)** The five *easy components* of the NMHV hexagon. Each black square represents a dual Grassmann variable η. For the hexagon these five components provide a complete base for all NMHV amplitudes.

For an hexagon we have only two pentagons and thus the easy components in (5.24) with $n = 6$ suffice to describe the NMHV hexagon, see figure 5.74. All other components can be trivially obtained by Ward identities. For example, we can use invariance under

$$Y_2 \cdot Q = \sum_k Y_2 \cdot Z_k \frac{\partial}{\partial \eta_k} = Y_2 \cdot Z_{-1} \frac{\partial}{\partial \eta_{-1}} + Y_2 \cdot Z_0 \frac{\partial}{\partial \eta_0} + Y_2 \cdot Z_4 \frac{\partial}{\partial \eta_4} \qquad (5.25)$$

to replace any component with an index associated to the edge 0 to a linear combination of components with η's associated to the top and bottom edges -1 and 4. Those, in turn, are the components which we can neatly compute from the OPE construction. For example, it immediately follows that

$$\mathcal{W}^{(-1,-1,-1,0)} = \alpha \, \mathcal{P}_{1234} \circ \mathcal{P} + \beta \, \mathcal{P}_{123} \circ \mathcal{P}_4 \,, \qquad (5.26)$$

with

$$\alpha = -\frac{Y_2 \cdot Z_{-1}}{Y_2 \cdot Z_0 \left((-\mathbf{1})_1\right)^4} \,, \qquad \beta = -\frac{Y_2 \cdot Z_4}{Y_2 \cdot Z_0 \left((-\mathbf{1})_1\right)^3 (\mathbf{4}_2)^1} \,. \qquad (5.27)$$

Similarly, we can easily write down any other hexagon NMHV component in terms of the OPE basis. Of course, this is equivalent to using the general inverse map (5.20), worked out in the previous section.

There are other components whose OPE expansions closely resemble those of the *nice* components (5.24). A notable example is the so-called *cusp-to-cusp* hexagon scalar component $\mathcal{R}^{\text{hex}}_{-1,0,3,4}$ and its heptagon counterpart $\mathcal{R}^{\text{hep}}_{-1,0,4,5}$. Such components were extensively

113

analyzed in the past using the OPE [82, 86, 94, 95].[7] What is nicest about them is their utter simplicity at tree level, being described by a simple scalar propagator from the bottom cusp $(-1, 0)$ to the top cusp $(n - 3, n - 2)$. Based on the OPE intuition, one would therefore imagine that this component should not behave that differently from the one in the middle line in (5.24). Indeed one observes that the expansion of this component and of the cusp-to-cusp components are exactly the same to leading order at large τ and to any loop order. Both are described by a single scalar flux tube excitation. However, as soon as two-particle contributions kick in – in the sub-leading collinear terms – these components start differing. A similar story is present for all other components in the family (5.24). For example, gluonic components were intensively studied in [84]. A simple tree-level gluonic example of this universality for the leading terms in the OPE was considered in detail in [96]. The hexagon fermionic component $\mathcal{W}^{(-1,-1,-1,4)}$ was recently studied in [97].[8]

Finally let us note that the weight factors showing up in (5.24) are not a novelty. Already in [82] it was explained that to properly deal with weight free quantities we better remove the weight of each pentagon by dividing out by the corresponding charged counterpart, see (132) and surrounding discussion in [82]. Nevertheless, in practice, in all previous OPE studies of super amplitudes, the weights $(-\mathbf{1})_1$ and $(\mathbf{n} - \mathbf{2})_{n-5}$ of the bottom and top twistors with respect to the corresponding pentagons were, for the most part, ignored. Sometimes this is fine. For instance, if we are interested in amplitudes at loop level we can always divide the ratio function by its tree level expression obtaining a weight free function of cross-ratios which we can unambiguously match with the OPE. Said differently, we can always normalize the tree level result by hand such that it agrees with the leading terms in the OPE. In particular, for the purpose of comparing with the hexagon function program [98–102] and using the OPE to generate high loop order predictions, it is overkilling to carry these weights around. Moreover, with the choice of twistors in [82], such weights actually evaluate to 1 which is one further reason why we never needed to take them into account.

Having said all that, of course, to be mathematically rigorous, weight free quantities (5.24) are what we should always manipulate. In particular, for higher n-gons, and as soon as we also charge middle pentagons, it is important to keep track of these weights to properly make contact with the OPE predictions.

---

[7]Recall once again that we are using here a slightly unconventional labelling of the edges as indicated in figure F.1.b; These same cusp-to-cusp component were denoted $\mathcal{R}_{6134}$ and $\mathcal{R}_{7145}$ in [82] and $\mathcal{R}_{2356}$ in [94].

[8]This component was denoted $\mathcal{W}^{(1114)}$ in the cyclic labelling in [97].

5.2.5 Parity

The charged pentagon construction provides us with a novel intuition about how to understand parity at the Wilson loop level.

Recall that the action of parity on a scattering amplitude is very simple. It is a symmetry of the amplitude under which a positive helicity gluon transforms into a negative helicity one, a positive helicity fermion transforms into its negative helicity conjugate counterpart and finally a scalar excitation is trivially conjugated. All in all, this can be summarized in the following nice relation [103]

$$\int \prod_{i=-1}^{n-2} d^4\tilde{\eta}_i \; e^{\sum_{i=-1}^{n-2} \bar{\tilde{\eta}}_i \tilde{\eta}_i} A[\tilde{\eta}, \lambda, \tilde{\lambda}] = A[\bar{\tilde{\eta}}, \tilde{\lambda}, \lambda] \,. \tag{5.28}$$

However, the relation between amplitudes and super Wilson loops involves stripping out the MHV tree-level factor along with going from the original amplitude $\tilde{\eta}$'s to the Wilson loop dual Grassman variables η's.[9] Together, these operations obscure the action of parity for this stripped object. How is parity symmetry realized on the super Wilson loop? Put differently, how does parity relate different ratio function components? Here we propose that – once decomposed using the OPE χ-components – parity at the Wilson loop level is no more complicated than in the original amplitude language. Precisely, we claim that our variables allow for a straightforward analogue of (5.28) in the Wilson loop picture as

$$\int \prod_{i=1}^{n-4} d^4\chi_i \; e^{\sum_{i=1}^{n-4} \bar{\chi}_i \chi_i} \mathcal{R}[\chi, Z] = \mathcal{R}[\bar{\chi}, W] \,, \tag{5.29}$$

where W_j are Hodge's *dual* momentum twistors [104]. The latter can be thought of as parity conjugate of the Z's and, up to an overall factor which drops out in (5.29), are given by[10]

$$W_j \equiv Z_{j-2} \wedge Z_j \wedge Z_{j+2} \,. \tag{5.30}$$

Note that this is nothing but the conventional definition of the dual twistor involving three consecutive edges; the shifts of 2 in the index are just an outcome or our labelling, see figure F.1.

---

[9]The convention for the labelling of the η's and $\tilde{\eta}$'s varies quite a lot in the literature. Our notation here is in line with [76] and [92] for example (modulo the non-cyclic labelling of the edges of course).

[10] Dual momentum twistors (as well as usual momentum twistors) are reviewed in some detail in appendix F.1, see formula (F.4) for an explicit expression relating them to the original momentum twistors, including all factors. Here we are dealing with weight free quantities and as a result, we can always safely drop any normalization from either Z's or W's on the left or right hand sides in (5.29).

The general relation (5.29) is a generating function for all parity relations between N^kNMHV components and N^{n-4-k}MHV components, such as the relation

$$\mathcal{P}_{1234} \circ \mathcal{P} = \mathcal{P} \circ \mathcal{P}_{1234}|_{Z \to W} \tag{5.31}$$

between two NMHV hexagon components, for instance, or the relation

$$\mathcal{P}_{123} \circ \mathcal{P}_{14} \circ \mathcal{P}_{234} = \mathcal{P}_4 \circ \mathcal{P}_{23} \circ \mathcal{P}_1|_{Z \to W} \tag{5.32}$$

relating NMHV and N^2MHV seven-point amplitudes. More precisely, to convert such identity into a relation for ratio function components, it is suffices to divide both sides by $\mathcal{W} = \mathcal{P} \circ \mathcal{P} \circ \mathcal{P}$.[11] After doing so, the same relation in (5.32) reads

$$\frac{\partial}{\partial \chi_1^1} \frac{\partial}{\partial \chi_1^2} \frac{\partial}{\partial \chi_1^3} \frac{\partial}{\partial \chi_2^1} \frac{\partial}{\partial \chi_2^4} \frac{\partial}{\partial \chi_3^2} \frac{\partial}{\partial \chi_3^3} \frac{\partial}{\partial \chi_3^4} \mathcal{R}^{\text{heptagon } N^2\text{MHV}} = \frac{\partial}{\partial \chi_1^4} \frac{\partial}{\partial \chi_2^2} \frac{\partial}{\partial \chi_2^3} \frac{\partial}{\partial \chi_3^1} \mathcal{R}^{\text{heptagon NMHV}} \Bigg|_{Z \to W} \tag{5.33}$$

where the χ derivatives are given in terms of conventional η derivatives in (5.10). Another more extreme example following from (5.29) is the relation

$$\mathcal{P}_{1234} \circ \mathcal{P}_{1234} \circ \mathcal{P}_{1234} = \mathcal{P} \circ \mathcal{P} \circ \mathcal{P}|_{Z \to W} \tag{5.34}$$

which encodes the fact that for seven points N^3MHV is the same as $\overline{\text{MHV}}$. It is straightforward to generate more such relations by picking different components in (5.29).

Note that relations such (5.33) are quite unconventional. We are not entitled to compare different η-components of the ratio function simply because they do not carry the same helicity weights. Equating different η-components would be tantamount to comparing apples and oranges. In contrast, when extracting the χ-components as in (5.33) we generate weight free quantities since the χ's – contrary to the η's – carry no weight. This is what allows us to write parity relations at the level of the Wilson loop in terms of simple relations such as (5.32)–(5.33) or, simply, in terms of the master relation (5.29), without the need of dressing the components by additional weight factors.

Having decoded in detail the notation behind our main claim (5.29), let us now explain how the relations (5.32)–(5.33) are nicely suggested by the pentagon approach. Then, we will explain what sort of checks/derivations we have performed.

Parity, first and foremost, is a symmetry that swaps the helicity of the external particles in the $\mathcal{N} = 4$ supermultiplet that are being scattered, see (5.28). Similarly, parity also flips

---

[11]The latter is symmetric under $Z \to W$ so we can evaluate it with either twistors Z or dual twistors W.

the helicity of the flux-tube excitations. Flipping the helicity of a flux-tube excitation is trivial: it can be accomplished by simply flipping the signs of all angles ϕ_j's, while keeping the times τ_j and distances σ_j invariant [79,81,82]. This is precisely what the transformation $Z \leftrightarrow W$ accomplishes![12]

This explains the substitution rule in the right hand side of (5.31)–(5.34). To complete the picture we also have to act with parity on the pentagon transitions. Naturally, it is expected to swap the several super pentagon components in (5.1) in exactly the same way that it acts on the usual super-field multiplet expansion (replacing the positive helicity gluon with no $\tilde{\eta}$'s with the negative helicity gluon with 4 $\tilde{\eta}$'s and so on.). This translates into

$$\mathcal{P}_{1234} \leftrightarrow \mathcal{P} \ , \qquad \mathcal{P}_{123} \leftrightarrow \mathcal{P}_4 \ \text{ etc,} \tag{5.35}$$

which is precisely what is encoded in (5.32)–(5.33) or, more generally, in (5.29). In particular, these prescriptions neatly relate N^kMHV and N^{n-k-4}MHV amplitudes, as expected for parity.

While (5.29) is what the OPE naturally suggests, the previous paragraph is obviously not a proof. In any case, (5.29) is a concrete conjecture for the realization of parity at the Wilson loop level that we should be able to establish (or disprove) rather straightforwardly starting from (5.28), without any reference whatsoever to the OPE. It would be interesting if a simple and elegant derivation of (5.29) existed, perhaps following the same sort of manipulations as in [75]. This would elucidate further the origin of the (weight free) super OPE Grassmann variables χ.

What we did was less thorough. To convince ourselves of the validity of (5.29) we did two simpler exercises: On the one hand, using the very convenient package by Bourjaily, Caron-Huot and Trnka [93] we extensively tested (5.29) for a very large number of ratio functions from NMHV hexagons to N^3MHV decagons, both at tree and at one loop level.[13] On the other hand, we also looked for an analytic derivation of (5.29) from (5.28). We did not find a particularly illuminating proof that establishes this in full generality but we did manage to prove several sub-examples.

---

[12]More precisely, it is a very instructive exercise to observe that under $Z_j \rightarrow W_j$ the cross-ratios in formula (160) in [82] precisely transform as $(\tau_j, \sigma_j, \phi_j) \rightarrow (\tau_j, \sigma_j, -\phi_j)$. When preforming such check it is important to take into account the conversion between the edge labelling used here and there, see caption of figure F.1.

[13]When checking such identities for a very large number of edges, the package becomes unpractically slow. The trick is to open the package and do a "find/replace operation" to eliminate several `Simplify` and `FullSimplify` throughout. For analytical checks of relations such as (5.32)–(5.33), these simplifications are superfluous.

5.3   The POPE integrand

We are now in condition to make the OPE expansion for super Wilson loops precise. The OPE integrand factorizes into considerably simpler building blocks which we can analyse separately. It is perhaps worth mentioning from the get-go that this factorization is by no means obvious. It stands as another wonderful (but mysterious) $\mathcal{N} = 4$ SYM gift. Were it not for it, one would hardly imagine bootstrapping the multi-particle contributions with ease. Indeed, except for the first few particles contributions, almost no explicit form factor summands for correlation functions in integrable theories are explicitly worked out. A notable exception is the $2d$ Ising model. The unexpected simplicity we are encountering in $\mathcal{N} = 4$ SYM theory motivates its portrait as the *Ising model of Gauge Theories*.

The three building blocks into which the OPE integrand factorizes are dubbed the *dynamical part*, the *matrix part* and the *form factor part*,

$$\texttt{integrand} = (\texttt{dynamical part}) \times (\texttt{matrix part}) \times (\texttt{form factors part}), \quad (5.36)$$

with the latter form factors being non-trivial for non-MHV processes only. Here is what we know about these building blocks :

Dynamical part - This is the part of the OPE integrand that is universally present, which applies to all cases, MHV or non-MHV, and which treats all flux tube excitations on a same footing, regardless of their quantum numbers / R-charges. It is the most dynamical component of the integrand, hence its name, and not surprisingly it exhibits the most complicated coupling dependence. Its overall form is however extremely simple since it is factorized into a product over elementary pentagon transitions linking the various flux tube excitations and a product over square measures and Boltzmann weights of each excitation. The geometry of the scattering amplitude, in particular, only enters through these Boltzmann weights. All the transitions, measures, energies and momentum appearing here are also rather universal. They are written in the appendix G.

Matrix part - The matrix part takes care of the $SU(4)$ group theoretical factor of the integrand. It can only show up when flux tube excitations with R-indices are present, and is otherwise totally absent. This component of the integrand has the distinguished feature of being a *coupling independent* rational function of the particles' rapidities, with no obvious factorization. Taming this group theoretical factor is an interesting algebraic problem on its own [105] but it is beyond the scope of this thesis.

Form factors part - Lastly, we have the non-MHV form factors. They are only needed for non-MHV amplitudes, which are composed of so-called *charged* pentagon transitions [29, 82, 97]. Luckily, these form factors are not independent objects. Instead, we can construct them from their relation to the bosonic (or MHV) transitions with fermionic excitations frozen to zero momentum. Applying this logic, we will obtain their expressions for all excitations and transitions. The final result is then checked against perturbative as well as self-consistency checks such as parity symmetry.

5.4   The abelian part

In this section we present the expression for the abelian part of the POPE integrand. It captures by definition what remains of the full integrand after stripping out the matrix part. (In some cases, when there is just no matrix part, the abelian part is of course everything. This is the case for instance for states made out of gluons or their bound states, which are intrinsically abelian.) As explained in the introduction, the abelian part is composed of the dynamical and form factors parts,

$$\texttt{abelian} = (\texttt{dynamical part}) \times (\texttt{non-MHV form factors part}). \qquad (5.37)$$

Conventionally, for MHV, only the dynamical part remains. For non-MHV, the latter remains the same, but form factors should be added to the story. These ones are not really independent and can be directly derived from suitable MHV processes, as we shall explain in this section.

5.4.1   The dynamical part

We start with the main component. This one captures, in particular, the information about the geometry, i.e. the cross ratios σ_i, τ_i, ϕ_i of the polygon, and can be written as [81]

$$
\begin{aligned}
\texttt{dynamical part} = {}& P(\ 0\ |\boldsymbol{\Psi}^{(1)})\,\mu(\boldsymbol{\Psi}^{(1)})\,e^{-E(\boldsymbol{\Psi}^{(1)})\tau_1 + ip(\boldsymbol{\Psi}^{(1)})\sigma_1 + im(\boldsymbol{\Psi}^{(1)})\phi_1} \\
&\times P(\overline{\boldsymbol{\Psi}}^{(2)}|\overline{\boldsymbol{\Psi}}^{(1)})\,\mu(\boldsymbol{\Psi}^{(2)})\,e^{-E(\boldsymbol{\Psi}^{(2)})\tau_2 - ip(\boldsymbol{\Psi}^{(2)})\sigma_2 + im(\boldsymbol{\Psi}^{(2)})\phi_2} \\
&\times P(\boldsymbol{\Psi}^{(2)}|\boldsymbol{\Psi}^{(3)})\,\mu(\boldsymbol{\Psi}^{(3)})\,e^{-E(\boldsymbol{\Psi}^{(3)})\tau_3 + ip(\boldsymbol{\Psi}^{(3)})\sigma_3 + im(\boldsymbol{\Psi}^{(3)})\phi_3} \\
&\times P(\overline{\boldsymbol{\Psi}}^{(4)}|\overline{\boldsymbol{\Psi}}^{(3)})\dots ,
\end{aligned}
\qquad (5.38)
$$

where $E(\boldsymbol{\Psi})$, $p(\boldsymbol{\Psi})$ and $m(\boldsymbol{\Psi})$ are the energy, momentum and angular momentum of the multi-particle state $\boldsymbol{\Psi}$. We have $n-5$ such states in total, in accordance with the number
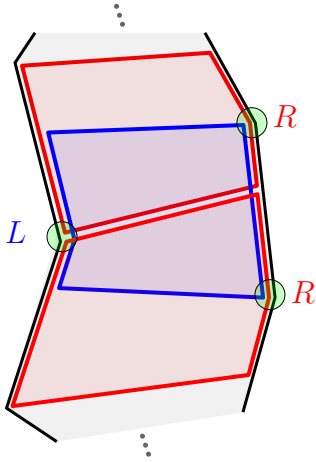
Figure 5.6: Every two successive pentagons in the POPE decomposition are flipped with respect to each other. Namely, if the cusp of one pentagon is pointing to the right then the next one is pointing to the left and so on, $\cdots \to \mathcal{P}^R \to \mathcal{P}^L \to \mathcal{P}^R \to \mathcal{P}^L \to \cdots$.

of middle squares in the tessellation, and for each of them we have a corresponding square measure $\mu(\boldsymbol{\Psi})$, see [81]. Finally, two consecutive squares with multi-particle states $\boldsymbol{\Phi}$ and $\boldsymbol{\Psi}$ are connected by means of a pentagon transition $P(\boldsymbol{\Phi}|\boldsymbol{\Psi})$ or $P(\overline{\boldsymbol{\Psi}}|\overline{\boldsymbol{\Phi}})$, where the bar stands for the state where all excitations are replaced by their conjugate and their order reversed. The fact that each other pentagon appears with such reversed states is a direct consequence of the alternating nature of the pentagon tessellation as illustrated in figures 5.6 and 5.7. The alternating signs multiplying the momenta of the states in consecutive middle squares have the same origin.

The factorization observed above is not a surprise and follows from symmetry considerations of the OPE. In contrast, the simplicity of $\mathcal{N} = 4$ SYM theory starts to manifest itself as soon as we start exploring the multi-particle nature of the various pieces. What happens here is that all the above mentioned blocks factorize further into one- and two-particle blocks! To describe this factorization we introduce the notation Ψ_n with $n = 1, \ldots, N$ to indicate the n-th excitation of the multi-particle state $\boldsymbol{\Psi}$. Then, the energy, momentum,
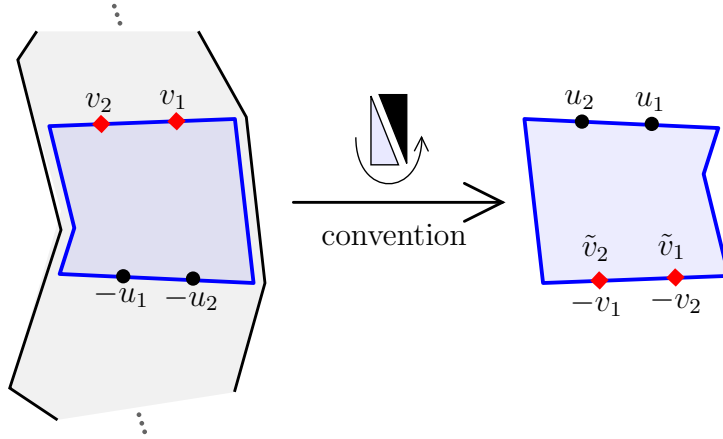
Figure 5.7: When inserting the resolution of the identity between each pentagon it is desirable to relate one sort of pentagon in figure 5.6 (say the ones with the cusp to the left) to the other kind to render things more uniform. We relate a pentagon with its cusp to the left to a pentagon with its cusp to the right by a "rotation", which maps the bottom to the top and the top to the bottom. In this convention, after rotating the pentagon we relabel the associated rapidities as illustrated in this figure. This leads to an alternating sign $(-1)^j$ multiplying the flux tube space variables as written in (5.38).

angular momentum and measure all factorize into their single particle counterparts as[14]

$$\mu(\boldsymbol{\Psi})\, e^{-E(\boldsymbol{\Psi})\tau \pm ip(\boldsymbol{\Psi})\sigma + im(\boldsymbol{\Psi})\phi} = \prod_{n=1}^{N} \mu(\Psi_n)\, \exp\left[-E(\Psi_n)\tau \pm ip(\Psi_n)\sigma + im(\Psi_n)\phi\right]\,, \quad (5.39)$$

where the sign $\pm = (-1)^{j+1}$ multiplying the momenta for states in the j-th middle square is a simple outcome of the conventions mentioned above, see figure 5.7. It is convenient to use a hatted measure $\hat{\mu}$ to denote collectively the measure and the accompanying Boltzmann factor, since these ones always come together. With this notation, the factorization we just described would simply read $\hat{\mu}(\boldsymbol{\Psi}) = \prod_n \hat{\mu}(\Psi_n)$. Most importantly, we observe a similarly neat factorization for the pentagon transitions into fundamental 2-particle transitions [81,

---

[14]In [81] the measure part also included combinatorial factors for identical excitations. These factors can instead be associated to the summation over the flux excitation that should be done in a way that avoids double counting.

82, 84, 87, 106][15]

$$P(\mathbf{\Phi}|\mathbf{\Psi}) = \frac{\prod\limits_{n,m} P(\Phi_n|\Psi_m)}{\prod\limits_{n>n'} P(\Phi_n|\Phi_{n'}) \prod\limits_{m<m'} P(\Psi_m|\Psi_{m'})} \ . \tag{5.40}$$

The measures themselves are not independent from the pentagon transitions. On the contrary, they can be extracted from the decoupling pole present in 2-particle transitions involving identical in- and out- going particles,

$$\operatorname*{Res}_{v=u} P_{\Psi|\Psi}(u|v) = \frac{i}{\mu_\Psi(u)} \ . \tag{5.41}$$

We see that to fully describe the dynamical part all we need are the two-particle pentagon transitions between any pair of single particle excitations. Most of them were already written down in the literature, see e.g. [82–84, 87, 97, 107]. It was found that, for any pair of excitations $\{\Psi, \Phi\}$, the pentagon transition takes the rather universal form

$$P_{\Psi|\Phi}(u|v)^2 = \mathcal{F}_{\Psi\Phi}(u,v)\frac{S_{\Psi\Phi}(u,v)}{S_{\star\Psi\Phi}(u,v)} \ , \tag{5.42}$$

where $S_{\Psi\Phi}(u,v)$ is the scattering phase (in the symmetric channel) for the excitations Ψ and Φ and $S_{\star\Psi\Phi}(u,v)$ is its mirror counterpart.[16] The functions $\mathcal{F}_{\Psi\Phi}(u,v)$ are simple functions of the rapidities, involving eventually the Zhukowski variables. In table 5.1 we present our ansatz for these functions for all pairs of excitations.

In the end, to evaluate the transition we still need to take the square-root of (5.42) which poses some ambiguity on the branch choice. This ambiguity can be partially fixed through comparison with data or with help of some reasonable normalization conditions as done in appendix G. Explicit expressions for all the transitions and measures are also given in this appendix (altogether with the transitions involving bound states of gluons and small fermions [83]).

---

[15]Let us stress again that formula (5.40) only captures the dynamical part of the transition. In the case where $\mathbf{\Phi} = \mathbf{0}$ and $\mathbf{\Psi} = \phi\phi$, for example, we get from (5.40) that $P_{\phi\phi}(0|u,v) = 1/P_{\phi|\phi}(u|v)$ while in [83] we had $P_{\phi\phi}(0|u,v) = 1/(g^2(u-v+2i)(u-v+i)) \times 1/P_{\phi|\phi}(u|v)$ which differs by a rational prefactor and by the factor $1/g^2$. The former rational factor is interpreted here as being part of the matrix part and thus discarded, while the power of $1/g^2$ is just absent because of our new normalization of $P_{\phi|\phi}$ (see appendix G).

[16]When Ψ is a gluon or scalar excitation, the mirror S-matrix is given by analytically continuing the physical one in the standard way, $S_{\star\Psi\Phi}(u,v) = S_{\bar\Psi\Phi}(u^\gamma, v)$. For fermions, the lack of a mirror transformation u^γ renders the relation between the mirror S-matrix and the physical one less straightforward. It involves a so-called anomalous mirror transformation as detailed in [83], see e.g. appendix A.4 therein.

$$\mathcal{F}_{\phi F}(u|v) = 1\,,$$

$$\mathcal{F}_{\phi\psi}(u|v) = -\frac{1}{(u - v + \frac{i}{2})}\,,$$

$$\mathcal{F}_{\phi\phi}(u|v) = \frac{1}{(u - v)(u - v + i)}\,,$$

$$\mathcal{F}_{FF}(u|v) = \frac{(x^+ y^+ - g^2)(x^+ y^- - g^2)(x^- y^+ - g^2)(x^- y^- - g^2)}{g^2 x^+ x^- y^+ y^- (u - v)(u - v + i)}\,,$$

$$\mathcal{F}_{F\psi}(u|v) = -\frac{(x^+ y - g^2)(x^- y - g^2)}{g\sqrt{x^+ x^-}\,y(u - v + \frac{i}{2})}\,,$$

$$\mathcal{F}_{F\bar\psi}(u|v) = -\frac{g\sqrt{x^+ x^-}\,y(u - v + \frac{i}{2})}{(x^+ y - g^2)(x^- y - g^2)}\,,$$ (5.43)

$$\mathcal{F}_{F\bar F}(u|v) = \frac{g^2 x^+ x^- y^+ y^- (u - v)(u - v + i)}{(x^+ y^+ - g^2)(x^+ y^- - g^2)(x^- y^+ - g^2)(x^- y^- - g^2)}\,,$$

$$\mathcal{F}_{\psi\psi}(u|v) = -\frac{(xy - g^2)}{\sqrt{gxy}(u - v)(u - v + i)}\,,$$

$$\mathcal{F}_{\psi\bar\psi}(u|v) = -\frac{\sqrt{gxy}}{(xy - g^2)}\,,$$

Table 5.1: Summary of prefactors for all twist-one squared transitions, with $x = x(u), y = x(v)$ and $x = \frac{1}{2}(u + \sqrt{u^2 - 4g^2})$ the Zhukowski variable. They agree with those found in the literature up to minor redefinitions (see appendix G for details).

In concluding, we should mention that there are two main axioms behind these ansätze. The most important (and still mysterious) one is the *fundamental relation*

$$P_{XY}(u|v) = \pm S_{XY}(u, v) P_{YX}(v|u)\,,$$ (5.44)

which comes with a minus sign whenever both X and Y are fermionic. Combined with the factorization property (5.40) it guarantees that general transitions fulfill proper Watson and decoupling equations. The other essential constraint is dubbed the *mirror axiom* which states that

$$P_{X|Y}(u^{-\gamma}|v) = P_{\bar Y|X}(v|u)\,, \quad \text{or more generally} \quad P_{X|\Psi}(u^{-\gamma}|\mathbf{v}) = P_{\bar\Psi|X}(\mathbf{v}|u)\,,$$ (5.45)

where $-\gamma$ denotes the inverse mirror rotation and with $\mathbf{v}$ a set of spectator rapidities.[17] Combined with (5.44) the mirror axiom can be used to argue for the ansatz (5.42) as

---

[17]Technically, X in this equation is restricted to be a gluonic or a scalar excitation. This is because, as

well as to solve for the prefactor $\mathcal{F}$. Finally, it is worth stressing that the solution to such bootstrap axioms are by no means unique and comparison with perturbative data is therefore crucial in backing up our proposals. This shall be discussed at length below.

5.4.2   Charged transitions and form factors

The physics that takes place on the flux tube is essentially the same regardless of whether some of the pentagons are charged or not. What can possibly differ is the R-charge flow throughout the pentagon evolution. Since the R-charge dependence was factored out into the matrix part at the very beginning, one can ask if the abelian part proposed in (5.40) can also be applied as it stands to these charged processes. The answer turns out to be positive up to a minor modification: the inclusion of the so-called non-MHV form factors, as sketched in (5.37). The need for these form factors is not a novelty and was previously stressed in [82,87] from the study of certain components of the NMHV hexagon. To pave the way to our general discussion, let us start by reviewing briefly, on a simple example, why these form factors are needed at all, or equivalently why is the dynamical part not enough for describing the abelian part of non-MHV amplitudes.

Consider the χ-component $\mathcal{P}_{1234} \circ \mathcal{P}$, or equivalently $\mathcal{P} \circ \mathcal{P}_{1234}$, of an NMHV hexagon mentioned in section 5.2.4. From R-charge conservation the excitations allowed on these transitions are the same as in the bosonic MHV case $\mathcal{P} \circ \mathcal{P}$. As such, at twist zero we have the vacuum, at twist one the positive and negative helicity gluons, F and $\bar{F}$, etc. Despite this similarity, one does not expect the transitions, integrands, and full amplitude to be the same for the two processes, since e.g. the MHV process treats symmetrically positive and negative helicity gluons while the non-MHV one does not. (This is also immediately confirmed at weak coupling by looking at the corresponding amplitudes.) At the level of the POPE integrand for a single gluon,

$$
\begin{aligned}
\mathcal{P} \circ \mathcal{P} &= 1 + \int \frac{du}{2\pi}\, \hat{\mu}_F(u) && + \int \frac{du}{2\pi}\, \hat{\mu}_{\bar{F}}(u) && + \dots\,, \\
\mathcal{P}_{1234} \circ \mathcal{P} &= 1 + \int \frac{du}{2\pi}\, \hat{\mu}_F(u)\, f(u) + \int \frac{du}{2\pi}\, \hat{\mu}_{\bar{F}}(u)\, \bar{f}(u) + \dots\,, && (5.46) \\
\mathcal{P} \circ \mathcal{P}_{1234} &= 1 + \int \frac{du}{2\pi}\, \hat{\mu}_F(u)\, \bar{f}(u) + \int \frac{du}{2\pi}\, \hat{\mu}_{\bar{F}}(u)\, f(u) + \dots\,,
\end{aligned}
$$

this difference follows from the fact that the gluons are either produced or annihilated in the presence of a charged transition $P^{[4]}$ in the NMHV cases and it results in the gluonic form

---

explained in [83], the mirror rotation for the fermions is of a more exotic type, mapping the fermions into higher-twist excitations.

factors f and $\bar{f}$. In other words, the dynamical part described before must be completed with the knowledge of these form factors, which in the present cases simply read [82]

$$f(u) = \frac{x^+ x^-}{g^2} = 1/\bar{f}(u) \,, \tag{5.47}$$

where $x^\pm = x(u \pm \frac{i}{2})$ with $x(u) = (u + \sqrt{u^2 - 4g^2})/2$ the Zhukowski map of the rapidity u. Note that such factor cannot be absorbed in the matrix part both because the matrix part is, by definition, independent of the coupling and because in this abelian case there is no matrix part.

Our main proposal is that the same structure persists for generic transitions. Namely, the effect of charging a pentagon, ignoring the matrix part, is to dress the abelian part by elementary form factors associated to each excitation present on the pentagons. More specifically, we propose that the charged version of (5.40) reads

$$P^{[r]}(\boldsymbol{\Phi}|\boldsymbol{\Psi}) = g^{\frac{r(r-4)}{8}} \times \left[\prod_i \left(h_{\Phi_i}\right)^r \times \prod_i \left(h_{\bar{\Psi}_i}\right)^r \right] \times P(\boldsymbol{\Phi}|\boldsymbol{\Psi}) \,, \tag{5.48}$$

where $\boldsymbol{\Phi} = \{\Phi_i\}$ is the incoming set of excitations at the bottom square of the pentagon, $\boldsymbol{\Psi} = \{\Psi_i\}$ the outgoing set of excitations at the top, and $r = 0, 1, \ldots, 4$ the amount of R-charge carried by the pentagon. The rules of the game are extremely simple. The result is factorized and for each excitation, or more precisely for each field creating the excitation at the bottom or conjugate field annihilating it at the top, we associate a form factor. The form factor can thus be thought of as being attached to the field and represents the net effect of charging the transition, as illustrated in figure 5.8.

We immediately verify that the general rule (5.48) properly reduces to (5.46) in the case of a single gluon. Indeed, as mentioned earlier, the form factor f above accounts for the difference between a gluon F produced on top of a charged and an uncharged pentagon, i.e.

$$f(u) = P^{[4]}_{0|F}(0|u)/P_{0|F}(0|u) \,. \tag{5.49}$$

By convention, or equivalently by applying (5.40) blindly, $P(0|u) = 1$, while (5.48) gives us

$$P^{[4]}_{0|F}(0|u) = g^0 \times (h_{\bar{F}}(u))^4 \times 1 \,, \tag{5.50}$$

that is

$$f(u) = (h_{\bar{F}}(u))^4 \qquad \Leftrightarrow \qquad h_{\bar{F}}(u) = \left(\frac{x^+ x^-}{g^2}\right)^{\frac{1}{4}} \,. \tag{5.51}$$

$$P^{[r]}(\mathbf{\Psi}|\mathbf{\Phi}) = \boxed{\begin{array}{c} \bar{\bar{\Phi}} \\ \mathcal{Q}^r \\ \Psi \end{array}} = \boxed{\begin{array}{c} (h_{\bar{\Phi}})^r \\ \bar{\bar{\Phi}} \\ \Psi \\ (h_{\Psi})^r \end{array}} = (h_{\mathbf{\Psi}})^r \times P(\mathbf{\Psi}|\mathbf{\Phi}) \times (h_{\bar{\Phi}})^r$$

Figure 5.8: The net effect of charging a pentagon is to dress each excitation on its edges by a corresponding form factor. This one is attached to the field that creates or annihilates the corresponding excitation in the bottom to top evolution picture. The picture above illustrates our conventions, with a state Ψ at the bottom being created by a field Ψ and a state Φ at the top being annihilated by the field $\bar{\Phi}$. The form factors associated to these fields are then $(h_{\Psi})^r$ and $(h_{\bar{\Phi}})^r$, with r the R-charge of the charged pentagon, or equivalently, the number of times we act with a supercharge $\mathcal{Q}$.

Similarly, we would read that

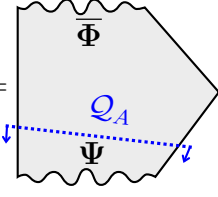$$h_F(u) = \left(\frac{g^2}{x^+ x^-} \right)^{\frac{1}{4}} . \tag{5.52}$$

The remaining questions are what are the form factors for the other excitations, why is the form factor for a composite state a product of elementary ones, and why is (5.48) valid at all? The quick answers are that, due to their expected simple dependence (see (5.47)), form factors are easily extracted from data analysis, as done in [82], and that their factorized form is consistent with all the constraints the charged transitions must fulfill, as shall be discussed in section 5.4.3 below. However, one can do much better than that and actually *derive* the rule (5.48) *directly* from the uncharged transitions (5.40). The important observation [29] is that charging a pentagon is the same as acting with a supersymmetry generator on one of its edges, as we will now explain.

To start with, we recall that one can view the pentagon transitions as form factors for a pentagon operator acting on the flux tube Hilbert space of states

$$P(\mathbf{\Psi}|\mathbf{\Phi}) = \langle \mathbf{\Phi}|\mathcal{P}|\mathbf{\Psi} \rangle = \boxed{\begin{array}{c} \bar{\bar{\Phi}} \\ \\ \Psi \end{array}} \tag{5.53}$$

As explained in [29], all we need to do in order to add a unit of R-charge to a pentagon $\mathcal{P}$ is to act with a supersymmetry generator $\mathcal{Q}$ on the bottom state or, equivalently, with

$-\mathcal{Q}$ on the top state. Here $\mathcal{Q}$ is the unique supercharge that commutes with $\mathcal{P}$ and is represented by ∂_χ on the super loop (5.6), see [29]. This leads to the relation :

$$P_A(\mathbf{\Psi}|\mathbf{\Phi}) = \langle \mathbf{\Phi}|\mathcal{P}_A|\mathbf{\Psi}\rangle = \langle \mathbf{\Phi}|\mathcal{P}\mathcal{Q}_A|\mathbf{\Psi}\rangle = $$

$$(5.54)$$

Importantly, supersymmetry generators are realized on the flux as zero momentum fermions [108]. That is, to act on the state $|\mathbf{\Psi}\rangle$ with a supercharge $\mathcal{Q}_A$, we add to it a fermion and then send the momentum of that fermion to zero. This directly links the charged transitions to their un-charged counterparts, allowing us to extract all information about the former from the latter.

Let us show more precisely how this works. Consider for example the transition from the vacuum at the bottom to a single fermion $\bar{\psi}(u)$ at the top. Such transition is only possible if we equip the transition with R-charge as in the charged transition $P_A(0|u) = \langle\bar{\psi}(u)|\mathcal{P}_A|0\rangle$. To obtain the latter transition from an uncharged one we can start with a similar fermion $\bar{\psi}(v)$ at the bottom, i.e. from $P_{\bar{\psi}\bar{\psi}}(v|u)$. We now wish to take the limit in which the momentum of the fermion $\bar{\psi}(v)$ goes to zero, so that it becomes a supersymmetry generator acting at the bottom. In appendix G.5 we show carefully how the zero momentum limit should be taken and in particular what is the proportionality factor. We find that

$$\mathcal{Q}|0\rangle = \sqrt{\frac{\Gamma_{\text{cusp}}}{2g}} \lim_{p\to 0}|p\rangle = \lim_{v\to\infty}\sqrt{\frac{\Gamma_{\text{cusp}}}{2ig}\frac{d\check{v}}{dp_{\bar{\psi}}}\mu_{\bar{\psi}}(\check{v})}\,|\bar{\psi}(\check{v})\rangle\,, \qquad (5.55)$$

where, following the notations of [83], the 'check mark' on top of the rapidity v, i.e. $\check{v}$, indicates that the analytical continuation to the rapidity plane neighbouring the zero momentum point (reached at $v = \infty$) has been done (see [83] for further details). Using this prescription, as well as the large v behaviours given in appendix G.4, we conclude that

$$P^{[1]}_{0|\bar{\psi}}(0|u) = \lim_{v\to\infty}\sqrt{\frac{\Gamma_{\text{cusp}}}{2ig}\frac{d\check{v}}{dp_{\bar{\psi}}}\mu_{\bar{\psi}}(\check{v})}\times P_{\bar{\psi}|\bar{\psi}}(\check{v}|u) = g^{-\frac{3}{8}}\left(\frac{g}{x(u)}\right)^{\frac{1}{4}}\,, \qquad (5.56)$$

where the upper label in $P^{[1]}$ indicates the amount of R-charge or equivalently the number of χ's carried by the pentagon. The fermionic creation transition (5.56) is obviously of the

type (5.48)[18]

$$P_{0|\bar\psi}^{[1]}(0|u) \equiv g^{-\frac{3}{8}} \times h_\psi(u) \times P_{0|\bar\psi}(0|u) = g^{-\frac{3}{8}} \times h_\psi(u) , \tag{5.57}$$

with

$$h_\psi(u) = (g/x)^{1/4} \tag{5.58}$$

the form factor for a single antifermion. As expected it shows a simple dependence on the rapidity u of the excitation, once expressed in terms of the Zhukowski variable $x = x(u)$, as found earlier for the gluons.

It is not so much difficult to include more excitations in the top and check the factorization of the form factors. Suppose, for instance, that we start with a multi-particle transition involving fermions and send the momentum of one of them to zero as prescribed by (5.55). As a result of the multi-particle factorization (5.40), the multi-particle form factors must factorize as well.[19]

We can see this at work on simple examples, using the same $P^{[1]}$ procedure as before. For instance, we can at no cost consider the same fermion creation transition with a gluonic excitation $F_a(w)$ added on the top. This yields

$$P_{0|\bar\psi F_a}^{[1]}(0|u,w) = \lim_{v\to\infty} \sqrt{\frac{\Gamma_{\rm cusp}}{2ig}\frac{d\check v}{dp_{\bar\psi}}}\mu_{\bar\psi}(\check v) \times P_{\bar\psi|\bar\psi F_a}(\check v|u,w) , \tag{5.59}$$

where, again, the upper index indicates that this new transition is taking place on top of a pentagon carrying one unit of R-charge. It exactly differs from the chargeless transition defined through (5.40) by the form factors. Indeed, using the factorization of the dynamical part (5.40) together with (5.56) and $(G.4)$, we derive that

$$P_{0|\bar\psi F_a}^{[1]}(0|u,w) \equiv P_{0|\bar\psi F_a}(0|u,w)\, h_\psi(u)h_{F_{-a}}(w) , \tag{5.60}$$

where

$$h_{F_a}(u) = \left[\frac{g^2}{x\left(u+\frac{ia}{2}\right)x\left(u-\frac{ia}{2}\right)}\right]^{(\operatorname{sign}a)/4} , \tag{5.61}$$

in agreement with (5.51) and (5.52) for $a = -1$ and $a = +1$, respectively.

Instead of adding matter to the fermion $\bar\psi$ at the top, one can imagine replacing it by a pair $\phi\psi$ or a triplet $\psi\psi\psi$ (always with the small fermion $\bar\psi(\check v)$ at the bottom) and

[18]Recall that following (5.40) we are working in a convention where the un-charged creation transition of any excitation X is trivial. With the χ-labelling this reads $P_{0|X}^{[0]}(0|u) = 1$.

[19]To see this in full generality one also needs the matrix part [105].

hence access to the as-yet-unknown ϕ and $\bar{\psi}$ form factors. A proper analysis would require introducing a matrix part, whose main role is to project the pair/triplet to the $SU(4)$ channel with one unit of R-charge. However, in both cases, the matrix part plays no role as far as the form factors are concerned.[20] One can thus proceed without knowing its explicit form and directly relate the ϕ and $\bar{\psi}$ form factors to the large v behaviours of the $P_{\bar{\psi}|\phi}(\check{v}|u)$ and $P_{\bar{\psi}|\psi}(\check{v}|u)$ transitions. Using expressions in appendix G.4 one gets the system of equations

$$h_\phi(u)h_{\bar{\psi}}(w) = g^{3/8} \lim_{v\to\infty} \sqrt{\frac{\Gamma_{\text{cusp}}}{2ig}\frac{d\check{v}}{dp_{\bar{\psi}}}\mu_{\bar{\psi}}(\check{v})} \times P_{\bar{\psi}|\psi}(\check{v}|u)P_{\bar{\psi}|\phi}(\check{v}|w) = \left(\frac{x(w)}{g}\right)^{1/4},$$

$$\prod_{i=1}^{3} h_{\bar{\psi}}(u_i) = g^{3/8} \lim_{v\to\infty} \sqrt{\frac{\Gamma_{\text{cusp}}}{2ig}\frac{d\check{v}}{dp_{\bar{\psi}}}\mu_{\bar{\psi}}(\check{v})} \times \prod_{i=1}^{3} P_{\bar{\psi}|\psi}(\check{v}|u_i) = \left(\frac{x(u_1)x(u_2)x(u_3)}{g^3}\right)^{1/4},$$

$$(5.62)$$

whose only reasonable solution is

$$h_\phi(u) = 1, \qquad h_{\bar{\psi}}(u) = (x/g)^{1/4}. \tag{5.63}$$

Equations (5.58), (5.61), and (5.63) finalize our proposal for the charged transitions (5.48). A couple of consistency checks for it will be given in the next sub-section. One easy test can actually be run immediately. It comes from the physical requirement that a pair of conjugate excitations should decouple on a charged transition exactly as they do in the un-charged case. That is, the *square limit* (5.41) must remain the same on a charged transition.[21] Including the form factors, this condition translates into

$$\operatorname*{Res}_{v=u} P_{\Phi|\Phi}(u|v)\, h_\Phi(u)h_{\bar{\Phi}}(v) = \frac{i}{\mu_\Phi(u)}, \tag{5.64}$$

which enforces

$$h_\Phi(u)h_{\bar{\Phi}}(u) = 1. \tag{5.65}$$

This relation is easily seen to be satisfied.

In the end our form factors are all simply given in terms of Zhukowski variables. Putting them together, for a polygon with n edges, gives us the full form factors part in (5.36) as

$$\texttt{form factors part} = \prod_{i=0}^{n-5} g^{\frac{r_i(r_i-4)}{8}} \left(h_{\boldsymbol{\Psi}(i)}\right)^{r_i} \left(h_{\bar{\boldsymbol{\Psi}}(i+1)}\right)^{r_i}, \tag{5.66}$$

---

[20]For completeness, we have indeed that the matrix part is $\propto 1/(u-w+3i/2)$ and $\propto 1/\prod_{i<j}(u_i-u_j+i)$ for the two cases at hand, i.e. for a state $\phi(u)\psi(w)$ and $\psi(u_1)\psi(u_2)\psi(u_3)$ at the top, respectively. Because it shows no dependence at all on the rapidity v of the fermion $\bar{\psi}(\check{v})$ at the bottom, it cannot contribute to the form factors.

[21]Put differently, the propagation on the square is diagonal, so it cannot be charged.
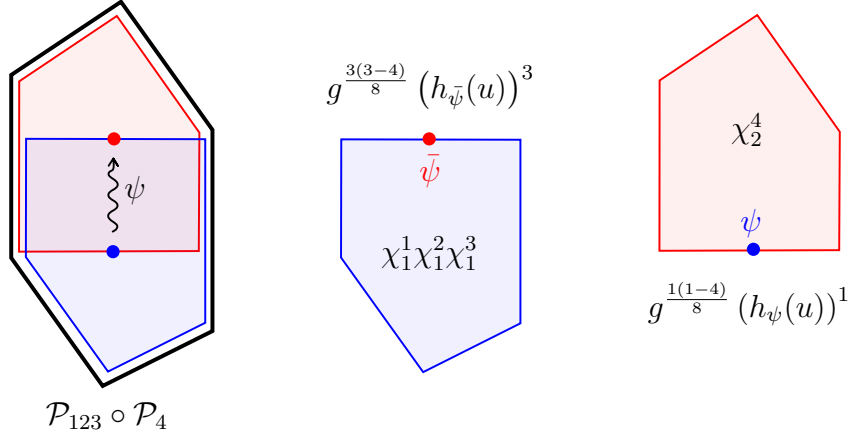
$$\mathcal{P}_{123} \circ \mathcal{P}_4$$

Figure 5.9: Leading twist transition for the hexagon component $\mathcal{P}_{123} \circ \mathcal{P}_4$. In this example, we assign the form factor $\left(h_{\bar{\psi}}(u)\right)^3$ to the bottom (blue) pentagon and $\left(h_\psi(u)\right)^1$ to the top (red) pentagon.

where the index i on top of the matter fields refers to the i'th square, with $i = 0$ being the first one at the very bottom and $i = n - 4$ the last one at the very top,[22] while the *same* index i in r_i refers to the i'th pentagon transition between states $\mathbf{\Psi}^{(i)}$ and $\mathbf{\Psi}^{(i+1)}$, with r_i units of R-charge. Note in particular that each excitation in a given square is assigned two form factors – one for each of the pentagons that overlap on this particular square. A simple example is depicted in figure 5.9.

As a summary, we can now write the OPE decomposition for a polygon with n edges in a rather compact form. Up to the matrix part of course, we have

$$\mathbb{P} \circ \mathbb{P} \circ \ldots \circ \mathbb{P}|_X = \sum \prod_{i=0}^{n-5} \hat{\mu}_{\mathbf{\Psi}^{(i)}} \, g^{\frac{r_i(r_i-4)}{8}} \left(h_{\mathbf{\Psi}^{(i)}}\right)^{r_i - r_{i-1}} P^{R/L}\big(\mathbf{\Psi}^{(i)}|\mathbf{\Psi}^{(i+1)}\big), \qquad (5.67)$$

with X a choice of χ component, with r_i Grassmann variables χ's in pentagon i, and with $P^{R/L}\big(\mathbf{\Psi}^{(i)}|\mathbf{\Psi}^{(i+1)}\big) = P\big(\mathbf{\Psi}^{(i)}|\mathbf{\Psi}^{(i+1)}\big)$ or $P\big(\overline{\mathbf{\Psi}}^{(i+1)}|\overline{\mathbf{\Psi}}^{(i)}\big)$ for i even or odd.

In what follows we shall perform two sort of checks of our proposal. The first kind of checks – with which we will conclude this section – are internal self-consistency checks of the POPE proposal. The second sort of checks concern explicit comparison against perturbative data and are the main focus of section 5.5.

---

[22]We recall that the states in the very bottom ($i = 0$) and very top ($i = n - 4$) squares are both vacuum with measure and form factors equal to one.

5.4.3   Consistency checks

In this section we shall present two consistency checks of the non-MHV form factors presented above. Namely, we will first see that they are consistent with parity and finally observe that they are compatible with the fundamental bootstrap axioms (and hence can be regarded as factorized CDD factors).

Parity

As we have seen in section 5.2.5, parity symmetry establishes the following relation between the OPE components

$$\mathbb{P} \circ \mathbb{P} \circ \ldots \circ \mathbb{P}|_X = (\mathbb{P} \circ \mathbb{P} \circ \ldots \circ \mathbb{P}|_{\bar{X}})|_{\phi \to -\phi}. \tag{5.68}$$

where $\bar{X}$ is the complement of the component X, namely

$$\bar{X} = \int \prod_{i=1}^{n-4} d^4 \chi_i \, e^{\sum_{i=1}^{n-4} \bar{\chi}_i \chi_i} X \Big|_{\bar{\chi} \to \chi}. \tag{5.69}$$

For example, we can relate an NMHV component with $X = \chi_1^1 \chi_1^2 \chi_1^3 \chi_2^4$ to an $\mathrm{N}^{n-5}\mathrm{MHV}$ with its complement $\bar{X} = \chi_1^4 \chi_2^1 \chi_2^2 \chi_2^3 \cdots \chi_{n-4}^1 \chi_{n-4}^2 \chi_{n-4}^3 \chi_{n-4}^4$. For parity to be a symmetry of the super Wilson loop, the POPE decomposition should be invariant under $r \to 4 - r$ together with a flip of the chirality of all the flux tube excitations, namely

$$\sum_{} \prod_{i=0}^{n-5} \hat{\mu}_{\boldsymbol{\Psi}^{(i)}} \, g^{\frac{r_i(r_i-4)}{8}} \left(h_{\boldsymbol{\Psi}^{(i)}}\right)^{r_i - r_{i+1}} P^{R/L}\big(\boldsymbol{\Psi}^{(i)} | \boldsymbol{\Psi}^{(i+1)}\big) \tag{5.70}$$

$$= \sum_{} \prod_{i=0}^{n-5} \hat{\mu}_{\bar{\boldsymbol{\Psi}}^{(i)}} \, g^{\frac{(r_i-4)r_i}{8}} \left(h_{\bar{\boldsymbol{\Psi}}^{(i)}}\right)^{(4-r_i)-(4-r_{i+1})} P^{R/L}\big(\overline{\boldsymbol{\Psi}}^{(i)} | \overline{\boldsymbol{\Psi}}^{(i+1)}\big) \Big|_{\phi_i \to -\phi_i},$$

up to an unphysical relative normalization. Note that the overall power of g is parity invariant by itself. Now, the pentagon transitions and measures change at most by a sign under this transformation (namely when fermions are involved) but they do not distinguish the chirality of the flux tube excitations otherwise. Finally, using the relation (5.65) we see that the form factor part is also invariant and thus parity is nicely satisfied.

Bootstrap axioms

In a way, the pentagon transitions in (5.42) constitute the simplest solutions to the bootstrap axioms they are expected to satisfy [81–84]. However, these solutions are by no means unique. Any other solution to the bootstrap equations would differ from (5.42) by a sort of CDD factor. As we shall now see, the form factors derived above can also be interpreted as such CDD factors. Namely, the charged transitions (5.48) still go through all the bootstrap axioms.

The most non-trivial axiom is the fundamental relation to the flux-tube S-matrix (5.44). Clearly, this relation is unaltered by the form factors due to their factorized form. It remains to check the *mirror axiom* (5.45) which was introduced when bootstrapping the pentagon transitions involving gluons or scalars. For this mirror relation to be satisfied by the charged transitions, the form factor should obey the relation

$$h_\Phi(u^{-\gamma}) = h_{\bar\Phi}(u) \,. \tag{5.71}$$

This relation is trivially satisfied for scalars while for gluons it follows from the relation $x^\pm(u^{-\gamma}) = g^2/x^\pm(u)$.[23] In fact, the validity of both axioms directly follows from the relation between the charged transition and a zero momentum fermion (5.55) (taken to be one of the $\mathbf{\Psi}$ excitations in (5.45) for example).

5.5 Comparison with data

We would like now to test our proposal (5.67) for the POPE integrand against available data at weak coupling. Historically, this comparison was absolutely instrumental in unveiling the general ansatz for the form factors.

The data we use is extracted from the package [93], which generates non-MHV amplitudes at tree level for any number of particles. The same package also yields one loop amplitudes but for the purpose of this thesis we restrict our attention to tree-level checks only.

In the POPE we have essentially five different types of elementary excitations, $F, \psi, \phi, \bar\psi, \bar F$, and fifteen different pairings of them into transitions. These two numbers are in correspondence with the five independent NMHV hexagons and fifteen independent NMHV heptagons, respectively. At leading twist, the hexagons essentially probe the measures

---

[23]Beware that mirror transformation takes different form for scalars and gluons [82, 109].

and the form factors. The heptagons on the other hand probe all building blocks of the integrand and, in particular, the pentagon transitions involving mixed types of particles. In this section we will confront our predictions against both hexagons and heptagons thus probing all these ingredients at once.

At the same time, these checks also provide us with a strong test of the map between N^kMHV amplitudes and charged pentagons proposed in [29]. This one maps any N^kMHV amplitude, as specified by choosing an η-component of the super loop, to a very precise linear combination of the OPE friendly χ-components (5.6) and vice-versa. It is the latter χ-components that admit a neat OPE interpretation and thus offer direct access to the various pentagon transitions.

To illustrate this point, let us consider a random η-component, say the NMHV heptagon component $\mathcal{W}^{(-1,-1,1,2)}$ multiplying the monomial $\eta_{-1}^A \eta_{-1}^B \eta_1^C \eta_2^D \epsilon_{ABCD}$ (see figure 5.12.**a** for the convention of the edge labelling). According to our discussion, we expect it *not* to have an obvious OPE expansion and indeed this is precisely what we find. To see it we extract this tree-level component[24] from the package [93] as

```
evaluate@superComponent[{1,2},{3},{},{},{},{4},{}]@treeAmp[7,1]
```

and, to make it into a weight free quantity, multiply it by the weights $((-\mathbf{1})_1)^2\,(\mathbf{1})_1\,(\mathbf{2})_2$ with $(\mathbf{i})_j$ the weight of the twistor Z_i in the jth pentagon (see [29] for more details), which we can express in terms of OPE variables using the twistors in Appendix F.2.[25] We denote this properly normalized heptagon component as $\mathbb{W}^{(-1,-1,1,2)}$. In terms of OPE variables we have

$$\mathbb{W}^{(-1,-1,1,2)} = \frac{e^{-\sigma_1 - \frac{i\phi_1}{2}}}{1 + e^{-2\tau_1}} = e^{-\sigma_1 - \frac{i\phi_1}{2}} - e^{-\sigma_1 - 2\tau_1 - \frac{i\phi_1}{2}} + \mathcal{O}(e^{-4\tau_1}), \qquad (5.72)$$

which clearly defies any reasonable OPE interpretation![26]

---

[24]Actually, the package extracts the ratio function component $\mathcal{R}^{(i,j,k,l)} = \mathcal{W}^{(i,j,k,l)}/\mathcal{W}_{\mathrm{MHV}}$, but at tree level they are the same.

[25]As is often the case, while this is the correct mathematical procedure, the naive evaluation of $\mathcal{W}^{(-1,-1,1,2)}$ with the twistors in Appendix F.2 would yield the very same result since, in this case, the weights simply evaluate to 1.

[26]To start with, it simply does not depend on the OPE variables τ_2, σ_2, ϕ_2 at all, as if only the vacuum were propagating in the second square of this heptagon. Even if we were to accept that, other puzzles would immediately appear when interpreting the large τ_1 expansion: the first term looks like a twist zero contribution – like the vacuum does – but with a non-trivial σ_1 and ϕ_1 dependence – contrary to the vacuum. There is no natural candidate for what anything like this would be. Also suspicious is the fact that only even twists show up once we expand the result out at large τ_1. Moreover terms in the near collinear expansion shout trouble: their dependence in σ_1 is so simple that they would not have any

Of course, this does *not* mean that we cannot describe this component within the POPE approach. On the contrary, as explained in [29], once using the inverse map we can express any component as a linear component of the nice χ-components which in turn we can describe at any loop order within the POPE. In this case, using the expression (21) of [29] we would find

$$
\begin{aligned}
\mathbb{W}^{(-1,-1,1,2)} = {}& \mathcal{P}_{12} \circ \mathcal{P} \circ \mathcal{P}_{34}\, e^{-\sigma_1-\sigma_2-\tau_2+\frac{i\phi_1}{2}} + \\
& \mathcal{P}_{12} \circ \mathcal{P}_3 \circ \mathcal{P}_4 \left(e^{-2\sigma_1-\tau_1-\tau_2-\frac{i\phi_1}{2}-\frac{i\phi_2}{2}} + e^{-\sigma_1-\tau_2+\frac{i\phi_1}{2}-\frac{i\phi_2}{2}} + e^{-\sigma_1-\sigma_2-2\tau_2+\frac{i\phi_1}{2}+\frac{i\phi_2}{2}} - \right. \\
& \left. e^{-\sigma_1-\sigma_2+\frac{i\phi_1}{2}+\frac{i\phi_2}{2}} \right) + \\
& \mathcal{P}_{12} \circ \mathcal{P}_{34} \circ \mathcal{P} \left(-e^{-2\sigma_1-\tau_1-\frac{i\phi_1}{2}} - e^{-\sigma_1-\sigma_2-\tau_2+\frac{i\phi_1}{2}+i\phi_2} - e^{-\sigma_1+\frac{i\phi_1}{2}} \right) + \\
& \mathcal{P}_{123} \circ \mathcal{P} \circ \mathcal{P}_4 \left(e^{-2\sigma_1-\tau_2-\frac{i\phi_2}{2}} + e^{-\sigma_1-\sigma_2-\tau_1+i\phi_1+\frac{i\phi_2}{2}} + e^{-\sigma_2+\frac{i\phi_2}{2}} \right) + \\
& \mathcal{P}_{123} \circ \mathcal{P}_4 \circ \mathcal{P} \left(e^{-\sigma_1-\tau_1-i\phi_1} + e^{-\sigma_1-\tau_1+i\phi_1} + e^{-\sigma_2-\tau_2+i\phi_2} + e^{-\sigma_1-\sigma_2-\tau_1-\tau_2+i\phi_1+i\phi_2} + \right. \\
& \left. e^{-2\sigma_1-2\tau_1} - e^{-2\sigma_1} + 1 \right) + \\
& \mathcal{P}_{1234} \circ \mathcal{P} \circ \mathcal{P} \left(e^{-2\sigma_1-\tau_1+\frac{i\phi_1}{2}} + e^{-\sigma_1-\frac{i\phi_1}{2}} \right).
\end{aligned}
$$

$$(5.73)$$

It is amusing to see how this precise linear combination of χ-components, each with a nice OPE expansion, combines into the component (5.72) without any obvious OPE picture. Conversely, and perhaps less trivially, according to [29], a generic χ-component is a precise linear combination of several η- components. These are the components that we shall directly confront against the integrability inspired predictions in the following subsections.

5.5.1 NMHV Hexagon

Due to R-charge conservation, different NMHV components will support different flux tube transitions. The hexagon – made out of two pentagons – is the simplest case where we can clearly see this at work. For the components $\mathcal{P}_{1234} \circ \mathcal{P}$ and $\mathcal{P} \circ \mathcal{P}_{1234}$, encountered before, the excitations flowing in the middle square should form an R-charge singlet (for example we could have the vacuum, any bound state of gluons, a pair $\psi_1 \bar{\psi}_{234}$, etc.). For $\mathcal{P}_{123} \circ \mathcal{P}_4$ ($\mathcal{P}_1 \circ \mathcal{P}_{234}$) we should have excitations with the same total R-charge as for a fermion (anti-fermion), that is the state should be in the fundamental (antifundamental) representation of $SU(4)$. Finally for $\mathcal{P}_{12} \circ \mathcal{P}_{34}$ we need the same R-charge as for a scalar,

---

sensible Fourier transform into momentum space. In short: this component is as weird as it could be from an OPE perspective.

i.e. a state in the vector representation of the R-symmetry group. As we have seen, these five components form a basis over which we can expand any other component [29].

We can write explicitly the OPE integrand for these *easy* components. At leading twist, they are (see figures 5.74 and 5.9)

$$
\mathcal{P}_{1234} \circ \mathcal{P} = 1 + \int_{\mathbb{R}} \frac{du}{2\pi} \hat{\mu}_{F_1}(u) \left(h_{F_{-1}}(u)\right)^4 \left(h_{F_1}(u)\right)^0 + \int_{\mathbb{R}} \frac{du}{2\pi} \hat{\mu}_{F_{-1}}(u) \left(h_{F_1}(u)\right)^4 \left(h_{F_{-1}}(u)\right)^0 + \dots ,
$$

$$
\mathcal{P}_{123} \circ \mathcal{P}_4 = g^{-\frac{3}{4}} \int_{\mathcal{C}} \frac{du}{2\pi} \hat{\mu}_{\psi}(u) \left(h_{\bar{\psi}}(u)\right)^3 h_{\psi}(u) + \dots , \tag{5.74}
$$

$$
\mathcal{P}_{12} \circ \mathcal{P}_{34} = g^{-1} \int_{\mathbb{R}} \frac{du}{2\pi} \hat{\mu}_{\phi}(u) \left(h_{\phi}(u)\right)^2 \left(h_{\phi}(u)\right)^2 + \dots ,
$$

$$
\mathcal{P}_1 \circ \mathcal{P}_{234} = g^{-\frac{3}{4}} \int_{\mathcal{C}} \frac{du}{2\pi} \hat{\mu}_{\bar{\psi}}(u) \, h_{\psi}(u) \left(h_{\bar{\psi}}(u)\right)^3 + \dots ,
$$

$$
\mathcal{P} \circ \mathcal{P}_{1234} = 1 + \int_{\mathbb{R}} \frac{du}{2\pi} \hat{\mu}_{F_{-1}}(u) \left(h_{F_1}(u)\right)^0 \left(h_{F_{-1}}(u)\right)^4 + \int_{\mathbb{R}} \frac{du}{2\pi} \hat{\mu}_{F_1}(u) \left(h_{F_{-1}}(u)\right)^0 \left(h_{F_1}(u)\right)^4 + \dots .
$$

Although in the first and last line we have the same allowed excitations, the form factors break the symmetry between the positive and negative helicity gluons. In particular, the first terms in $\mathcal{P}_{1234} \circ \mathcal{P}$ and $\mathcal{P} \circ \mathcal{P}_{1234}$ appear at tree level and the last terms are delayed to two loops, as confirmed from data.

As thoroughly described in [83], the contour of the integration $\mathcal{C}$ for the fermions is over a two-sheeted Riemann surface and can be conveniently splitted into two contributions: the large and small sheet contours. The large sheet contour is performed over the real axis with a small positive imaginary part whereas the small sheet contour is a counter-clockwise half-moon on the lower complex plane. It is then natural to treat these contributions independently as coming from a large fermion ψ_L and a small fermion ψ_S. In appendix G.2 we provide the explicit formulae for the analytic continuation of the pentagon transitions from the large to the small sheet.

Let us now study in detail the component $\mathcal{P}_{123} \circ \mathcal{P}_4$ at leading twist as an illustration of a check against data (see figure 5.9). The OPE integral splits into two terms corresponding to the large and small fermion contributions

$$
\mathcal{P}_{123} \circ \mathcal{P}_4 = g^{-\frac{3}{4}} \int_{\mathcal{C}_{\text{large}}} \frac{du}{2\pi} \hat{\mu}_{\psi_L}(u) \left(h_{\bar{\psi}_L}(u)\right)^3 h_{\psi_L}(u) + g^{-\frac{3}{4}} \int_{\mathcal{C}_{\text{small}}} \frac{du}{2\pi} \hat{\mu}_{\psi_S}(u) \left(h_{\bar{\psi}_S}(u)\right)^3 h_{\psi_S}(u) .
$$

$$\tag{5.75}$$

In this case the contour of integration $\mathcal{C}_{\text{small}}$ does not enclose any singularity, resulting in a vanishing contribution of the second term. We are only left with the first term that should be integrated slightly above the real axis. Using the explicit expressions for the measure and form factor at leading order in the coupling, we obtain

$$\mathcal{P}_{123} \circ \mathcal{P}_4 = e^{-\tau+i\phi/2} \int\limits_{\mathbb{R}+i0} \frac{du}{2\pi} \frac{-i\pi}{\sinh(\pi u)} e^{2iu\sigma} + \mathcal{O}(g^2)\,. \tag{5.76}$$

According to the map worked out in [29], this component should relate to a component of the super amplitude as follows

$$\mathcal{P}_{123} \circ \mathcal{P}_4 = \left((-\mathbf{1})_1\right)^3 (\mathbf{4})_2\, \mathcal{W}^{(-1,-1,-1,4)}\,, \tag{5.77}$$

where, as before, the pre-factor $(\mathbf{i})_j$ stands for the weight of the twistor Z_i in the jth pentagon. In order to extract this component we use the aforementioned package by running the following line in Mathematica

```
evaluate@superComponent[{1,2,3},{},{},{4},{},{}]@treeAmp[6,1]
```

still using the twistors given in Appendix F.2.[27] Upon expanding the outcome at leading order in the twist and taking into account the weights, we obtain a perfect match validating our conjecture for this particular transition.

The same type of checks are straightforward to generalize to the rest of the components or to one loop level using the same package [93]. These probe the expressions for the form factors presented in (5.66) at weak coupling. We have also verified the correctness of our conjectures beyond leading twist when also the pentagon transitions start to play a role. In the next section, we probe them more directly using the NMHV heptagon.

5.5.2 NMHV Heptagon

The NMHV heptagon is the appropriate laboratory to test the pentagon transitions involving all possible pairings of the fundamental excitations. In particular, it is the first polygon where the transitions between excitations in different squares arise. All the POPE building blocks take now part in and consequently they are all scrutinised.

---

[27]Note that one should convert between the OPE friendly and the cyclic labelling of the edges. Figure 5.74.**a** shows both labellings for the hexagon.

The heptagon has fifteen independent components [29], represented in figure 5.10. Five of them, in the top line of that figure, can be constructed in a similar manner to the hexagon by charging the outermost pentagons. To generate the remaining ten independent components, it is unavoidable charging the middle pentagon. According to [29], charging the middle pentagon typically involves rather nontrivial linear combinations of the super amplitude η- components. Since we are also interested in testing this map, in what follows we will focus mostly on such examples in which the middle pentagon is charged.

To leading twist each of the fifteen heptagon components probes a different pentagon transition, see figure 5.10. We verified that their near collinear expansions are indeed in perfect agreement with the proposals of the previous section once expanded out to leading order in perturbation theory. Interesting as they are, the analysis of these cases follow [82] almost verbatim and is therefore not particularly illuminating to present it in detail. Instead, in this section we will consider a richer example involving multi-particle states in both middle squares. These examples allow one to get a good picture of how generic transitions show up at weak coupling. They also probe considerably more structures in a very non-trivial way and allow us to stress the important role of the so-called *small fermions*. The matrix part in the first one is trivially equal to 1 and in the second case it is simple and has been determined before in [83].

The examples where more complicated matrices appear were also tested but we leave them for a future publication, where the general construction of the matrix part will be presented. All in all, we have tested *all* possible transitions at tree level up to twists three in one square and two in the second one and several twist three (in both squares) transitions with simple matrix part (in a total of 429 processes).

It is instructive to present one such example in detail. We will analyse the $\mathcal{P} \circ \mathcal{P}_{123} \circ \mathcal{P}_4$ component through the POPE lens. As mentioned above, to make things more interesting and nontrivial we will look at some high twist contribution involving several particles and/or bound-states. To be precise we shall consider the term proportional to

$$e^{-3\tau_1 - 3i\phi_1} \times e^{-3\tau_2 + 5/2i\phi_2} \tag{5.78}$$

as illustration. What flux tube physical processes govern this contribution? To answer this question it suffices to list everything that has the right quantum numbers to be allowed to flow. In the case at hand we are looking at states with twist 3 both in the first middle square and the second square. We are searching for states with helicity -3 in the first square and $+5/2$ in the second square. Finally, we have R-charge considerations. For the sequence $\mathcal{P} \circ \mathcal{P}_{123} \circ \mathcal{P}_4$ we necessarily have an R-charge singlet in the first middle square and a state in the fundamental (**4**) representation of $SU(4)$ in the second middle square.
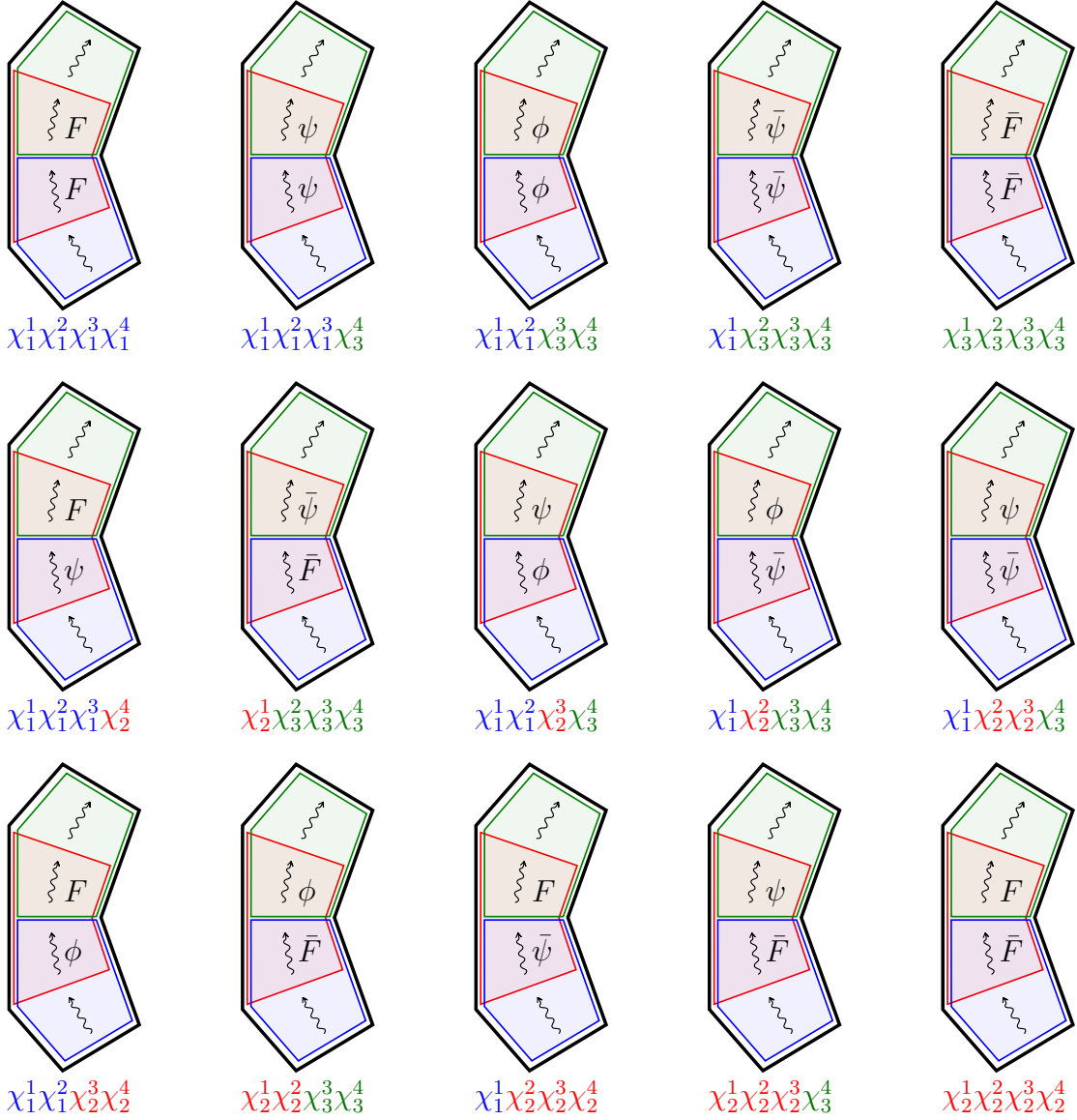
137

Figure 5.10: Fifteen independent components for the NMHV heptagon with the corresponding excitations at twist one. The components in the first line involve charging the bottom and top pentagons only while the second and third line correspond to the remaining ten components where the middle pentagon is also charged. As illustrated here, each such component can be used as a direct probe of a pentagon transition.
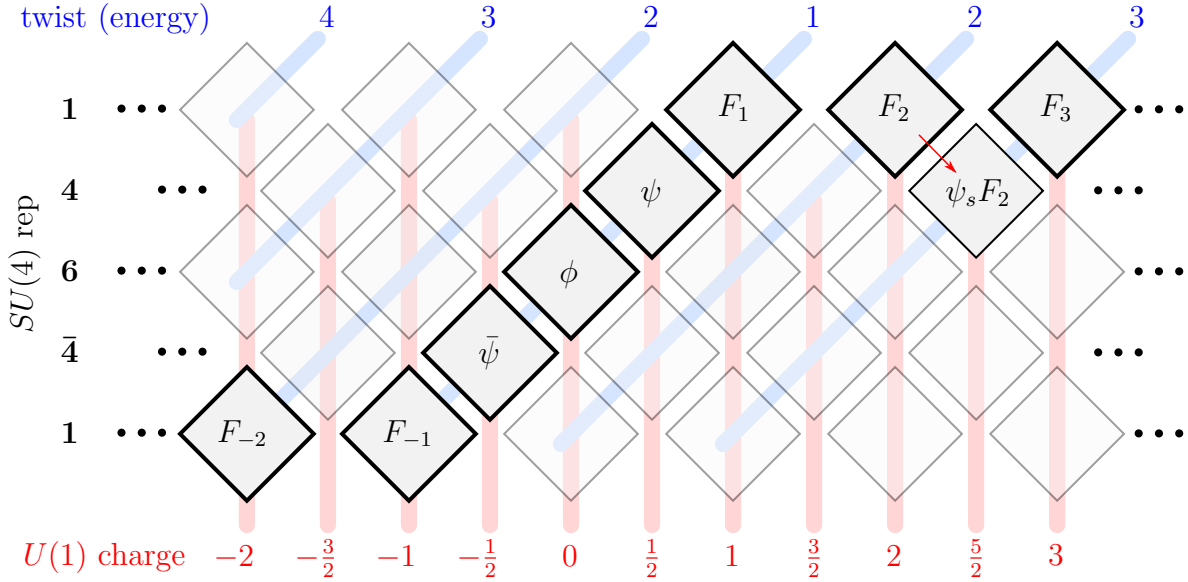
Figure 5.11: Fundamental excitations together with the effective excitation $\psi_s F_2$ (a.k.a. $\mathcal{D}_{1\dot{2}}^2 \psi$) used in the example.

All in all, this information restricts the matter content enormously.

In the first square, for example, the absolute value of the helicity is maximal, equal to the twist of the state. This saturation is achieved for purely gluonic states only, see figure 5.11. There are therefore only three possible states in the first middle square,

$$|F_{-1}(u)F_{-1}(v)F_{-1}(w)\rangle\,, \qquad |F_{-2}(u)F_{-1}(v)\rangle\,, \qquad |F_{-3}(u)\rangle\,. \qquad (5.79)$$

The first two are multi-particle states and kick in at higher loop orders. The last one, corresponding to a bound-state of three negative helicity gluons, is the only one showing up at leading order at weak coupling.

In the second square things are more interesting. With helicity $5/2$ there are only two possible states we could envisage:

$$|F_1(u)F_1(v)\psi(w)\rangle\,, \qquad |\psi(w)F_2(u)\rangle\,. \qquad (5.80)$$

At first we could imagine discarding both since they are both multi-particle states; however, when fermions are involved the coupling analysis is more subtle. The point is that fermions can be either small or large and in the former case they act as sort of symmetry

139

generators [83]. As such each of the states in (5.80) can be split into two cases depending on whether the fermion is small or large. In particular, the second state $|F_2(u)\psi(v)\rangle$ with the fermion evaluated in the small fermion domain can be seen as a supersymmetry generator acting on the excitation $F_2(u)$ thus generating a *single* effective weak coupling excitation – see figure 5.11 – and as such might show up already at leading order at weak coupling. (At the same time the first state $|F_1(u)F_1(v)\psi(w)\rangle$ with ψ being a small fermion would behave as a two particle state and thus show up only at higher orders in perturbation theory.)

In sum, to match against tree level data it suffices to focus on the process

$$\texttt{vacuum} \to F_{-3}(u) \to \psi(w)F_2(v) \to \texttt{vacuum}, \tag{5.81}$$

which is what we turn to now. In this case the matrix part is trivial. Indeed, the R-charge index of the fermion is unambiguously fixed once we pick an R-charge configuration for the various χ's. In other words, the matrix part in (5.36) is equal to one and the full integrand is just a product of the dynamical part and the form factor contribution. According to (5.38) and (5.66) these read

$$\texttt{dynamical part} = \hat{\mu}_{F_{-3}}(u)\,\hat{\mu}_\psi(w)\,\hat{\mu}_{F_2}(v)\,\frac{P_{\bar{\psi}|F_3}(w|u)P_{F_{-2}|F_3}(v|u)}{P_{\bar{\psi}|F_{-2}}(w|v)P_{F_2|\psi}(v|w)}, \tag{5.82}$$

$$\texttt{form factors part} = \frac{1}{g^{\frac{3}{4}}}\,(h_{F_3}(u))^0\,(h_{F_{-3}}(u))^3\,(h_{\bar{\psi}}(w))^3\,(h_{F_{-2}}(v))^3\,h_\psi(w)\,h_{F_2}(v) \tag{5.83}$$

which we simply multiply together to obtain the POPE prediction

$$\mathcal{W}_{F_{-3}\to\psi F_2} = \int_{\mathbb{R}}\frac{du}{2\pi}\int_{\mathbb{R}}\frac{dv}{2\pi}\int_{\bar{\mathcal{C}}_{\text{small}}}\frac{dw}{2\pi}\,(\texttt{dynamical part})\times(\texttt{form factors part}), \tag{5.84}$$

where $\bar{\mathcal{C}}_{\text{small}}$ is the *complex conjugate* version of the half-moon contour mentioned below (5.74), hence running in the upper half u plane, in agreement with the alternating conventions in (5.38). (Equivalently, depending on the $\pm$ sign in front of $ip\sigma$ in (5.38) we use an $\pm i\epsilon$ prescription for integration around zero momentum fermions in the corresponding square.) Plugging all the building blocks together, we therefore arrive at

$$\mathcal{W}_{F_{-3}\to\psi F_2} = e^{-3\tau_1-3i\phi_1}\times e^{-3\tau_2+5/2i\phi_2}\times \tag{5.85}$$

$$\times\int_{\mathbb{R}}\frac{du}{2\pi}\int_{\mathbb{R}}\frac{dv}{2\pi}\int_{\bar{\mathcal{C}}_{\text{small}}}\frac{dw}{2\pi}\,\frac{w\,\Gamma\left(\frac{5}{2}+iu\right)\Gamma(2-iv)\Gamma\left(\frac{7}{2}-iu+iv\right)}{2i\left(u^2+\frac{9}{4}\right)(v^2+1)\left((v-w)^2+1\right)}e^{2iu\sigma_1-2i(v+w)\sigma_2}+\mathcal{O}(g^2),$$

and verify that, despite the funny fractional powers of the coupling appearing in the individual ingredients, the resulting integrand has a regular expansion in g^2 and starts at tree level, as expected.

One of the three integrals involves a small fermion $\psi(w)$ integrated over its corresponding small fermion contour $\bar{\mathcal{C}}_{\text{small}}$. An important universal property of small fermions is that they can always be straightforwardly integrated out (at any value of the coupling in fact). In this tree level example we see that the only singularity inside the half moon encircling the upper half plane is the single pole at $w = v + i$. The fermion integral thus collapses into the corresponding residue contribution which freezes w to be attached to the rapidity v in a Bethe string like pattern. The interpretation of such strings is that the fermion is acting as a symmetry generator on the other excitation in this square, the bound-state of gluons $F_2(v)$. The result of this action is an effective twist 3 weak coupling excitation, see figure 5.11, which is described by the Bethe string.

In sum, after integrating out the small fermion we end up with the integrations in u and v for a single effective particle in each square. The resulting integral can then be straightforwardly performed leading to the prediction

$$
\begin{aligned}
\mathcal{W}_{F_{-3} \to \psi F_2} = \; & \frac{e^{-3\tau_1 - 3\tau_2 - 3i\phi_1 + 5i\phi_2/2}}{\left(e^{2\sigma_1} + 1\right)^3 \left(e^{2\sigma_2} + 1\right)^3 \left(e^{2\sigma_2 + 2\sigma_1} + e^{2\sigma_2} + e^{2\sigma_1}\right)^5} \times \big(e^{13\sigma_1 + 2\sigma_2} + 5\,e^{11\sigma_1 + 4\sigma_2} + 8\,e^{13\sigma_1 + 4\sigma_2} \\
& + 10\,e^{9\sigma_1 + 6\sigma_2} + 35\,e^{11\sigma_1 + 6\sigma_2} + 28\,e^{13\sigma_1 + 6\sigma_2} + 10\,e^{7\sigma_1 + 8\sigma_2} + 60\,e^{9\sigma_1 + 8\sigma_2} + 105\,e^{11\sigma_1 + 8\sigma_2} \\
& + 56\,e^{13\sigma_1 + 8\sigma_2} + 5\,e^{5\sigma_1 + 10\sigma_2} + 35\,e^{7\sigma_1 + 10\sigma_2} + 105\,e^{9\sigma_1 + 10\sigma_2} + 130\,e^{11\sigma_1 + 10\sigma_2} + 55\,e^{13\sigma_1 + 10\sigma_2} \\
& + e^{3\sigma_1 + 12\sigma_2} + 8\,e^{5\sigma_1 + 12\sigma_2} + 28\,e^{7\sigma_1 + 12\sigma_2} + 56\,e^{9\sigma_1 + 12\sigma_2} + 55\,e^{11\sigma_1 + 12\sigma_2} + 20\,e^{13\sigma_1 + 12\sigma_2} \big) .
\end{aligned}
\tag{5.86}
$$

This example clearly illustrates the importance of checking the integrability against perturbative data. After all, it is clearly a tall order to reproduce any result of the complexity of (5.86). According to the proposal in [29], the amplitude $\mathcal{P} \circ \mathcal{P}_{123} \circ \mathcal{P}_4$ can be extracted from standard η-components as

$$
\left(\frac{\partial}{\partial\chi_2}\right)^3 \frac{\partial}{\partial\chi_3} \mathcal{W} = \frac{(\mathbf{5})_3}{((\mathbf{1})_2(\mathbf{2})_2(\mathbf{3})_2)^3} \left(\langle 1,2,3,-1\rangle \frac{\partial}{\partial\eta_{-1}} + \langle 1,2,3,0\rangle \frac{\partial}{\partial\eta_0} \right)^3 \frac{\partial}{\partial\eta_5} \mathcal{W}
\tag{5.87}
$$

$$
= \frac{(\mathbf{5})_3}{((\mathbf{1})_2(\mathbf{2})_2(\mathbf{3})_2)^3} \big(\langle 1,2,3,-1\rangle^3\, \mathcal{W}^{(-1,-1,-1,5)} + \langle 1,2,3,-1\rangle^2 \langle 1,2,3,0\rangle\, \mathcal{W}^{(-1,-1,0,5)}
$$

$$
+ \langle 1,2,3,-1\rangle \langle 1,2,3,0\rangle^2\, \mathcal{W}^{(-1,0,0,5)} + \langle 1,2,3,0\rangle^3\, \mathcal{W}^{(0,0,0,5)} \big) .
\tag{5.88}
$$

Each of these components can be obtained by running similar code lines in Mathematica as in the previous example of the hexagon, using the heptagon twistors in the Appendix
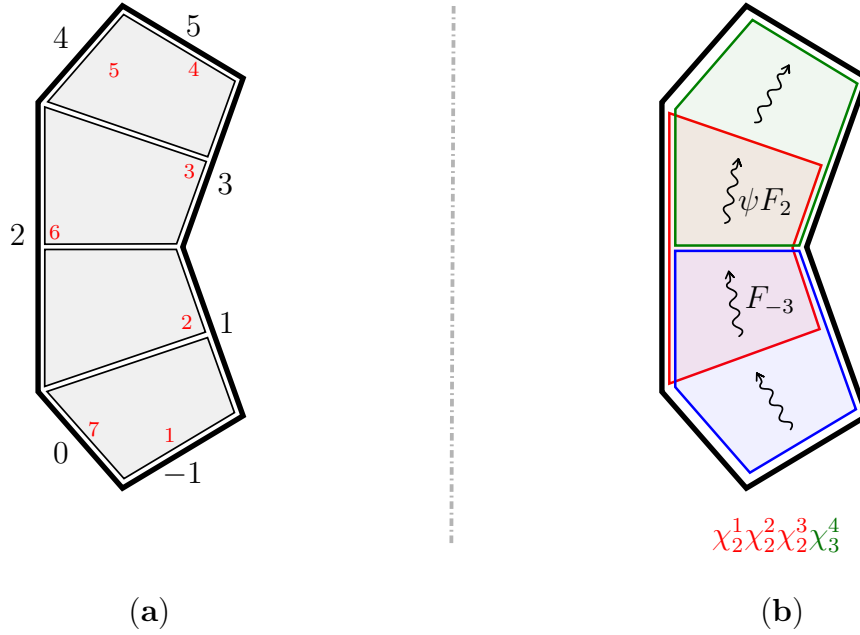
Figure 5.12: (**a**) The POPE friendly edge labelling used in this chapter (big black outer numbers) versus the more conventional cyclic labelling (small red inner numbers) for the heptagon. (**b**) The NMHV heptagon process analysed in this section.

F.2. Once we evaluate the brackets and the weights, we expand the result at large τ_1 and τ_2 and pick the term proportional to (5.78). In this way we obtain a perfect match with the expression (5.86)!

These are formidable checks of the full POPE construction as they are probing, at the same time, the map between charging pentagons and charging edges of [29] as well as the (weak coupling expansion of) the various elements of the POPE integrand. We performed several other checks of this sort (more than a hundred of them) always obtaining a perfect match. We also explored some higher loop data but our analysis there was much less thorough. It would be interesting to push it much further both in higher twists and higher loops. In particular, it would be nice to make contact with the very interesting recently uncovered heptagon bootstrap [110]. This ends the second part of this thesis.

Chapter 6

Final remarks

Solving a non-trivial interacting four dimensional quantum field theory seems now conceivable for the first time. Planar $\mathcal{N} = 4$ SYM appears to be a gifted point in the space of quantum field theories, combining so many symmetries that we can aim at obtaining non-perturbative solutions for many observables. In this regard, integrability is at the core of the main developments of the last years. In this thesis, we have explored two main classes of such observables: the higher point correlation functions and the scattering amplitudes/Wilson loops. In the correlation function problem, we have studied both the weak and strong coupling regimes, where integrability emerges in two distinct ways with no *a priori* connection. At weak coupling, the representation of the single trace operators in terms of spin chains allows us to make use of technology that often appears on integrable condensed matter or statistical physics systems, such as Bethe ansatz, scalar products of Bethe states and integrable form factors. It contrasts with the strong coupling side of the problem, where integrability is associated to the classical two dimensional sigma model describing the world-sheet. The computation of a correlation function in this regime is that of determining the area of a minimal surface embedded in AdS with specific boundary conditions. This problem turns out to be solvable precisely due to the integrability of the sigma model.

In the study of scattering amplitudes, we have seen that this quantity is dual to the expectation value of a null polygonal Wilson loop. This Wilson loop supports a 1+1 dimensional integrable flux tube, whose spectrum and S-matrix of its excitations are known non-perturbatively. In order to compute its expectation value, it was proposed to break the polygon into more fundamental building blocks, namely the *pentagons*, that could be bootstrapped using integrability. Later we glued them back together by performing a sum over all propagating states in the Wilson loop.

Let us now put the results of this thesis in the broader context of the state-of-the-art of integrability in $\mathcal{N} = 4$ SYM. The weak coupling computation of the three point function we have presented here proved to be an important check point for the most recent integrability based bootstrap proposal of [31] (see also [112]). In this groundbreaking paper, the authors proposed a framework to compute the all-loop structure constants in planar $\mathcal{N} = 4$ SYM. The three point function is pictured as a pair of pants, which can be regarded as the splitting of a closed string into two other closed strings. Then the main step was to cut the pair of pants into two hexagons which are more fundamental objects. Each of these hexagons inherit some of the excitations associated to the original closed string states. The dynamics of these excitations is integrable which allows to bootstrap the hexagons pretty much in analogy with the pentagons of the Wilson loop. Later these hexagons are glued back together by summing over the excitations along the cuts.

In both three-point function and scattering amplitudes problems, the all-loop solutions involve the idea of breaking an object into smaller building blocks that are bootstrappable by integrability, and then gluing them back together by performing a certain sum over states whose charges and dynamics are fully under control at all loops. In the case of the three point functions, these states are described by excitations above the BMN vacuum whereas in the case of scattering amplitudes it is over the GKP vacuum. In both cases there is an an all-loop Bethe ansatz description.

On the other hand, at strong coupling there is also some sort of unifying picture in both problems. As mentioned in the core of the thesis, the scenario we have described for the correlation functions is analogous for the scattering amplitudes. From the string theory point of view, the scattering amplitude is also given by the area of a minimal surface in AdS ending on a null polygonal contour. This problem was solved for general null polygons in [57] and for smooth Wilson loops in [111]. It is natural to ask how the non-perturbative proposals just described give rise to this more geometrical picture emerging in the string side. In fact, part of it was already answered in [31] for the three-point functions and [81] for scattering amplitudes, where the bootstrap solutions were shown to be consistent with the minimal surfaces results. It would be very interesting to reconstruct the four point function from the non-perturbative knowledge of the structure constants and recover the strong coupling results presented in this thesis.

In addition to these two non-perturbative results for three point functions and scattering amplitudes/Wilson loops, the solution of the spectral problem is also available in the literature and given in its most advanced form by the so-called *Quantum Spectral Curve* [24]. The method behind the spectral curve is different from cutting and gluing as in the other examples, even though it might be possible to apply that logic by considering a cylinder (which is the topology of the closed string associated to the two point function problem),

145

break it into squares and bootstrap them. Nevertheless, in the Quantum Spectral Curve there is no such sum over excitations and the efficiency of the method is truly remarkable. One might wonder whether such powerful technology can possibly exist for these other observables.

Zooming out a little bit more, planar $\mathcal{N} = 4$ SYM seems to be very special among all quantum field theories which raises many interrogations about what is really transferable from solving it. One obvious question is how dependent of the large N limit this solution is. Can we go beyond the planar limit? So far the studies of non-planar corrections to anomalous dimensions did not yet reveal any traces of integrability (see [113] for a review). In particular, the first $1/N$ correction to the dilatation operator involves the splitting and joining of spin chains, and all the sites interact with each other. It is therefore unclear how to define an asymptotic regime and integrability concepts like asymptotic S-matrix or two-particle scattering are not applicable at least in the standard way. Related to this question, is the somehow curious fact that for computing some *planar* structure constants, namely those associated with extremal three-point functions, it is important to consider the mixing of single with double trace operators which requires a diagonalization of the non-planar dilatation operator. Perhaps methods inspired on the integrable bootstrap for (non-extremal) three point functions [31] can be extended for the extremal case and from there we might access some non-planar information of the theory. In any case, this issue is clearly calling for an ingenious way out.

Along the same lines, how extendable and useful are these results to attack less symmetric theories like QCD? One particular connection that we might hope to establish is with the QCD string or flux tube. As we have seen, the $\mathcal{N} = 4$ flux tube is integrable. There is no reason to expect the same to happen for the QCD flux tube though. That said, it is interesting to point out that approximate low energy integrability of the worldsheet theory was recently used [114, 115] for perturbative calculations of the spectrum of confining strings in non-supersymmetric theories. The search for integrable flux tubes on less symmetric theories is certainly an important route and the first steps were already taken in [116].

On a more speculative guise, the origin of integrability and whether there is a connection between integrability and dualities with string theories remain obscure despite of all exact results already obtained. How do exactly gauge fields become strings and vice-versa in $\mathcal{N} = 4$ SYM as we tune the coupling? Is it a general mechanism that can be exported to other examples of gauge/gravity dualities and aid at constructing new duals of gauge theories?

The solutions we just described constitute the state-of-the-art of the first complete

all-loop description of a gauge theory in four dimensions. We believe this will stand as a reference model to test new techniques or ideas that might emerge in the future for quantum field theories, in similar fashion to the role that the Onsager's solution of the two dimensional Ising model played in the development of statistical physics and field theory. Many doors are being opened right now and the depth of our questions is increasing as our knowledge of existing theories expands. For these reasons, the next years promise to be exciting. This is the end of the thesis.

APPENDICES

Appendix A

One-loop perturbative computation details

A.1 Notation and conventions

In this Appendix, we fix our conventions for the perturbative computations. The $\mathcal{N} = 4$ SYM with $SU(N)$ gauge group has the Lagrangian given by formula (1.7) presented in the introduction. The propagators extracted from this Lagrangian are (we are suppressing the gauge indices and taking the leading order in N)

$$\langle \Phi^{ab}(x)\Phi_{cd}(0)\rangle = \frac{\bar{\delta}^{ab}_{cd}}{8}\frac{1}{(2\pi)^2(-x^2+i\epsilon)}\,,$$

$$\langle \psi^a_\alpha(x)\bar{\psi}_{\dot{\beta}b}(0)\rangle = \frac{i\,\delta^a_b}{2}\sigma^\mu_{\alpha\dot{\beta}}\partial_\mu\frac{1}{(2\pi)^2(-x^2+i\epsilon)}\,,$$

$$\langle A_\mu(x)A_\nu(0)\rangle = -\frac{\eta_{\mu\nu}}{2}\frac{1}{(2\pi)^2(-x^2+i\epsilon)}\,,$$

where $\bar{\delta}^{ab}_{cd} \equiv \delta^a_c\delta^b_d - \delta^b_c\delta^a_d$. We are using the Minkowski metric $(+---)$ and the Feynman gauge. The action of the (classical) supersymmetry generators are given by [118]

$$[q^\alpha{}_a, \Phi^{bc}] = \frac{i\sqrt{2}}{2}\left(\delta^b_a\psi^{\alpha c} - \delta^c_a\psi^{\alpha b}\right)\,,$$

$$[q^\alpha{}_a, \psi^b_\beta] = \delta^b_a F^\alpha_\beta\,,$$

$$[q^\alpha{}_a, \bar{\psi}^{\dot{\beta}}_b] = 2\sqrt{2}\,\mathcal{D}^{\dot{\beta}\alpha}\Phi_{ab}\,,$$

150

and the conjugate expressions for the action of $\bar{q}^a{}_{\dot{\alpha}}$. The action of the R-symmetry generators is given by

$$[r^a{}_b, \Phi^{cd}] = \delta^c_b \, \Phi^{ad} + \delta^d_b \, \Phi^{ca} - \frac{1}{2}\delta^a_b \, \Phi^{cd} \,,$$

$$[r^a{}_b, \psi^c] = \delta^c_b \, \psi^a - \frac{1}{4}\delta^a_b \, \psi^c \,.$$

In the computations of the Feynman diagrams, in particular for the evaluation of the integrals, we analytical continued to Euclidean space by using

$$x^0 = ix^4 \,, \qquad \sigma^0_M = -\sigma^0_E \,, \qquad \sigma^i_M = i\sigma^i_E \,,$$

where the subscripts M means Minkowski space and E means Euclidean space,

$$\sigma^0_M = \mathrm{Id}_{2\times2} \,,$$

and, finally, σ^i_M are the usual Pauli matrices.

A.2 Details of the perturbative computation

We now present the details of the perturbative computation of the three-point functions at one-loop using the point splitting regularization. As reviewed in the main text, in order to obtain scheme and normalization independent structure constants we also need to know the results of the two-point functions.

Typically three kinds of integrals will appear in the computations

$$Y_{123} = \int d^4u \, I_{x_1 u} I_{x_2 u} I_{x_3 u} \,,$$

$$X_{1234} = \int d^4u \, I_{x_1 u} I_{x_2 u} I_{x_3 u} I_{x_4 u} \,,$$

$$H_{12,34} = \int d^4u \, d^4v \, I_{x_1 u} I_{x_2 u} I_{uv} I_{x_3 v} I_{x_4 v} \,,$$

where $I_{x_a x_b}$ is the (euclidean) scalar propagator defined as

$$I_{x_a x_b} \equiv \frac{1}{(2\pi)^2(x_a - x_b)^2} \,.$$

151

The Y and X integrals are well-known and explicit expressions for them can be found for instance in [36, 119]. The integral H is not known analytic, however, only its derivatives will be needed. In particular, the following combination [119] turns out to be useful

$$
\begin{aligned}
F_{12,34} &\equiv \frac{(\partial_1 - \partial_2) \cdot (\partial_3 - \partial_4) H_{12,34}}{I_{x_1 x_2} I_{x_3 x_4}} \qquad\qquad\qquad\qquad\qquad\qquad\text{(A.1)} \\
&= \frac{X_{1234}}{I_{x_1 x_3} I_{x_2 x_4}} - \frac{X_{1234}}{I_{x_1 x_4} I_{x_2 x_3}} + G_{1,34} - G_{2,34} + G_{3,12} - G_{4,12}\,,
\end{aligned}
$$

where

$$
G_{a,bc} = \frac{Y_{abc}}{I_{x_a x_c}} - \frac{Y_{abc}}{I_{x_a x_b}}\,.
$$

We will need several limits of the expressions for Y and X, namely when pairs of distinct points collapse into each other

$$
Y_{113} \equiv \lim_{x_2 \to x_1} Y_{123} = \left(2 - \log\left(\frac{\epsilon^2}{x_{13}^2}\right)\right) \frac{I_{x_1 x_3}}{16\pi^2}\,,
$$

$$
X_{1134} \equiv \lim_{x_2 \to x_1} X_{1234} = \left(2 - \log\left(\frac{\epsilon^2 x_{34}^2}{x_{13}^2 x_{14}^2}\right)\right) \frac{I_{x_1 x_3} I_{x_1 x_4}}{16\pi^2}\,,
$$

where we are considering $x_2^\mu = x_1^\mu + \epsilon^\mu$ with $\epsilon^\mu \to 0$. We can also take a further limit of the last expression above when $x_4 \to x_3$ giving

$$
X_{1133} = \left(1 - \log\left(\frac{\epsilon^2}{x_{13}^2}\right)\right) \frac{I_{x_1 x_3}^2}{8\pi^2}\,.
$$

Moreover, we also need limits of the first and second derivatives of both the Y and the X integrals. We include the results of them below for completeness. The first derivatives are given by

$$
\lim_{x_2 \to x_1} \partial_{1,\mu} Y_{123} = \frac{\epsilon_\mu}{\epsilon^2} \frac{I_{x_1 x_3}}{8\pi^2} - \left(1 - \log\left(\frac{\epsilon^2}{x_{13}^2}\right)\right) \frac{x_{13,\mu} I_{x_1 x_3}^2}{4} - \frac{x_{13,\nu} \epsilon^\nu \epsilon_\mu I_{x_1 x_3}^2}{2\epsilon^2}\,, \qquad\text{(A.2)}
$$

$$
\lim_{x_2 \to x_1} \partial_{3,\mu} Y_{123} = \left(1 - \log\left(\frac{\epsilon^2}{x_{13}^2}\right)\right) \frac{x_{13,\mu} I_{x_1 x_3}^2}{2}\,, \qquad\qquad\qquad\qquad\qquad\text{(A.3)}
$$

$$
\begin{aligned}
\lim_{x_2 \to x_1} \partial_{1,\mu} X_{1234} =\ & \frac{\epsilon_\mu}{\epsilon^2} \frac{I_{x_1 x_3} I_{x_1 x_4}}{8\pi^2} - \left(1 - \log\left(\frac{\epsilon^2 x_{34}^2}{x_{13}^2 x_{14}^2}\right)\right) \frac{x_{13,\mu} I_{x_1 x_3}^2 I_{x_1 x_4} + x_{14,\mu} I_{x_1 x_3} I_{x_1 x_4}^2}{4} \\
& - \frac{x_{14,\nu} \epsilon^\nu \epsilon_\mu I_{x_1 x_3} I_{x_1 x_4}^2}{2\epsilon^2} - \frac{x_{13,\nu} \epsilon^\nu \epsilon_\mu I_{x_1 x_3}^2 I_{x_1 x_4}}{2\epsilon^2}\,,
\end{aligned}
$$

$$
\lim_{x_2 \to x_1} \partial_{3,\mu} X_{1234} = -\frac{x_{34,\mu} I_{x_1 x_3} I_{x_1 x_4} I_{x_3 x_4}}{2} + \left(1 - \log\left(\frac{\epsilon^2 x_{34}^2}{x_{13}^2 x_{14}^2}\right)\right) \frac{x_{13,\mu} I_{x_1 x_3}^2 I_{x_1 x_4}}{2}\,,
$$

As before, one can take further limits of these expressions when needed. The second derivatives read

$$
\begin{aligned}
\lim_{x_2 \to x_1} \partial_{1,\mu} \partial_{2,\nu} Y_{123} \;=\;& -\frac{\epsilon_\mu \epsilon_\nu}{\epsilon^4} \frac{I_{x_1 x_3}}{4\pi^2} + \frac{\epsilon_\mu \epsilon_\nu I_{x_1 x_3}^2}{\epsilon^2} \Big(\frac{1}{6} + \frac{x_{13,\rho}\, \epsilon^\rho}{\epsilon^2} - \frac{16\pi^2 x_{13,\rho}\, \epsilon^\rho x_{13,\sigma}\, \epsilon^\sigma I_{x_1 x_3}}{3\epsilon^2} \Big) \\
+\;& \frac{\epsilon_\nu}{\epsilon^2} \frac{x_{13,\mu} I_{x_1 x_3}^2}{2} - \frac{\epsilon_\mu}{\epsilon^2} \frac{x_{13,\nu} I_{x_1 x_3}^2}{2} + \frac{8\pi^2 x_{13,\rho}\, \epsilon^\rho I_{x_1 x_3}^3}{3\epsilon^2} \left(2x_{13,\nu} \epsilon_\mu - x_{13,\mu} \epsilon_\nu \right) \\
+\;& \frac{1}{\epsilon^2} \frac{\delta_{\mu\nu} I_{x_1 x_3}}{8\pi^2} - \delta_{\mu\nu} I_{x_1 x_3}^2 \Big(\frac{11}{36} + \frac{x_{13,\rho} \epsilon^\rho}{2\epsilon^2} - \frac{8\pi^2 x_{13,\rho}\, \epsilon^\rho x_{13,\sigma}\, \epsilon^\sigma I_{x_1 x_3}}{3\epsilon^2} \Big) \\
+\;& \frac{1}{12} \log \Big(\frac{\epsilon^2}{x_{13}^2} \Big) I_{x_1 x_3}^2 \delta_{\mu\nu} + \frac{2\pi^2}{9} \Big(1 - 6 \log \Big(\frac{\epsilon^2}{x_{13}^2} \Big) \Big) x_{13,\mu} x_{13,\nu} I_{x_1 x_3}^3 \,, \\[4pt]
\lim_{x_2 \to x_1} \partial_{1,\mu} \partial_{3,\nu} Y_{123} \;=\;& \frac{\epsilon_\mu \epsilon_\nu I_{x_1 x_3}^2}{\epsilon^2} + \frac{\epsilon_\mu}{\epsilon^2} x_{13,\nu} I_{x_1 x_3}^2 - 2\pi^2 \Big(1 - 2 \log \Big(\frac{\epsilon^2}{x_{13}^2} \Big) \Big) x_{13,\mu} x_{13,\nu} I_{x_1 x_3}^3 \\
+\;& \frac{1}{4} \Big(1 - \log \Big(\frac{\epsilon^2}{x_{13}^2} \Big) \Big) I_{x_1 x_3}^2 \delta_{\mu\nu} - \frac{8\pi^2 x_{13,\nu}\, \epsilon_\mu\, x_{13,\rho}\, \epsilon^\rho I_{x_1 x_3}^3}{\epsilon^2} \,, \qquad\text{(A.4)}
\end{aligned}
$$

153

$$
\begin{aligned}
\lim_{x_2 \to x_1} \partial_{1,\mu}\partial_{2,\nu} X_{1234} \;=\;\; & -\frac{\epsilon_\mu\,\epsilon_\nu}{\epsilon^4}\frac{I_{x_1x_3}I_{x_1x_4}}{4\pi^2} + \frac{\epsilon_\mu\,\epsilon_\nu I_{x_1x_3}^2 I_{x_1x_4}^2}{6\epsilon^2}\left(\frac{1}{I_{x_3x_4}} - \frac{32\pi^2 x_{13,\rho}\,\epsilon^\rho\,x_{14,\sigma}\,\epsilon^\sigma}{\epsilon^2}\right) \\[4pt]
& + \frac{\epsilon_\mu\,\epsilon_\nu\,\epsilon^\rho I_{x_1x_3}I_{x_1x_4}}{\epsilon^4}\left(x_{14,\rho}I_{x_1x_4} + x_{13,\rho}I_{x_1x_3}\right) \\[4pt]
& - \frac{16\pi^2\,\epsilon_\mu\,\epsilon_\nu\,\epsilon^\rho\,\epsilon^\sigma I_{x_1x_3}I_{x_1x_4}}{3\epsilon^4}\left(x_{14,\rho}x_{14,\sigma}I_{x_1x_4}^2 + x_{13,\rho}x_{13,\sigma}I_{x_1x_3}^2\right) \\[4pt]
& - \frac{\epsilon_\mu I_{x_1x_3}I_{x_1x_4}}{2\epsilon^2}\left(x_{14,\nu}I_{x_1x_4} + x_{13,\nu}I_{x_1x_3}\right) \\[4pt]
& + \frac{\epsilon_\nu I_{x_1x_3}I_{x_1x_4}}{2\epsilon^2}\left(x_{14,\mu}I_{x_1x_4} + x_{13,\mu}I_{x_1x_3}\right) \\[4pt]
& + \frac{8\pi^2\epsilon_\mu\,\epsilon^\rho I_{x_1x_3}I_{x_1x_4}}{3\epsilon^2}\left(2x_{14,\nu}\,x_{14,\rho}\,I_{x_1x_4}^2 + x_{13,\rho}\,x_{14,\nu}\,I_{x_1x_3}I_{x_1x_4}\right) \\[4pt]
& + \frac{8\pi^2\epsilon_\mu\,\epsilon^\rho I_{x_1x_3}I_{x_1x_4}}{3\epsilon^2}\left(2x_{13,\nu}\,x_{13,\rho}\,I_{x_1x_3}^2 + x_{14,\rho}\,x_{13,\nu}\,I_{x_1x_3}I_{x_1x_4}\right) \\[4pt]
& - \frac{4\pi^2\epsilon_\nu\,\epsilon^\rho I_{x_1x_3}I_{x_1x_4}}{3\epsilon^2}\left(2x_{14,\mu}\,x_{14,\rho}I_{x_1x_4}^2 + x_{13,\rho}\,x_{14,\mu}I_{x_1x_3}I_{x_1x_4}\right) \\[4pt]
& - \frac{4\pi^2\epsilon_\nu\,\epsilon^\rho I_{x_1x_3}I_{x_1x_4}}{3\epsilon^2}\left(2x_{13,\mu}\,x_{13,\rho}I_{x_1x_3}^2 + x_{14,\rho}\,x_{13,\mu}I_{x_1x_3}I_{x_1x_4}\right) \\[4pt]
& + \frac{1}{\epsilon^2}\frac{I_{x_1x_3}I_{x_1x_4}\delta_{\mu\nu}}{8\pi^2} - \frac{I_{x_1x_3}I_{x_1x_4}\delta_{\mu\nu}}{4}\left(I_{x_1x_4} + I_{x_1x_3}\right) \\[4pt]
& - \frac{I_{x_1x_3}I_{x_1x_4}\delta_{\mu\nu}\,\epsilon^\rho}{2\epsilon^2}\left(x_{14,\rho}\,I_{x_1x_4} + x_{13,\rho}\,I_{x_1x_3}\right) \\[4pt]
& + \frac{8\pi^2 I_{x_1x_3}I_{x_1x_4}\,\delta_{\mu\nu}\,\epsilon^\rho\,\epsilon^\sigma}{3\epsilon^2}\left(x_{14,\rho}\,x_{14,\sigma}\,I_{x_1x_4}^2 + x_{13,\rho}\,x_{13,\sigma}\,I_{x_1x_3}^2\right) \\[4pt]
& + \frac{8\pi^2 I_{x_1x_3}I_{x_1x_4}\,\delta_{\mu\nu}\,\epsilon^\rho\,\epsilon^\sigma}{3\epsilon^2}\,x_{13,\rho}\,x_{14,\sigma}\,I_{x_1x_3}I_{x_1x_4} \\[4pt]
& + \frac{1}{36}\left(-2 + 3\log\left(\frac{\epsilon^2 x_{34}^2}{x_{13}^2 x_{14}^2}\right)\right)\frac{I_{x_1x_3}^2 I_{x_1x_4}^2\delta_{\mu\nu}}{I_{x_3x_4}} \\[4pt]
& + \frac{2\pi^2}{9}\left(1 - 6\log\left(\frac{\epsilon^2 x_{34}^2}{x_{13}^2 x_{14}^2}\right)\right)x_{13,\mu}x_{13,\nu}I_{x_1x_3}^3\,I_{x_1x_4} \\[4pt]
& - \frac{2\pi^2}{9}\left(1 + 3\log\left(\frac{\epsilon^2 x_{34}^2}{x_{13}^2 x_{14}^2}\right)\right)\left(x_{13,\nu}x_{14,\mu} + x_{13,\mu}x_{14,\nu}\right)I_{x_1x_3}^2 I_{x_1x_4}^2 \\[4pt]
& + \frac{2\pi^2}{9}\left(1 - 6\log\left(\frac{\epsilon^2 x_{34}^2}{x_{13}^2 x_{14}^2}\right)\right)x_{14,\mu}x_{14,\nu}I_{x_1x_3}I_{x_1x_4}^3\,,
\end{aligned}
$$

$$\lim_{x_2 \to x_1} \partial_{1,\mu} \partial_{3,\nu} X_{1234} = \frac{\epsilon_\mu \epsilon_\nu}{\epsilon^2} \frac{I^2_{x_1 x_3} I_{x_1 x_4}}{2} + 2\pi^2 \log\left(\frac{\epsilon^2 x^2_{34}}{x^2_{13} x^2_{14}}\right) x_{13,\nu} x_{14,\mu} I^2_{x_1 x_3} I^2_{x_1 x_4}$$

$$+ \quad \frac{x_{13,\nu} \, \epsilon_\mu I^2_{x_1 x_3} I_{x_1 x_4}}{\epsilon^2} \left(1 - 4\pi^2 x_{14,\rho} \, \epsilon^\rho I_{x_1 x_4} - 8\pi^2 x_{13,\rho} \, \epsilon^\rho I_{x_1 x_3}\right)$$

$$+ \quad 2\pi^2 \left(-1 + 2\log\left(\frac{\epsilon^2 x^2_{34}}{x^2_{13} x^2_{14}}\right)\right) x_{13,\mu} x_{13,\nu} I^3_{x_1 x_3} I_{x_1 x_4}$$

$$- \quad \frac{1}{4}\left(-1 + \log\left(\frac{\epsilon^2 x^2_{34}}{x^2_{13} x^2_{14}}\right)\right) I^2_{x_1 x_3} I_{x_1 x_4} \delta_{\mu,\nu}$$

$$+ \quad 2\pi^2 x_{13,\mu} x_{34,\nu} I^2_{x_1 x_3} I_{x_1 x_4} I_{x_3 x_4} + 2\pi^2 x_{14,\mu} x_{34,\nu} I_{x_1 x_3} I^2_{x_1 x_4} I_{x_3 x_4} \,,$$

$$\lim_{x_2 \to x_1} \partial_{3,\mu} \partial_{4,\nu} X_{1234} = \frac{\delta_{\mu\nu}}{2} I_{x_1 x_3} I_{x_1 x_4} I_{x_3 x_4} - 4\pi^2 x_{34,\mu} x_{34,\nu} I_{x_1 x_3} I_{x_1 x_4} I^2_{x_3 x_4}$$

$$- \quad 4\pi^2 x_{14,\nu} \, x_{34,\mu} \, I_{x_1 x_3} I^2_{x_1 x_4} I_{x_3 x_4} + 4\pi^2 x_{13,\mu} \, x_{34,\nu} \, I^2_{x_1 x_3} I_{x_1 x_4} I_{x_3 x_4}$$

$$- \quad 4\pi^2 x_{13,\mu} \, x_{14,\nu} \, \log\left(\frac{\epsilon^2 x^2_{34}}{x^2_{13} x^2_{14}}\right) I^2_{x_1 x_3} I^2_{x_1 x_4} \,.$$

Using the above results, we can proceed to the computation of the two- and three-point functions. The result of all the non-zero Feynman diagrams relevant for us is given in figure A.1, where we have omitted terms involving $\epsilon^{\mu\nu\rho\lambda}$ that must either vanish when a pair of point collide or cancel when all the diagrams are summed. This is the case in order to preserve conformal invariance and parity.

The results of figure A.1 only contain derivatives of the function $H_{12,34}$ and it is possible to evaluate them explicitly [120]. Consider the case when the derivatives act on either the first or the second pair of points of H, namely $\partial_1 \cdot \partial_2 H_{12,34}$, and also the case when they act on a point belonging to the first pair and a point belonging to the second pair, for instance $\partial_1 \cdot \partial_4 H_{12,34}$. The first case is straightforward to compute by using integration by parts and the property of the euclidean propagator $\Box_x I_{xy} = -\delta^{(4)}(x - y)$. The result is

$$\partial_1 \cdot \partial_2 H_{12,34} = \frac{1}{2}\left(Y_{134} I_{x_1 x_2} + Y_{234} I_{x_1 x_2} - X_{1234}\right) . \tag{A.5}$$

For computing the second case, we need the function $F_{12,34}$ defined in (A.1) and some identities of $H_{12,34}$. Firstly, note that H satisfies the equation

$$\left(\partial_{1,\mu} + \partial_{2,\mu} + \partial_{3,\mu} + \partial_{4,\mu}\right) H_{12,34} = 0 \,, \tag{A.6}$$

which can be proved by integration by parts. Similarly, it is possible to show that the following identity holds

$$\partial_i \cdot \partial_j H_{12,34} = \frac{1}{2}\left(\Box_k + \Box_l - \Box_i - \Box_j\right) H_{12,34} + \partial_k \cdot \partial_l H_{12,34} \tag{A.7}$$

155

for $i \neq j \neq k \neq l$. In order to get $\partial_1 \cdot \partial_4 H_{12,34}$, it is convenient to write it as

$$\partial_1 \cdot \partial_4 H_{12,34} = \frac{1}{2} \left(\partial_1 \cdot \partial_3 + \partial_1 \cdot \partial_4 \right) H_{12,34} - \frac{1}{2} \left(\partial_1 \cdot \partial_3 - \partial_1 \cdot \partial_4 \right) H_{12,34} \,. \tag{A.8}$$

Now using (A.7), one can show that the first term on the right-hand side of (A.8) can be written as

$$\frac{1}{2} \left(\partial_1 \cdot \partial_3 + \partial_1 \cdot \partial_4 \right) H_{12,34} = -\frac{1}{2} \left(\Box_1 H_{12,34} + \partial_1 \cdot \partial_2 H_{12,34} \right) \tag{A.9}$$

where $\Box_i H_{12,34}$ can be computed using the equation defining the euclidean propagator and $\partial_1 \cdot \partial_2 H_{12,34}$ is known from (A.5). Using (A.6), the second term on the right-hand side of (A.8) can be written as

$$\frac{1}{2} \left(\partial_1 \cdot \partial_3 - \partial_1 \cdot \partial_4 \right) H_{12,34} = \frac{1}{4} \left(F_{12,34} I_{x_1 x_2} I_{x_3 x_4} + (\Box_4 - \Box_3) H_{12,34} \right) \,. \tag{A.10}$$

Finally, substituting (A.9) and (A.10) in (A.8), one gets an expression for $\partial_1 \cdot \partial_4 H_{12,34}$. The expressions for the remaining cases where the derivatives act on other points can be deduced analogously.

In order to get the two-point functions, one takes the limit where two pairs of points collapse into each other that is $x_4 \to x_1$ and $x_3 \to x_2$. The result of these limits gives the Hamiltonian (1.12) mentioned in the introduction of this thesis.

We now proceed to the three-point functions. In order to obtain the constant coming from each diagram, one takes the limit of the expressions given in figure A.1 where a single pair of points collapses into each other. After taking that limit, the result will have constant terms, divergent logarithmic terms and eventually Y functions and their derivatives. The derivatives of the Y functions can be expressed in terms of the Y function itself by using some of its properties. This will be explained in detail in the Appendix A.3. After this procedure, the logarithmic terms will contribute to the standard regulator dependence in (2.33) and the remaining Y functions will cancel with similar contributions from other diagrams in a way that the conformal invariance is restored. One can then read the constant part of the diagram. The final step is to subtract one half the constant coming from the same diagram but when the two pairs of points collapse into each other as described in figure 2.3. The results are given in figure 2.4.

Let us comment now on a detail of this computation. Our final results presented in the figures 2.4 and A.1 do not contain the Feynman diagrams of figure A.3. This is the case because the first two graphs of this figure turn out to cancel among them. They can give a non-zero contribution in our setup only when either $b = c = 4$ and $a = 3$ or $a = c = 2$ and

$b = 3$. However, as these two graphs always appear with the same weight and opposite signs, they end up canceling. The last graph of the figure A.3 must vanish when $|x_{12}| \to 0$ because it is

$$\propto \ \epsilon^{\gamma\delta}\epsilon^{\dot\gamma\dot\delta}\sigma^{\mu}_{E\gamma\dot{1}}\sigma^{\nu}_{E\delta\dot{1}}\sigma^{\rho}_{E1\dot\gamma}\sigma^{\lambda}_{E1\dot\delta} \int d^4v\, d^4u\, (\partial^v_\mu I_{x_1 v})(\partial^v_\nu I_{x_2 v}) I_{vu} (\partial^u_\rho I_{x_3 u})(\partial^u_\lambda I_{x_4 u}) \ \to 0\,.$$

If it was non-vanishing it would produce a term with a different tensor structure of (2.33) which would violate conformal invariance.

A.3 Some examples of three-point functions

We now give two examples of three-point functions. The first one is the case of three half-BPS operators. It is well-known that this correlator is protected and therefore it constitutes a check for our computations. Then we compute a non-protected three-point function both by brute force and by using our prescription of inserting the operator $\mathcal{F}$ at the splitting points.

A.3.1 Three half-BPS operators

Consider the following three half-BPS operators

$$\mathcal{O}_1 \ = \ \mathrm{Tr}\,(ZZ)\,, \tag{A.11}$$

$$\mathcal{O}_2 \ = \ \mathrm{Tr}\,(\bar\Psi\bar Z)\,, \tag{A.12}$$

$$\mathcal{O}_3 \ = \ (r^2{}_4\, r^1{}_3)\cdot\mathrm{Tr}\,(\Psi Z) = \mathrm{Tr}\,(\Psi\bar Z) + \mathrm{Tr}\,(\psi^2\,\Phi^{14})\,. \tag{A.13}$$

At tree-level the result is simply given by the sum of the two diagrams of figure A.4 and reads

$$\langle\mathcal{O}_1(x_1)\mathcal{O}_2(x_2)\mathcal{O}_3(x_3)\rangle = \frac{2}{(2\pi)^6 8^2 x_{12}^2 x_{13}^2}(\sigma^{\mu}_E)_{1\dot{1}}\partial_{3,\mu}\frac{1}{2x_{23}^2}\,. \tag{A.14}$$

At one-loop, one has to sum the diagrams of figure A.5 and use the results given in figure A.1 taking the appropriate limits. Some diagrams will still contain the function Y and its first derivatives. The Y function depends on the external points in a way that does not respect the spacetime dependence fixed by conformal symmetry, see equation (2.33). However, when one sums the different diagrams this non-conformal spacetime dependence turns out to cancel identically.

At the end of the day, summing all the diagrams gives a vanishing one-loop contribution

to the structure constant in agreement with the non-renormalization theorem for the three-points functions of half-BPS operators introduced in [56]. Equivalently, one can also use our prescription to reproduce this one-loop result. One simply has to sum over the insertions represented in figure A.6 obtaining zero as expected.

A.3.2 Two non-BPS and one half-BPS operators

We consider now a non-protected three-point function. This example serves as an illustration of some of the technical details of the brute force computation. Moreover, we also use it to check our prescription of the $\mathcal{F}$ operator insertion at the splitting points. The operators at one-loop level that we will consider are

$$
\begin{align}
\mathcal{O}_1 &= \text{Tr}\left(Z\Psi\Psi Z\right), \tag{A.15}\\
\mathcal{O}_2 &= \text{Tr}\left(\bar{Z}\bar{\Psi}\bar{\Psi}\bar{\Psi}\right), \tag{A.16}\\
\mathcal{O}_3 &= (r^2{}_4\, r^1{}_3)\cdot \text{Tr}\left(\Psi Z\right) = \text{Tr}\left(\Psi\bar{Z}\right) + \text{Tr}\left(\psi^2\,\Phi^{14}\right). \tag{A.17}
\end{align}
$$

Note that the $\mathcal{O}_1$ and $\mathcal{O}_2$ are not half-BPS and therefore they will receive corrections as explained in section 2.2.1. However, to compute the Feynman diagrams contribution we do not need to take them into account. At tree-level the result is simply the sum of the two diagrams of figure A.7 which gives

$$
\begin{aligned}
\langle \mathcal{O}_1(x_1)\mathcal{O}_2(x_2)\mathcal{O}_3(x_3)\rangle_0 = & -\frac{2}{(2\pi)^{10}8^2 x_{13}^2 x_{12}^2}\\
& \times \left((\sigma_E^\mu)_{1\mathrm{i}}\partial_{1,\mu}\frac{1}{2x_{12}^2}\right)\left((\sigma_E^\nu)_{1\mathrm{i}}\partial_{1,\nu}\frac{1}{2x_{12}^2}\right)\left((\sigma_E^\rho)_{1\mathrm{i}}\partial_{3,\rho}\frac{1}{2x_{23}^2}\right).
\end{aligned}
$$

The diagrams contributing at one-loop are represented in figure A.8.

As in the previous example, the dependence of each diagram on the Y function and its derivatives will cancel when we sum over all the diagrams. This ensures that we obtain a conformal invariant result. However, this cancellation is not immediate and it relies on several properties of the Y function. The first observation is that the function Y is given by

$$
Y_{123} = \frac{\pi^2\phi(r,s)}{(2\pi)^4}I_{x_1,x_3}, \tag{A.18}
$$

where $r = \frac{x_{12}^2}{x_{13}^2}$ and $s = \frac{x_{23}^2}{x_{13}^2}$ and an explicit expression for $\phi(r,s)$ can be found in [119].

The important information for us is that the function ϕ satisfies the following differential equations [36]

$$\phi(r,s) + (s + r - 1)\partial_s\phi(r,s) + 2r\partial_r\phi(r,s) = -\frac{\log r}{s} \,, \tag{A.19}$$

$$\phi(r,s) + (s + r - 1)\partial_r\phi(r,s) + 2s\partial_s\phi(r,s) = -\frac{\log s}{r} \,,$$

which can be used to relate the first derivatives of Y with Y itself. In addition, one can take derivatives with respect to r and s of both the equations above to arrive at a system of equations that relates second derivatives of ϕ with first derivatives and the function ϕ itself. Using then (A.18), it is trivial to get rid of the second derivatives of Y. These properties of the function ϕ ensure that the non-conformal dependence of the three-point function indeed cancel when all diagrams are summed over.

The final result is given by

$$\langle \mathcal{O}_1(x_1)\mathcal{O}_2(x_2)\mathcal{O}_3(x_3)\rangle = \langle \mathcal{O}_1\mathcal{O}_2\mathcal{O}_3\rangle_0 \left(1 + 4g^2\left(-1 + 2\log\left(\frac{\epsilon^2}{x_{12}^2}\right)\right) + \mathcal{O}(g^4)\right)$$

which comparing with (2.33) gives the correct anomalous dimensions of the operators. This is a non-trivial consistency check of our computation.

The structure constant can now be obtained by also computing the constants from the two-point functions. We have all the tools at hand to perform such calculation and read the one-loop constant. We obtain the following contribution from the Feynman diagrams to the structure constant

$$C_{123}^{(1)}\bigg|_{\text{Feynman diagrams contribution}} = -\frac{3}{2} \,. \tag{A.20}$$

Recall that this is not the final result, one also has to add the extra contribution from the corrected two-loop Bethe states.

Finally, it is possible to test our prescription of inserting the $\mathcal{F}$ operator at the splitting points, see figure A.9. Summing over all these insertions gives precisely the contribution (A.20) to the structure constant.

A.4   Wilson line contribution

As mentioned before, the point splitting regularization breaks explicitly the gauge invariance due to the fact that some fields inside the trace are now at a slightly different spacetime

points. The introduction of a Wilson line connecting these fields restore the gauge invariance at the price of introducing extra Feynman diagrams. In this Appendix, we show that these extra diagrams do not contribute to the scheme and normalization independent structure constant $C_{123}^{(1)}$ defined in (2.33).

A.4.1 Wilson line connecting two scalars

In our conventions the Wilson line operator is defined by

$$W_l = \mathcal{P} \exp \left[i\, g_{YM} \int A_\mu \, d\vec{x}^\mu \right] .$$

When inserting a Wilson line connecting two scalars, it is necessary to consider the one-loop graphs corresponding to the gluon emission depicted in figure A.10(a). Let us define $\epsilon^\mu = x_4^\mu - x_3^\mu$ and at the end of the day we will take the limit $\epsilon^\mu \to 0$. Then we can conveniently parametrize the Wilson line by $x^\mu(z) = x_3^\mu + z\epsilon^\mu$. The result of the sum of the diagrams is

$$\text{figure } A.10(a) = \frac{\lambda}{128} \int_0^1 dz\, \epsilon_\mu \left(I_{x_2 x_3}\, \partial_1^\mu Y_{1x4} - I_{x_1 x_4}\, \partial_2^\mu Y_{2x3} + I_{x_1 x_4}\, \partial_3^\mu Y_{2x3} - I_{x_2 x_3}\, \partial_4^\mu Y_{1x4} \right),$$

$$(A.21)$$

where we have suppressed both the R-charge and the gauge indices which are the same as in the tree-level case. From the formula (A.3), it follows that the first and second terms of the above result are of order ϵ and therefore vanish in the limit $\epsilon \to 0$. However, from (A.2) we see that the third and last term give a finite contribution.

In order to compute the scheme and normalization structure constant $C_{123}^{(1)}$ of (2.33), we have to subtract from the previous result one half of the one-loop diagrams from the two-point functions as shown in figure A.11 (we take both the limits $x_4 \to x_3$ and $x_2 \to x_1$). It is simple to show that the contribution of these diagrams cancels exactly the constant coming from the expression (A.21). So, at this order in perturbation theory we do not get any further contribution to $C_{123}^{(1)}$ and therefore we can safely ignore the Wilson lines.

A.4.2 Wilson line connecting either a scalar and a fermion or two fermions

In the case of a scalar and a fermion connected by a Wilson line, the contribution of the diagrams depicted in A.10(b) is given by

$$
\text{figure } A.10(b) = \frac{\lambda}{32} \int_0^1 dz\, \epsilon^\mu \Big[I_{x_2 x_3} (\sigma_{E\mu 1\dot{1}} \partial^4 \cdot \partial^1 Y_{1x4} - \sigma^\nu_{E1\dot{1}} \partial^4_\nu \partial^1_\mu Y_{1x4} - \sigma^\nu_{E1\dot{1}} \partial^4_\mu \partial^1_\nu Y_{1x4}
$$
$$
-\epsilon_{\rho\mu\lambda\nu}\, \sigma^\nu_{E1\dot{1}}\, \partial^{4,\lambda} \partial^{1,\rho} Y_{1x4}) + \sigma^\nu_{E1\dot{1}} \partial^1_\nu I_{x_1 x_4} (\partial^3_\mu Y_{2x3} - \partial^2_\mu Y_{2x3}) \Big]. \tag{A.22}
$$

Using the expressions (A.2-A.4), one can easily see that this gives a finite contribution in the limit when ϵ goes to zero (in particular, the term with $\epsilon_{\rho\mu\lambda\nu}$ vanishes). To this result, we have again to subtract one half of the one-loop diagrams from the two-point functions as was done in the previous subsection for the case of two scalars. Once again, the contribution of these diagrams cancels exactly the expression (A.22).

In the case when we have a Wilson line connecting two fermions, the same argument holds. Hence at one-loop level, we can ignore the Wilson lines contributions in all cases.

$$\Phi^{ef}(x_4) \quad \Phi^{gh}(x_1)$$

$$= -\frac{\lambda}{128} F_{12,34} I_{x_1 x_2} I_{x_3 x_4} \bar{\delta}^{ef}_{ab} \bar{\delta}^{gh}_{cd}$$

$$\Phi_{ab}(x_3) \quad \Phi_{cd}(x_2)$$

$$\Phi^{ef}(x_4) \quad \Phi^{gh}(x_1)$$

$$= \frac{\lambda}{128} X_{1234} \left(2\,\bar{\delta}^{gh}_{ab} \bar{\delta}^{ef}_{cd} - \bar{\delta}^{ef}_{ab} \bar{\delta}^{gh}_{cd} - \epsilon_{abcd}\epsilon^{efgh} \right)$$

$$\Phi_{ab}(x_3) \quad \Phi_{cd}(x_2)$$

$$\Phi^{cd}(x_2)$$

$$= \quad + \quad + \quad + \quad = -\frac{\lambda}{4} Y_{112}\,\bar{\delta}^{cd}_{ab}$$

$$\Phi_{ab}(x_1)$$

$$\bar{\psi}_{\dot\alpha = \dot{1}\, b}(x_4) \quad \Phi_{ef}(x_1)$$

$$= \frac{\lambda}{32}\,\sigma^\mu_{E\alpha\dot\alpha} \Big(\partial_{3,\mu}\partial_2 \cdot \partial_4 + \partial_{4,\mu}\partial_2 \cdot \partial_3$$
$$+\partial_{1,\mu}\partial_3 \cdot \partial_4 - \partial_{2,\mu}\partial_3 \cdot \partial_4$$
$$- \partial_{3,\mu}\partial_1 \cdot \partial_4 - \partial_{4,\mu}\partial_1 \cdot \partial_3 \Big) H_{12,34}\,\delta^a_b\,\bar{\delta}^{cd}_{ef}$$

$$\psi^a_{\alpha=1}(x_3) \quad \Phi^{cd}(x_2)$$

$$\bar{\psi}_{\dot\alpha = \dot{1}\, b}(x_2)$$

$$= \quad + \quad = -2\lambda\,\sigma^\mu_{E\alpha\dot\alpha}\,\partial_{2,\mu} Y_{112}\,\delta^a_b$$

$$\psi^a_{\alpha=1}(x_1)$$

$$\bar{\psi}_{\dot\alpha = \dot{1}\, d}(x_4) \quad \Phi_{ef}(x_1)$$

$$= \frac{\lambda}{16}\,\sigma^\mu_{E\alpha\dot\alpha} \Big(\partial_{4,\mu}\partial_2 \cdot \partial_3 - \partial_{3,\mu}\partial_2 \cdot \partial_4$$
$$- \partial_{2,\mu}\partial_2 \cdot \partial_4 - \partial_{2,\mu}\partial_1 \cdot \partial_4 \Big) H_{12,34}\,\bar{\delta}^{ab}_{kd}\bar{\delta}^{kc}_{ef}$$

$$\Phi^{ab}(x_3) \quad \psi^c_{\alpha=1}(x_2)$$

$$\bar{\psi}_{\dot\alpha = \dot{1}\, c}(x_4) \quad \bar{\psi}_{\dot\beta = \dot{1}\, d}(x_1)$$

$$= \frac{\lambda}{4}\sigma^\mu_{E\alpha\dot\alpha}\sigma^\nu_{E\beta\dot\beta} \Big(\partial_{2,\nu}\partial_{4,\mu}\partial_1 \cdot \partial_3 + \partial_{1,\nu}\partial_{3,\mu}\partial_2 \cdot \partial_4$$
$$- \partial_{1,\mu}\partial_{2,\nu}\partial_3 \cdot \partial_4 - \partial_{3,\mu}\partial_{4,\nu}\partial_1 \cdot \partial_2 \Big) H_{12,34}\,\delta^a_c\,\delta^b_d$$

$$\psi^a_{\alpha=1}(x_3) \quad \psi^b_{\beta=1}(x_2)$$

Figure A.1: The results of the Feynman diagrams computation omitting both terms that must vanish or cancel when summing all the diagrams (see text) and factors of N. The solid, wiggly and dashed lines represent the scalars, gluons and fermions, respectively. The $\bar{\delta}$ was defined in Appendix A.

162
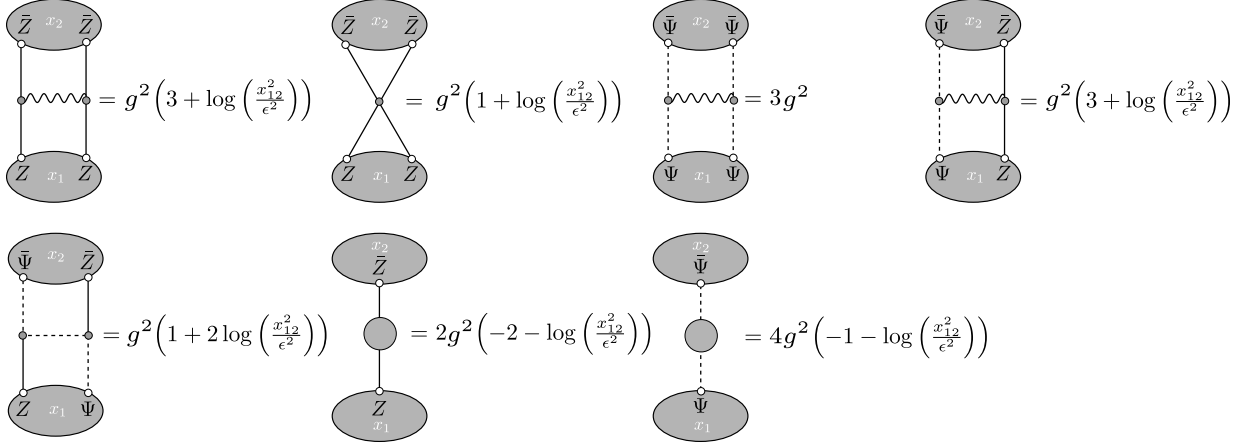
Figure A.2: The results of the Feynman diagrams for the two-point functions. They are obtained by taking the limits $x_3 \to x_2$ and $x_4 \to x_1$ of the expressions in figure A.1.
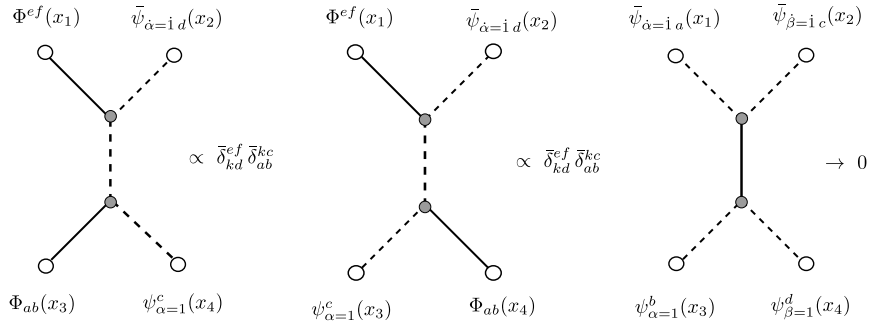
Figure A.3: The additional Feynman diagrams that do not contribute in the setup considered in this work. The solid and dashed lines represent the scalars and fermions, respectively.
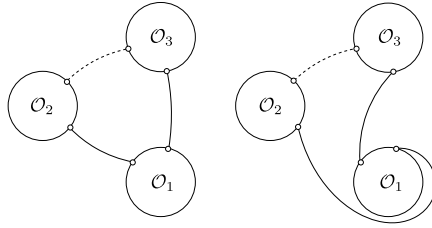
Figure A.4: The tree-level diagrams for the three-point functions of the three half-BPS operators considered in (A.11)-(A.13). Note that only the first term of $\mathcal{O}_3$ in (A.13) gives a non-zero contribution at this order in perturbation theory as the second term clearly gives a vanishing contribution due to R-charge conservation.
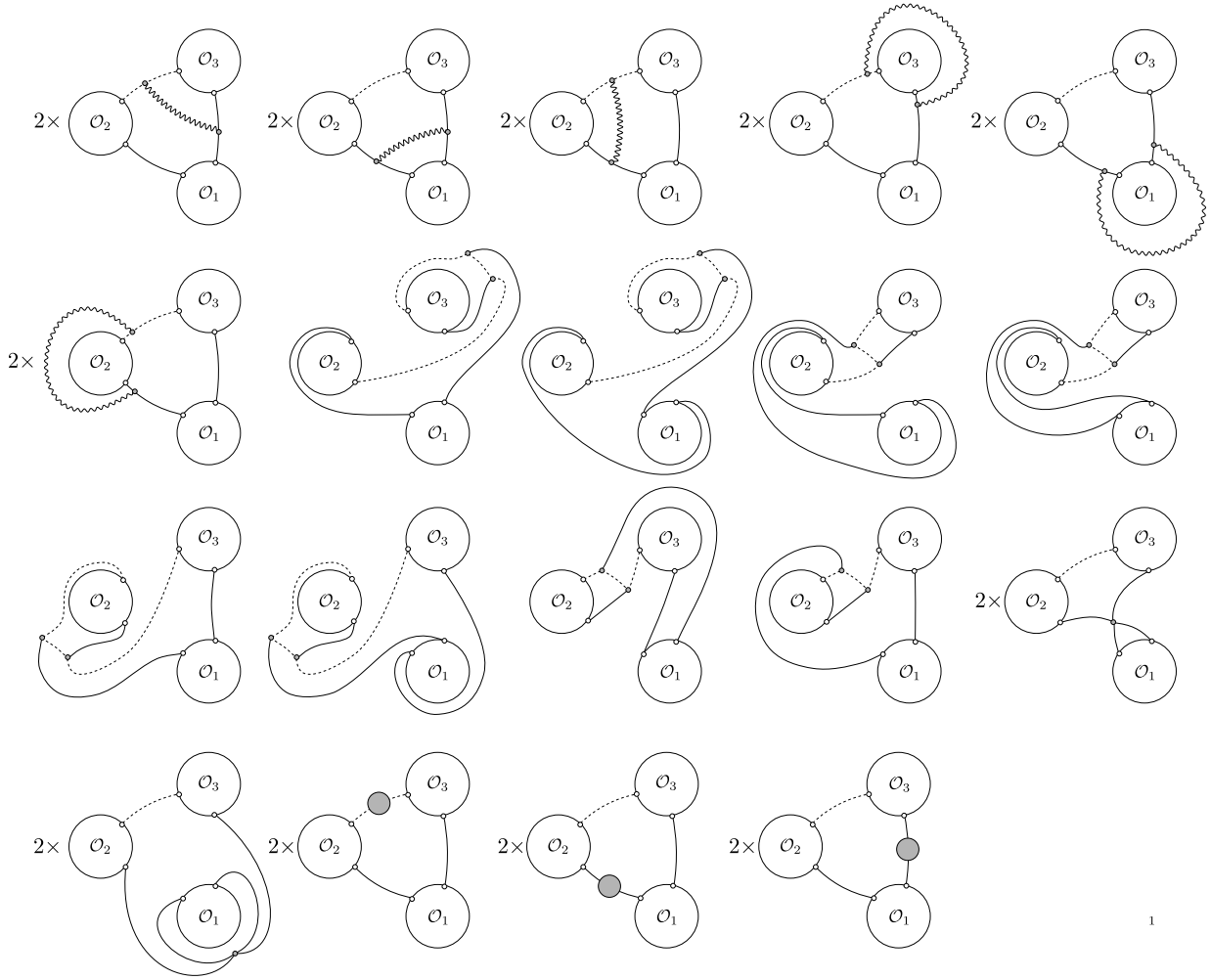
Figure A.5: The one-loop diagrams contributing to the three-point function of the three half-BPS operators considered in (A.11)-(A.13). In the last four diagrams of the second row, the second term of $\mathcal{O}_3$ (see expression (A.13)) gives a non-zero result. In all other diagrams only the first term of $\mathcal{O}_3$ contributes.
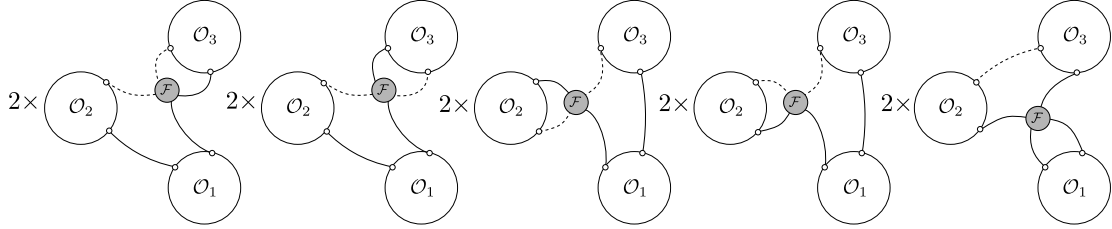
Figure A.6: Inserting the $\mathcal{F}$ operator at the splitting points, one reproduces the vanishing result expected for a three-point function of half-BPS operators. Apart from the graphics in the figure, there are similar graphics with the operator $\mathcal{F}$ acting in the remaining splitting points.
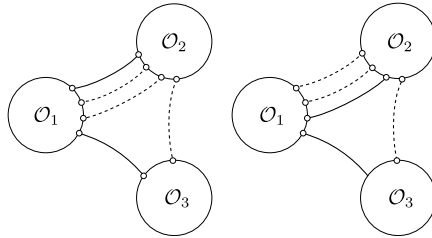
Figure A.7: The tree-level diagrams contributing to the three-point function of the operators (A.15)-(A.17). Once again, we only need to consider the first term of (A.17) at this order in perturbation theory.

167
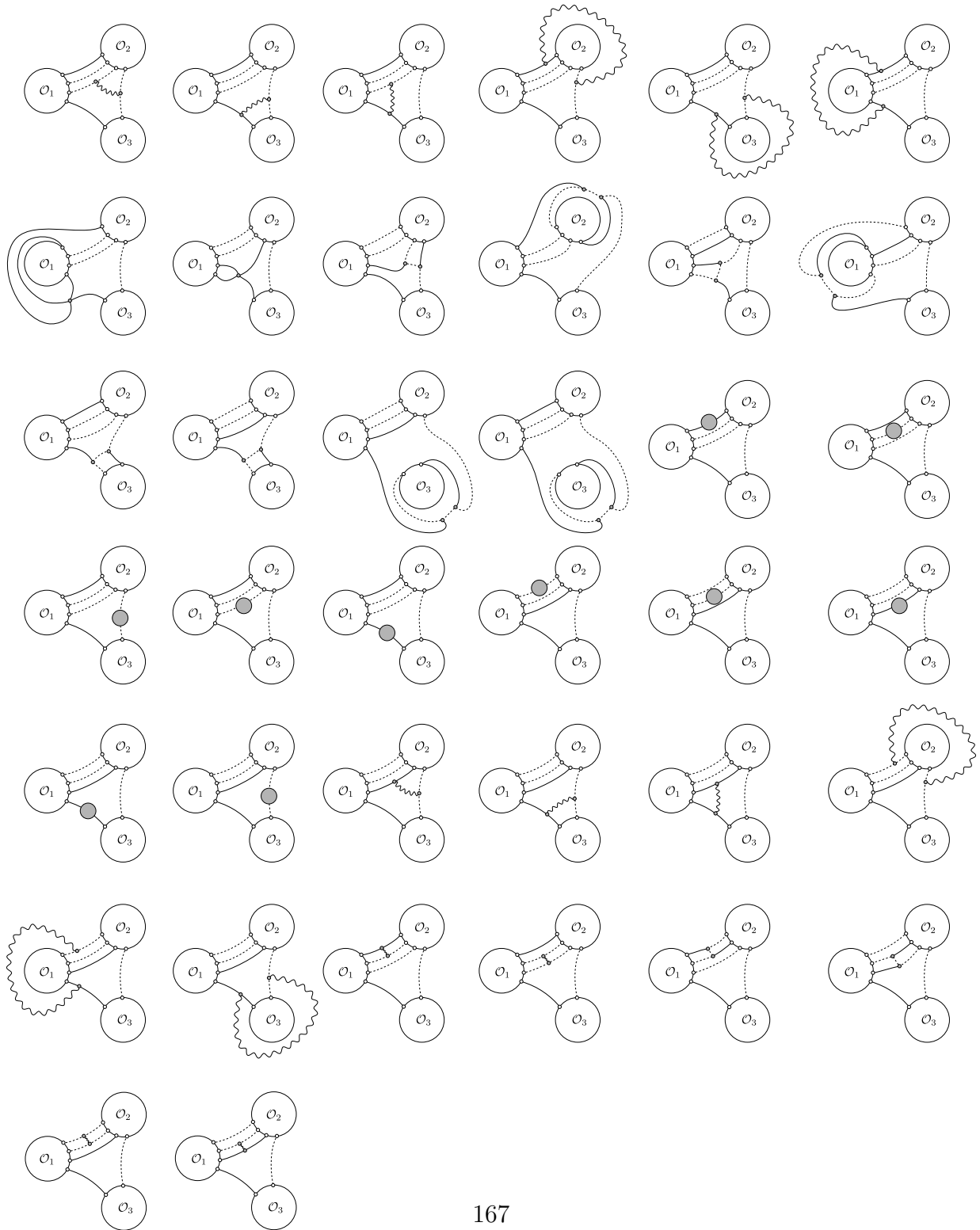
Figure A.8: The relevant one-loop diagrams for the three-point function of the operators (A.15)-(A.17). The second term of (A.17) gives a non-zero contribution namely the first four diagrams of the third row.
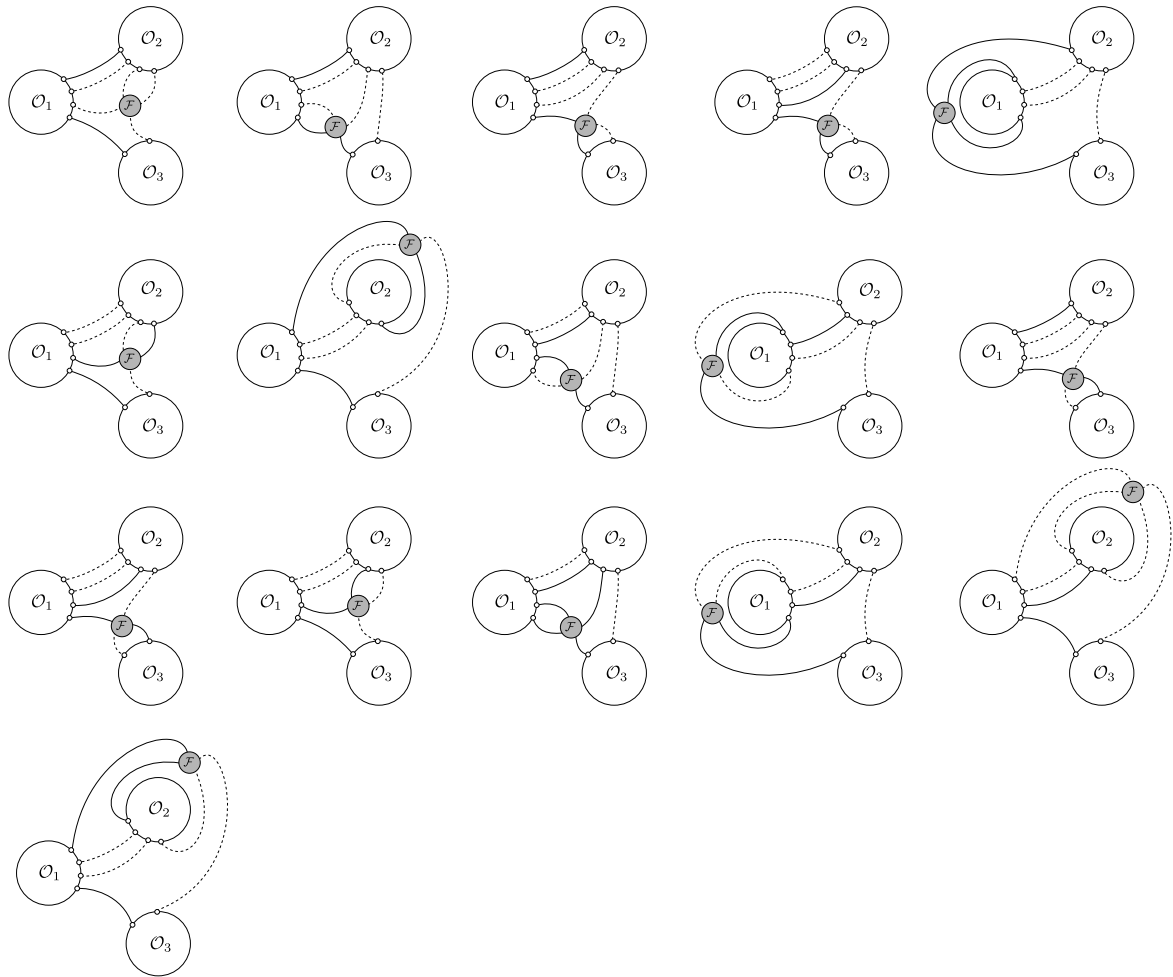
Figure A.9: Inserting the operator $\mathcal{F}$ at the splitting points reproduce the result of the one-loop Feynman diagrams.
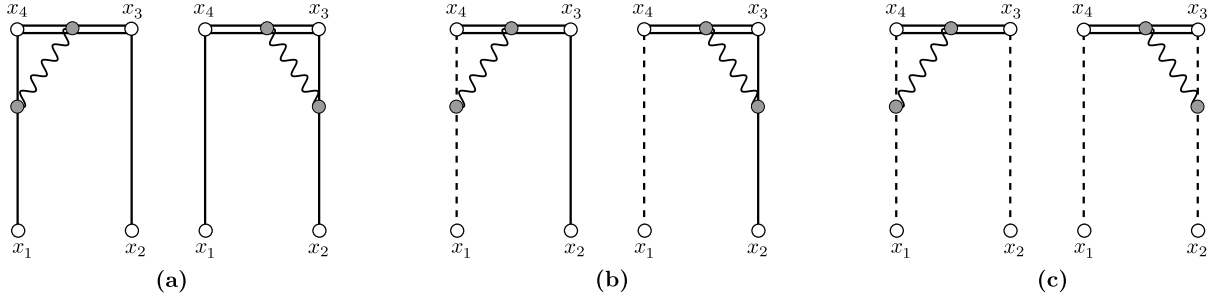
Figure A.10: The one-loop additional graphs coming from the Wilson line.
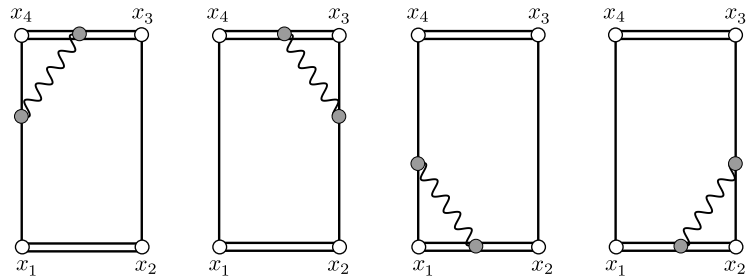
Figure A.11: The Wilson line contributions to the two-point functions. In the combination of the two- and the three-point diagrams that provide the scheme independent structure constant (2.33), all the extra diagrams coming from the Wilson lines cancel each other at this order in perturbation theory. In the figure, the diagram corresponding to the emission of a gluon between the two Wilson lines is not depicted, since it is proportional to ϵ^2 and vanishes in the limit $\epsilon \to 0$.

Appendix B

The linear problem

B.1 Summary of the linear problem

The linear problem associated with (3.10) is given by

$$\left(\partial + J_w\right)\psi = 0, \qquad \left(\bar{\partial} + J_{\bar{w}}\right)\psi = 0 \tag{B.1}$$

where the connection has the form

$$J_w = \frac{1}{\xi}\Phi_w + A_w, \qquad J_{\bar{w}} = \xi\Phi_{\bar{w}} + A_{\bar{w}} \tag{B.2}$$

$$\Phi_w = \begin{pmatrix} 0 & -\frac{1}{2}e^{\widetilde{\gamma}} \\ -\frac{1}{2}Te^{-\widetilde{\gamma}} & 0 \end{pmatrix} \tag{B.3}$$

$$\Phi_{\bar{w}} = \begin{pmatrix} 0 & -\frac{1}{2}\bar{T}e^{-\widetilde{\gamma}} \\ -\frac{1}{2}e^{\widetilde{\gamma}} & 0 \end{pmatrix} \tag{B.4}$$

$$A_w = \partial_w \begin{pmatrix} \frac{1}{2}\widetilde{\gamma} & 0 \\ 0 & -\frac{1}{2}\widetilde{\gamma} \end{pmatrix} \tag{B.5}$$

$$A_{\bar{w}} = \partial_{\bar{w}} \begin{pmatrix} -\frac{1}{2}\widetilde{\gamma} & 0 \\ 0 & \frac{1}{2}\widetilde{\gamma} \end{pmatrix} \tag{B.6}$$

For compactness we have introduced the combination $\widetilde{\gamma} = 1/2(\gamma + \log\sqrt{T\bar{T}})$. The function γ is defined as the solution of the following problem

$$\begin{aligned} \partial\bar{\partial}\gamma &= \sqrt{T\bar{T}}\sinh\gamma \\ \gamma &\to \pm\frac{1}{2}\log T\bar{T} \quad (w \to z_a) \\ \gamma &\to 0 \quad\qquad (w \to w_a) \end{aligned} \tag{B.7}$$

where z_a and w_a are the zeros and the poles of T, respectively.

For the near-puncture analysis as well as the WKB analysis it is useful to make the field redefinition $\psi \to \hat{\psi} = \hat{G}\psi$ where

$$\hat{G} = \frac{1}{2}\begin{pmatrix} +e^{-\gamma/2}T^{1/4}\bar{T}^{-1/4} & 1 \\ -e^{-\gamma/2}T^{1/4}\bar{T}^{-1/4} & 1 \end{pmatrix} \tag{B.8}$$

This is usually refered to as 'diagonal gauge' in the literature. In diagonal gauge we have

$$\hat{\Phi}_w = \frac{1}{2}\sqrt{T}\begin{pmatrix} -1 & 0 \\ 0 & 1 \end{pmatrix} \tag{B.9}$$

$$\hat{\Phi}_{\bar{w}} = \frac{1}{2}\sqrt{\bar{T}}\begin{pmatrix} -\cosh\gamma & \sinh\gamma \\ -\sinh\gamma & \cosh\gamma \end{pmatrix} \tag{B.10}$$

$$\hat{A}_w = \partial_w \begin{pmatrix} \frac{1}{4}\gamma-\frac{1}{8}\log(T\bar{T}) & -\frac{1}{2}\gamma \\ -\frac{1}{2}\gamma & \frac{1}{4}\gamma-\frac{1}{8}\log(T\bar{T}) \end{pmatrix} \tag{B.11}$$

$$\hat{A}_{\bar{w}} = \partial_{\bar{w}} \begin{pmatrix} \frac{1}{4}\gamma+\frac{1}{8}\log(T\bar{T}) & 0 \\ 0 & \frac{1}{4}\gamma+\frac{1}{8}\log(T\bar{T}) \end{pmatrix} \tag{B.12}$$

We are now ready to consider the behavior of the solutions near the points w_a and z_a.

B.2 Solutions near w_a

Let us first consider the solutions of the linear problem in the neighborhood of one of the punctures. From $(B.7)$ and the explicit expressions for $\hat{\Phi}$ and $\hat{A}$ for $w \to w_a$ we have

$$\hat{\Phi}_w \to \frac{1}{2}\sqrt{T}\begin{pmatrix} -1 & 0 \\ 0 & +1 \end{pmatrix}, \quad \hat{\Phi}_{\bar{w}} \to \frac{1}{2}\sqrt{\bar{T}}\begin{pmatrix} -1 & 0 \\ 0 & +1 \end{pmatrix} \tag{B.13}$$

$$\hat{A}_w \to \partial_w \left(-\frac{1}{8}\log T\bar{T}\right)\begin{pmatrix} +1 & 0 \\ 0 & +1 \end{pmatrix}, \quad \hat{A}_{\bar{w}} \to \partial_{\bar{w}} \left(\frac{1}{8}\log T\bar{T}\right)\begin{pmatrix} +1 & 0 \\ 0 & +1 \end{pmatrix} \tag{B.14}$$

Then the solution in the vicinity of puncture P_a is given by:

$$\hat{\psi}^{\pm}(w) \equiv \left(T/\bar{T}\right)^{1/8} e^{\pm\frac{1}{2}\int^w \xi^{-1}\omega + \xi\bar{\omega}}|\pm\rangle \sim (w-w_a)^{\pm\frac{1}{4}\Delta_a\xi^{-1}-\frac{1}{4}}\,(\bar{w}-\bar{w}_a)^{\pm\frac{1}{4}\bar{\Delta}_a\xi+\frac{1}{4}}\,|\pm\rangle \tag{B.15}$$

where $|\pm\rangle$ are the eigenvectors of the Pauli matrix σ^3. Note the characteristic monodromy of the solutions about w_a.

171

B.3   Solutions near z_a

Now we will consider the behavior of the solutions near the zeros z_a of T. Notice from (B.3) - (B.6) and (B.7) that the connection is regular or singular at z_a depending on the direction of the spike in γ at z_a. More specifically, the connection is regular if $\gamma \sim -\log|w - z_a|$ and thus the solution will be regular in the vicinity of a d-spike. However, the connection has a singularity if $\gamma \sim +\log|w - z_a|$ and at the u-spikes one can check that in gauge (B.3) - (B.6) there are two linearly independent solutions behaving as

$$\Psi \sim \Psi_{z_a} \equiv \begin{pmatrix} (w-z_a)^{-1/4}(\bar{w}-\bar{z}_a)^{+1/4} & 0 \\ 0 & (w-z_a)^{+1/4}(\bar{w}-\bar{z}_a)^{-1/4} \end{pmatrix} \tag{B.16}$$

where we have written the two solutions in matrix form as in (3.71). Notice that Ψ has square-root type singularity at z_a since it has a monodromy of $\Psi \to (-1)\,\Psi$ about z_a. The solutions associated with the punctures $\{s_P\}$ and $\{\tilde{s}_P\}$ inherit this square-root singularity as one can see by expanding them in the basis (B.16) near z_a.

In our analysis it is crucial to account for the additional monodromies originating from u-spikes. Let us explain our conventions for doing this. If there is a u-spike at z_a, one can always make the gauge-transformation $\Psi \to \Psi_{z_a}^{-1}\Psi$ that removes the square root singularity (Ψ_{z_a} is given in (B.16)). Of course this gauge transformation contains the same multivaluedness and one must still account for it at the end of the day. In the main text we use the point of view that this gauge transformation has been performed for each u-spike. The connection in this gauge will only have singularities at the punctures and the solutions in this gauge will only have non-trivial monodromies around the punctures. In this way we can define small solutions that are single valued throughout some Q_E, as is the prescription of [58]. We must then be sure to account for the multivaluedness of these gauge transformations whenever we have a holonomy that encloses an odd number of u-spikes. Such holonomies arise in the WKB expansion of the coordinates and we will return to this issue below.

B.4   WKB analysis

B.4.1   Statement of the WKB approximation

As we have discussed above, it is essential to have control over the $\xi \to 0, \infty$ asymptotics of the inner products. It is clear from ($B.1 - B.2$) that these are both singular limits, and the basic idea of extracting this singularity is as follows. As discussed above, we have good

control over the solutions in the neighborhood of the punctures. Thus what we would like to study is the transport

$$\text{Pexp}\left[-\int_{\mathcal{C}(w_a' \to w)} \frac{1}{\xi}\Phi + A + \xi\bar{\Phi}\right]\psi\left(w_a'\right) \tag{B.17}$$

where $\mathcal{C}\left(w_a' \to w\right)$ is a curve starting at w_a', a point in the neighborhood of w_a, and terminating at a generic point w. Note that at any point on the punctured sphere C the Higgs field Φ has the two eigenvalues $\mp\omega/2 = \mp\sqrt{T}/2\, dw$ (which are single valued on the double cover $\widetilde{\Sigma}$), and thus we can choose a gauge along $\mathcal{C}$ where Φ is diagonal and given by

$$\Phi = \frac{1}{2}\begin{pmatrix} -\omega & 0 \\ 0 & \omega \end{pmatrix} \tag{B.18}$$

Now consider the $\xi \to 0$ limit. First consider an infinitesimal segment of $\mathcal{C}$ in the neighborhood of P_a. In the neighborhood of P_a the connection (in diagonal gauge) becomes diagonal (see (B.13)-(B.14)) and thus one can break apart the path-ordered exponential. In particular, one can isolate the singular part $e^{-\int \Phi/\xi}|\pm\rangle$ which will have one component growing exponentially and one component decaying. Let us choose the branch of Φ such that the $|+\rangle$ component is the one that is growing as we transport along $\mathcal{C}$ *away* from P_a (although for the moment we are still working in a neighborhood of P_a). This will correspond to the small solution at P_a since it is exponentially decaying as it is transported *toward* from P_a. The *WKB approximation* is the statement that the exponentially growing part of the solution as $\xi \to 0$ will continue to be given by $e^{-\int \Phi/\xi}|+\rangle$ as we transport away from the neighborhood of P_a (now leaving the neighborhood of P_a) as long as we follow a curve such that at every point we have

$$\text{Re}\left(\omega/\xi\right) > 0 \tag{B.19}$$

This condition is satisfied most strongly along a curve such that

$$\text{Im}\left(\omega/\xi\right) = 0 \tag{B.20}$$

Condition (B.19) is called the *WKB condition* and curves satisfying (B.20) are called *WKB curves* [58]. Along a WKB curve defined for $\text{Arg}\left(\xi\right) = \theta$ the WKB condition is satisfied for $\text{Arg}\left(\xi\right) \in \left(\theta - \pi/2, \theta + \pi/2\right)$ and the WKB approximation is guaranteed to hold in this range. For example, suppose there is a WKB line connecting P_a to P_b for $\theta \in \left(\theta_-, \theta_+\right)$ but not outside that range. Then the WKB approximation will reliably give the $\xi \to 0, \infty$ asymptotic for $\theta \in \left(\theta_- - \pi/2, \theta_+ + \pi/2\right)$. These statements are proven in [58] and we refer the reader there for a more detailed discussion.

B.4.2 Subleading WKB

We will now consider the $\xi \to 0$ limit of the inner products (or Wronskians) $(s_b \wedge s_a)(\xi)$. We consider the case when P_a and P_b are connected by a WKB line which will be an edge E_{ab} in the WKB triangulation. From the analysis of B.2 we know s_a and s_b in the neighborhood of P_a and P_b respectively. In order to evaluate the Wronskian we need to know the solutions at a common point. The approach here is to use the connection to transport the solution s_a along E_{ab} to a point w_b' in the neighborhood of P_b and then to evaluate the Wronskian at w_b'. That is, we want to study the $\xi \to 0$ behavior of

$$\langle s_b | \text{Pexp} \left[- \int_0^1 dt \, \frac{1}{\xi} H_0 + V \right] | s_a \rangle \tag{B.21}$$

where we defined

$$H_0 = \dot{w} \hat{\Phi}_w, \qquad V = \dot{w} \hat{A}_w + \dot{\bar{w}} \hat{A}_{\bar{w}} + \xi \dot{\bar{w}} \hat{\Phi}_{\bar{w}} \tag{B.22}$$

The contour of integration in (B.21) is the edge E_{ab} and the components of (B.22) are defined in appendix B. The basic idea of the computation is to expand in a perturbative series where $\xi^{-1} H_0$ acts as the free Hamiltonian. Such a procedure will be valid so long as the free part of the Hamiltonian is sufficiently larger than V for all points along the curve, which will be true along the edges of the WKB triangulation. Then we can expand (B.21) in the Born series

$$(-1)\hat{\psi}_b^- \hat{\psi}_a^+ \Big(\langle + | e^{-\int_0^1 H_0/\xi} | + \rangle - \int_0^1 dt_1 \langle + | e^{-\int_{t_1}^1 H_0/\xi} V(t_1) e^{-\int_0^{t_1} H_0/\xi} | + \rangle \tag{B.23}$$

$$+ \int_0^1 dt_2 \int_0^{t_2} dt_1 \langle + | e^{-\int_1^{t_2} H_0/\xi} V(t_2) e^{-\int_{t_1}^{t_2} H_0/\xi} V(t_1) e^{-\int_0^{t_1} H_0/\xi} | + \rangle \Big)$$

Let us explain a subtle point regarding the 'external states' in the above expression. We start with the small solution at P_a which we take to be ψ_a^+. We then transport it to P_b and then extract the coefficient of the exponentially growing part – that is, we take the inner product with the small part of this transported solution. Since $\psi_a^+ \sim |+\rangle$ grows as we transport it along a WKB curve (i.e. it decays as one follows the curve into P_a and thus grows as we transport it away from P_a) and H_0 is diagonal, we infer that the small part of the solution at P_b is the solution proportional to $|-\rangle$. Thus we take the out-state to be $\langle -|\psi_b^-$. Finally, since the inner product is antisymmetric the $\langle -|$ gets flipped to a $\langle +|$.

Using the fact that $|\pm\rangle$ are eigenstates of the free Hamiltonian we can easily evaluate

the order $\mathcal{O}(V^0)$ and $\mathcal{O}(V^1)$ terms in (B.23). For the $\mathcal{O}(V^2)$ term, we insert the identity $|+\rangle\langle+| + |-\rangle\langle-|$ between the two insertions of V. We find

$$
(-1)\hat{\psi}_b^- \hat{\psi}_a^+ \, e^{+\frac{1}{2}\int_0^1 \omega/\xi} \left(1 - \int_0^1 dt_1 \langle+|V(t_1)|+\rangle + \frac{1}{2} \left[\int_0^1 dt_1 \langle+|V(t_1)|+\rangle \right]^2 + \qquad \text{(B.24)}
$$

$$
\int_0^1 dt_2 \int_0^{t_2} dt_1 e^{-\int_{t_1}^{t_2} \omega/\xi} \langle+|V(t_2)|-\rangle\langle-|V(t_1)|+\rangle \right)
$$

Now concentrate on the second term on the $\mathcal{O}(V^2)$ contribution. As $\xi \to 0$ the factor $\exp\left(-\int_{t_1}^{t_2} \omega/\xi\right)$ will suppress the integrand except for the small range $t_2 = t_1 + \mathcal{O}(\xi)$ and thus the result of the first integration will already be $\mathcal{O}(\xi)$. So to order ξ we can take ω to be constant and $V(t_1) \to V(t_2)$. We then find for the second term in the $\mathcal{O}(V^2)$ contribution

$$
e^{\frac{1}{2}\int_0^1 \omega/\xi} \int_0^1 dt_2 \xi \frac{|\langle+|V(t_2)|-\rangle|^2}{\dot{w}\sqrt{T}} \qquad \text{(B.25)}
$$

Putting everything together, we see that the result re-exponentiates and we find

$$
(-1)\hat{\psi}_b^- \hat{\psi}_a^+ \exp\left[+\frac{1}{\xi}\int_0^1 dt \frac{1}{2}\sqrt{T} - \int_0^1 dt \langle+|V(t)|+\rangle + \xi \int_0^1 dt \frac{|\langle+|V(t)|-\rangle|^2}{\dot{w}\sqrt{T}} \right] \qquad \text{(B.26)}
$$

Grouping each term based on its order in ξ (including the prefactors $\hat{\psi}_b^- \hat{\psi}_a^+$ whose explicit expression are given in (B.15)) we find

$$
(s_b \wedge s_a)(\xi) \sim \exp\left[+\frac{1}{2}\xi^{-1}\varpi_{ab} + \alpha_{ab} + \frac{1}{2}\xi\overline{\varpi}_{ab} + \xi\eta_{ab} \right] \qquad \text{(B.27)}
$$

where

$$
\varpi_{ab} = \lim_{w_a' \to w_a} \lim_{w_b' \to w_b} \left[\int_{E_{ab}} \sqrt{T} dw + \frac{\Delta_a}{2}\log(w_a - w_a') + \frac{\Delta_b}{2}\log(w_b - w_b') \right] \qquad \text{(B.28)}
$$

$$
\alpha_{ab} = -\int_{E_{ab}} \left(\frac{1}{4}\partial_w \left(\gamma - \log\sqrt{T\bar{T}} \right) dw + \frac{1}{4}\partial_{\bar{w}} \left(\gamma + \log\sqrt{T\bar{T}} \right) d\bar{w} \right) \qquad \text{(B.29)}
$$

$$
\eta_{ab} = \int_{E_{ab}} \left(\frac{1}{2}\sqrt{\bar{T}} \left(\cosh\gamma - 1 \right) d\bar{w} + \frac{1}{4\sqrt{T}}(\partial\gamma)^2 dw \right) \qquad \text{(B.30)}
$$

This completes the derivation of formula (3.26) used in the main text. The integral ϖ_{ab} is defined as in (3.58). Note that the logarithmic terms in ϖ_{ab} in (B.27) are due to the

prefactor $\hat{\psi}_b^- \hat{\psi}_a^+$. These terms precisely cancel the singularities at the endpoints of the integral $\int_a^b \omega$ so that ϖ_{ab} is finite as we continue the limits of integration all the way up the to punctures at w_a and w_b [46].

B.4.3 WKB expansion of the coordinates

In the previous section we derived the $\xi \to 0$ WKB expansion of $(s_a \wedge s_b)$ up to order $\mathcal{O}(\xi)$. To compute the WKB expansion of the coordinate χ_E we simply combine the expansions for each edge of the quadrilateral Q_E, taking care to account for the directions of the WKB lines as discussed in section 3.3.6. When this is done each of the integrals (B.28) - (B.30) become closed integrals along the cycle γ_E. The asymptotics of the χ-functions are needed for the inversion of the χ-system described in section 3.3.9. For that purpose only the non-vanishing contributions are needed in the $\xi \to 0, \infty$ limits.

There is one very important subtlety that must be addressed here, which is that of the monodromy around u-spikes discussed in appendix B.3. We take the point of view that we have made the (multi-valued) gauge-transformation (B.16) that removes the monodromy about each u-spike. The small solutions in this gauge are single valued throughout Q_E, but we must account for the monodromy of the gauge transformation about Q_E. This monodromy is simply $(-1)^{u_E}$ where u_E is the number of u-spikes in Q_E.

Combining the above discussion with (B.29), the constant term in the WKB expansion of χ_E is given by

$$C_E^{(0)} = \log(-1)^{u_E} - \frac{1}{4} \int_{\gamma_E} \left(d\gamma + *d\log \sqrt{T\bar{T}} \right) = \log(-1)^{u_E} \pm i\pi \qquad (B.31)$$

To arrive at the last equality (B.31) we have used the fact that γ is single-valued on the 4-punctured sphere so that the integral of $d\gamma$ on any closed contour is zero. The integral of $*d\log\sqrt{T\bar{T}}$ is simple to do explicitly and gives the $\pm i\pi$ factor.[1]

The discussion of the $\xi \to \infty$ limit follows along the same lines as the $\xi \to 0$ limit. The singular term is given by $e^{\xi \int_{\gamma_E} \bar{\omega}/2}$. The constant term is the same. Thus the full non-vanishing WKB asymptotic is given by

$$\chi_E \sim (-1)^{u_E} \exp\left[\frac{1}{2} \int_{\gamma_E} \left(\xi^{-1}\omega + \xi\bar{\omega} \right)\right] \qquad (B.32)$$

---

[1] The $\pm$ depends on the orientation of γ_E but both signs have the same overall effect so that the $\pm$ is irrelevant.

where we recall that u_E is the number of u-spikes enclosed in γ_E. This is the expression (3.40) used in the main text.

Appendix C

Fold lines and Properties of γ

In this appendix we discuss some properties of the function γ and how they are related to geometric features of the string embedding. In appendix C.1 we show that the world-sheet contours where $\gamma = 0$ map to the fold-lines of the target space solution; in appendix C.2 we discuss how the geometry of the string embedding near the boundary is deduced from the structure of these $\gamma = 0$ contours near the points w_a; finally, in section C.2.1 we show how the global structure of the $\gamma = 0$ contours is deduced from the choice of spikes in γ. The point of this appendix is to give the background details that were omitted in the discussion of section 3.2.3.

C.1 Fold lines

In this section we show that the contours on the worldsheet where $\gamma = 0$ map to the fold lines of the string embedding. This was pointed out in [46]. Recall the relation between γ and the world-sheet metric

$$\sqrt{T\bar{T}}\cosh\gamma = \frac{\partial x\bar{\partial}x + \partial z\bar{\partial}z}{z^2} \tag{C.1}$$

Furthermore, we have

$$T(w) = \frac{(\partial x)^2 + (\partial z)^2}{z^2}, \quad \bar{T}(\bar{w}) = \frac{(\bar{\partial}x)^2 + (\bar{\partial}z)^2}{z^2} \tag{C.2}$$

Now, suppose that $\mathcal{C}$ is a curve on the worldsheet that maps to a fold-line of the string and consider a point $\mathcal{P}$ in that curve. We can choose local coordinates at $\mathcal{P}$ so that

the derivative takes the form $\partial_w \to e^{i\phi}(\partial_t + i\partial_n)$ where the direction ∂_n is chosen such that $\partial_n z = 0$. The prefactor $e^{i\phi}$ is the Jacobian of the coordinate transformation (just a translation and rotation). The defining property of the fold-line is then that the x-coordinate reaches an local extrema and thus we also have $\partial_n x = 0$ as we cross the fold. Therefore along the fold-line we have (with $\partial_t x = \dot{x}$)

$$\sqrt{T\bar{T}}\cosh\gamma \to \frac{\dot{x}^2 + \dot{z}^2}{z^2}, \quad T(w) \to e^{2i\phi}\frac{\dot{x}^2 + \dot{z}^2}{z^2}, \quad \bar{T}(\bar{w}) \to e^{-2i\phi}\frac{\dot{x}^2 + \dot{z}^2}{z^2} \tag{C.3}$$

Using the last two equations to solve for $\sqrt{T\bar{T}}$ we see that they are consistent with the first equation only if $\gamma = 0$. Therefore, the worldsheet contours where $\gamma = 0$ map to the fold-lines of the string-embedding. For this reason, we frequently refer to the contours where $\gamma = 0$ as fold-lines.

C.2   Structure of γ near w_a

To gain some intuition about the structure of the contours where $\gamma = 0$ it is useful to study the behavior of γ near the points w_a. Recall that γ is defined as the solution to the PDE:

$$\partial\bar{\partial}\gamma = \sqrt{T\bar{T}}\sinh\gamma \tag{C.4}$$

subject to the boundary conditions

$$\gamma \; \to \; \pm\frac{1}{2}\log T\bar{T} \quad (w \to z_a) \tag{C.5}$$

$$\gamma \; \to \; 0 \quad\quad\quad (w \to P_a) \tag{C.6}$$

The boundary condition (C.6) simply imposes that γ is non-singular at the singularities of T and this condition is automatically imposed if we demand the solution be regular away from the zeros of T.

Since we know that γ must vanish at singularities of T, it's natural to study the function in the neighborhood of these points. Let us consider some P_a and use polar coordinates (r, ϕ) in which the origin is at w_a. Since γ is vanishing, we can linearize the RHS of (C.4). Further, we can take $\sqrt{T\bar{T}} \sim |\Delta|^2/(4r^2)$. The PDE becomes linear and separable and using standard techniques one finds the series solution

$$\gamma \sim g_0 \, r^{\frac{1}{2}\Delta} + \sum_{m=1}^{\infty} g_m \sin\left(m\phi + \delta_m\right) r^{\frac{1}{2}\sqrt{\Delta^2 + 4m^2}} \tag{C.7}$$
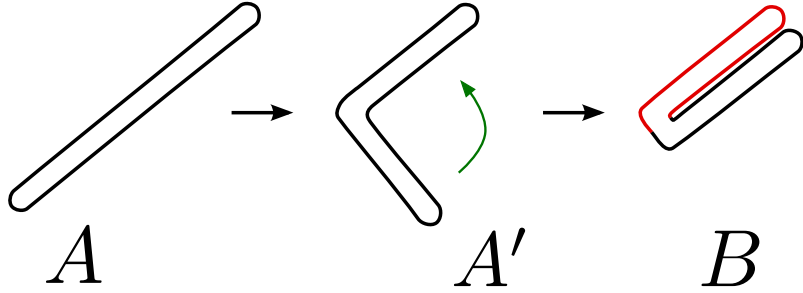
179

Figure C.1: Single-folded and double-folded string in panels A and B respectively.

Now consider a small circle centered at $r = 0$. As $r \to 0$ the series (C.7) is dominated by the lowest mode in the expansion. Thus along an infinitesimal circle centered at $r = 0$ the series (C.7) will vanish $2m^*$ times, where g_{m^*} is the smallest non-zero coefficient g_m, $m = 0, 1, 2, ...$ in the series. Thus, if g_0 is the smallest non-zero coefficient then the series will vanish only at the point w_a which will be a local extrema. If $m^* = 1$ then the series will vanish along a single curve passing through P_a; if $m^* = 2$ then γ will vanish along two curves that intersect at P_a, and so on.

The fact that the contours where $\gamma = 0$ map to fold-lines of the target-space solution gives a clear geometric meaning to each possible behavior $m^* = 1, 2, ...$ near an insertion point. For $m^* = 1$ we will cross two fold-lines as the world-sheet coordinate traverses a small loop around the point w_a. This means that near the insertion point the string is single-folded as shown in figure C.1A. For $m^* = 2$ we will cross two fold-lines as the world-sheet coordinate traverses a small loop around the point w_a. This means that near the insertion point the string is double-folded as shown in figure C.1B, for example. In general for $n > 0$ the case $m^* = n$ should correspond to an n-folded string. The only subtle case seems to be $m^* = 0$. Apparently if $m^* = 0$, as we traverse a closed loop around w_a the contour swept out in the target space does not close since there is no point at which the coordinates (x, z) can 'turn around'. In this section we are only interested in solutions that are closed (i.e. the embedding coordinates have trivial monodromies around operator the insertion points x_a) and thus we will only study cases for which $m^* > 0$ at all w_a. This is further discussed in appendix C.2.1.

It is important to keep in mind that (as we mentioned above) the behavior of γ at P_a is not our choice, and is determined by regularity and the conditions (C.5). In other words, for fixed T the only remaining conditions one can specify are the choice of signs in (C.5). For each choice of signs there will be a unique m^* for each P_a. In the next section we demonstrate how this works using the T of the 4-point function discussed in the main text.

180

C.2.1 Structure of contours where $\gamma = 0$

In this section we describe why the spike configurations of figure 3.4 are the only two physically relevant configurations. Furthermore, we deduce the structure of the contours where $\gamma = 0$ for each of these spike configurations.

Consider T fixed to be that of the 4-point function discussed in the main text (see equation (3.60) and figure 3.15). There are 4 zeros and therefore 2^4 ways to choose the signs in (C.5). Because of the symmetry of (C.4) under $\gamma \to -\gamma$, without loss of generality we can fix one of the spikes to be up which leaves 2^3 choices. Now, because the string is embedded in AdS_2 we know that it must be folded. Moreover we know that the operator insertions x_a will sit along the fold-lines of the target-space solution. In the world-sheet coordinates this translates to the statement that we should require $m^* > 0$ at each w_a. That is, there should be at least one contour where $\gamma = 0$ running through each insertion point w_a. For the 4-point function T (see equation (3.60) and figure 3.15) the only obvious way to accomplish this in general is to choose the spikes such that $\gamma \to -\gamma$ under reflection about the real axis. This leaves only the spike configurations of figure C.2A,B, which are those of figure 3.4 used in the main text. We will now discuss the global structure of the $\gamma = 0$ contours for these two choices of spikes.

In figure C.2 we show the fold-structure for three different spike configurations. The black lines schematically represent the contours where $\gamma = 0$ and one can read off the m^* associated with each puncture. The structure of these contours is determined purely by the choice of the directions of the spikes of γ. We refer to these contours as 'fold lines' since they map onto the fold-lines of the target-space embedding (see appendix C.1). We guess the structure of the fold lines for each choice of the spikes as follows: u spikes must be separated from d spikes by at least one fold line; we use the minimum number of fold lines needed to accomplish this for all spikes. Note that fold lines must encircle at least one zero of T.[1] This restriction is useful because, for example, it allows one to rule-out the possibility of fold-lines corresponding to the gray contours in figure C.2C. This is important because if it was possible for the gray contours to be fold-lines then it might

---

[1] Consider a closed contour along which $\gamma = 0$ and suppose (for a contradiction) that it does not enclose any zeros of T. Let $\mathcal{D}$ be the region enclosed by the contour. This contour must separate positive values from negative values (i.e. it cannot sit at the bottom of a 'valley' since this locally violates the equation (C.4)). Suppose for simplicity that $\gamma < 0$ in $\mathcal{D}$. Since γ is regular away from the zeros of T, there must be at least one local minimum inside $\mathcal{D}$, and therefore at least one point where $\left(\partial_x^2 + \partial_y^2\right)\gamma \geq 0$. Thus at such a point the LHS of (C.4) is positive or zero, but the RHS is strictly less than zero by assumption, which is the desired contradiction.
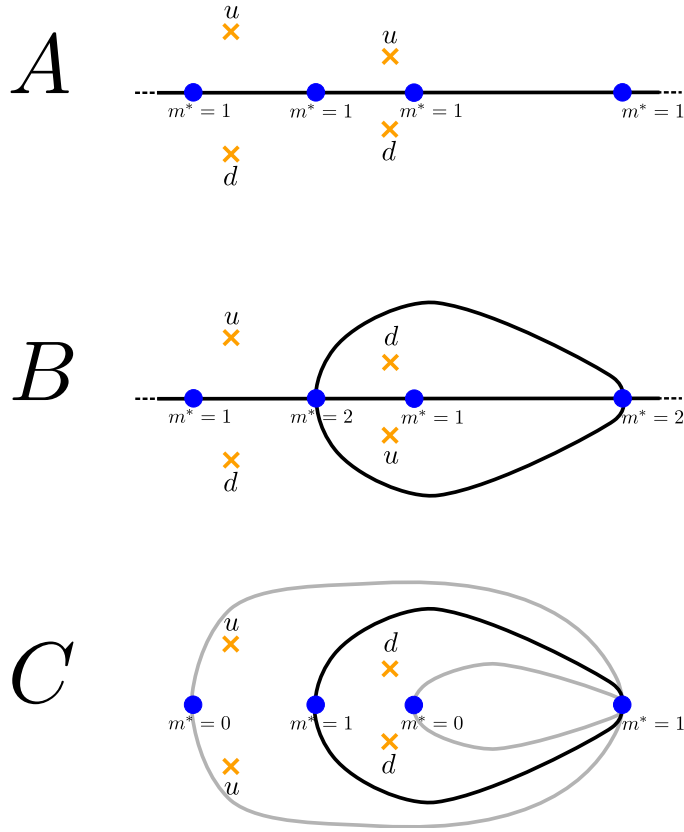
Figure C.2: Three different spike configurations and the corresponding structure of the $\gamma = 0$ contours. The black lines schematically represent the contours where $\gamma = 0$ and one can read off the m^* associated with each puncture. Panels A and B show the physically relevant configurations studied in the main text. Panel C shows a third spike configuration which is not physical due to the presence of $m^* = 0$ behavior at two of the insertion points. The gray contours in panel C indicate contours that cannot cannot correspond to fold-lines due to the restriction that $\gamma = 0$ contours must encircle at least one zero of T (see footnote 1). In this figure we are not indicating the location point w_4^* because it is not relevant for the present discussion (so long as it is located somewhere on the real axis).

be possible to have a solutions with all $m^* > 0$ for configuration C. Configurations A and B are the physical configurations that we study in this chapter and we have checked the fold structures of figure C.2A,B numerically. Configuration C is an example of a spike-configuration that does not correspond to a target-space solution with the desired

properties; the corresponding fold structure is only our best guess but we have not checked it numerically.

To summarize this appendix, in appendix C.1 we showed that the world-sheet contours where $\gamma = 0$ map to the fold-lines of the target space solution; in appendix C.2 we discussed how the geometry of the string embedding near the boundary is deduced from the structure of these $\gamma = 0$ contours near the points w_a; finally, in section C.2.1 we discussed how the global structure of the $\gamma = 0$ contours is deduced from the choice of spikes in γ. From all of this one can deduce some qualitative global features of the string embedding, which is discussed in detail in section 3.2.3.

Appendix D

Details of the 4-point function computation

D.1 Explicit expression for stress-energy tensor coefficients

For completeness we present the coefficients c_a of the stress-energy tensor in formula (3.60),

$$
\begin{aligned}
c_\infty &= \frac{\Delta_\infty^2}{4} \\
c_0 &= \frac{1}{4}\left[4\,U w_4 + 2 w_4\left(1 + w_4\right)\Delta_3^2 + \left(-1 + w_4\right)\left(2 w_4 \Delta_1^2 + \left(1 + w_4\right)\left(\Delta_2^2 - \Delta_4^2\right)\right)\right] \\
c_1 &= \frac{1}{2}\left[-2\,U + \left(-1 + w_4\right)^2\Delta_1^2 - \left(1 + w_4\right)^2\Delta_3^2\right] \\
c_2 &= \frac{1}{4}\left[-4\,U w_4 + 2\left(1 + w_4\right)\Delta_3^2 + \left(-1 + w_4\right)\left(-2\Delta_1^2 + \left(1 + w_4\right)\left(-\Delta_2^2 + \Delta_4^2\right)\right)\right] \tag{D.1}
\end{aligned}
$$

D.2 Explicit expressions for χ-functions and A_{PQ}

For reference, we include here the explicit expressions for the χ-functions for the triangulation of figure 3.15. They are given by

$$\chi_{12} = (-1)\frac{(s_1 \wedge M_1^{-1}s_4)(s_2 \wedge s_4)}{(M_1^{-1}s_4 \wedge s_2)(s_4 \wedge s_1)} \tag{D.2}$$

$$\chi_{23} = (-1)\frac{(s_2 \wedge M_3 s_4)(s_3 \wedge s_4)}{(M_3 s_4 \wedge s_3)(s_4 \wedge s_2)} \tag{D.3}$$

$$\chi_{34} = (-1)\frac{(s_4 \wedge s_2)\left(s_3 \wedge M_3^{-1}s_2\right)}{(s_2 \wedge s_3)\left(M_3^{-1}s_2 \wedge s_4\right)} \tag{D.4}$$

$$\chi_{14} = (-1)\frac{(s_4 \wedge M_1 s_2)\left(s_1 \wedge s_2\right)}{(M_1 s_2 \wedge s_1)\left(s_2 \wedge s_4\right)} \tag{D.5}$$

$$\chi_{24} = (-1)\frac{(s_2 \wedge s_3)(s_4 \wedge s_1)}{(s_3 \wedge s_4)(s_1 \wedge s_2)} \tag{D.6}$$

$$\chi_{\hat{2}4} = (-1)\frac{(M_3^{-1}s_2 \wedge M_4 s_1)(s_4 \wedge s_3)}{(M_4 s_1 \wedge s_4)(s_3 \wedge M_3^{-1}s_2)} \tag{D.7}$$

One can check that these coordinates satisfy the rule (3.37) at each puncture. The χ-system obeyed by these coordinates is given by

$$\chi_{24}\chi_{24}^{++} = \left(\chi_{\hat{2}4}\chi_{\hat{2}4}^{++}\right)^{-1} = \frac{(1+A_{23})(1+A_{14})}{(1+A_{34})(1+A_{12})} \tag{D.8}$$

$$\chi_{12}\chi_{12}^{++} = \left(\chi_{14}\chi_{14}^{++}\right)^{-1} = \chi_{34}\chi_{34}^{++} = \left(\chi_{23}\chi_{23}^{++}\right)^{-1} = \frac{(1+A_{24})}{(1+A_{\hat{2}4})} \tag{D.9}$$

where the A_{PQ} are given by

$$A_{12} = \frac{\chi_{12}(1+\chi_{14})(1+\hat{\chi}_{24}(1+\chi_{23}(1+\chi_{24})))}{(1-\mu_1^2)(1-\mu_2^2)} \tag{D.10}$$

$$A_{23} = \frac{\chi_{23}(1+\chi_{34})(1+\chi_{24}(1+\chi_{12}(1+\chi_{\hat{2}4})))}{(1-\mu_2^2)(1-\mu_3^2)} \tag{D.11}$$

$$A_{34} = \frac{\chi_{34}(1+\chi_{23})(1+\hat{\chi}_{24}(1+\chi_{14}(1+\chi_{24})))}{(1-\mu_3^2)(1-\mu_4^2)} \tag{D.12}$$

$$A_{14} = \frac{\chi_{14}(1+\chi_{12})(1+\chi_{24}(1+\chi_{34}(1+\hat{\chi}_{24})))}{(1-\mu_1^2)(1-\mu_4^2)} \tag{D.13}$$

$$A_{24} = \frac{\chi_{24}(1+\chi_{12}(1+\chi_{\hat{2}4}(1+\chi_{23})))(1+\chi_{43}(1+\chi_{\hat{4}2}(1+\chi_{41})))}{(1-\mu_2^2)(1-\mu_4^2)} \tag{D.14}$$

$$A_{\hat{2}4} = \frac{\hat{\chi}_{24}(1+\chi_{23}(1+\chi_{24}(1+\chi_{12})))(1+\chi_{41}(1+\chi_{42}(1+\chi_{43})))}{(1-\mu_2^2)(1-\mu_4^2)} \tag{D.15}$$

Using the explicit expressions for the coordinates (D.2)-(D.7), schouten identity and the shift relation (3.43) one can directly verify the functional equations (D.8)-(D.9).

D.3   Finite part of AdS

In this section, we present some intermediate steps in the derivation of our formula (3.66) for the finite part of the AdS contribution. We want to compute

$$A_{fin} = \frac{\pi}{3} - \frac{i}{2}\left(\oint_{\gamma_a}\omega\right)I_{ab}^{-1}\left(\oint_{\gamma_b}\eta\right). \tag{D.16}$$

according to the steps outline in section 3.4.1. The complete basis of five a-cycles and five b-cycles that we chose is depicted in figure D.1. From this figure we also read-off the intersection matrix $I_{ab} = (\delta_{a+1,b} - \delta_{a-1,b})$ using the conventions described in the caption. The only other ingredient we need is

$$\int_{a_i}\eta = 0, \quad i = 2,\ldots,5 \tag{D.17}$$

which follows from the regularity of η at the poles of T. Plugging into (D.16) and computing we find

$$A_{fin} = \frac{\pi}{3} + i\left(\omega_{a_1}\eta_{z_3,z_2} + \omega_{a_2}\eta_{-1,z_2} + \omega_{a_3}\eta_{z,z_2} + \omega_{a_4}\eta_{1,z_2} + \omega_{a_5}\eta_{\infty,z_2}\right) - i\left(\sum_{i=1}^{5}\omega_{b_i}\right)\eta_{z_3,z_4} \tag{D.18}$$
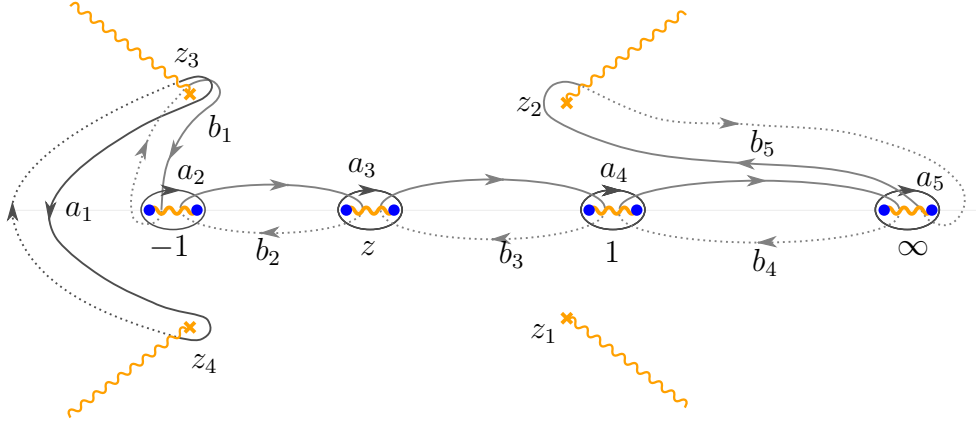
Figure D.1: The cycles for Riemann bilinear identity. The dashed line represents a contour in a different Riemann sheet. The wavy lines represent a choice of branch cuts. From this picture we also read the intersection matrix I_{ab} of the cycles. For each pair of cycles, say γ_a and γ_b, intersecting at a point with tangent vectors ∂_a and ∂_b respectively, we assign $I_{ab} = +1\,(-1)$ if $\det\left[\{\partial_a, \partial_b\}\right] > 0\,(<0)$.

where we are using the notation $\eta_{ab} = \int_a^b \eta$ and $\omega_{\mathcal{C}} = \int_{\mathcal{C}} \omega$ and the contours are defined in figures D.1 and D.2.

Each of these η_{ab} can be written as a linear combination of the $\eta_{E_{ab}} = \int_{E_{ab}} \eta$ where the integral is taken along the WKB-line from P_a to P_b and the direction of the contour is the same as that of the WKB line. The idea is to combine the $\eta_{E_{ab}}$ to form the contour that we want. Let us exemplify with η_{1,z_2}. From the WKB configuration, see figure D.2, we see that the large θ expansion of the ratio $\frac{(s_1 \wedge s_2)(s_1 \wedge s_4)}{(s_2 \wedge s_4)}$ involves a cycle that can be continuously deformed into *twice* the line integral connecting the puncture at $w = 1$ and the zero at $w = z_2$. Therefore we have

$$\eta_{1,z_2} = \frac{1}{2} \int_{-\infty}^{\infty} \frac{d\theta}{\pi} e^{-\theta} \log\left[\frac{\left(1 + A_{12}^-\right)\left(1 + A_{14}^-\right)}{\left(1 + A_{24}^-\right)}\right] = \frac{1}{2}\left(\eta_{E_{12}} + \eta_{E_{14}} - \eta_{E_{24}}\right) \tag{D.19}$$
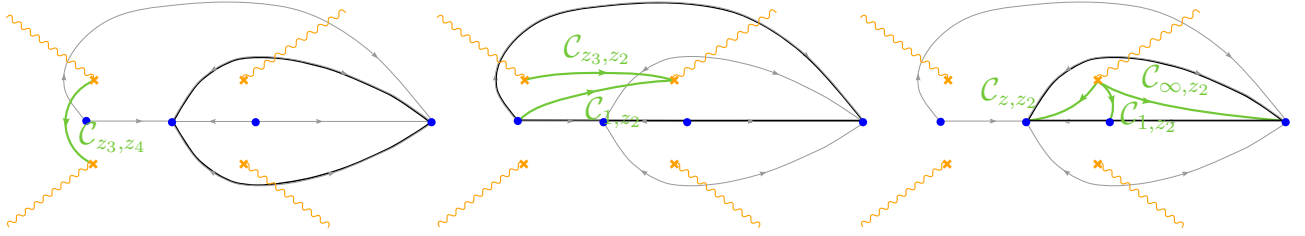
In the same way we obtain

Figure D.2: To extract line integrals connecting a zero to puncture or connecting two zeros we combine products of elementary solutions that have WKB expansions involving integrals over the paths indicated by the black lines. The resulting closed contours can be continuously deformed into the contour that we want, indicated by the green lines. The precise way of combining these products is dictated by the direction of the WKB lines indicated by the gray arrows.

$$\eta_{z_3, z_4} = \frac{1}{2} \left(\eta_{24} - \eta_{\hat{2}4} \right) \tag{D.20}$$

$$\eta_{-1, z_2} = \frac{1}{2} \left(2\eta_{34} + \eta_{12} - \eta_{14} - \eta_{24} \right) \tag{D.21}$$

$$\eta_{z, z_2} = \frac{1}{2} \left(\eta_{12} - \eta_{14} - \eta_{24} \right) \tag{D.22}$$

$$\eta_{\infty, z_2} = \frac{1}{2} \left(\eta_{14} - \eta_{12} - \eta_{24} \right) \tag{D.23}$$

$$\eta_{z_3, z_2} = \frac{1}{2} \left(\eta_{12} + \eta_{34} - \eta_{14} - \eta_{23} \right) \tag{D.24}$$

where the notation is the natural simplification of that used in (D.19). Plugging these expressions into (D.18) and re-collecting each η_E, one finds that the coefficient of η_E is simply ω_E where ω_E is the ω-cycle the intersects edge E, *not* the integral of ω along edge E (which would be divergent). That is, it's (1/2 of) the ω-cycle associated with the coordinate χ_E which are shown in figure 3.15. Thus we have

$$A_{fin} = \frac{\pi}{3} - i \sum_{E \in \mathcal{T}} \omega_E \, \eta_E \tag{D.25}$$

which is formula (3.66) as desired.

Equation (D.25) is perhaps the simplest possible result one could write from the triangulation data. Given this simplicity, it is probably possible to derive the result in a much more elegant way and perhaps even for any number of punctures. We have not pursued this issue but feel that it merits further exploration.

Appendix E

Three-point function in GMN language

In this section we apply the method developed in section 3.3 to the three point correlation function studied in [46]. We use the setup of [46], namely the same stress-energy tensor. We aim at deriving a set of functional equations to extract the cycles used there.

As a starting point, we introduce the WKB triangulation for this configuration from which we define the coordinates, see figure E.1. From this figure, we easily derive the χ-system. Since the quadrilateral is very degenerate it follows from (3.46) that the right hand side of the χ-system is equal to 1. The reason is that the same auxiliary A_{PQ}'s appear both in numerator and denominator canceling each other. Hence, the solution of the functional equations is simply given by the WKB asymptotics. More explicitly, the χ functions take the form

$$\chi_{ac} = (-1)\exp\left(\frac{1}{2}e^{\theta}\int_{\gamma_{ac}}\omega + \frac{1}{2}e^{-\theta}\int_{\gamma_{ac}}\bar{\omega}\right) = -\frac{\mu_a\mu_c}{\mu_b} \tag{E.1}$$

where a, b and c are distinct.[1] The spikes must be in pointing in opposite direction as follows from the discussion of appendix C. This is the the origin of the (-1) prefactor in (E.1). The cycles of ω are given in terms of the dimensions of the operators,

$$\int_{\gamma_{ac}}\omega = i\pi(-\Delta_a - \Delta_c + \Delta_b) \tag{E.2}$$

---

[1]This result also follows directly from the definition of the coordinates in terms of the small solutions, $\chi_{ac} = -\frac{(s_c\wedge s_b)(s_a\wedge M_a^{-1}s_b)}{(M_a^{-1}s_b\wedge s_c)(s_b\wedge s_a)}$ for distinct a, b and c; all the inner-products cancel and one is left with only the monodromy factors in (E.1).
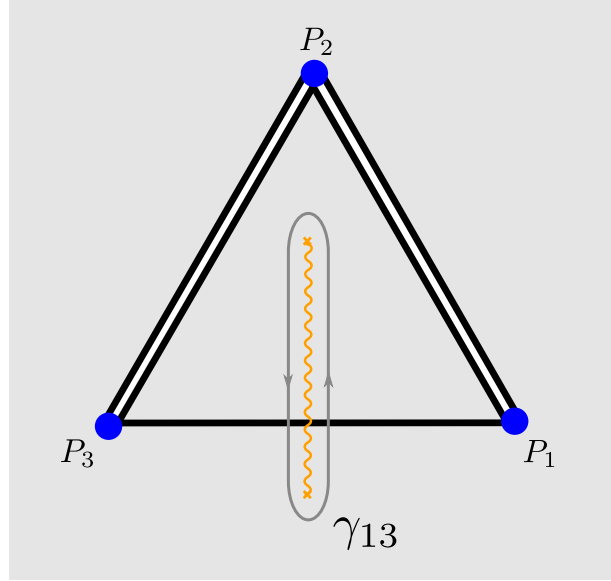
Figure E.1: The WKB triangulation for the 3-point function is composed of 3 edges forming two triangles on the sphere. Here we show the construction of the coordinate χ_{13}. We are using the edge-splitting procedure discussed in section 3.3.5 (in particular, see figure 3.12). The gray contour shows the cycle associated with the coordinate χ_{13}.

Having the solutions of the functional equations, we can easily find the auxiliary quantities A_{PQ} using the rules of section 3.3.8. The determination of the η-cycles is also straightforward. To compare with the result in [46] let us set $\Delta_1 = \Delta_2 = \Delta$ and $\Delta_3 = \Delta_\infty$. We use expression 3.57 to compute the cycles, and we get

$$\int_{-1}^{1} \eta = \int_{\mathbb{R}} \frac{d\theta}{\pi} e^{-\theta} \log(1 + A_{12}^-) = h(2\Delta - \Delta_\infty) + h(2\Delta + \Delta_\infty) - 2h(2\Delta) \qquad \text{(E.3)}$$

$$\int_{1}^{\infty} \eta = \int_{\mathbb{R}} \frac{d\theta}{\pi} e^{-\theta} \log(1 + A_{23}^-) = h(\Delta_\infty) + h(2\Delta + \Delta_\infty) - h(2\Delta) - h(2\Delta_\infty) \qquad \text{(E.4)}$$

where we define

$$h(x) = \int_{\mathbb{R}} \frac{d\theta}{\pi} \cosh\theta \log\left(1 - e^{-x\pi \cosh\theta}\right) . \qquad \text{(E.5)}$$

This is precisely the result obtained in [46]. A last comment about the expression for the area in the three point function. It is easy to show using the same type of manipulation of the four point function case that the area can be expressed in terms of elements of the

WKB triangulation as

$$A_{fin} = \frac{\pi}{6} - i \sum_{E \in \mathcal{T}} \omega_E \eta_E \qquad (E.6)$$

where the sum is over the edges of the triangulation of figure E.1. As in the case of the four point function, we define $\eta_{E_{ab}}$ as the η-cycle that passes along edge E_{ab} from P_a to P_b and $\omega_{E_{ab}}$ as the ω-cycle that intersects edge E_{ab}.

Appendix F

Review of twistors and geometry

In this appendix we review some known facts about the geometry of amplitudes and in particular, pentagons.

F.1 Variables

Scattering Amplitudes and null polygonal Wilson loops are conventionally parametrized by a plethora of very useful variables. Amongst them, we have momentum twistors Z, spinor helicity variables λ and their parity conjugate $\tilde{\lambda}$, and dual momentum twistors W. Let us introduce them in our notation following [104] closely. We shall start by the momentum twistors Z and construct all other variables from them.

A momentum twistor is a four dimensional projective vector $Z_j \sim \lambda Z_j$. It is associated to each edge of the null polygon, see figure F.1. Momentum twistors allow us to parametrize the shape of the polygon in an unconstrained way, this being one of their main virtues. Moreover, they transform linearly under conformal transformations and are therefore very useful when dealing with a conformal theory such as $\mathcal{N} = 4$ SYM.

Note the labelling of edges we are using in this chapter is tailored from an OPE analysis and is *not* the conventional cyclic labelling commonly used to describing color ordered partial amplitudes. In particular, in our convention, Z_j and Z_{j+1} (or Z_{j-1}) are *not* neighbours; instead they nicely face each other in the polygon tessellation, see figure F.1. The trivial conversion between our labelling and a more conventional numbering of the edges is presented in the caption of figure F.1.
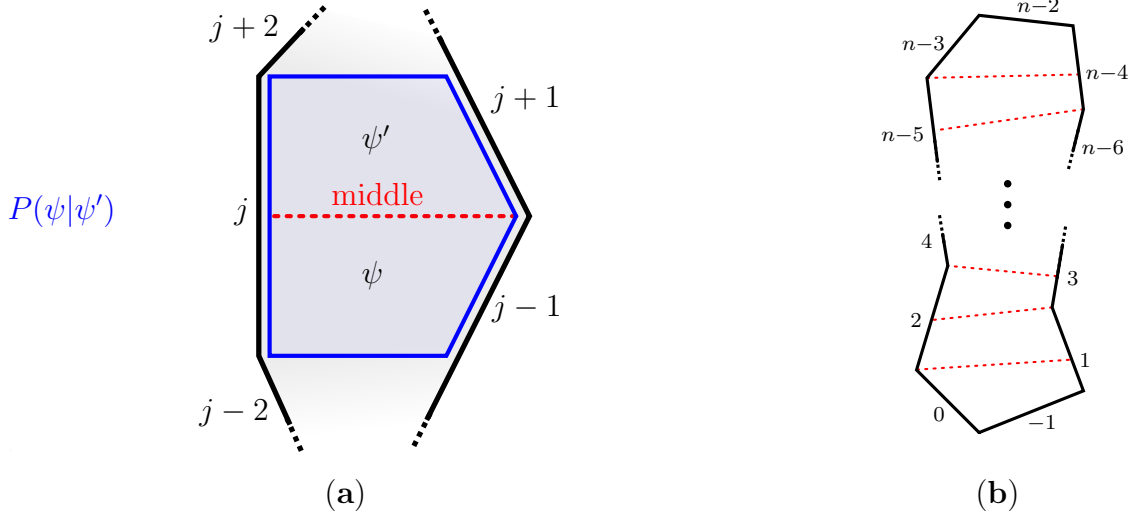
Figure F.1: **a**) The pentagon transitions are the building blocks of null polygonal Wilson loops. They represent the transition $\psi \to \psi'$ undergone by the flux-tube state as we move from one square to the next in the OPE decomposition. This breaking into squares is univocally defined by specifying the middle (or inner dashed) edge of the pentagon to be $Z_{\text{middle}} \propto \langle j-2, j, j+2, j-1 \rangle Z_{j+1} - \langle j-2, j, j+2, j+1 \rangle Z_{j-1}$. **b**) In the OPE-friendly labelling of edges, adopted in this chapter, the middle edge of the j-th pentagon ends on the j-th edge. As a result, the very bottom edge is edge -1 while the very top one is edge $n-2$. The map between the OPE index j and the more common cyclic index j_{cyc} reads $j_{\text{cyc}} = \frac{3}{4} - \frac{1}{4}(-1)^j(2j+3) \bmod n$.

Out of four momentum twistors we can build conformal invariant angle brackets

$$\langle ijkl \rangle \equiv \epsilon_{abcd} Z_i^a Z_j^b Z_k^c Z_l^d \qquad \text{or} \qquad \langle ijkl \rangle \equiv Z_i \wedge Z_j \wedge Z_k \wedge Z_l \,. \tag{F.1}$$

We construct spinor helicity variables λ by extracting the first two components of each

four dimensional momentum twistors[1]

$$\lambda_i \equiv \begin{pmatrix} 1 & 0 & 0 & 0 \\ 0 & 1 & 0 & 0 \end{pmatrix} \cdot Z_i . \tag{F.2}$$

With these spinor helicity variables we can construct Lorentz invariant two dimensional angle brackets

$$\langle i, j \rangle \equiv \epsilon^{\alpha\beta} \lambda_{i,\alpha} \lambda_{j,\beta} \qquad \text{or} \qquad \langle i, j \rangle \equiv Z_i \cdot \mathbb{I} \cdot Z_j \tag{F.3}$$

where $\mathbb{I}_{ab}$ is the usual infinite twistor which one can read off from the first definition. Next we introduce the dual momentum twistors W which can be thought of as the parity conjugate of the Z's. The dual momentum twistors are defined by using three neighbouring standard momentum twistors as

$$W_{j,a} \equiv \epsilon_{abcd} \frac{Z^b_{j-2} Z^c_j Z^d_{j+2}}{\langle j-2, j \rangle \langle j, j+2 \rangle} \qquad \text{or} \qquad W_j \equiv \frac{Z_{j-2} \wedge Z_j \wedge Z_{j+2}}{\langle j-2, j \rangle \langle j, j+2 \rangle} . \tag{F.4}$$

Note that with this convenient normalization the dual momentum twistor W_j has the opposite helicity weight as the momentum twistor Z_j. For the very bottom and top we need to tweak the definition (F.4) due to the non-cyclic labelling we are using.[2]

With the dual momentum twistors we can now construct four brackets once more, now denoted with square brackets

$$[ijkl] \equiv \epsilon^{abcd} W_{i,a} W_{j,b} W_{k,c} W_{l,d} \qquad \text{or} \qquad [ijkl] \equiv W_i \wedge W_j \wedge W_k \wedge W_l . \tag{F.5}$$

Finally, we come to the parity conjugate spinor helicity variables $\tilde{\lambda}$.[3] They can be now

---

[1] More precisely, we can always apply a global $GL(4)$ rotation U to all the twistors (before extracting the first two components) plus a residual $GL(2)$ transformation V to all the spinors (after extracting them from the first two components) such that in total $\lambda_i \equiv V \cdot \begin{pmatrix} 1 & 0 & 0 & 0 \\ 0 & 1 & 0 & 0 \end{pmatrix} \cdot U \cdot Z_i$. Henceforth we set U and V to be the identity matrices. Nevertherless, it is worth keeping in mind that sometimes such transformations can be quite convenient. For instance, the twistors in previous OPE studies – see e.g. appendix of [82] – contain several zero components and will lead to singular λ's if extracted blindly. In those cases, it is quite convenient to preform such generic conformal transformations when constructing the spinor helicity variables.

[2] Explicitly, the only tricky definitions are $W_0 \equiv \frac{Z_2 \wedge Z_0 \wedge Z_{-1}}{\langle 2,0 \rangle \langle 0,-1 \rangle}$, $W_{-1} \equiv \frac{Z_0 \wedge Z_{-1} \wedge Z_1}{\langle 0,-1 \rangle \langle -1,1 \rangle}$ at the bottom and $W_{n-2} \equiv \frac{Z_{n-4} \wedge Z_{n-2} \wedge Z_{n-3}}{\langle n-4,n-2 \rangle \langle n-2,n-3 \rangle}$ and $W_{n-3} \equiv \frac{Z_{n-2} \wedge Z_{n-3} \wedge Z_{n-5}}{\langle n-2,n-3 \rangle \langle n-3,n-5 \rangle}$ at the top, see figure F.1.

[3] Literally, the transformation $(\lambda, \bar{\lambda}) \to (\bar{\lambda}, \lambda)$ acts on the momentum $p_\mu \sigma^\mu_{\alpha\dot\alpha} = \lambda_\alpha \tilde{\lambda}_{\dot\alpha}$ as a reflection of p_2 since the corresponding Pauli matrix is antisymmetric while all others are symmetric. Once combined with an 180° rotation in the 1-3 plane, we get what is conventionally denoted by parity. In sum, since rotation symmetries are an obvious symmetry, one often slightly abuses notation to denote as parity any transformation whose determinant is -1.

194

defined as the *last* two components of the dual twistors,

$$\tilde{\lambda}_i = \begin{pmatrix} 0 & 0 & 1 & 0 \\ 0 & 0 & 0 & 1 \end{pmatrix} \cdot W_i \, . \tag{F.6}$$

Out of two such twistors we can construct the Lorentz invariant square brackets

$$[ij] \equiv \epsilon^{\dot{\alpha}\dot{\beta}} \tilde{\lambda}_{i,\dot{\alpha}} \tilde{\lambda}_{j,\dot{\beta}} \qquad \text{or} \qquad [ij] = W_i \cdot \tilde{\mathbb{I}} \cdot W_j \tag{F.7}$$

where the dual infinity twistor $\tilde{\mathbb{I}}^{ab}$ can once gain be read off from the first definition.

A beautiful outcome of the construction above is that momentum conservation

$$0 = \sum_i \lambda_{i,\alpha} \tilde{\lambda}_{i,\dot{\alpha}} \qquad \text{for } \alpha = 1,2 \text{ and } \dot{\alpha} = \dot{1},\dot{2} \tag{F.8}$$

automatically follows from the definitions above. In other words, as is well known, the use of twistors trivializes momentum conservation.

To summarize: At this point, each edge of our polygon is endowed with a momentum twistor Z_j, a dual momentum twistor W_j and a pair of spinors λ_j and $\tilde{\lambda}_j$. There are also other null segments which play a critical role in our construction: the middle edges that define our tessellation which are represented by the red dashed lines in figure F.1 and whose corresponding momentum twistors are given in the caption of that same figure. We quote here for convenience:

$$Z_{\text{middle}} = \langle j-2, j, j+2, j-1 \rangle Z_{j+1} - \langle j-2, j, j+2, j+1 \rangle Z_{j-1} \, . \tag{F.9}$$

Let us briefly explain how this equation can be established. This simple exercise beautifully illustrates the power of Hodges' momentum twistors when dealing with the geometry of null lines. First, since $Z_{\text{middle}} \wedge Z_{j-1}$, $Z_{\text{middle}} \wedge Z_{j+1}$ and $Z_{j-1} \wedge Z_{j+1}$ all correspond to the same right cusp in figure F.1a, we immediately have that $Z_{\text{middle}} = \alpha Z_{j+1} + \beta Z_{j-1}$. At the same time the point $Z_{\text{middle}} \wedge Z_j$ – where the middle line intercepts the left edge in figure F.1a – lies on the line $Z_{j+2} \wedge Z_j + t Z_{j-2} \wedge Z_j$ between the two left cusps. As such, the middle twistor is also a linear combination of the twistors Z_j, Z_{j-2} and Z_{j+2} and thus $\langle j, j-2, j+2, Z_{\text{middle}} \rangle = 0$. This condition immediately fixes the ratio β/α to be as in (F.9). The normalization of the projective twistor can be fixed arbitrarily with (F.9) being one such choice. Following the logic above, we can now also associate to each middle edge a dual twistor W_{middle} and a pair of spinors λ_{middle} and $\tilde{\lambda}_{\text{middle}}$. They will indeed show up below.

We close this section with two useful identities which we shall use latter. The first is

$$\frac{\langle i\hat{i}j\hat{j}\rangle}{[i\hat{i}j\hat{j}]} = \frac{\langle i\hat{i}\rangle\langle j\hat{j}\rangle}{[i\hat{i}][j\hat{j}]} \tag{F.10}$$

where $\hat{i}$ and i are neighbouring edges and so are $\hat{j}$ and j. The second is

$$\langle abcd \rangle = \langle ab \rangle \langle bc \rangle \langle cd \rangle [bc] \qquad \text{and} \qquad [abcd] = [ab][bc][cd]\langle bc \rangle \tag{F.11}$$

which holds for any four consecutive twistors (starting with a followed by b, then c and then d at the end). Note that the second equality in (F.11) follows from the first equality there together with (F.10). It also follows trivially from the first equality in (F.11) under parity which simply interchanges square and angle brackets.

F.2 Hexagon and Heptagon twistors

In figure F.2 we include the twistors we used in this thesis for the hexagon and heptagon Wilson loop [82]. The symmetries of the middle squares are generated by the following matrices

$$M_1 = \begin{pmatrix} e^{\sigma_1 - \frac{i\phi_1}{2}} & 0 & 0 & 0 \\ 0 & e^{-\sigma_1 - \frac{i\phi_1}{2}} & 0 & 0 \\ 0 & 0 & e^{\tau_1 + \frac{i\phi_1}{2}} & 0 \\ 0 & 0 & 0 & e^{-\tau_1 + \frac{i\phi_1}{2}} \end{pmatrix}. \tag{F.12}$$
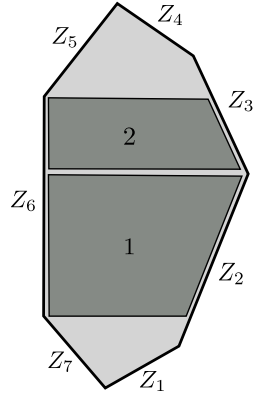
and

$$M_2 = \begin{pmatrix} e^{-\sigma_2 - \frac{i\phi_2}{2}} & 0 & 0 & -e^{-\sigma_2 - \frac{i\phi_2}{2}} + e^{\tau_2 + \frac{i\phi_2}{2}} \\ 0 & e^{\sigma_2 - \frac{i\phi_2}{2}} & 0 & 0 \\ 0 & e^{\sigma_2 - \frac{i\phi_2}{2}} - e^{\frac{i\phi_2}{2} - \tau_2} & e^{\frac{i\phi_2}{2} - \tau_2} & -e^{\frac{i\phi_2}{2} - \tau_2} + e^{\tau_2 + \frac{i\phi_2}{2}} \\ 0 & 0 & 0 & e^{\tau_2 + \frac{i\phi_2}{2}} \end{pmatrix}. \tag{F.13}$$

F.3 Pentagons and Weights

In a tessellation of an n-sided polygon, each two consecutive null squares form a pentagon. As depicted in figure F.1, each such pentagon shares some edges with the larger polygon

196
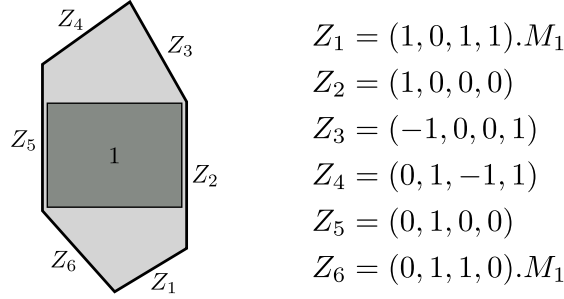
$$Z_1 = (1, 0, 1, 1).M_1$$
$$Z_2 = (1, 0, 0, 0)$$
$$Z_3 = (-1, 0, 0, 1)$$
$$Z_4 = (0, 1, -1, 1)$$
$$Z_5 = (0, 1, 0, 0)$$
$$Z_6 = (0, 1, 1, 0).M_1$$

$$Z_1 = (1, 0, 1, 1).M_1.M_2$$
$$Z_2 = (1, 0, 0, 0).M_1.M_2$$
$$Z_3 = (-1, 0, 0, 1)$$
$$Z_4 = (-1, 1, -1, 3)$$
$$Z_5 = (0, 2, -1, 1)$$
$$Z_6 = (0, 1, 0, 0).M_2$$
$$Z_7 = (0, 1, 1, 0).M_1.M_2$$

Figure F.2: In this figure we present the hexagon and heptagon twistors used in the main text. The respective middle squares are also indicated. The matrices M_1 and M_2 preserve these middles squares and they are used to generate a family of hexagons and heptagons parametrized by the coordinates τ_i, σ_i, ϕ_i with $i = 1, 2$ for the respective square.

while some (either one or two) edges are middle edges defined by the tessellation, see also (F.9).

These pentagons play a prominent role in our construction. In particular, here we want to describe their importance in defining the *weight* of a given edge *with respect to a given pentagon*. To simplify our discussion we label the edges of a generic pentagon as a, b, c, d, e.[4]

Pentagons have no cross-ratios. Nevertheless, they are not totally trivial. For instance, they allow us to read of the weight of an edge of the pentagon (with respect to that

---

[4]For example, this pentagon could be the first pentagon in the tessellation in figure F.1b. In this case we would set $a = Z_2$, $b = Z_0$, $c = Z_{-1}$, $d = Z_1$ and $e = Z_{\text{middle line ending on edge 2}}$.

pentagon) through the pentagon NMHV ratio function components as

$$\mathcal{R}^{(abcd)} = \frac{1}{\mathbf{abcd}} \ , \qquad \mathcal{R}^{(aabc)} = \frac{1}{\mathbf{a^2bc}} \ , \qquad \mathcal{R}^{(aaaa)} = \frac{1}{\mathbf{a^4}} \ , \tag{F.14}$$

and so on. All such components can be extracted from a single R-invariant beautifully written using momentum twistors in [75, 104],

$$\mathcal{R}^{\text{NMHV pentagon}} = \frac{\prod\limits_{A=1}^{4} \left(\langle abcd \rangle \eta_e^A + \langle bcde \rangle \eta_a^A + \langle cdea \rangle \eta_b^A + \langle deab \rangle \eta_c^A + \langle eabc \rangle \eta_d^A \right)}{\langle abcd \rangle \langle bcde \rangle \langle cdea \rangle \langle deab \rangle \langle eabc \rangle} \ . \tag{F.15}$$

From the relations (F.14) we read

$$\mathbf{a^4} = \frac{\langle abcd \rangle \langle cdea \rangle \langle deab \rangle \langle eabc \rangle}{\langle bcde \rangle^3} \ . \tag{F.16}$$

We can also re-write this relation using (F.11) as

$$\mathbf{a^4} = \frac{\langle ab \rangle^4 \langle ea \rangle^4}{\langle ab \rangle \langle bc \rangle \langle de \rangle \langle ea \rangle \langle cd \rangle} \Big/ \frac{[cd]^4}{[ab][bc][cd][de][ea]} \tag{F.17}$$

where the familiar Parke-Taylor chains nicely show up.

Furthermore, note that a product of three weights with respect to the same pentagon can be traded by the weight of any of the other two twistors of the pentagon using the first relation in (F.14) with $\mathcal{R}^{(abcd)} = 1/\langle abcd \rangle$. In particular, it follows that

$$\frac{1}{\mathbf{bce}} = \frac{\mathbf{a}}{\langle abce \rangle} = \frac{\mathbf{d}}{\langle dbce \rangle} \ . \tag{F.18}$$

This allows us to massage slightly some of the formulae in the main text. For example, (5.10) can be written a bit more economically using

$$\frac{1}{(\mathbf{j-1})_j \, (\mathbf{j})_j \, (\mathbf{j+1})_j} = \frac{(\mathbf{t_j})_j}{W_j \cdot Z_{t_j}} \qquad \text{or} \qquad \frac{1}{(\mathbf{j-1})_j \, (\mathbf{j})_j \, (\mathbf{j+1})_j} = \frac{(\mathbf{b_j})_j}{W_j \cdot Z_{b_j}} \tag{F.19}$$

where t_j and b_j indicate the top or bottom twistors of pentagon j respectively, see figure F.3. Note that it is irrelevant that we do not fix the normalizations of these top and bottom twistors: they drop out in the ratios here constructed.
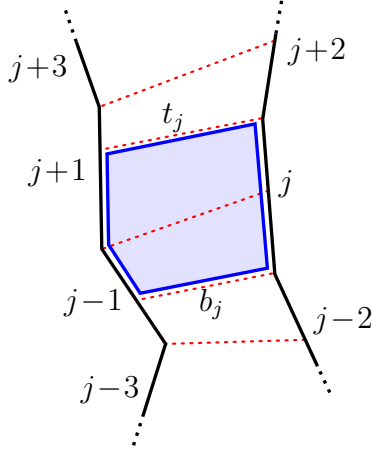
Figure F.3: The weight factor $(\mathbf{j} - \mathbf{1})_j(\mathbf{j})_j(\mathbf{j} + \mathbf{1})_j$ associated to the j-th pentagon can be expressed in terms of the twistors of the larger polygon. It involves the seven closest edges to that pentagon, as illustrated in the figure. It is clear from this example the advantage of using this edge labelling as opposed to the cyclic one.

We can also explicitly evaluate (F.19) by plugging in (F.16) the expressions for the middle momentum twistors (F.9), see figure F.3. When doing so, one finds[5]

$$
\left(\frac{1}{(\mathbf{j} - \mathbf{1})_j(\mathbf{j})_j(\mathbf{j} + \mathbf{1})_j}\right)^4 = \tag{F.20}
$$

$$
= \frac{\langle j - 3, j - 1, j + 1, j + 3\rangle\langle j - 2, j - 1, j, j + 2\rangle\langle j - 2, j, j + 1, j + 2\rangle}{\langle j - 2, j - 1, j, j + 1\rangle^2\langle j - 1, j, j + 1, j + 2\rangle^2\langle j - 1, j, j + 1, j + 3\rangle\langle j - 3, j - 1, j, j + 1\rangle} .
$$

---

[5]As usual, for the bottom and top pentagons we need to adjust this formula slightly. For instance, for $j = 1$ we find Z_{-2} in the right hand side which is not defined, see figure F.1. The fix is very simple: we should simply replace Z_{-2} by the very bottom twistor, that is Z_{-1}. Similarly for the top pentagon, where we should replace Z_{n-1} by the very top twistor Z_{n-2}.

Appendix G

Pentagon transitions and measures

In this appendix we summarize our knowledge about elementary transitions $P_{X|Y}$, with (X, Y) being any pair of flux tube excitations. Their general structure is

$$
P_{X|Y}(u|v) = f_X(u) F_{XY}(u, v) f_Y(-v)
$$
$$
\times \exp\left[2(\kappa_X(u) - i\tilde{\kappa}_X(u))^t \cdot \mathcal{M} \cdot \kappa_Y(v) + 2i(\kappa_X(u) + i\tilde{\kappa}_X(u))^t \cdot \mathcal{M} \cdot \tilde{\kappa}_Y(v) \right],
$$

$$\text{(G.1)}$$

where all the objects in the exponent were explicitly given in the appendix C of [83] for all sorts of excitations of the flux tube (with $\mathcal{M} = \mathbb{Q} \cdot \mathbb{M}$ in the notations of [83], see also [84]). We also found convenient to strip out the factor

$$
\log f_X(u) = \int_0^\infty \frac{dt}{t} (J_0(2gt) - 1) \frac{\frac{1}{2}J_0(2gt) + \frac{1}{2} - e^{-q_X t/2} e^{-iut}}{e^t - 1}, \qquad \text{(G.2)}
$$

for each excitation, with $J_0(z) = 1 + O(z^2)$ the Bessel function of the first kind and $q_X = -1/2, 0, 1/2, 1, \dots$ for scalar, large fermion, elementary gluon, bound state of two gluons, etc. (Note that in the case of a small fermion, i.e. $X = \psi_S$ or $\bar{\psi}_S$, we have $f_X(u) = 1$ identically, see G.2 below.)

The factor (G.2) as well as the term in the exponent above are quite universal and, in particular, only depend on the absolute values of the $U(1)$ charges (e.g. they cannot distinguish between $(X, Y) = (\psi, \psi), (\psi, \bar{\psi}), (\bar{\psi}, \psi),$ or $(\bar{\psi}, \bar{\psi})$). As such, the function $F_{XY}(u, v)$ has the same conjugation property as its parent transition. Since all our transitions obey[1]

$$
P_{X|Y}(u|v)^* = P_{\bar{Y}|\bar{X}}(v|u), \qquad \text{(G.3)}
$$

---

[1] We failed to find a reason for this simple property, but noticed that it is consistent both with the fun-

upon complex conjugation (for real rapidities), with of course $\bar{\phi} = \phi$ for a scalar, $\bar{F}_a = F_{-a}$ for a gluon, etc., then the exact same relation holds true for the corresponding functions F.

The factor (G.2) as well as the exponential in (G.1) are also both irrelevant to leaden order at weak coupling, with both $\log f_X$ and the exponent in (G.1) being of order $O(g^2)$. (This estimate is not uniform in the rapidities and holds only away from the locations of singularities, which are at imaginary half integer values at weak coupling.) The leading order weak coupling results can thus be directly obtained from the prefactors F_{XY}.

G.1   Summary of transitions

Knowing the transitions is equivalent to knowing the prefactors F in (G.1). For them, which as we just said are also all we need to know to leading order at weak coupling, we have the following lists. (Up to few exceptions involving gluonic bound states, all the transitions given below already appeared in [82–84, 87, 97, 107].[2])

Transitions involving a gluon or a bound state of gluons

We start by the cases involving a gluon or a bound state of gluons.

The purely gluonic transitions are given by

$$
\begin{aligned}
F_{F_a F_b}(u,v) &= \sqrt{(x^{[+a]}y^{[-b]} - g^2)(x^{[-a]}y^{[+b]} - g^2)(x^{[+a]}y^{[+b]} - g^2)(x^{[-a]}y^{[-b]} - g^2)} \\
&\times \frac{(-1)^b \Gamma(\frac{|a|-|b|}{2} + iu - iv)\Gamma(\frac{|a|+|b|}{2} - iu + iv)}{g^2 \Gamma(1 + \frac{|a|}{2} + iu)\Gamma(1 + \frac{|b|}{2} - iv)\Gamma(1 + \frac{|a|-|b|}{2} - iu + iv)}, \quad \text{for } ab > 0, \\
F_{F_a F_b}(u,v) &= \frac{1}{\sqrt{\left(1 - \frac{g^2}{x^{[+a]}y^{[-b]}}\right)\left(1 - \frac{g^2}{x^{[-a]}y^{[+b]}}\right)\left(1 - \frac{g^2}{x^{[+a]}y^{[+b]}}\right)\left(1 - \frac{g^2}{x^{[-a]}y^{[-b]}}\right)}} \\
&\times \frac{\Gamma(1 + \frac{|a|+|b|}{2} + iu - iv)}{\Gamma(1 + \frac{|a|}{2} + iu)\Gamma(1 + \frac{|b|}{2} - iv)}, \quad \text{for } ab < 0,
\end{aligned}
\tag{G.4}
$$

damental relation (5.44), since $S_{XY}(u,v)^* = S_{YX}(v,u) = S_{\bar{Y}\bar{X}}(v,u)$, and with the mirror equation (5.45). In the latter case, one needs to use that $u^{-\gamma}$ turns into $u^{+\gamma}$ upon conjugation and that (5.45) is equivalent to $P_{X|Y}(u|v^\gamma) = P_{Y|\bar{X}}(v|u)$.

[2]Mixed transitions involving gluonic bound states were independently obtained by A. Belitsky.

and the mixed ones by

$$F_{F_a\phi}(u,v) = F_{\phi F_a}(-v,-u) = \frac{\sqrt{x^{[+a]}x^{[-a]}}\Gamma(\frac{1}{2} + \frac{|a|}{2} + iu - iv)}{g\Gamma(1 + \frac{|a|}{2} + iu)\Gamma(\frac{1}{2} - iv)}\,, \tag{G.5}$$

for any a, and by

$$F_{F_a\psi}(u,v) = F_{\psi F_a}(-v,-u) = -\frac{iy(x^{[+a]}x^{[-a]})^{3/4}\Gamma(\frac{a}{2} + iu - iv)\sqrt{(1 - \frac{g^2}{x^{[+a]}y})(1 - \frac{g^2}{x^{[-a]}y})}}{g^{3/2}\Gamma(1 + \frac{a}{2} + iu)\Gamma(1 - iv)}\,,$$

$$F_{F_{-a}\psi}(u,v) = F_{\psi F_{-a}}(-v,-u) = \frac{(x^{[+a]}x^{[-a]})^{1/4}\,\Gamma(1 + \frac{a}{2} + iu - iv)}{g^{1/2}\Gamma(1 + \frac{a}{2} + iu)\Gamma(1 - iv)\sqrt{(1 - \frac{g^2}{x^{[+a]}y})(1 - \frac{g^2}{x^{[-a]}y})}}\,,$$

$$\tag{G.6}$$

for $a > 0$. In all cases, we have $x = x(u)$, $x^{[\pm a]} = x(u \pm ia/2)$, $y = x(v)$, $y^{[\pm b]} = x(v \pm ib/2)$, $x(u) \equiv \frac{1}{2}(u + \sqrt{u^2 - (2g)^2})$ and $\Gamma(z)$ the Euler Gamma function. Transitions involving $\bar{\psi}$ can be obtained by conjugating those with ψ, as in (G.3).

(Note that all the factors above are normalized such that the associated transitions are equal to 1 to leading order at strong coupling, in the perturbative regime, i.e. for excitations with momenta of the same order as their masses. This is the expected decoupling property of the gluons at strong coupling.)

Transitions involving only scalars or fermions

We proceed with the remaining set of functions F_{XY} involving scalars and fermions. They read

$$F_{\phi\phi}(u,v) = \frac{\Gamma(iu - iv)}{g\Gamma(\frac{1}{2} + iu)\Gamma(\frac{1}{2} - iv)}\,,$$

$$F_{\phi\psi}(u,v) = F_{\phi\bar{\psi}}(u,v) = \frac{\sqrt{y}\,\Gamma\left(\frac{1}{2} + iu - iv\right)}{g\Gamma(\frac{1}{2} + iu)\Gamma(1 - iv)}\,,$$

$$F_{\bar{\psi}\psi}(u,v) = -F_{\psi\bar{\psi}}(u,v) = \frac{(xy)^{3/4}\Gamma(1 + iu - iv)}{g^{3/4}\Gamma(1 + iu)\Gamma(1 - iv)\sqrt{xy - g^2}}\,, \tag{G.7}$$

$$F_{\psi\psi}(u,v) = -F_{\bar{\psi}\bar{\psi}}(u,v) = \frac{i(xy)^{1/4}\Gamma(iu - iv)\sqrt{xy - g^2}}{g^{5/4}\Gamma(1 + iu)\Gamma(1 - iv)}\,.$$

(The branch choice for the mixed transitions above was mostly driven by the goal of getting the sign-free large (positive) v behaviours (G.15).)

202

The lists (G.4), (G.5), (G.6) and (G.7) cover all the pentagon transitions of the OPE program.

G.2 Analytic continuation to small fermions

It is also convenient to store the representation for small fermions. This one is obtained by direct analytical continuation, $x(v) \to x(\check{v}) = g^2/x(v)$, and it was thoroughly exemplified in [83]. The squared transitions, for instance, read as :

$$
\begin{aligned}
P_{\phi\psi}(u|\check{v})^2 &= -\frac{S_{\phi\psi}(u, \check{v})}{(u - v + \frac{i}{2})S_{\star\phi\psi}(u, \check{v})} , \\
P_{F\psi}(u|\check{v})^2 &= -\frac{g\sqrt{x^+x^-}y(u - v - \frac{i}{2})S_{F\psi}(u, \check{v})}{(x^+y - g^2)(x^-y - g^2)S_{\star F\psi}(u, \check{v})} , \\
P_{F\bar{\psi}}(u|\check{v})^2 &= -\frac{(x^+y - g^2)(x^-y - g^2)S_{F\bar{\psi}}(u, \check{v})}{g\sqrt{x^+x^-}y(u - v - \frac{i}{2})S_{\star F\bar{\psi}}(u, \check{v})} , \\
P_{\psi\psi}(u|\check{v})^2 &= -\frac{\sqrt{gxy}\,S_{\psi\psi}(u, \check{v})}{(xy - g^2)(u - v + i)S_{\star\psi\psi}(u, \check{v})} , \quad\quad\quad (G.8) \\
P_{\psi\bar{\psi}}(u|\check{v})^2 &= -\frac{(xy - g^2)S_{\psi\bar{\psi}}(u, \check{v})}{\sqrt{gxy}\,(u - v)S_{\star\psi\bar{\psi}}(u, \check{v})} , \\
P_{\psi\psi}(\check{u}|\check{v})^2 &= \frac{(xy - g^2)S_{\psi\psi}(\check{u}, \check{v})}{\sqrt{gxy}\,(u - v)(u - v + i)S_{\star\psi\psi}(\check{u}, \check{v})} , \\
P_{\psi\bar{\psi}}(\check{u}|\check{v})^2 &= \frac{\sqrt{gxy}\,S_{\psi\bar{\psi}}(\check{u}, \check{v})}{(xy - g^2)S_{\star\psi\bar{\psi}}(\check{u}, \check{v})} ,
\end{aligned}
$$

where, again, 'check marked' rapidities indicate analytical continuation to the small momentum sheet.

More explicitly, and including bound states as well, we can take all the transitions listed before and perform the continuation. The explicit form of the analytically continued transitions still preserves the structure (G.1), but the prefactors as well as the functions in the exponent are changed. The continuation of the exponent was explicitly worked out in [83] and here we provide once again only the expressions for the prefactors. We stress in particular that $f_{\psi_S}(u) \neq f_\psi(\check{u})$ and $F_{X\psi_S}(u, v) \neq F_{X\psi}(u, \check{v})$, since upon continuation of the *full* transition some extra terms are produced by the exponent in (G.1) and transferred to

the prefactors. Instead, the correct analytic continuation produces $f_{\psi_S}(u) = 1$ and

$$F_{F_a\psi_S}(u,v) = F_{\psi_S F_a}(-v,-u) = -\frac{\sqrt{g}(u-v+ia/2)}{y(x^{[+a]}x^{[-a]})^{1/4}\sqrt{(1-\frac{g^2}{x^{[+a]}y})(1-\frac{g^2}{x^{[-a]}y})}}, \quad \text{for } a > 0,$$

$$F_{F_a\psi_S}(u,v) = F_{\psi_S F_a}(-v,-u) = \frac{(x^{[+a]}x^{[-a]})^{1/4}}{\sqrt{g}}\sqrt{\left(1-\frac{g^2}{x^{[+a]}y}\right)\left(1-\frac{g^2}{x^{[-a]}y}\right)}, \quad \text{for } a < 0,$$

$$\text{(G.9)}$$

and

$$F_{\phi\psi_S}(u,v) = 1/\sqrt{y}, \qquad\qquad F_{\psi_S\phi}(u,v) = 1/\sqrt{x},$$

$$F_{\psi\psi_S}(u,v) = \frac{g^{1/4}}{x^{1/4}y^{3/4}}\Big/\sqrt{1-\frac{g^2}{xy}}, \qquad F_{\psi\bar{\psi}_S}(u,v) = -\frac{1}{g^{1/4}}\left(\frac{x}{y}\right)^{1/4}\sqrt{1-\frac{g^2}{xy}},$$

$$F_{\psi_S\psi}(u,v) = -\frac{g^{1/4}}{x^{3/4}y^{1/4}}\Big/\sqrt{1-\frac{g^2}{xy}}, \qquad F_{\psi_S\bar{\psi}}(u,v) = -\frac{1}{g^{1/4}}\left(\frac{y}{x}\right)^{1/4}\sqrt{1-\frac{g^2}{xy}}, \quad \text{(G.10)}$$

$$F_{\psi_S\psi_S}(u,v) = -\frac{(xy)^{1/4}}{g^{1/4}(u-v)}\sqrt{1-\frac{g^2}{xy}}, \qquad F_{\psi_S\bar{\psi}_S}(u,v) = -\frac{g^{1/4}}{(xy)^{1/4}}\Big/\sqrt{1-\frac{g^2}{xy}}.$$

G.3 Measures

We recall that the measures are obtained from the direct transition through

$$\text{Res}_{v=u} P_{\Phi|\Phi}(u|v) = \frac{i}{\mu_\Phi(u)}. \tag{G.11}$$

For a given field X, they have the universal structure

$$\mu_X(u) = \frac{M_X(u)}{f_X(u)f_X(-u)}\exp\left[2\tilde{\kappa}_X(u)^t\cdot\mathcal{M}\cdot\tilde{\kappa}_X(u)-2\kappa_X(u)^t\cdot\mathcal{M}\cdot\kappa_X(u)\right] \tag{G.12}$$

and the functions M_X are given by

$$M_\phi(u) = \frac{\pi g}{\cosh(\pi u)},$$

$$M_\psi(u) = -i\frac{\pi g^{5/4}u}{\sqrt{x}\sinh(\pi u)\sqrt{x^2-g^2}}, \tag{G.13}$$

$$M_{F_a}(u) = \frac{(-1)^a g^2 \Gamma(1+\frac{a}{2}+iu)\Gamma(1+\frac{a}{2}-iu)}{\Gamma(a)(x^{[+a]}x^{[-a]}-g^2)\sqrt{((x^{[+a]})^2-g^2)((x^{[-a]})^2-g^2)}}, \quad \text{for } a > 0.$$

204

Moreover, we have that $\mu_{F_{-a}}(u) = \mu_{F_a}(u)$ and $\mu_{\bar{\psi}}(u) = -\mu_\psi(u)$. Upon analytical continuation to the small fermion sheet, we obtain

$$M_{\psi_S}(u) = i \frac{g^{1/4}\sqrt{x}}{\sqrt{x^2 - g^2}} \,. \tag{G.14}$$

G.4 Zero momentum limit

Given a transition $P_{\bar{\psi}|Y}(\check{u}|v)$ it is immediate to derive its scalings at $u = \infty$, i.e. for a zero momentum fermion. This one can be read directly from the function $F_{\bar{\psi}_S Y}(u, v)$ listed before, since the remaining factors in (G.1) all go to 1 in this limit. We get this way

$$
\begin{aligned}
P_{\bar{\psi}|\bar{\psi}}(\check{u}|v) &\sim \frac{g^{1/4}}{u^{3/4}y^{1/4}} \,, \\
P_{\bar{\psi}|\phi}(\check{u}|v) &\sim \frac{1}{\sqrt{u}} \,, \\
P_{\bar{\psi}|\psi}(\check{u}|v) &\sim \frac{1}{g^{1/4}} \left(\frac{y}{u}\right)^{1/4} \,, \\
P_{\bar{\psi}|F_a}(\check{u}|v) &\sim \frac{\sqrt{g}}{(y^{[+a]}y^{[-a]})^{1/4}} \,, \quad \text{for } a < 0 \,, \\
P_{\bar{\psi}|F_a}(\check{u}|v) &\sim \frac{(y^{[+a]}y^{[-a]})^{1/4}}{\sqrt{g}} \,, \quad \text{for } a > 0 \,,
\end{aligned}
\tag{G.15}
$$

where, again, $y = x(v)$ and $y^{[\pm a]} = x(v \pm i\frac{a}{2})$. This information was used to obtain the non-MHV form factors $h_{\bar{Y}}(v)$ of the excitation $Y(v)$ in the main text, with help of the asymptotic behaviour of the Jacobian factor

$$\sqrt{\frac{\Gamma_{\text{cusp}}}{2ig} \mu_{\bar{\psi}}(\check{u}) \frac{du}{dp_{\bar{\psi}}}(\check{u})} \sim \frac{u^{3/4}}{g^{3/8}} \,, \tag{G.16}$$

itself following from

$$\mu_{\bar{\psi}}(\check{u}) \sim -\frac{ig^{1/4}}{\sqrt{u}} \,, \qquad \frac{dp_{\bar{\psi}}}{du}(\check{u}) \sim -\frac{\Gamma_{\text{cusp}}}{2u^2} \,. \tag{G.17}$$

G.5 The superconformal charge $\mathcal{Q}$ and the flux Goldstone fermion

In section 5.4.2 we used the realization of the superconformal generator $\mathcal{Q}_A$ as a zero momentum fermion. The precise relation is (5.55) and is repeated here for convenience

$$\mathcal{Q}|0\rangle = \sqrt{\frac{\Gamma_{\text{cusp}}}{2g}} \lim_{p\to 0} |p\rangle = \lim_{v\to\infty} \sqrt{\frac{\Gamma_{\text{cusp}}}{2gi} \frac{d\check{v}}{dp_{\bar{\psi}}} \mu_{\bar{\psi}}(\check{v})} \, |\bar{\psi}(\check{v})\rangle \, . \tag{G.18}$$

In this appendix we will derive this relation.

G.5.1 The zero momentum fermion

The non-trivial part of (G.18) is the factor dressing the zero momentum fermion state. To derive it, we should first fix the normalization of that flux-tube state $|\bar{\psi}\rangle$. It is instructive to do this in two steps. First we note that we have a well defined flux tube square measure μ, which allows us to overlap states in the flux Hilbert space. Using the supersymmetry algebra, this measure leads to a precise representation of the superconformal generators on the flux, that we denote by $\mathbb{Q}_A$. There is no reason however for this realization of the supercharge on the flux tube to be normalized in the same way as its realization on the generating function of amplitudes or equivalently, the super loop. Namely, the two may differ by an overall proportionality constant $\mathbb{Q}_A = c_0 \times \mathcal{Q}_A$.[3] We shall now first relate $\mathbb{Q}_A$ to a zero momentum fermion using the measure and the supersymmetry algebra. We will then fix the constant c_0 by demanding that pentagon NHMV amplitude is the same as the MHV one as appears in the generating function (5.6).

Consider first a delta-function normalized momentum states

$$\langle p(u)|\tilde{p}(v)\rangle = 2\pi\delta(p(u) - \tilde{p}(v)) \qquad \Rightarrow \qquad \langle p = 0|\tilde{p} = 0\rangle = 2\pi\delta(0) = \text{Vol}(\sigma) \tag{G.19}$$

where $\text{Vol}(\sigma)$ is the infinite volume of the flux in the coordinate σ conjugate to p. These momentum states differ by a simple normalization factor (involving the measure $\mu_{\bar{\psi}}$) from the rapidity states, which we conventionally normalize as [82]

$$\langle v|u\rangle = \frac{2\pi}{\mu_{\bar{\psi}}(u)}\delta(v - u) \qquad \Rightarrow \qquad |p(u)\rangle = \sqrt{-i\frac{dv}{dp_{\bar{\psi}}}\mu_{\bar{\psi}}(u)} \, |u\rangle \tag{G.20}$$

---

[3]See [76] for a very similar relation.

On the other hand, with respect to this square measure, we have

$$2||\mathbb{Q}_A|0\rangle||^2 = \langle 0|\{\mathbb{Q}_A, \bar{\mathbb{Q}}^A\}|0\rangle \tag{G.21}$$

where $|0\rangle$ is the GKP vacuum, normalized so that $\langle 0|0\rangle = 1$. The commutator is a special conformal generator that can be written in terms of the symmetries of the square as

$$\sum_{A=1}^{4}\{\mathbb{Q}_A, \bar{\mathbb{Q}}^A\} = 2(\delta_\tau - i\delta_\phi) + \mathcal{C} , \tag{G.22}$$

where the total helicity $\mathcal{C} = 0$ in our case and for simplicity, we have summed over the R-charged index, see section G.5.2. The GKP vacuum does not carry $U(1)$ charge while δ_τ measures its energy. We conclude that

$$||\mathbb{Q}_A|0\rangle||^2 = \frac{1}{4}E_{\text{GKP}}\langle 0|0\rangle = \frac{1}{4}\Gamma_{\text{cusp}} \text{Vol}(\sigma) \tag{G.23}$$

where in the last step we used the interpretation of Γ_{cusp} as the energy density of the flux in the σ direction [108]. It then follows that

$$\mathbb{Q}|0\rangle = \sqrt{\frac{\Gamma_{\text{cusp}}}{4}} \lim_{p\to 0} |p\rangle = \lim_{v\to\infty} \sqrt{\frac{\Gamma_{\text{cusp}}}{4i} \frac{d\check{v}}{dp_{\bar{\psi}}}\mu_{\bar{\psi}}(\check{v})} \, |\bar{\psi}(\check{v})\rangle \tag{G.24}$$

where the check over the fermion rapidity ($\check{v}$) indicates that it is on the so-called *small fermion sheet* where the zero momentum point is, see [83].

Next, we shall fix the proportionality constant c_0. This is done by demanding that the pentagon NHMV amplitude is the same as the MHV one. Translated to the POPE notations, this condition reads

$$1 = P(0|0) \overset{!}{=} P^{[4]}(0|0) \tag{G.25}$$

$$= \frac{1}{c_0^4}\left(\frac{\Gamma_{\text{cusp}}}{4}\right)^2 \prod_{j=1}^{4} \lim_{v_j\to\infty} \sqrt{-i\frac{d\check{v}_j}{dp_{\bar{\psi}}}\mu_{\bar{\psi}}(\check{v}_j)} \times P_{\bar{\psi}^4|0}(\check{v}_1, \check{v}_2, \check{v}_3, \check{v}_4|0) \times (\texttt{matrix part}) = \frac{g^2}{4c_0^4}$$

where in the last step we used the large v behaviours quoted in G.4, together with

$$P_{\bar{\psi}|\bar{\psi}}(\check{v}|\check{u}) \sim \frac{(vu)^{\frac{1}{4}}}{g^{\frac{1}{4}}(u - v)} ,$$

207

that can be read from the expressions in G.2, and, finally, the expression for the matrix part (which is nontrivial in this case) given by [105]

$$\texttt{matrix part} = \frac{1}{\prod\limits_{i>j}^{4}(v_i - v_j + i)} \, .$$

We deduce that $c_0 = \sqrt{g/2}$ and hence the relation (G.18). In the following subsection we elaborate on the commutation relation (G.22).

G.5.2   The commutator of superconformal charges

We shall now derive the relation relation (G.22) used above. For that aim, it is convenient to decompose any twistor in the basis of the square four twistors, (see for example appendix A of [82] for an explicate choice)

$$Z = z_b \, Z_{\text{bottom}} + z_t \, Z_{\text{top}} + z_r \, Z_{\text{right}} + z_l \, Z_{\text{left}} \, . \tag{G.26}$$

In this basis, the three symmetries of the square are generated by

$$\delta_\tau = z_b \delta_{z_b} - z_t \delta_{z_t} \, , \qquad \delta_\sigma = z_r \delta_{z_r} - z_l \delta_{z_l} \quad \text{and} \quad \delta_\phi = \frac{i}{2} \left(z_b \delta_{z_b} + z_t \delta_{z_t} - z_r \delta_{z_r} - z_l \delta_{z_l} \right) \, . \tag{G.27}$$

The relation (G.22) is an algebra relation between superconformal generators and therefore we can use any representation of the generators to test it. When acting on the generating function of helicity amplitudes, the supercharge is represented as $Q_A^\alpha = Z^\alpha \delta_\eta$. The operator $\mathcal{Q}_A$ is a specific component of the superconformal generator Q_A^α which was specified in [29]. To translate between (G.26) and the notations of [29] we may think of the square here as the bottom square of the j'th pentagon in the POPE decomposition. Then, equations (10)-(11) in [29] for the component of Q_A^α read

$$\mathcal{Q}_A = \delta_{\chi_j^A} \; \propto \; (Z_{j-1} \wedge Z_j \wedge Z_{j+1}) \cdot Z \delta_\eta \; \propto \; z_b \delta_{\eta^A} \tag{G.28}$$

where we used that $Z_j = Z_{\text{left}}$, $Z_{j-1} = Z_{\text{right}}$ and Z_{j+1} is a linear combination of Z_{right} and Z_{top}. Here, we drop the proportionality factors in (G.28) as it drops out in the commutator (G.22). We can now use the conjugate operator in this representation to evaluate the

commutator in (G.22). We find[4]

$$\sum_A \{\mathcal{Q}_A, \bar{\mathcal{Q}}^A\} = \sum_A \{z_b \delta_{\eta^A}, \eta^A \delta_{z_b}\} = 4z_b \delta_{z_b} + \sum_A \eta^A \delta_{\eta^A} \qquad \text{(G.29)}$$

$$= 2(\delta_\tau - i\delta_\phi) + (z_b \delta_{z_b} + z_t \delta_{z_t} + z_r \delta_{z_r} + z_l \delta_{z_l}) + \sum_A \eta^A \delta_{\eta^A}$$

$$= 2(\delta_\tau - i\delta_\phi) + \mathcal{C}$$

Here, the summation over the R-charge index was done for simplicity. Otherwise, on the right hand side we would also had an R-charge generator. Alternatively to this derivation, (G.22) can be read from equation (3.9) in [91] by specifying to the corresponding component.

---

[4]Note that the commutation relation (G.29) is independent of the measure one uses to realise it and thus $\{\mathcal{Q}_A, \bar{\mathcal{Q}}^A\} = \{\mathbb{Q}_A, \bar{\mathbb{Q}}^A\}$.

Appendix H

Copyright Permissions

Bibliography

[1] http://home.web.cern.ch/about/updates/2015/06/lhc-season-2-first-physics-13-tev-start-tomorrow

[2] G. 't Hooft, "A Planar Diagram Theory for Strong Interactions," Nucl. Phys. B **72**, 461 (1974).

[3] L. N. Lipatov, "High-energy asymptotics of multicolor QCD and exactly solvable lattice models," hep-th/9311037.

[4] L. D. Faddeev and G. P. Korchemsky, "High-energy QCD as a completely integrable model," Phys. Lett. B **342**, 311 (1995) [hep-th/9404173].

[5] J. M. Maldacena, "The Large N limit of superconformal field theories and supergravity," Adv. Theor. Math. Phys. **2**, 231 (1998) [Int. J. Theor. Phys. **38**, 1113 (1999)] [arXiv:hep-th/9711200].

[6] A. B. Zamolodchikov and A. B. Zamolodchikov, "Factorized s Matrices in Two-Dimensions as the Exact Solutions of Certain Relativistic Quantum Field Models," Annals Phys. **120**, 253 (1979).

[7] S. R. Coleman and J. Mandula, "All Possible Symmetries of the S Matrix," Phys. Rev. **159**, 1251 (1967).

[8] L. Brink, J. H. Schwarz and J. Scherk, "Supersymmetric Yang-Mills Theories," Nucl. Phys. B **121**, 77 (1977).

[9] G. Georgiou, V. L. Gili and R. Russo, "Operator Mixing and the AdS/CFT correspondence," JHEP **0901** (2009) 082 [arXiv:0810.0499 [hep-th]].

[10] M. Staudacher, "The Factorized S-matrix of CFT/AdS," JHEP **0505**, 054 (2005) [hep-th/0412188].

[11] J. A. Minahan and K. Zarembo, "The Bethe ansatz for N=4 superYang-Mills," JHEP **0303**, 013 (2003) [hep-th/0212208].

[12] I. Bena, J. Polchinski and R. Roiban, "Hidden symmetries of the AdS(5) x S**5 superstring," Phys. Rev. D **69**, 046002 (2004) [hep-th/0305116].

[13] N. Beisert and M. Staudacher, "The N=4 SYM integrable super spin chain," Nucl. Phys. B **670**, 439 (2003) [hep-th/0307042].

[14] N. Beisert, "The su(2|3) dynamic spin chain," Nucl. Phys. B **682**, 487 (2004) [hep-th/0310252].

[15] N. Beisert, V. Dippel and M. Staudacher, "A Novel long range spin chain and planar N=4 super Yang-Mills," JHEP **0407**, 075 (2004) [hep-th/0405001].

[16] N. Beisert and M. Staudacher, "Long-range psu(2,2|4) Bethe Ansatze for gauge theory and strings," Nucl. Phys. B **727**, 1 (2005) [hep-th/0504190].

[17] N. Beisert, B. Eden and M. Staudacher, "Transcendentality and Crossing," J. Stat. Mech. **0701**, P01021 (2007) [hep-th/0610251].

[18] S. Frolov and A. A. Tseytlin, "Semiclassical quantization of rotating superstring in AdS(5) x S**5," JHEP **0206**, 007 (2002) [hep-th/0204226].

[19] R. Roiban and A. A. Tseytlin, "Strong-coupling expansion of cusp anomaly from quantum superstring," JHEP **0711**, 016 (2007) [arXiv:0709.0681 [hep-th]].

[20] N. Gromov, V. Kazakov, A. Kozak and P. Vieira, "Exact Spectrum of Anomalous Dimensions of Planar N = 4 Supersymmetric Yang-Mills Theory: TBA and excited states," Lett. Math. Phys. **91** (2010) 265 [arXiv:0902.4458 [hep-th]].

[21] D. Bombardelli, D. Fioravanti and R. Tateo, "Thermodynamic Bethe Ansatz for planar AdS/CFT: A Proposal," J. Phys. A **42**, 375401 (2009) [arXiv:0902.3930 [hep-th]].

[22] G. Arutyunov and S. Frolov, "Thermodynamic Bethe Ansatz for the AdS(5) x S(5) Mirror Model," JHEP **0905**, 068 (2009) [arXiv:0903.0141 [hep-th]].

[23] N. Gromov, V. Kazakov and P. Vieira, "Exact Spectrum of Anomalous Dimensions of Planar N=4 Supersymmetric Yang-Mills Theory," Phys. Rev. Lett. **103**, 131601 (2009) [arXiv:0901.3753 [hep-th]].

[24] N. Gromov, V. Kazakov, S. Leurent and D. Volin, "Quantum spectral curve for AdS_5/CFT_4," Phys. Rev. Lett. **112**, 011602 (2014) [arXiv:1305.1939 [hep-th]].

[25] N. Beisert, C. Ahn, L. F. Alday, Z. Bajnok, J. M. Drummond, L. Freyhult, N. Gromov and R. A. Janik *et al.*, "Review of AdS/CFT Integrability: An Overview," Lett. Math. Phys. **99**, 3 (2012) [arXiv:1012.3982 [hep-th]].

[26] J. Caetano and J. Escobedo, "On four-point functions and integrability in N=4 SYM: from weak to strong coupling," JHEP **1109**, 080 (2011) [arXiv:1107.5580 [hep-th]].

[27] J. Caetano and J. Toledo, "χ-Systems for Correlation Functions," arXiv:1208.4548 [hep-th].

[28] J. Caetano and T. Fleury, "Three-point functions and $\mathfrak{su}(1|1)$ spin chains," JHEP **1409**, 173 (2014) [arXiv:1404.4128 [hep-th]].

[29] B. Basso, J. Caetano, L. Cordova, A. Sever and P. Vieira, "OPE for all Helicity Amplitudes," arXiv:1412.1132 [hep-th].

[30] B. Basso, J. Caetano, L. Cordova, A. Sever and P. Vieira, "OPE for all Helicity Amplitudes II. Form Factors and Data analysis," arXiv:1508.02987 [hep-th].

[31] B. Basso, S. Komatsu and P. Vieira, "Structure Constants and Integrable Bootstrap in Planar N=4 SYM Theory," arXiv:1505.06745 [hep-th].

[32] S. Lee, S. Minwalla, M. Rangamani and N. Seiberg, "Three point functions of chiral operators in D = 4, N=4 SYM at large N," Adv. Theor. Math. Phys. **2**, 697 (1998) [hep-th/9806074].

[33] J. Escobedo, N. Gromov, A. Sever and P. Vieira, "Tailoring Three-Point Functions and Integrability," JHEP **1109**, 028 (2011) [arXiv:1012.2475 [hep-th]].

[34] O. Foda, "N=4 SYM structure constants as determinants," JHEP **1203**, 096 (2012) [arXiv:1111.4663 [math-ph]].

[35] K. Okuyama and L. -S. Tseng, "Three-point functions in N = 4 SYM theory at one-loop," JHEP **0408**, 055 (2004) [hep-th/0404190].

[36] L. F. Alday, J. R. David, E. Gava and K. S. Narain, "Structure constants of planar N = 4 Yang Mills at one loop," JHEP **0509**, 070 (2005) [hep-th/0502186].

[37] N. Gromov and P. Vieira, "Tailoring Three-Point Functions and Integrability IV. Theta-morphism," arXiv:1205.5288 [hep-th].

[38] Y. Jiang, I. Kostov, F. Loebbert and D. Serban, "Fixing the Quantum Three-Point Function," arXiv:1401.0384 [hep-th].

[39] P. Vieira and T. Wang, "Tailoring Non-Compact Spin Chains," [hep-th/1311.6404].

[40] V. Kazakov and E. Sobko, "Three-point correlators of twist-2 operators in N=4 SYM at Born approximation," JHEP **1306**, 061 (2013) [arXiv:1212.6563 [hep-th]].

[41] O. Foda, Y. Jiang, I. Kostov and D. Serban, "A tree-level 3-point function in the $su(3)$-sector of planar $N = 4$ SYM," arXiv:1302.3539 [hep-th].

[42] I. Balitsky, V. Kazakov and E. Sobko, "Three-point correlator of twist-2 operators in BFKL limit," arXiv:1506.02038 [hep-th].

[43] M. S. Costa, R. Monteiro, J. E. Santos and D. Zoakos, "On three-point correlation functions in the gauge/gravity duality," JHEP **1011**, 141 (2010) [arXiv:1008.1070 [hep-th]].

[44] K. Zarembo, "Holographic three-point functions of semiclassical states," JHEP **1009**, 030 (2010) [arXiv:1008.1059 [hep-th]].

[45] R. A. Janik, P. Surowka and A. Wereszczynski, "On correlation functions of operators dual to classical spinning string states," JHEP **1005**, 030 (2010) [arXiv:1002.4613 [hep-th]].

[46] R. A. Janik and A. Wereszczynski, "Correlation functions of three heavy operators: The AdS contribution," JHEP **1112**, 095 (2011) [arXiv:1109.6262 [hep-th]].

[47] Y. Kazama and S. Komatsu, "On holographic three point functions for GKP strings from integrability," JHEP **1201**, 110 (2012) [Erratum-ibid. **1206**, 150 (2012)] [arXiv:1110.3949 [hep-th]].

[48] Y. Kazama and S. Komatsu, "Wave functions and correlation functions for GKP strings from integrability," arXiv:1205.6060 [hep-th].

[49] Y. Kazama and S. Komatsu, "Three-point functions in the SU(2) sector at strong coupling," JHEP **1403**, 052 (2014) [arXiv:1312.3727 [hep-th]].

[50] J. A. Minahan, "Holographic three-point functions for short operators," JHEP **1207**, 187 (2012) [arXiv:1206.3129 [hep-th]].

[51] T. Bargheer, J. A. Minahan and R. Pereira, "Computing Three-Point Functions for Short Operators," JHEP **1403**, 096 (2014) [arXiv:1311.7461 [hep-th]].

[52] J. A. Minahan and R. Pereira, "Three-point correlators from string amplitudes: Mixing and Regge spins," JHEP **1504**, 134 (2015) [arXiv:1410.4746 [hep-th]].

[53] G. M. Sotkov and R. P. Zaikov, "Conformal Invariant Two Point and Three Point Functions for Fields with Arbitrary Spin," Rept. Math. Phys. **12**, 375 (1977).

[54] G. M. Sotkov and R. P. Zaikov, "On the Structure of the Conformal Covariant N Point Functions," Rept. Math. Phys. **19**, 335 (1984).

[55] M. S. Costa, J. Penedones, D. Poland and S. Rychkov, "Spinning Conformal Correlators," JHEP **1111**, 071 (2011) [arXiv:1107.3554 [hep-th]].

[56] S. Lee, S. Minwalla, M. Rangamani and N. Seiberg, "Three point functions of chiral operators in D = 4, N=4 SYM at large N," Adv. Theor. Math. Phys. **2**, 697 (1998) [hep-th/9806074].

[57] L. F. Alday, J. Maldacena, A. Sever and P. Vieira, "Y-system for Scattering Amplitudes," J. Phys. A A **43**, 485401 (2010) [arXiv:1002.2459 [hep-th]].

[58] D. Gaiotto, G. W. Moore and A. Neitzke, "Wall-crossing, Hitchin Systems, and the WKB Approximation," arXiv:0907.3987 [hep-th].

[59] E. I. Buchbinder and A. A. Tseytlin, "Semiclassical correlators of three states with large S^5 charges in string theory in $AdS_5 x S^5$," Phys. Rev. D **85**, 026001 (2012) [arXiv:1110.5621 [hep-th]].

[60] A. M. Polyakov, "Gauge fields and space-time," Int. J. Mod. Phys. A **17S1**, 119 (2002) [hep-th/0110196].

[61] A. A. Tseytlin, "On semiclassical approximation and spinning string vertex operators in AdS(5) x S**5," Nucl. Phys. B **664**, 247 (2003) [hep-th/0304139].

[62] S. S. Gubser, I. R. Klebanov and A. M. Polyakov, "A Semiclassical limit of the gauge / string correspondence," Nucl. Phys. B **636**, 99 (2002) [hep-th/0204051].

[63] E. D'Hoker, D. Z. Freedman, S. D. Mathur, A. Matusis and L. Rastelli, "Extremal correlators in the AdS / CFT correspondence," In *Shifman, M.A. (ed.): The many faces of the superworld* 332-360 [hep-th/9908160].

[64] B. Eden, P. S. Howe, C. Schubert, E. Sokatchev and P. C. West, "Extremal correlators in four-dimensional SCFT," Phys. Lett. B **472**, 323 (2000) [hep-th/9910150].

[65] L. J. Dixon, L. Magnea and G. F. Sterman, "Universal structure of subleading infrared poles in gauge theory amplitudes," JHEP **0808**, 022 (2008) [arXiv:0805.3515 [hep-ph]].

[66] Z. Bern, L. J. Dixon and V. A. Smirnov, "Iteration of planar amplitudes in maximally supersymmetric Yang-Mills theory at three loops and beyond," Phys. Rev. D **72**, 085001 (2005) [hep-th/0505205].

[67] H. Elvang and Y. t. Huang, "Scattering Amplitudes," arXiv:1308.1697 [hep-th].

[68] L. J. Dixon, "A brief introduction to modern amplitude methods," arXiv:1310.5353 [hep-ph].

[69] S. J. Parke and T. R. Taylor, "An Amplitude for n Gluon Scattering," Phys. Rev. Lett. **56**, 2459 (1986).

[70] L. F. Alday and J. M. Maldacena, "Gluon scattering amplitudes at strong coupling," JHEP **0706**, 064 (2007) [arXiv:0705.0303 [hep-th]].

[71] D. J. Gross and P. F. Mende, "The High-Energy Behavior of String Scattering Amplitudes," Phys. Lett. B **197**, 129 (1987).

[72] J. McGreevy and A. Sever, "Quark scattering amplitudes at strong coupling," JHEP **0802**, 015 (2008) [arXiv:0710.0393 [hep-th]].

[73] G. P. Korchemsky, J. M. Drummond, E. Sokatchev, "Conformal properties of four-gluon planar amplitudes and Wilson loops," Nucl. Phys. **B795**, (2008) 385-408 [arXiv:0707.0243] • A. Brandhuber, P. Heslop, G. Travaglini, "MHV amplitudes in N=4 super Yang-Mills and Wilson loops," Nucl. Phys. **B794**, (2008) 231-243 [arXiv:0707.1153] • Z. Bern, L. J. Dixon, D. A. Kosower, R. Roiban, M. Spradlin, C. Vergu and A. Volovich, "The Two-Loop Six-Gluon MHV Amplitude in Maximally Supersymmetric Yang-Mills Theory," Phys. Rev. D **78**, (2008) 045007 [arXiv:0803.1465] • J. M. Drummond, J. Henn, G. P. Korchemsky and E. Sokatchev, "Hexagon Wilson loop = six-gluon MHV amplitude," Nucl. Phys. B **815** (2009) 142

[arXiv:0803.1466] • N. Berkovits, J. Maldacena, "Fermionic T-Duality, Dual Superconformal Symmetry, and the Amplitude/Wilson Loop Connection," JHEP **0809**, (2008) 062 [arXiv:0807.3196].

[74] J. M. Maldacena, "Wilson loops in large N field theories," Phys. Rev. Lett. **80** (1998) 4859 [hep-th/9803002].

[75] L. J. Mason and D. Skinner, "Dual Superconformal Invariance, Momentum Twistors and Grassmannians," JHEP **0911** (2009) 045 [arXiv:0909.0250 [hep-th]].

[76] S. Caron-Huot, "Notes on the scattering amplitude / Wilson loop duality," [arXiv:1010.1167].

[77] R. Rattazzi, V. S. Rychkov, E. Tonni and A. Vichi, "Bounding scalar operator dimensions in 4D CFT," JHEP **0812**, 031 (2008) [arXiv:0807.0004 [hep-th]].

[78] A. V. Belitsky, G. P. Korchemsky and E. Sokatchev, "Are scattering amplitudes dual to super Wilson loops?," Nucl. Phys. B **855**, 333 (2012) [arXiv:1103.3008 [hep-th]].

[79] L. F. Alday, D. Gaiotto, J. Maldacena, A. Sever and P. Vieira, "An Operator Product Expansion for Polygonal null Wilson Loops," JHEP **1104** (2011) 088 [arXiv:1006.2788 [hep-th]].

[80] B. Basso, "Exciting the GKP string at any coupling," Nucl. Phys. B **857** (2012) 254 [arXiv:1010.5237].

[81] B. Basso, A. Sever and P. Vieira, "Spacetime and Flux Tube S-Matrices at Finite Coupling for N=4 Supersymmetric Yang-Mills Theory," Phys. Rev. Lett. **111** (2013) 9, 091602 [arXiv:1303.1396 [hep-th]].

[82] B. Basso, A. Sever and P. Vieira, "Space-time S-matrix and Flux tube S-matrix II. Extracting and Matching Data," JHEP **1401**, 008 (2014) [arXiv:1306.2058 [hep-th]].

[83] B. Basso, A. Sever and P. Vieira, "Space-time S-matrix and Flux-tube S-matrix III. The two-particle contributions," arXiv:1402.3307 [hep-th].

[84] B. Basso, A. Sever and P. Vieira, "Space-time S-matrix and Flux-tube S-matrix IV. Gluons and Fusion," JHEP **1409**, 149 (2014) [arXiv:1407.1736 [hep-th]].

[85] L. F. Alday, J. M. Maldacena, "Gluon scattering amplitudes at strong coupling," JHEP **0706**, (2007) 064 [arXiv:0705.0303].

[86] A. V. Belitsky, "A note on two-loop superloop," Phys. Lett. B **718** (2012) 205 [arXiv:1207.1924 [hep-th]].

[87] A. V. Belitsky, "On factorization of multiparticle pentagons," arXiv:1501.06860 [hep-th].

[88] L. J. Mason, D. Skinner, "The Complete Planar S-matrix of N=4 SYM as a Wilson Loop in Twistor Space," JHEP **1012**, (2010) 018 [arXiv:1009.2225].

[89] H. Elvang, D. Z. Freedman and M. Kiermaier, "Solution to the Ward Identities for Superamplitudes," JHEP **1010** (2010) 103 [arXiv:0911.3169 [hep-th]].

[90] J. M. Drummond, J. Henn, G. P. Korchemsky and E. Sokatchev, "Dual superconformal symmetry of scattering amplitudes in N=4 super-Yang-Mills theory," Nucl. Phys. B **828** (2010) 317 [arXiv:0807.1095].

[91] G. P. Korchemsky and E. Sokatchev, "Superconformal invariants for scattering amplitudes in N=4 SYM theory," Nucl. Phys. B **839** (2010) 377 [arXiv:1002.4625 [hep-th]].

[92] N. Arkani-Hamed, J. L. Bourjaily, F. Cachazo, S. Caron-Huot and J. Trnka, "The All-Loop Integrand For Scattering Amplitudes in Planar N=4 SYM," JHEP **1101** (2011) 041 [arXiv:1008.2958 [hep-th]]. ● N. Arkani-Hamed, J. L. Bourjaily, F. Cachazo, A. B. Goncharov, A. Postnikov and J. Trnka, "Scattering Amplitudes and the Positive Grassmannian," arXiv:1212.5605 [hep-th]. ● N. Arkani-Hamed and J. Trnka, "The Amplituhedron," arXiv:1312.2007 [hep-th].

[93] J. L. Bourjaily, S. Caron-Huot and J. Trnka, "Dual-Conformal Regularization of Infrared Loop Divergences and the Chiral Box Expansion," arXiv:1303.4734 [hep-th].

[94] A. Sever, P. Vieira and T. Wang, "OPE for Super Loops," JHEP **1111** (2011) 051 [arXiv:1108.1575 [hep-th]].

[95] A. Sever, P. Vieira and T. Wang, "From Polygon Wilson Loops to Spin Chains and Back," JHEP **1212** (2012) 065 [arXiv:1208.0841 [hep-th]].

[96] Tree Heptagon exercise on the first day of the 6th edition of the Mathematica School http://msstp.org/?q=node/289.

[97] A. V. Belitsky, "Fermionic pentagons and NMHV hexagon," Nucl. Phys. B **894** (2015) 108 [arXiv:1410.2534 [hep-th]].

[98] L. J. Dixon, J. M. Drummond and J. M. Henn, "Bootstrapping the three-loop hexagon," JHEP **1111** (2011) 023

[99] L. J. Dixon, J. M. Drummond, M. von Hippel and J. Pennington, "Hexagon functions and the three-loop remainder function," JHEP **1312**, 049 (2013)

[100] L. J. Dixon, J. M. Drummond, C. Duhr and J. Pennington, "The four-loop remainder function and multi-Regge behavior at NNLLA in planar N=4 super-Yang-Mills theory," arXiv:1402.3300 [hep-th].

[101] L. J. Dixon, J. M. Drummond, C. Duhr, M. von Hippel and J. Pennington, "Bootstrapping six-gluon scattering in planar N=4 super-Yang-Mills theory," PoS LL **2014** (2014) 077 [arXiv:1407.4724 [hep-th]].

[102] L. J. Dixon and M. von Hippel, "Bootstrapping an NMHV amplitude through three loops," JHEP **1410** (2014) 65 [arXiv:1408.1505 [hep-th]].

[103] N. Arkani-Hamed, F. Cachazo and J. Kaplan, "What is the Simplest Quantum Field Theory?," JHEP **1009** (2010) 016 [arXiv:0808.1446 [hep-th]].

[104] A. Hodges, "Eliminating spurious poles from gauge-theoretic amplitudes," JHEP **1305** (2013) 135 [arXiv:0905.1473 [hep-th]].

[105] B. Basso, F. Coronado, A. Sever and P. Vieira, "Spacetime and Flux Tube S-Matrices. The Matrix Part", to appear.

[106] A. V. Belitsky, S. E. Derkachov and A. N. Manashov, "Quantum mechanics of null polygonal Wilson loops," Nucl. Phys. B **882** (2014) 303 [arXiv:1401.7307 [hep-th]].

[107] A. V. Belitsky, "Nonsinglet pentagons and NMHV amplitudes," Nucl. Phys. B **896** (2015) 493 [arXiv:1407.2853 [hep-th]].

[108] L. F. Alday and J. M. Maldacena, "Comments on operators with large spin," JHEP **0711** (2007) 019 [arXiv:0708.0672].

[109] B. Basso and A. V. Belitsky, "Luescher formula for GKP string," Nucl. Phys. B **860** (2012) 1 [arXiv:1108.0999].

[110] J. M. Drummond, G. Papathanasiou and M. Spradlin, "A Symbol of Uniqueness: The Cluster Bootstrap for the 3-Loop MHV Heptagon," JHEP **1503** (2015) 072 [arXiv:1412.3763 [hep-th]].

[111] J. C. Toledo, "Smooth Wilson loops from the continuum limit of null polygons," arXiv:1410.5896 [hep-th].

[112] Z. Bajnok and R. A. Janik, "String field theory vertex from integrability," JHEP **1504**, 042 (2015) [arXiv:1501.04533 [hep-th]].

[113] C. Kristjansen, "Review of AdS/CFT Integrability, Chapter IV.1: Aspects of Non-Planarity," Lett. Math. Phys. **99**, 349 (2012) [arXiv:1012.3997 [hep-th]].

[114] S. Dubovsky, R. Flauger and V. Gorbenko, "Evidence from Lattice Data for a New Particle on the Worldsheet of the QCD Flux Tube," Phys. Rev. Lett. **111**, no. 6, 062006 (2013) [arXiv:1301.2325 [hep-th]].

[115] S. Dubovsky, R. Flauger and V. Gorbenko, "Flux Tube Spectra from Approximate Integrability at Low Energies," J. Exp. Theor. Phys. **120**, no. 3, 399 (2015) [arXiv:1404.0037 [hep-th]].

[116] P. Cooper, S. Dubovsky, V. Gorbenko, A. Mohsen and S. Storace, "Looking for Integrability on the Worldsheet of Confining Strings," JHEP **1504**, 127 (2015) [arXiv:1411.0703 [hep-th]].

[117] G. Georgiou, V. Gili, A. Grossardt and J. Plefka, "Three-point functions in planar N=4 super Yang-Mills Theory for scalar operators up to length five at the one-loop order," JHEP **1204**, 038 (2012) [arXiv:1201.0992 [hep-th]].

[118] B. Eden, P. Heslop, G. P. Korchemsky and E. Sokatchev, "The super-correlator/super-amplitude duality: Part I," Nucl. Phys. B **869** (2013) 329 [arXiv:1103.3714 [hep-th]].

[119] N. Beisert, C. Kristjansen, J. Plefka, G. W. Semenoff and M. Staudacher, "BMN correlators and operator mixing in N=4 superYang-Mills theory," Nucl. Phys. B **650**, 125 (2003) [hep-th/0208178].

[120] G. Georgiou and G. Travaglini, "Fermion BMN operators, the dilatation operator of N=4 SYM, and pp wave string interactions," JHEP **0404**, 001 (2004) [hep-th/0403188].